

NASA Conference Publication 2486

The 1986 Goddard Space Flight Center Battery Workshop

*G. Morrow and T. Yi, Editors
NASA Goddard Space Flight Center
Greenbelt, Maryland*

Proceedings of a workshop held at
NASA Goddard Space Flight Center
Greenbelt, Maryland
November 18-19, 1986



**National Aeronautics
and Space Administration**

**Scientific and Technical
Information Office**

1987

PREFACE

This document contains the proceedings of the 19th annual Battery Workshop held at Goddard Space Flight Center, Greenbelt, Maryland on November 18-19, 1986. The Workshop attendees included manufacturers, users, and Government representatives interested in the latest developments in battery technology as they relate to high reliability operations and aerospace use. The subjects covered included lithium cell technology and safety improvements, nickel-cadmium separator and electrode technology along with associated modifications, flight experience and life testing of nickel-cadmium cells, and nickel-hydrogen applications and technology.

PRECEDING PAGE BLANK NOT FILMED

INTRODUCTION

Thomas Y. Yi
Goddard Space Flight Center

On behalf of George Morrow, I would like to thank you for your continuing interest in the annual NASA/GSFC Battery Workshop. We sincerely hope that the 1986 Workshop was as informative and enlightening as past Workshops. The attendance at the workshop has been growing each year, as evidenced by our moving the workshop location to a much larger auditorium at the Goddard Space Flight Center to accommodate a larger crowd. We hope that this interest in our Workshop by the aerospace battery community will continue to grow.

In the 1986 Workshop, as in the past Workshops, we have placed emphasis on the existing test programs and recent improvements, changes or problems, if any, in the aerospace cells and batteries. We did make one change, however. In the last two Workshops, we dedicated one session to the advanced energy storage systems to provide you with an overview of research and development in the energy areas for future NASA and government-wide aerospace applications. This year, we decided to abandon the advanced energy storage topics; however, this area will be covered in the first annual Space Electrochemical Research and Technology Conference sponsored by the NASA/Lewis Research Center in April 1987. As a result, we have reduced the 2-1/2 day Workshop to a 2-day Workshop.

The first day began with a presentation on the NASA Aerospace Battery Flight Systems Program Plan. This was included to provide the attendees with an overview of what NASA is planning to do to improve performance, reliability, and safety of both the primary and secondary cells. This presentation was followed by a session on Lithium Cell Technology, and the first day ended with the Nickel Hydrogen Technology session. The second day was devoted to the nickel cadmium cell technology. The morning session concentrated on the Simulated Orbital Cycling and Flight Experience, while the afternoon session, on Nickel Cadmium Design Evaluation and Component Testing.

We would like to thank the attendees, and especially all the presenters for the time and effort they put in, for making the Workshop an active forum for discussion of aerospace cells and batteries.

PRECEDING PAGE BLANK NOT FILMED

PREVIOUS BATTERY WORKSHOP PROCEEDINGS PUBLICATIONS

For your information, we have included a list of the acquisition numbers for all Battery Workshop proceedings since 1970. Copies of previous publications are available upon request. The document numbers and the addresses are as follows:

YEAR	CONTENTS	ACCESSION NUMBER
1985	Workshop	N87-11072
1984	Workshop	N85-31371
1983	Workshop	N84-33668
1982	Workshop	N83-35230
1981	Workshop	N82-20402
1980	Workshop	N81-21493
1979	Workshop	N80-20820
1978	Workshop	N79-28669
1977	Workshop	N79-21565
1976	Workshop	N77-21550
1975	Workshop	N76-24704
1974	Workshop	N75-16976
1973	Workshop (1st day)	N75-15152
	Workshop (2nd day)	N75-17808
1972	Workshop (1st day)	N73-21956
	Workshop (2nd day)	N73-21957
1971	Workshop (Volume 1)	N72-27062
	Workshop (Volume 2)	N72-27062
1970	Workshop (1st day)	N71-28672
	Workshop (2nd day)	N71-28672

NASA may contact:

NASA Scientific and Technical Information Facility (STIF)
P. O. Box 8757
BWI Airport
Baltimore, MD 21240
(301) 859-5300

All other interested parties may contact:

National Technical Information Services (NTIS)
U.S. Department of Commerce
Springfield, VA 22161
(703) 487-4600

PRECEDING PAGE BLANK NOT FILMED

CONTENTS

1986 NASA/GSFC BATTERY WORKSHOP

CO-CHAIRMEN: George W. Morrow
Thomas Y. Yi
Goddard Space Flight Center

Page

PREFACE	iii
INTRODUCTION	v
PREVIOUS BATTERY WORKSHOP PUBLICATIONS	vii
NASA AEROSPACE FLIGHT SYSTEMS PROGRAM PLAN	
O. Gonzalez-Sanabria, NASA/LeRC	1

SESSION I

TOPIC:

LITHIUM CELL TECHNOLOGY

Chairman: G. Halpert, JPL

Presentations:

COMPUTER SIMULATION OF THERMAL MODELING OF PRIMARY LITHIUM CELLS

Y. Cho, Drexel University; H. Frank and G. Halpert, JPL 21

250 Ah/90A ACTIVE LiSOCl_2 CELL FOR CENTAUR-G APPLICATION

A. Zolla and D. Tura, Altus Corp. 61

THE MOLICEL® RECHARGEABLE LITHIUM SYSTEM: MULTICELL BATTERY ASPECTS

D. Fouchard and J. B. Taylor, MOLI Energy, Ltd. 73

FAULT TREE SAFETY ANALYSIS OF A LARGE Li/SOCl_2 SPACECRAFT BATTERY

O. M. Uy and R. Maurer, APL 93

CHEMICAL ANALYSIS OF CHARGED LiSO_2 CELLS

S. Subbarao, D. Lawson, H. Frank and G. Halpert, JPL;
J. Barnes and R. Bis, NSWC 121

SESSION II

TOPIC:

NICKEL HYDROGEN TECHNOLOGY

Chairman: L. Thaller, NASA/LeRC

Presentations:

BATTERY DEVELOPMENT AND TESTING AT ESA

J. Verniolle, ESA/ESTEC 141

CONTENTS (Continued)

	Page
NICKEL HYDROGEN LOW EARTH ORBIT TEST PROGRAM UPDATE AND STATUS C. Badcock and S. Donley, The Aerospace Corp; A. Felts and R. Haag, Naval Weapons Support Center/Crane	167
ADVANCES IN NICKEL-HYDROGEN TECHNOLOGY AT YARDNEY BATTERY DIVISION J. Bentley and A. Hall, Yardney Battery Division	189
FAILURE ANALYSIS OF A 3.5 INCH AMPERE-HOUR NICKEL-HYDROGEN CELL K. Fuhr, Martin Marietta Denver Aerospace	209
GRACE DAKASEP ALKALINE BATTERY SEPARATOR R. Giovannoni, J. Lundquist, and W. Choi, W. R. Grace & Co.	215

SESSION III

TOPIC:

SIMULATED ORBITAL CYCLING & FLIGHT EXPERIENCE

Chairman: T. Yi, NASA/GSFC

Presentations:

BRASILSAT A-2-GROUND AND IN-ORBIT ANOMALIES S. Ferreira, EMBRATEL	225
INTERNATIONAL ULTRAVIOLET EXPLORER (IUE) SPACECRAFT BATTERY PERFORMANCE UPDATE S. Tiller, NASA/GSFC	231
EARTH RADIATION BUDGET SATELLITE (ERBS) ORBITING PROFILES AND NI-CD USE M. Enciso, NASA/GSFC	247
EFFECTS OF LONG TERM STORAGE ON AEROSPACE NICKEL CADMIUM CELL PERFORMANCE T. Yi, NASA/GSFC	257
QUALIFICATION TESTING OF GENERAL ELECTRIC 50AH NICKEL-CADMIUM CELLS WITH PELLON 2536 SEPARATOR AND PASSIVATED POSITIVE PLATES G. Morrow, NASA/GSFC	277
FLIGHT EXPERIENCE OF SOLAR MESOSPHERE EXPLORER'S POWER SYSTEM OVER HIGH TEMPERATURE RANGES (Not presented at the Workshop) J. Faber & D. Hurley, University of Colorado	301

SESSION IV

TOPIC:

NICKEL CADMIUM DESIGN EVALUATION & COMPONENT TESTING

Chairman: G. Morrow, NASA/Goddard Space Flight Center

Presentations:

REAL TIME CHARGE EFFICIENCY MONITORING FOR NICKEL ELECTRODES IN NICD AND NIH ₂ CELLS A. Zimmerman, The Aerospace Corporation	311
---	-----

CONTENTS (Continued)

	Page
STATISTICALLY DETERMINED NICKEL CADMIUM PERFORMANCE RELATIONSHIPS	
S. Gross, Boeing Aerospace Company	335
TEST SUMMARY FOR ADVANCED H ₂ CYCLE NiCd CELL	
L. Miller, Eagle-Picher Industries, Inc.	343
FNC: A NEW TECHNOLOGY IN NiCd BATTERIES	
G. Waterman, Utah Research & Development Co.	351
LIST OF ATTENDEES	365

COMMON DATA POOL FOR NiCd CELLS (Not Received for Publication)

W. Hwang & S. Donley, The Aerospace Corporation

NASA AEROSPACE FLIGHT SYSTEMS PROGRAM PLAN

by
Olga D. Gonzalez-Sanabria

National Aeronautics and Space Administration
Lewis Research Center
Cleveland, Oh 44135

INTRODUCTION

Although batteries and related power systems have not been a major contributor to flight failures, their performance, at times, has caused concern within NASA. At the Agency's request, the Jet Propulsion Laboratory (JPL) performed a study of actual performance of flight power systems. A thorough assessment of the state of technology revealed possible solutions to problems and ways to improve the current status of primary and secondary batteries in addition to power system integration.

This plan outlines the necessary steps to re-establish the quality, safety and reliability of standard nickel-cadmium cells. It provides for the incorporation of new, advanced technologies and improvements in the performance and life of battery systems for future NASA missions. It also looks at the present status of the primary cells and batteries to reduce the large number of chemistries involved.

OBJECTIVES

The objective of this program is to provide NASA with a policy and posture which will increase safety, performance and reliability of space power systems. This will be accomplished through improved performance, safety and quality of primary and secondary cells, batteries and control over battery system integration.

PROGRAM PLAN OVERVIEW

This plan addresses NASA flight battery and related flight power system activities which are essential for safe, reliable, and technically adequate performance during ground and flight operations. The policy, standards, and specifications developed by this plan will provide guidance for NASA project and program managers. In addition this plan will provide for the safe and reliable operation of flight batteries, including operation at higher levels of performance. Measures for reliable power systems for flight vehicle applications will be identified. The identification of missing or insufficient technical controls within the Agency and the alleviation of these conditions are essential elements of this plan. Furthermore, the plan will provide for the timely identification of the future technical needs of NASA in terms of hardware development and research.

The NASA Aerospace Flight Battery System Program Plan is intended to be responsive to NASA's anticipated needs for high performance as well and safe and reliable energy storage space power systems. In the near term the program will: a) establish the necessary data bases, b) assure short-term mission requirements will be met, and c) improve the reliability of power systems. The long range goals are designed to improve the performance and reliability of energy storage power systems to meet NASA's future needs. It will also maintain a data base to ensure problem identification and resolution.

PROGRAM TASKS

This program is designed to enhance safety, reliability, and performance of NASA's aerospace primary and secondary batteries as well as battery power systems. It is also intended to bring NASA up to state-of-art with current battery technology. A total of four tasks are required, these will be briefly described in this section.

Program Management

To provide continuing coordination with all the NASA centers, JPL, NASA Headquarters and the Battery Steering Committee. To review progress and requirements in order to provide programmatic redirection as required. Will provide for technical management, cost and scheduling of the program.

Battery Systems Technology

To improve the reliability of energy storage space power system design, integration and checkout. This is to be achieved through the development of NASA handbooks, training programs, a problem reporting mechanism, and enhancement of communications throughout the agency.

Secondary Battery Technology

To improve the performance, quality, safety, and reliability of secondary battery systems. It will involve the establishment of a performance data base for SOA batteries. Also new procurement processes to resolve present manufacturing problems. This task will focus on the understanding of critical performance parameters, and the upgrading of the test facilities to maintain the necessary data bases.

Primary Battery Technology

To improve the performance, safety, and reliability of primary battery systems. To reduce the number of chemistries used for primary batteries in order to improve characterization and controls. The activity will also include the establishment of space qualified cells and guidelines for design and operation of primary batteries.

IMPLEMENTATION

Successful implementation of the program requires participation and cooperation throughout all NASA levels. The NASA Lewis Research Center has been assigned the responsibility of the lead center. The NASA Battery Steering Committee will provide guidance and recommend priorities for the activities covered. The different tasks will be performed by the assigned NASA center or JPL in agreement with each center expertise. Overall objective, guidelines and funding will be provided by NASA Headquarters, Code Q. An overview of the centers structure and responsibilities is shown in figure 1.

CONCLUDING REMARKS

The plan responds to battery/system problems. The goals of improved reliability, safety and performance is attainable. It will also enhance understanding and communications throughout the agency and a unified, coordinated effort for future problem avoidance. The plan is certainly an inexpensive effort relative to benefits. This program addresses flight battery and related flight power system activities which are essential for safe, reliable and technically adequate performance during ground and flight operations.

NASA AEROSPACE FLIGHT BATTERY PROGRAM

4

NASA GSFC BATTERY WORKSHOP

NOVEMBER 18, 1986

OUTLINE

- **BACKGROUND**
- **PLAN OVERVIEW**
- **TASK IMPLEMENTATION**
- **CONCLUDING REMARKS**

BACKGROUND

- **NASA ADMINISTRATION CONCERN**
 - **SHUTTLE SAFETY**
 - **REAL/PERCEIVED PROBLEMS**
 - **MAINTENANCE OF BATTERY EXPERTISE**
- **NASA POLICY/PLAN**

FLIGHT BATTERY PROBLEMS

THEIR CAUSES AND IMPACT

A SURVEY FOR NASA HEADQUARTERS

GERALD HALPERT

MAY 1986

CONCLUSIONS

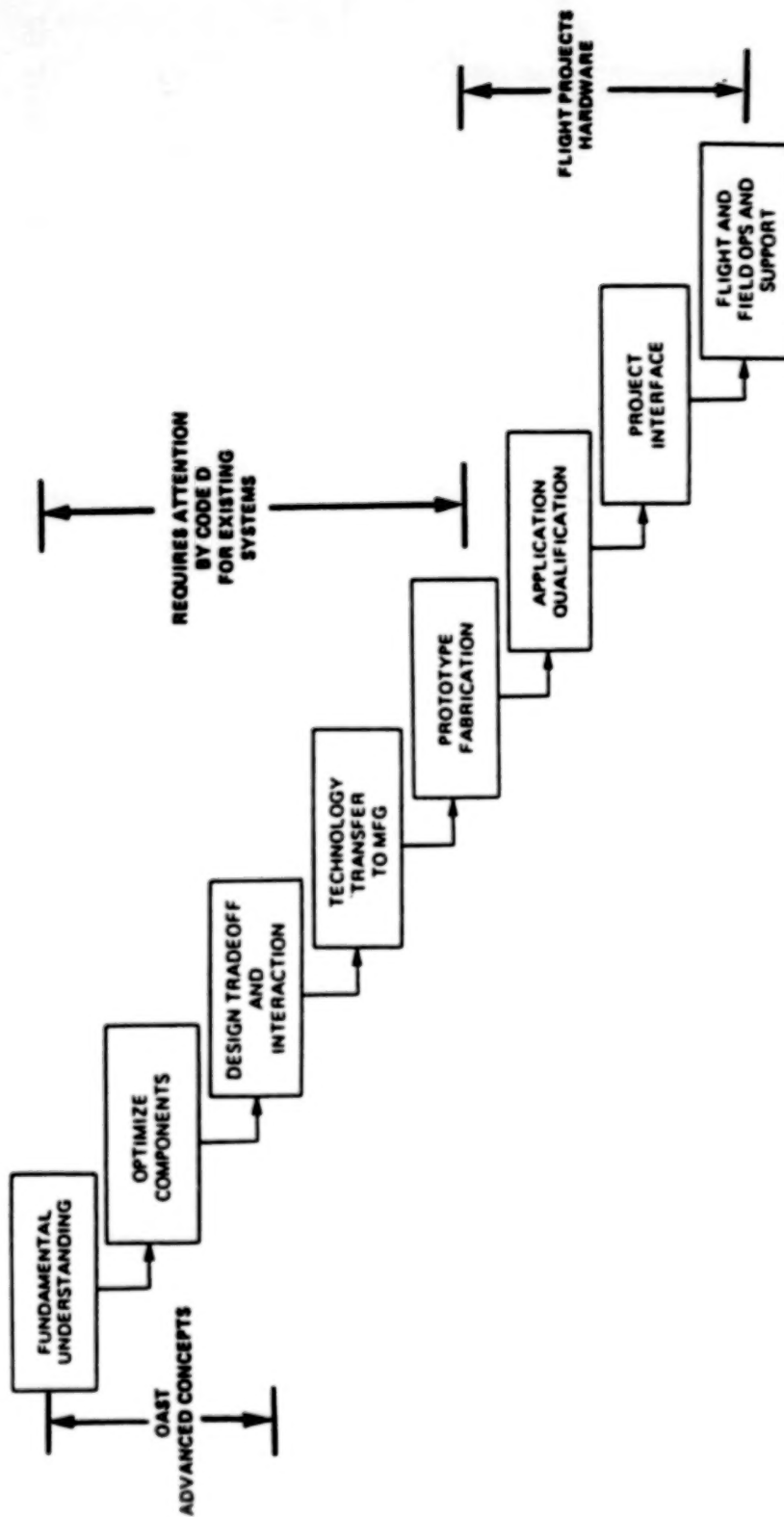
- 0 ELECTROCHEMICAL CELLS ARE COMPLEX ENERGY STORAGE DEVICES
- 0 THERE IS A CONFLICT IN MOTIVATION BETWEEN CELL MANUFACTURER, PRIME CONTRACTOR AND PROJECT OFFICE WHICH ULTIMATELY LEADS TO FAILURES COSTING MILLIONS OF DOLLARS
- 0 UNDER THE PRESENT MODE AND INVOLVEMENT OF BATTERY CADRE IN NASA FLIGHT PROJECT OPERATIONS, NASA IS VULNERABLE BECAUSE OF
 - INCONSISTENCIES IN MANUFACTURE
 - UNPREDICTABLE BEHAVIOR
 - SENSITIVITY TO OPERATING STRATEGIES
 - NAIVE UNDERSTANDING OF CELL/BATTERIES AND COMPLEX NATURE OF THE BEAST
- 0 ADDED CONTROLS AND ADEQUATE EVALUATION ARE NEEDED
- 0 IMPROVEMENTS IN RELIABILITY AND EDUCATION ARE NECESSARY
- 0 ADDITIONAL EFFORTS REQUIRED BY CODE Q TO AVOID REPETITION OF PAST OCCURRENCES AND ELIMINATE HORROR STORIES

RECOMMENDATIONS

FIVE RECOMMENDATIONS ARE MADE TO ADDRESS AND ALLEVIATE THE PROBLEMS IN THE FUTURE:

1. UNDERSTAND THE PERFORMANCE AND LIFE-LIMITING PROCESSES OF THE NI-Cd CELL
2. EVALUATE THE NEED TO ESTABLISH AND QUALIFY A SOURCE FOR AEROSPACE-QUALITY NI-Cd AND NI-H₂ CELLS
3. IMPROVE THE QUALITY AND COMMONALITY OF CELLS AND BATTERIES FOR STS OPERATIONS
4. EXPAND INVOLVEMENT WITH PROGRAM OFFICES THAT DO NOT HAVE OVERSIGHT OF BATTERY DESIGN AND APPLICATION
5. EDUCATE/TRAIN USERS AND OPERATORS ON PROPER TECHNIQUES

NASA MANAGEMENT APPROACH TO ELECTROCHEMICAL CELL TECHNOLOGY



HIGHLIGHTS OF THE NASA

AEROSPACE BATTERY SYSTEMS PROGRAM PLAN

THE NASA AEROSPACE BATTERY SYSTEMS PROGRAM PLAN

- 0 LERC MANAGEMENT VIEWS THIS EFFORT AS HIGHLY SIGNIFICANT
- 0 A COORDINATED UNIFIED ATTACK ON AN AGENCY PROBLEM
- 0 AN INEXPENSIVE INSURANCE POLICY AGAINST FUTURE PROBLEMS
- 0 A CHANCE TO PROMOTE AND DISPLAY INTERCENTER COOPERATION

OBJECTIVES OF THE PLAN

0 PROVIDE NASA WITH A POLICY AND POSTURE TO INCREASE SPACE POWER SYSTEM;

-SAFETY

-PERFORMANCE

-RELIABILITY

-QUALITY

-REDUCTION IN OVERALL PROGRAM RELATED DOLLARS

0 WILL BE ACCOMPLISHED BY:

-INCREASING THE FUNDAMENTAL UNDERSTANDING OF PRIMARY AND SECONDARY CELLS
AND BATTERIES

-PROVIDING GUIDELINES FOR PROPER DESIGN, HANDLING, AND INTEGRATION OF
BATTERY SYSTEMS

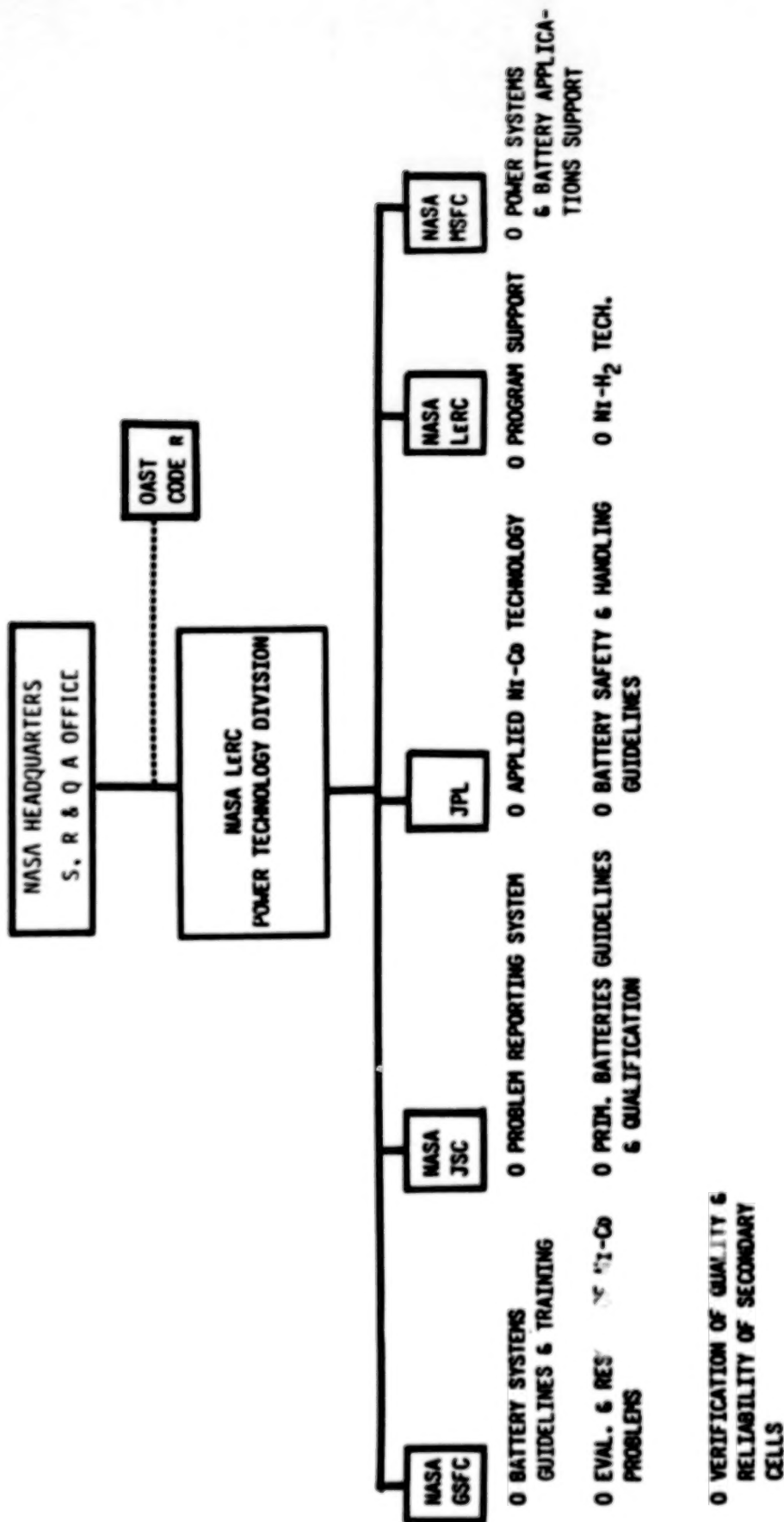
-ESTABLISHING NECESSARY DATA BASES

-PROVIDING UNIFIED INTERCENTER FOCUS TOWARD COMMON GOALS

BACKGROUND OF THE PLAN

- 0 PLAN ADDRESSES BOTH NEAR-TERM AND FAR-TERM ISSUES
- 0 WILL INVOLVE VARIOUS NASA FIELD CENTERS (LERC, GSFC, JSC, MSFC, KSC) AND JPL WITH THE OVERALL MANAGEMENT RESPONSIBILITY RESIDING AT THE LEWIS RESEARCH CENTER
- 0 WILL BE FUNDED BY NEW MONEY TO BE PROVIDED BY THE SRQM OFFICE (CODE Q) ALONG WITH THE BASE R&T OAST (CODE R) FUNDS THAT ARE ALREADY IN PLACE
- 0 INDIVIDUAL TASKS TO BE MANAGED BY THE VARIOUS CENTERS UNDER THE GUIDANCE OF THE LEWIS RESEARCH CENTER

ORGANIZATION OF TASKS



PROGRAM TASKS

- . TASK I PROGRAM MANAGEMENT**
- . TASK II BATTERY SYSTEMS TECHNOLOGY**
- . TASK III SECONDARY BATTERY TECHNOLOGY**
- . TASK IV PRIMARY BATTERY TECHNOLOGY**

CONCLUSIONS AND RECOMMENDATIONS

- 0 PLAN RESPONDS TO BATTERY/SYSTEM PROBLEMS
- 0 GOAL OF IMPROVED RELIABILITY, SAFETY, PERFORMANCE ATTAINABLE
- 0 ENHANCED UNDERSTANDING AND COMMUNICATIONS FOR PROBLEM AVOIDANCE
- 0 INEXPENSIVE RELATIVE TO BENEFITS
- 0 CODE Q COMMITMENT REQUIRED AND SUPPORT ESSENTIAL
- 0 FUNDING NOW REQUIRED TO IMPLEMENT PROGRAM

SESSION I

LITHIUM CELL TECHNOLOGY

Chairman: G. Halpert, JPL

Computer Simulation of Thermal Modeling of Primary Lithium Cells

Young I. Cho¹, Harvey Frank² and Gerald Halpert²
Drexel University (1) and Jet Propulsion Laboratory (2)

ABSTRACT

The objective was to gain a better understanding of the safety problem of primary Li-SOCl₂ and Li-SO₂ cells by carrying out detail thermal modeling work. In particular, the transient heat generation rates during moderate and extremely high discharge rate tests of Li-SOCl₂ cells were predicted and compared with those from the electrochemical heating. The difference between the two may attributed to the lithium corrosion and other chemical reactions. The present program was also tested for charging tests of Li-SO₂. In addition, the present methodology should be applicable to other primary cylindrical cells as well as rechargeable battery analyses with minor modifications.

INTRODUCTION

The present investigation is an extension of our earlier work of a simple transient model, which used the lumped-heat-capacity method to predict the time-dependent cell temperature of primary lithium-thionyl chloride (Li-SOCl₂) cells [1]. However, the thermal impact of internal thermal resistances on the overall heat dissipation was not included in the previous analysis. In addition, the heat transfer coefficient h , which is a function of temperature and position, was assumed to be constant in the previous study to demonstrate the validity of methodology.

The purpose of the present thermal modeling work was to develop a computer program to take into account the effects of internal thermal

resistances, non-linear heat transfer coefficient, and radiation. In so doing, we wanted to identify the mechanism of heat dissipation in typical cylindrical lithium cells. In addition, we wanted to calculate the net amount of heat generated from the cell during the discharging or charging procedure, from which the safety problem of Li-SOCl_2 and Li-SO_2 (lithium-sulfur dioxide) battery systems could be better understood.

Frank et al. pointed out in their study of safety hazards associated with the charging of Li-SO_2 cells [2] that the cell safety depended on a number of variables such as cell type, charging current, temperature and cell condition prior to charging (discharge history), etc. Results of the charging tests were reduced to the form of a curve called "safety envelope", that related time to explosion with charging current. The time required to reach a dangerous condition increased as the charging current was reduced. Hence, one of the objectives of the present investigation was to calculate the threshold time, which will allow the reliable prediction of the dangerous region for a system without first conducting extensive experimental measurements.

The available experimental data for Li-SO_2 cells were in the form of instantaneous cell wall temperature and operating cell voltage at a given charge current. All charging tests were carried out with power supplies, which were adjusted to provide a constant current, thus allowing voltages to float. During the charging tests the cells were placed in temperature-controlled chambers at a given temperature so that the ambient temperature was remained constant during the tests.

DESCRIPTION OF THE PROGRAM

Two computer programs were developed for the present thermal modeling work. The program A calculates instantaneous heat generation rates using the cell wall temperature as experimental input during discharging or charging test, while the program B calculates instantaneous cell wall temperature with heat generation rates if available from calorimetric measurements. In both cases the internal temperature distribution within the cell would be automatically produced. Also, electrolyte consumption schedules could be given as input such that a dry or flooded cell could be simulated. It was pointed out that the correct estimation of electrolyte during discharging or charging

test was important in the calculation of thermal mass of a cell, since electrolyte usually accounts more than fifty percent of the total thermal mass in a fully discharged condition.

Note that the programs were written in the Basic Language and can be run on the IBM PC XT or AT. Both programs are fully self-contained and the only input data required are either the transient cell wall temperature for program A or heat generation rate obtained from the calorimetric measurement for program B.

These computer programs were developed as a tool, with which one can carry out a computer experiment to identify several important safety problems such as the effects of the ambient temperature, time required to reach a dangerous condition, discharge or charge current, and amount of electrolyte, etc. To do this, one needs to have a set of data of both instantaneous cell wall temperature and heat generation rate obtained from the calorimetric measurement during discharging or charging test for a particular type of a cell. Once we establish the base line test conditions for the computer simulation by cross-checking the predicted temperature with experimental data, one can conduct a series of parametric studies by changing a parameter at a time such as ambient temperature, charging current, amount of electrolyte, etc.

In the following section, the thermal modeling work will be described in detail, which should help us to understand the full capability and limitation of the computer simulation based on the present thermal model.

DESCRIPTION OF THE THERMAL MODELING

From the heat transfer point of view, the total amount of heat generated from the cell can be expressed by the sum of the sensible heat stored within the cell and the heat dissipated out of the cell via convection and radiation mode. Although the heat transfer coefficient by a forced convection can be larger than that by a natural convection by an order of magnitude, the former was not considered here from the fact that the forced convection cooling requires power from the primary battery system, thus diluting the available power density. Hence, the convection in the present thermal modeling work

consists of the natural convection only.

When the cell wall temperature is near the ambient temperature, the heat dissipation by radiation is considered relatively small. However, with increasing cell temperature, the amount of heat to be dissipated out by radiation could be significant. This is true when a cell temperature is in the range of 80 to 120 °C, as illustrated in Fig. 1 which was for a D-size Li-SOCl₂ cell with heat generation rate of 10 W. The solid points in Fig. 1 represent the heat dissipation by convection only, while the open points include heat dissipation by radiation. As demonstrated, if radiation is not included in the heat dissipation analysis, the predicted temperature is well above the actual level by almost 100 percent even in the range of 80 to 120 °C. Thus, the radiation mode of heat dissipation is kept in the present thermal modeling. In summary, the total amount of heat generated from the cell during discharging or charging test can be written as

$$Q_{TOTAL} = Q_{CV} + Q_R + Q_{S1} + Q_{S2} \quad (1)$$

where

Q_{CV} = heat dissipation to the surroundings by convection

Q_R = heat dissipation to the surroundings by radiation

Q_{S1} = sensible heat (energy stored within the cell)

Q_{S2} = sensible heat correction due to the internal temperature variation by heat conduction.

The heat balance equation can be rewritten in terms of the actual parameters:

$$Q_{TOTAL} = h A (T_w - T_a) + F_{1-2} \epsilon \sigma A [T_w^4 - T_a^4] + C_p M \frac{dT}{dt} + Q_{S2} \quad (2)$$

where T_w and T_a are the cell wall temperature and ambient temperature, respectively. Since Q_{S2} includes the thermal resistance network introduced by Cho (i.e., Figure 8,[3]) and associated heat conduction analysis, the last term could not be expressed explicitly here.

HEAT CONVECTION

The first term in Eq. (2) represents the amount of heat removed from the cell surface to the environment via natural convection. In the cylindrical shape cell, there are three different areas, which are the side, top and bottom surfaces. The heat transfer coefficient from each surface is quite different and is a non-linear function of the wall temperature, which again varies with time. Note that the natural convection phenomena from the side, top and bottom walls of the cylindrical shape cell are well established. Hence, using the available experimental data, the dimensionless heat transfer on each wall surface was calculated as a function of the Prandtl and Rayleigh numbers, leading to the calculation of the Nusselt number. The mathematical expressions of the Nusselt numbers in the side, bottom and top surfaces were given in Cho [3]. In addition, the Prandtl number, thermal conductivity of air and the values of $g\beta/\nu^2$ necessary for the calculation of the Rayleigh number were given as a function of temperature in Cho [3]. This was converted into the corresponding heat transfer coefficient using a characteristic length such as the cell height or diameter. Using the local heat transfer coefficient, the amount of heat convected out from each wall surface was calculated and summed together to produce the total heat convected to the surroundings.

In so doing, the bottom wall surface posed some uncertainty because the cell could be placed on top of a plastic, wood, or metal shelf during the discharge or charge tests, thus preventing natural convection from occurring from the bottom wall. Depending on the shelf material and the contact resistance between the cell bottom surface and shelf, the conduction heat transfer from bottom surface to shelf could vary significantly. However, the effect of the shelf was not considered in the present thermal modeling, and heat was assumed to be removed from the bottom wall by the natural convection mode alone. Of note is that from the calculation of the present thermal modeling the heat dissipation from the bottom wall by convection was found to be relatively small compared with those from the side one.

When one has a fairly large size heat sink under the bottom wall, the effect of the heat sink can be significant and should be carefully examined. However, in many aerospace applications, such addition of heat sink is

considered not beneficial due to the associated weight gain, which is directly related to the launch cost. Also note that for a multi-cell arrangement as found in most practical applications of these lithium cells, the active surface area available for heat convection (and radiation) is lesser per cell than a single cell condition. Thus, the heat convection calculation based on the actual cell arrangement should be carried out to estimate the correct amount of heat dissipated out by convection. The multi-cell analysis should constitute future work.

HEAT RADIATION

The second term, radiation heat, represents the energy dissipated out by the radiation mode. The amount of radiated energy is proportional to the fourth power of the surface temperature (in the absolute temperature scale), in Eq. (2). Hence, with increasing cell temperature, the role of radiated energy becomes quite important. In general, the amount of heat transferred by radiation depends on the following parameters;

- F_{1-2} = configuration factor from wall to the surroundings
(geometric constant)
- ϵ = emmissivity (surface property)
- A = active area for radiation
- T_w, T_a = cell surface temperature and ambient temperature, respectively.

The values of the configuration factor and the emmissivity of the lithium cells used in the present analysis were unity and 0.8, respectively, simulating a single cell test condition. The total surface area of the cell was used as the active radiation area in the present analysis. However, the radiation from the bottom wall should not be included in the analysis when the cell is placed on a shelf. Note that for a multi-cell test one has to calculate the configuration factor using the actual multi-cell arrangement, which could be substantially smaller than unity.

SENSIBLE HEAT

The sensible energy means the energy stored within the cell due to a temperature rise of a cell during discharge or charge process. The third term in Eq. (3) represents the product of the total thermal mass and wall temperature rise during Δt , assuming that the cell internal temperature is the same as the wall temperature.

However, cell internal temperatures vary from cell wall temperature at any given time t during discharging or charging process, which was caused by the outward heat conduction. Hence, the sensible heat must be corrected to take into account the effects of internal temperature variation within the cell. To determine the local temperature in each cell component at time t , the thermal resistance of each cell component (such as cathode, anode, separator, electrolyte, and case can) was calculated in a similar manner introduced by Cho [3]. Accordingly, the sensible heat correction was obtained using the local temperature rise of each cell component. Of note is that the present program has the cell specifications of geometry and component materials for cylindrical D-size Li-SOCl₂ and Li-SO₂ (i.e., Navy's sonobuoy cell) cells. Thus, the only geometric input required for the calculation of the thermal resistance of cell components is to specify D for the D size cell or N for the Li-SO₂ cell.

In addition, the amount of liquid electrolyte varies with the depth of discharge. Since the thermal mass, defined as the product of mass and specific heat, of electrolyte, is about one third or half of the total thermal mass of the primary lithium cells, it is very important to provide a correct information on the actual amount of electrolyte as a function of time. For example, the electrolyte limited cell will have almost no liquid electrolyte near the end of discharge. Thus, substantially less thermal energy can be stored within the cell near the end of discharge. Hence, the thermal modeling presented here was developed to take into account the effect of actual electrolyte consumption as a function of discharge.

Intuitively, the flooded cell should provide more thermal mass during discharge process, thus being safer from the heat management point of view than the electrolyte limited cell. The present thermal model can be used to find how much better the flooded cell would be compared with the electrolyte limited cell, or what amount of the excessive electrolyte is needed to avoid or

delay the unsafe condition for a given type of a cell. Thus, the initial amount of electrolyte and the consumption rate could be given as a part of input data, if desired.

RESULTS AND DISCUSSION

Looking at the discharge mechanism of the lithium primary cells, the total amount of heat generated from the cell during discharge is the sum of that from the electrochemical reaction and chemical reactions. In general, the amount of the heat from the electrochemical reaction is given by the product of the polarization voltage and discharge current, while that of chemical reaction is not established well.

During the charging procedure, the amount of total input energy can be expressed by the product of the charging current and the operating cell voltage. Similarly, the excessive input energy applied during the charging test may be given by the product of the charging current and the voltage difference between the open-circuit-voltage (OCV) and operating voltage. However, it is not known what percentage of the excessive input energy would be converted into heat. The present thermal modeling work was partly initiated in an attempt to answer this question.

Li-SOCl₂ cells

a) Moderate Discharge Rate Test

A D-size cell was discharged under a constant load of 0.5 ohms. The cell wall temperature and operating cell voltage were recorded as a function of time and shown in Fig. 2. The cell wall temperature was gradually increased from the ambient condition of 22 °C to an asymptotic value of 85 °C, while the cell voltage dropped from the maximum value of 3 V at $t = 60$ min to 1.19 V near the end of test (i.e., at $t = 282$ min). The transient cell wall temperature was used as the input for the present program and the corresponding heat generation rate was calculated accordingly.

Figure 3 shows the predicted heat generation rate from the present model together with the electrochemical heatings based on the thermoneutral potential

(E_H) of 3.72 V (see the dashed line in Fig. 3). The predicted heat rates are in good agreement with those calculated with the thermoneutral potential in the range of $t = 0$ to 120 min. After $t = 120$ min when the cell operating cell voltage began to show substantial drop, the actual predicted heat rate was consistently smaller than those of electrochemical heating, indicating that the electrochemical heating based on the polarization during this period (i.e., approaching the end of discharge) is not a good measure of the total heat produced in the cell.

Figure 4 shows the contributions of energy used in the form of convection, radiation, sensible energy, and sensible energy correction due to heat conduction. As shown in the figure, the sensible energy was a dominant mode of the energy use in the beginning of discharge, while near the end of test convection and radiation accounted almost all the heat produced within the cell. In addition, the sensible heat correction due to heat conduction was negligible throughout the entire discharge period.

b) Extremely High Discharge Rate Test

To test the present program, an extremely high discharge rate test was chosen. The mechanism of heat dissipation from the cell was examined for this extreme case. Experimental data were taken from Dey [4] and shown in Fig. 5, which was obtained by external short circuit using a typical jellyroll type D-size Li-SOCl₂ cell. Of note is that the cell was exploded at $t = 9.6$ min.

The predicted core temperature together with the experimental wall temperature was presented in Fig. 6. Prior to the explosion, the temperature difference between wall and core was found to be 28 °C. The core temperature almost reached the melting point of lithium (i.e., 179 °C) while the wall temperature was well below that.

Figure 7 shows the predicted heat generation rate (see the solid line) and the electrochemical heatings based on E_H (see the dashed line). Of note is that the curves of electrochemical heating was shifted to the right by 0.5 min to match the initial slopes with the predicted one. The predicted heat rate gave a good agreement with the calculated one with E_H , confirming the validity of the present program.

To understand the mechanism of heat dissipation during the extremely high discharge rate test, the contributions of convection, radiation, sensible heat and sensible heat correction due to heat conduction are shown in Fig. 8. In the beginning of discharge, the sensible accounted almost all the heat produced within the cell. However, approaching the explosion, the contribution of the sensible heat, Q_{S1} , decreased gradually while the amount of heat due to convection, radiation and conduction increased. It is interesting to note that the sum of convection and radiation only accounted about 40 percent, while the conduction took the largest portion of the total heat, approximately 35 percent. This clearly indicates that one must include the sensible heat correction due to heat conduction in the thermal modeling of high discharge rate tests of lithium cells.

Li-SO₂ Cells

The present program was tested for charging tests of Li-SO₂ cells. Some of the results will be briefly described. The predicted instantaneous heat generation rate obtained from the Navy's Li-SO₂ cells (identified as cell#4 for the State-Of-Charge effect test at JPL) was found to be smaller than the excessive amount of input energy calculated using OCV. Note that the excessive input energy was defined as the product of the current and the difference between the cell operating voltage and OCV, $I(E_o - OCV)$. However, approaching a large explosion point, the present model predicted a significant increase in the heat generation rate, suggesting that a vigorous chemical reaction might have started during this period.

Considering the fact that during discharging tests the predicted heat rate was almost equal to or larger than the electrochemical heating, the results obtained from the simulation of charging tests showed the opposite trend. The excessive input energy was substantially larger than the predicted heat rate, indicating that a good part of input energy was consumed for some unknown chemical reactions during charging tests.

The break-down of the heat generation rate into convection, radiation, sensible heat, and sensible heat correction due to conduction was also examined. In the beginning and ending periods of the charging test, the

sensible heat was large, absorbing the significant percentage of the total heat generated from the cell. However, in the middle period of the test, the sensible heat was found to be very small due to the fact that the cell temperature remained almost unchanged during this period. In contrast, the heat dissipated out by convection and radiation were found to increase consistently with time.

SUMMARY AND CONCLUSIONS

Two programs were developed as a tool to investigate the thermal performance of primary lithium cells. Program A predicts the instantaneous heat generation rate while Program B calculates the instantaneous wall temperature. In both cases, internal temperature distributions were automatically produced, and the contributions of heat convection, radiation, internal energy stored within the cell (i.e., sensible heat) and its correction due to heat conduction were also identified. These results were used to understand the mechanism of heat dissipation from the lithium cells during discharging or charging tests.

Internal thermal resistance of each cell component was calculated based on the actual design parameters, built-in in the present program. In addition, electrolyte consumption schedules could be given as input such that a dry or flooded cell could be simulated. The major findings will be briefly highlighted below:

1. During discharging test runs, the predicted heat rate gave a good agreement with those obtained with the electrochemical heating based on thermoneutral potential, $I(E_H - E_0)$.
2. Under normal discharge rate conditions, convection and radiation were dominant heat dissipation modes.
3. However, approaching the explosion or for extremely high discharge rate cases such as external short circuits, convection and radiation accounted only

forty percent of the total heat produced.

4. During the most period of the charging test, the predicted heat generation rate was found to be consistently smaller than the excessive input energy given by $I(E_0 - OCV)$. However, approaching the explosion point, the predicted heat rate showed a significant increase, suggesting a vigorous chemical reaction occurring within the cell.

5. Time-history of convection, radiation, sensible heat, and conduction was calculated from the thermal modeling analysis both Li-SOCl₂ and Li-SO₂ cell, which helps us to better understand the overall thermal behavior of the cell during discharging charging tests.

A series of parametric investigations using the present thermal modeling program might help us to identify the unsafe operating condition of the primary lithium cells. Of note is that the present program is applicable to other primary cylindrical cells with minor modifications. In addition, the present methodology should be valid for prismatic or button type lithium cells as well as for rechargeable battery analyses, in general.

ACKNOWLEDGEMENT

The first author acknowledges the support from the Jet Propulsion Laboratory, California Institute of Technology.

NOMENCLATURE

A	: cross sectional area
C_p	: specific heat
E_H	: thermoneutral potential of the lithium cell
E_o	: operating cell voltage
F_{1-2}	: configuration factor used in radiation analysis
h	: convection heat transfer coefficient
I	: Current
M	: mass of cell
OCV	: Open-circuit-voltage
Q	: Heat generation rate
T	: Temperature
t	: time

Greeks

ϵ	: emissivity
σ	: Stefan-Boltzman constant

Subscriptions

a	: ambient
w	: cell wall

REFERENCES

1. Y.I. Cho and G. Halpert, Heat Dissipation of High Rate Li-SOCl₂ Primary Cells, J. of Power Sources, 18, (1986), pp.109-115. Also, presented at the 1985 Goddard Space Flight Center Battery Workshop, Nov. 19-21, 1985, Greenbelt, MD.
2. H. Frank, G. Halpert, D.D. Lawson, J.A. Barnes and R.F. Bis, Safety Hazards Associated with the Charging of Lithium /Sulfur Dioxide Cells, J. Power Sources, 18, (1986), pp.89-99.
3. Y.I. Cho, Thermal Modeling of High Rate Li-SOCl₂ Primary Cylindrical Cells, to be published in the J. Electrochemical Society.
4. A. N. Dey, Sealed Primary Lithium-Inorganic Electrolyte Cell, Final Report ERADCOM-TR-74-0109 F, July (1978).

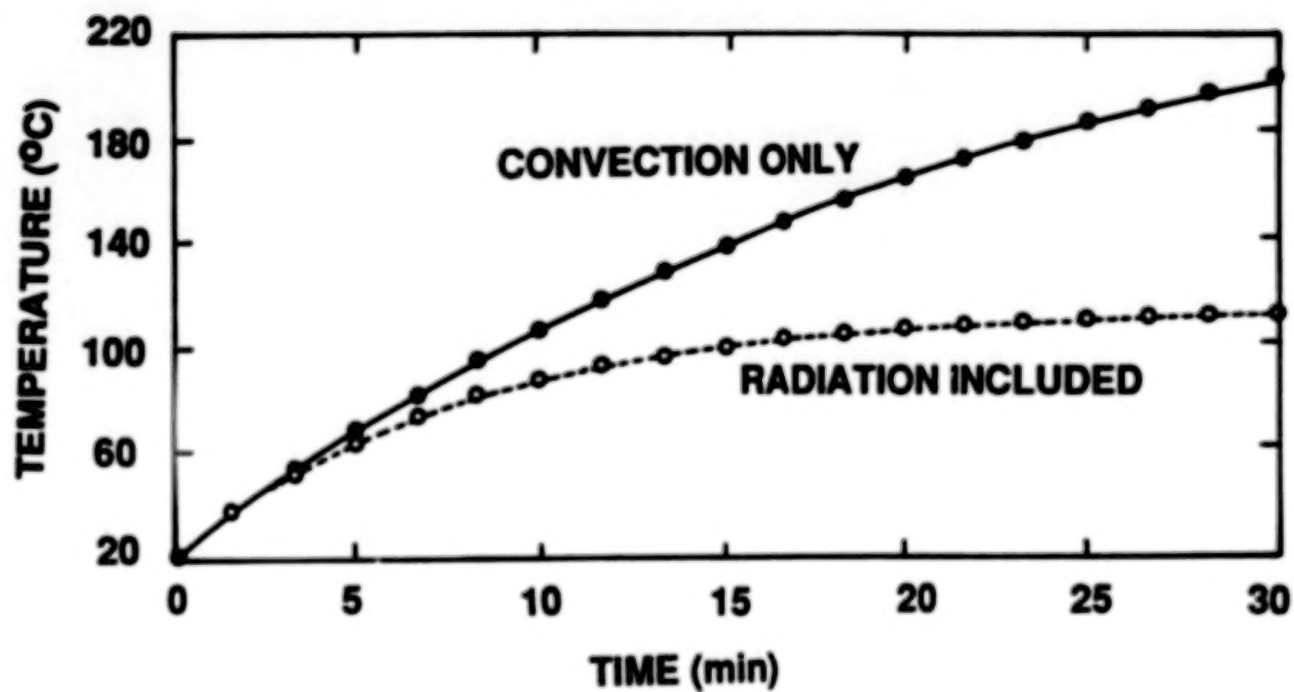


Figure 1. Predicted temperatures for a D-size Li-SOCl_2 cell with heat generation rate of 10 W.

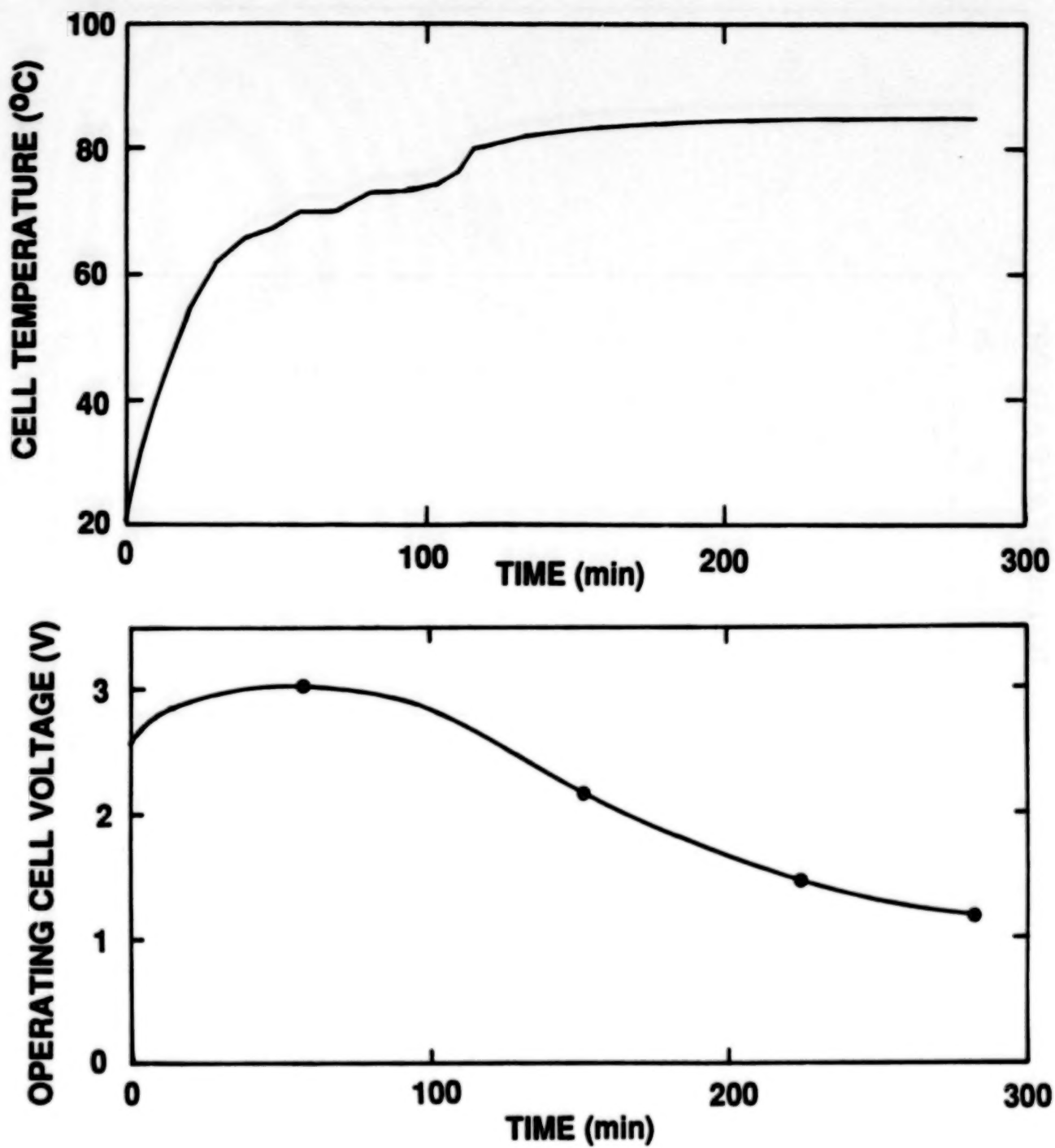


Figure 2. Experimentally measured cell wall temperature and operating cell voltage vs. time during the discharge test under a constant load.

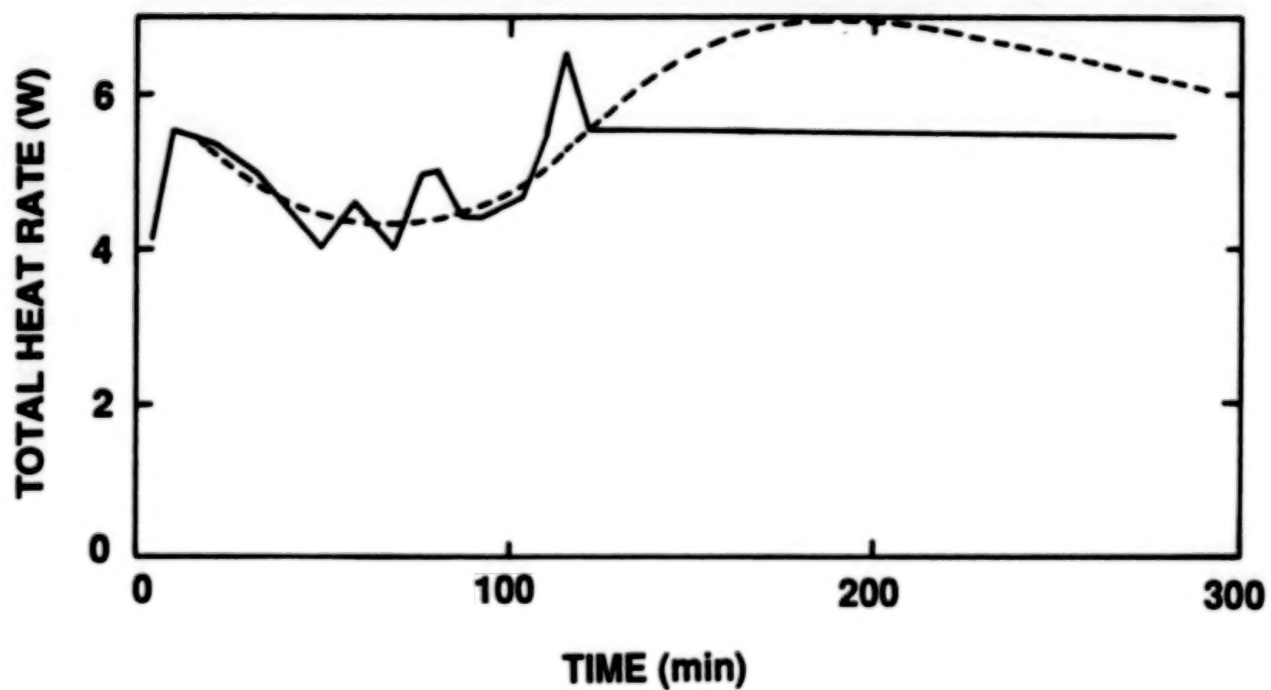


Figure 3. Prediction of the total heat rates from the present model (solid line) and the calculated results based on the thermoneutral potential of 3.72 V (dashed line) for the discharge test under constant load.

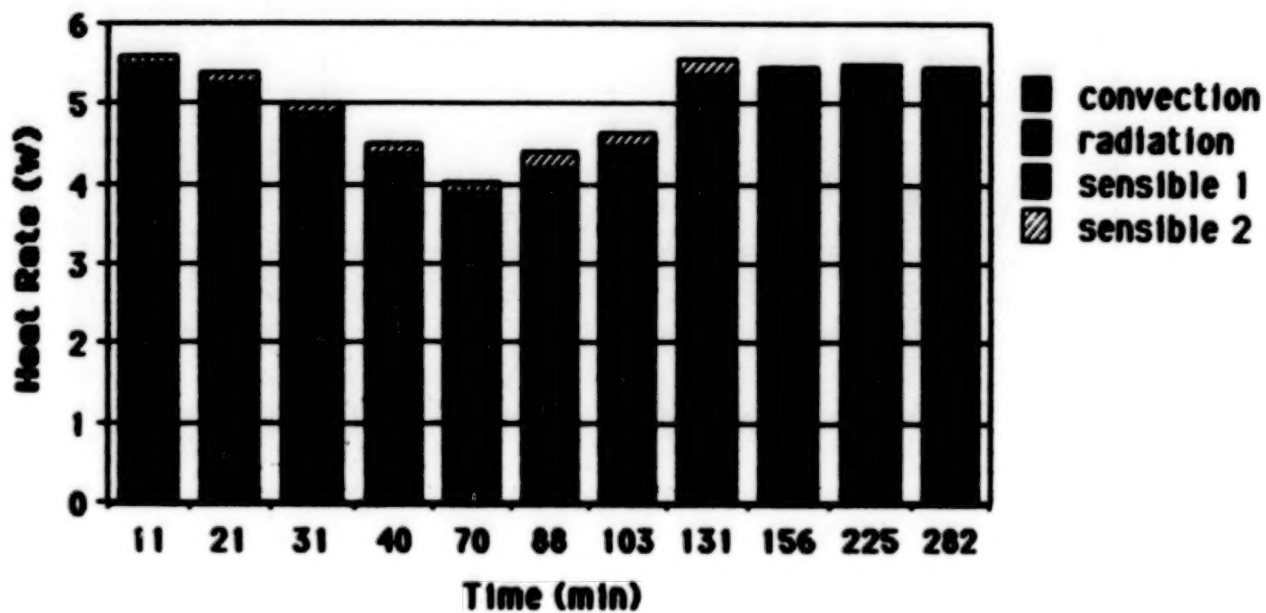


Figure 4. Contributions of convection, radiation, sensible energy (1) and sensible energy correction due to conduction (2) for the discharge test under constant load.

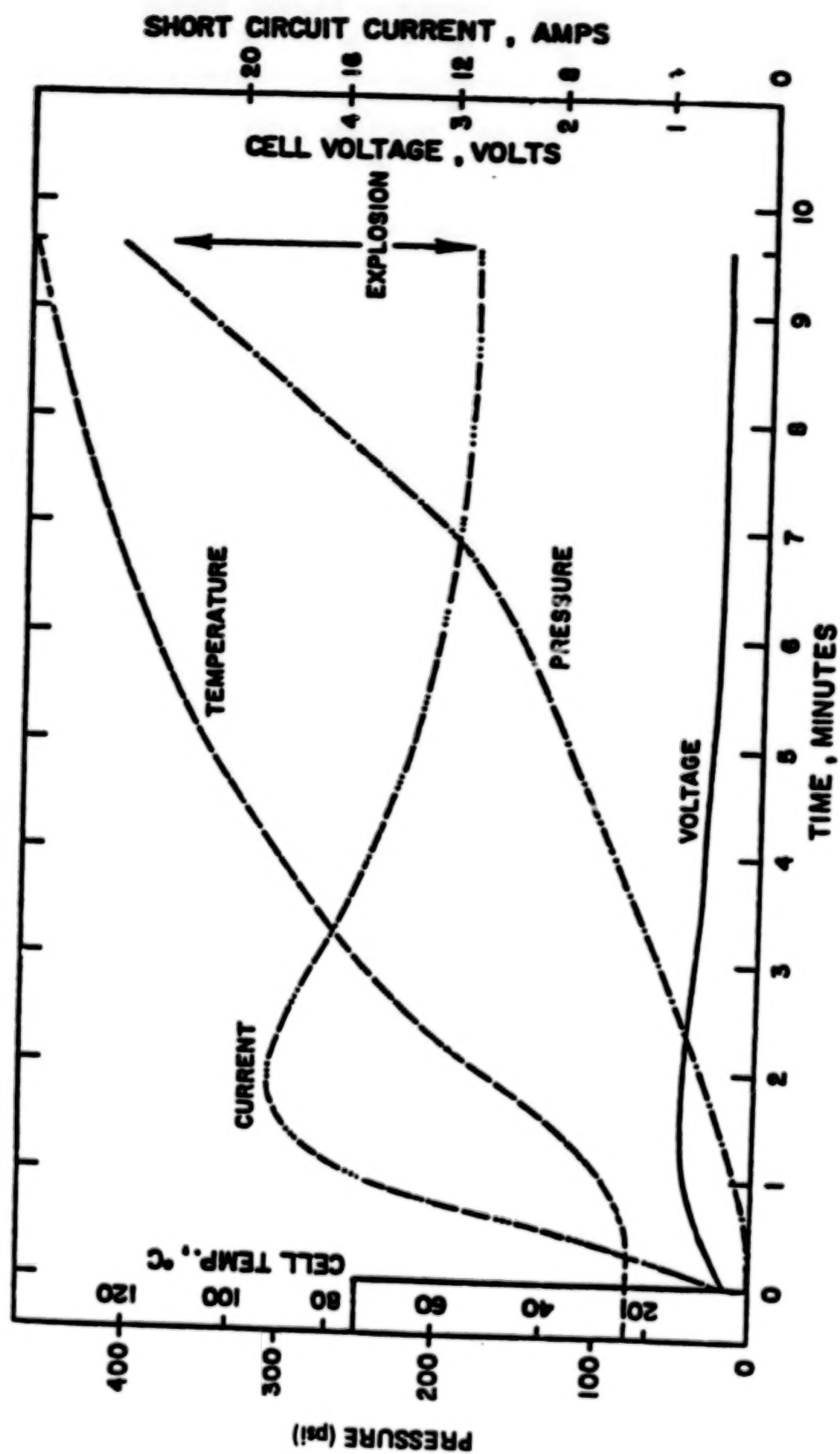


Figure 5. Experimental data during external short circuit from Dey (4).

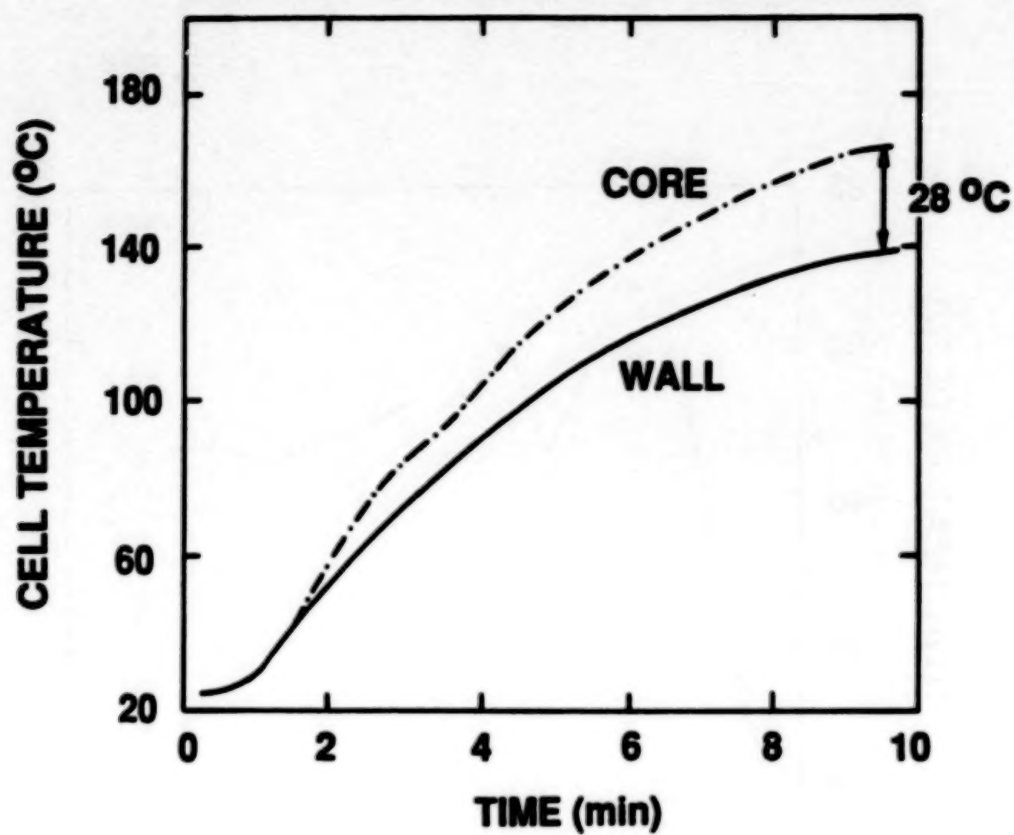


Figure 6. Prediction of core and wall temperatures from the present model for the short circuit test.

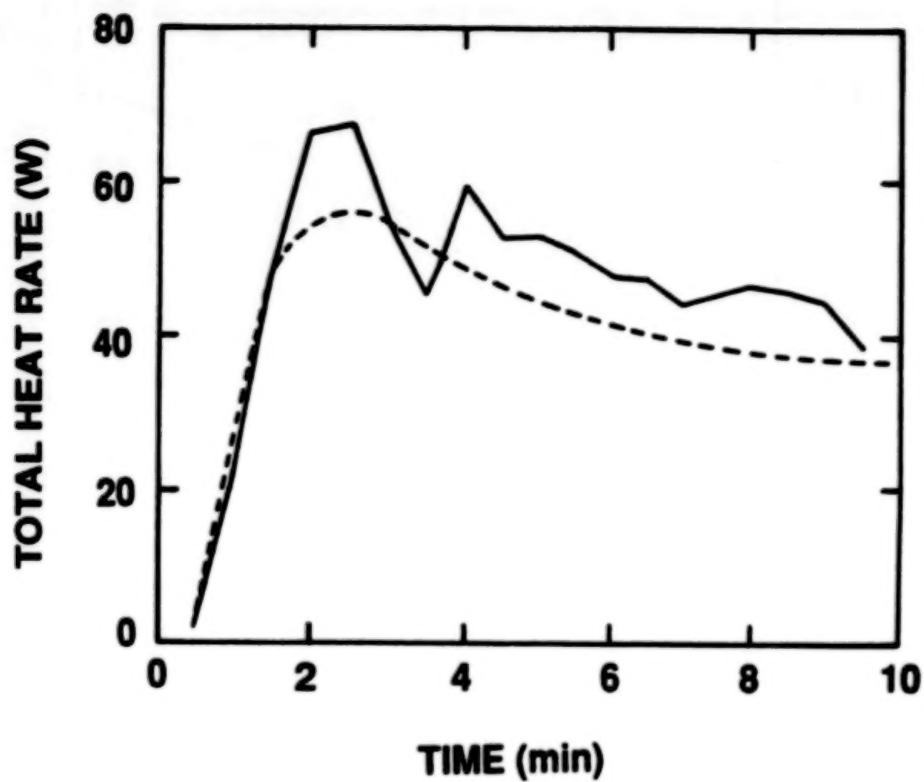


Figure 7. Prediction of total heat rates from the present model (solid line) and the calculated results based on the thermoneutral potential of 3.72 V (dashed line) for the short circuit test.

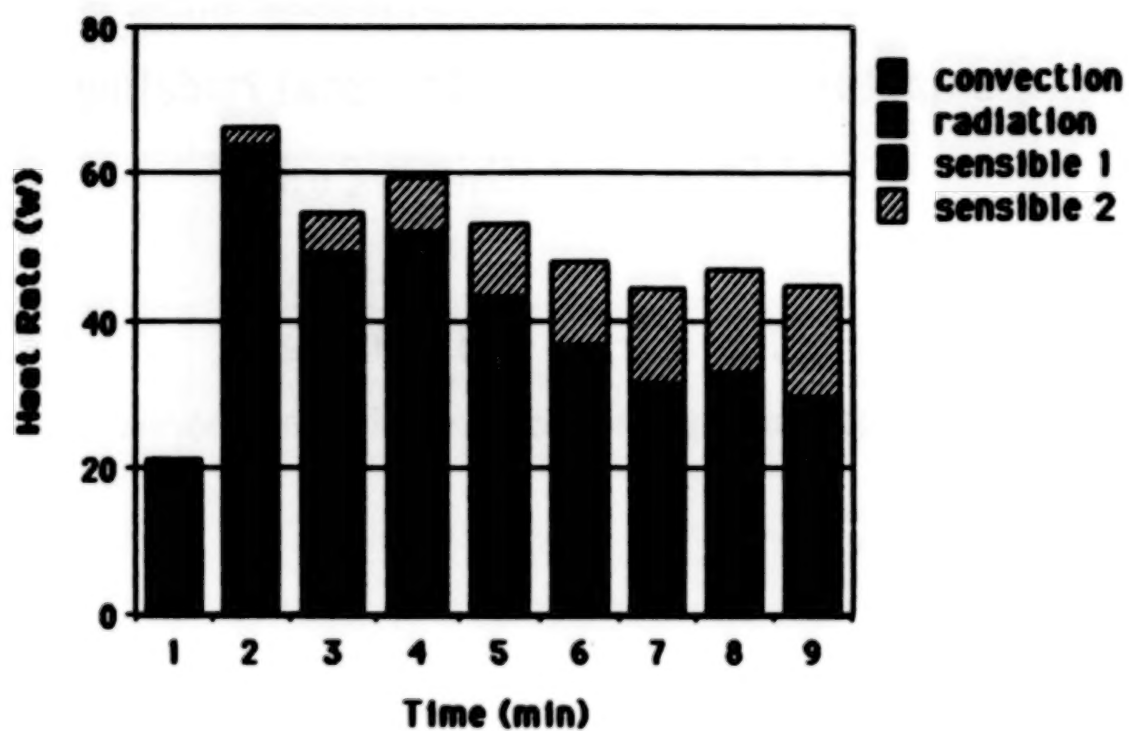


Figure 8. Contributions of convection, radiation, sensible energy (1) and sensible energy correction due to conduction (2) for the short circuit test.

Computer Simulation of Thermal Modeling of Primary Lithium Cells

**Y. Cho, H. Frank and G. Halpert
Drexel University and Jet Propulsion Laboratory**

**November 18, 1986
Goddard Space Flight Center Battery Workshop**

OBJECTIVES

The goal was to better understand the safety problem of primary Li-SOCl₂ and Li-SO₂ cells by conducting the thermal modeling work.

Specifically, we wanted

- i) to predict the total amount of heat generation rate during high discharge rate conditions, and**
- ii) to understand the mechanism of heat dissipation from the cell**

OBJECTIVES-CONTINUED

- o The time required to reach unsafe conditions for a given cell and given test conditions should be calculated.
- o The net difference between the predicted total heat rate from the model q_t and the heat calculated from $I(OCV - E_1)$ is due to lithium corrosion and/or other chemical reactions.

Total Heat Dissipation consists of

- o heat convection from cell wall to the surroundings**
- o heat radiation from cell wall to the surroundings**
- o energy stored within the cell (sensible energy)**
- o sensible energy correction due to heat conduction**

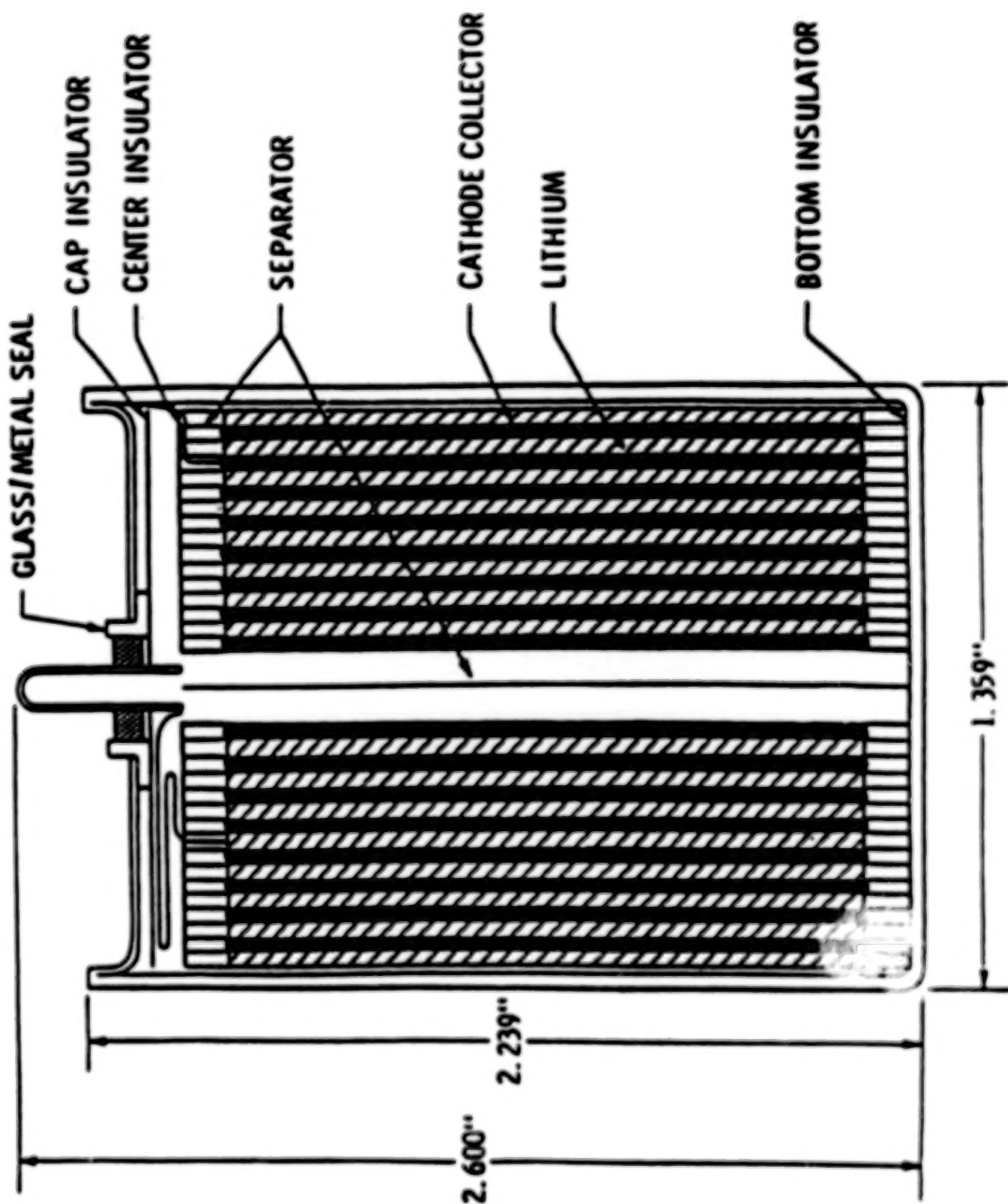


Figure 1.

The total heat generation rate is the sum of all four.

$$q_{\text{total}} = q_{\text{cv}} + q_r + q_{s1} + q_{s2}$$

The heat balance equation becomes

$$q_{\text{total}} = h(T_w, r) A (T_w - T_a) + F_{1-2} A \sigma \epsilon (T_w^4 - T_a^4)$$

$$c_p M \frac{dT_w}{dt} + q_{s2}$$

where T_w is a function of time.

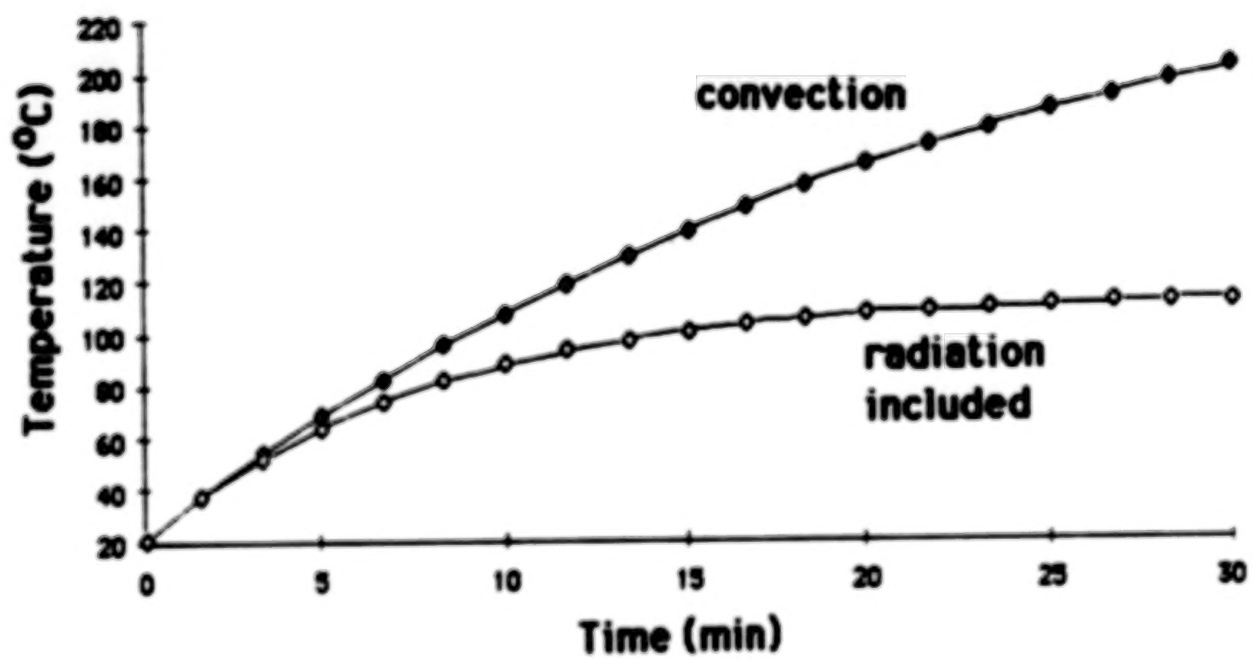


Figure 2.

THE PRESENT COMPUTER CODE CONSISTED OF TWO PARTS.

Program A : to predict total heat generation rate from the cell wall temperature as a function of time

Program B : to predict transient cell temperature from the heat generation rate data

In both cases,

- i) internal temperature distributions were automatically produced, and
- ii) contributions of heat convection, radiation, internal energy stored within the cell, and heat conduction were automatically identified.

USER-FRIENDLY CODE:

**Any cylindrical cell can be simulated.
In particular,**

- i) Detail information on the geometry and cell component materials for Li-SOCl₂ (D-size cell) and Li-SO₂ (Navy's sonobuoy cell) was built-in.**
- ii) Internal thermal resistances were automatically calculated based on these information to produce internal temperature distributions.**
- iii) Electrolyte consumption schedules could be given such that a dry or flooded cell could be simulated.**

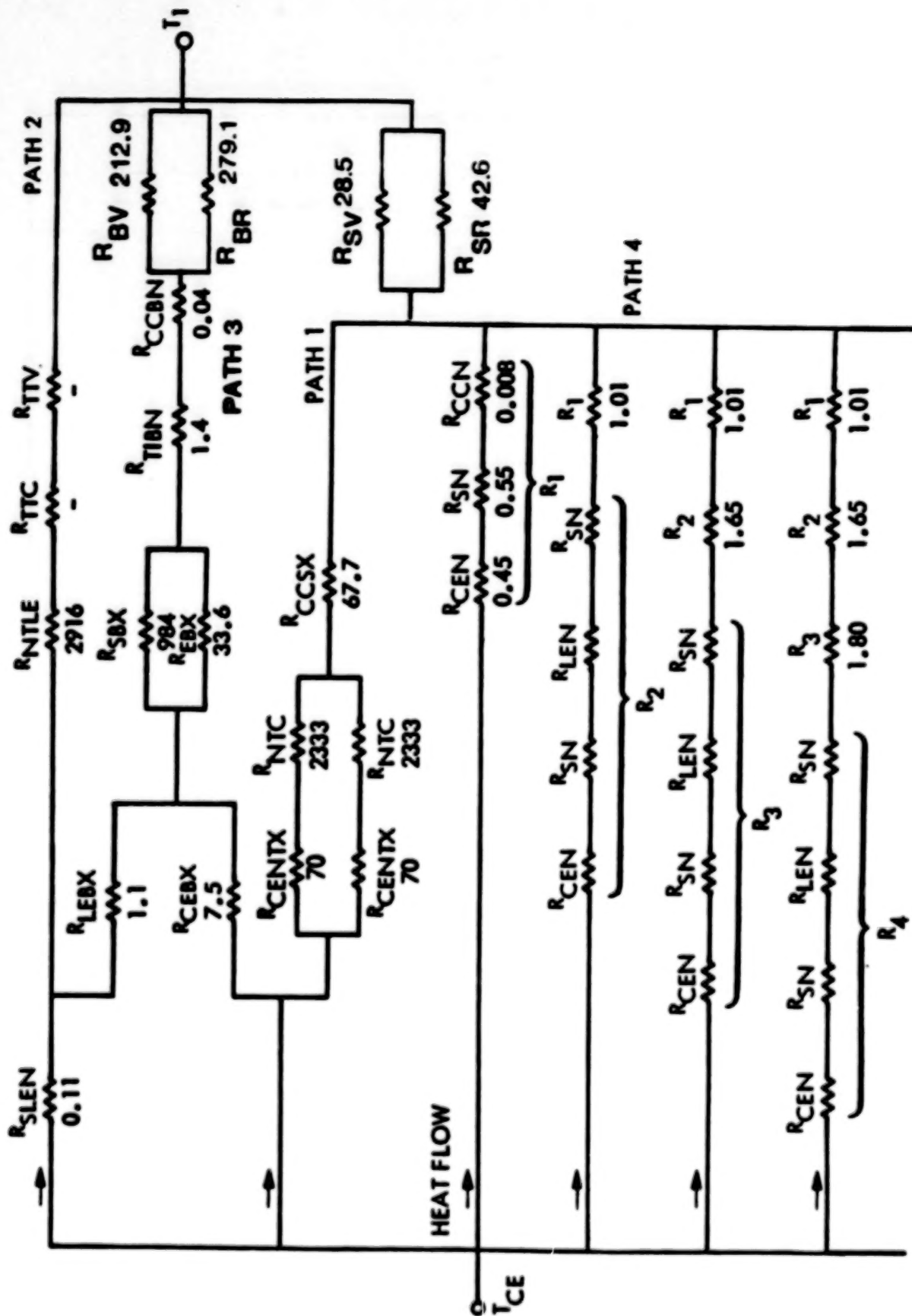


Figure 3.

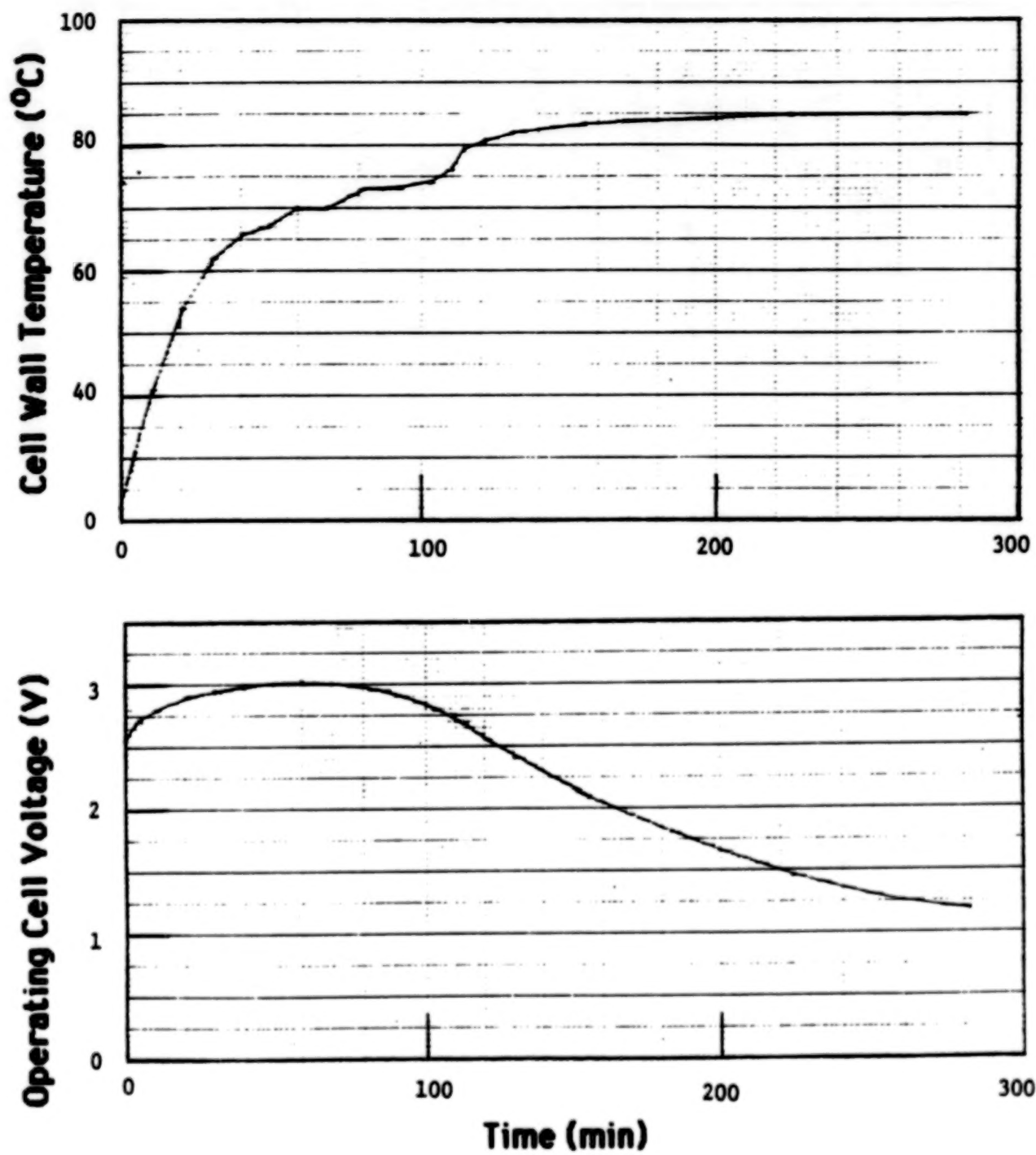


Figure 4. Discharge test under a constant load.

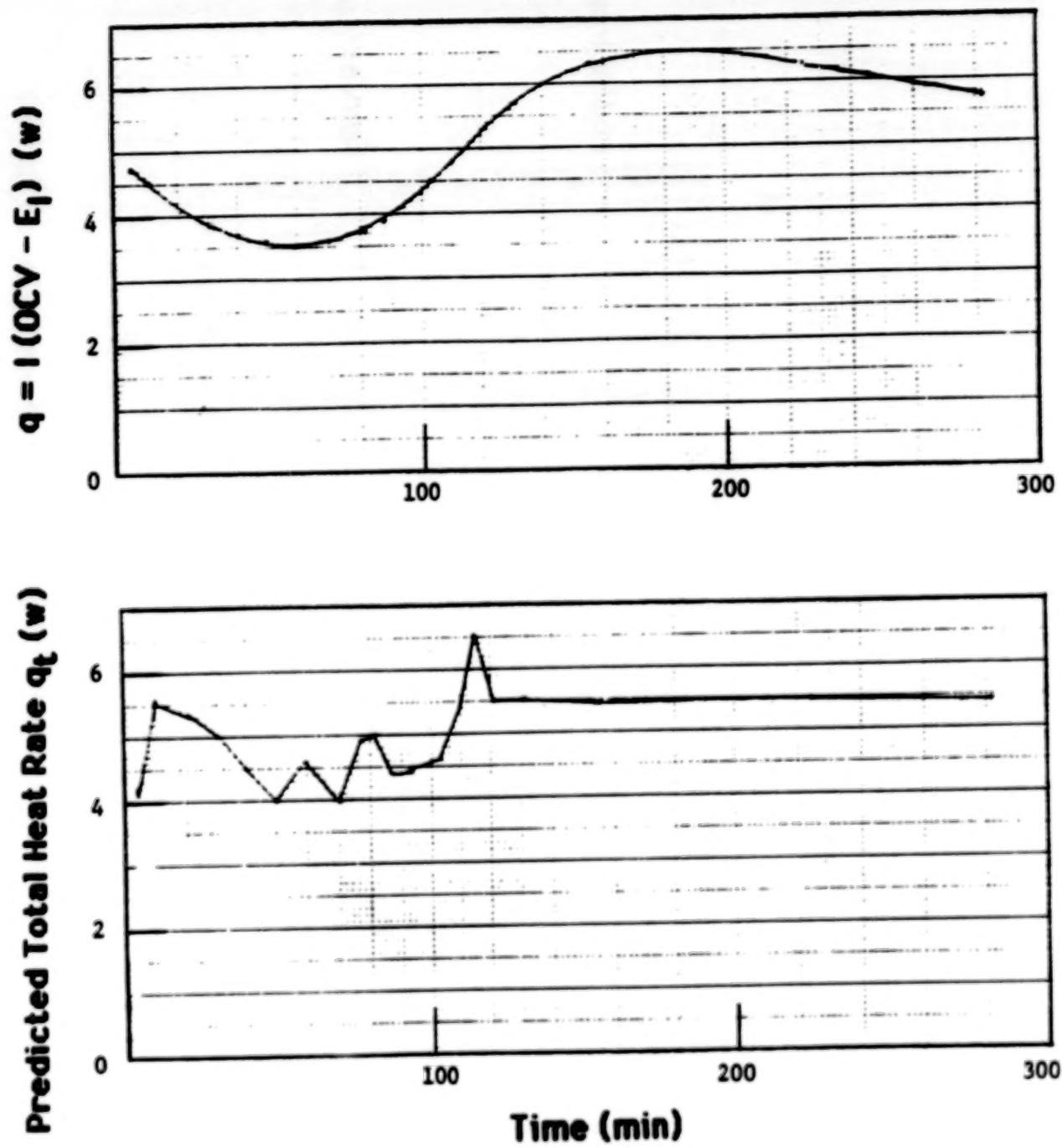


Figure 5. Discharge test under a constant load.

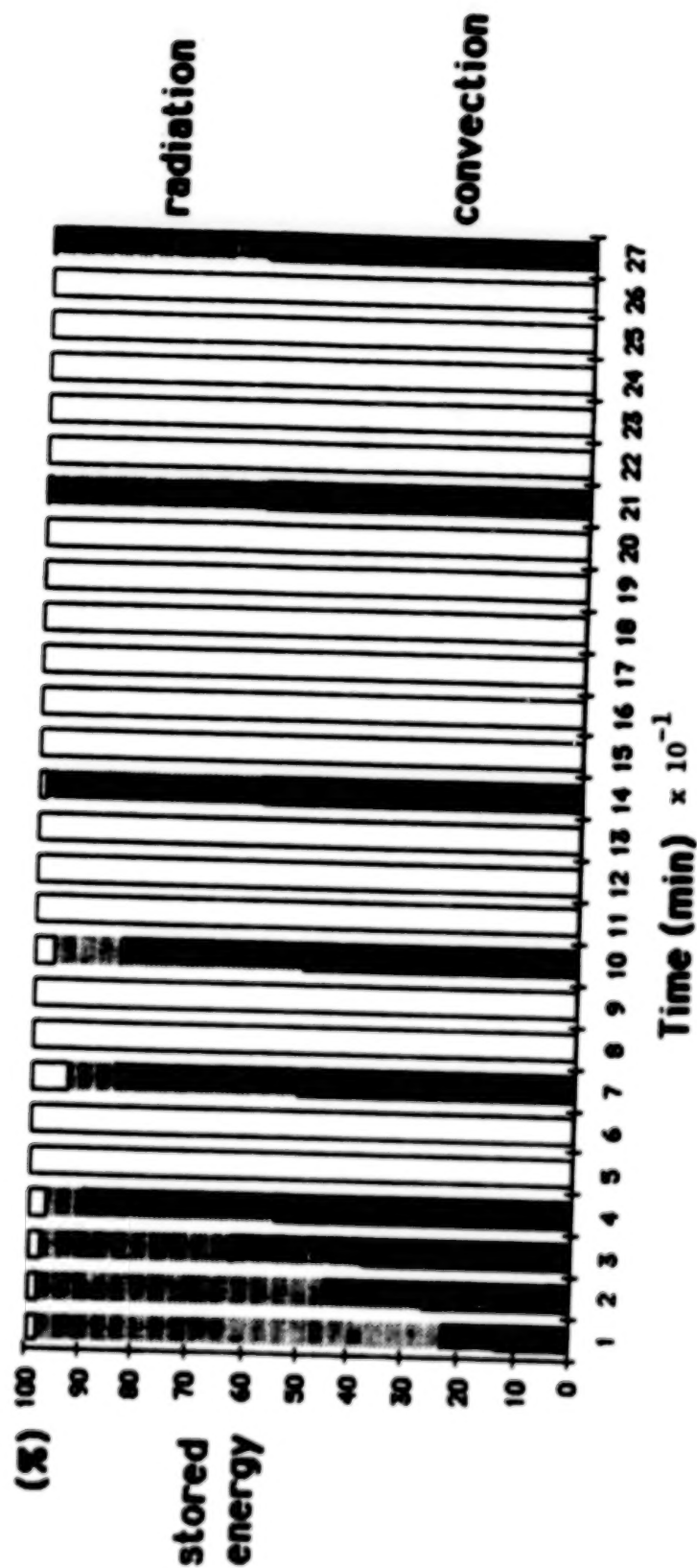


Figure 6. Discharge test under a constant load.

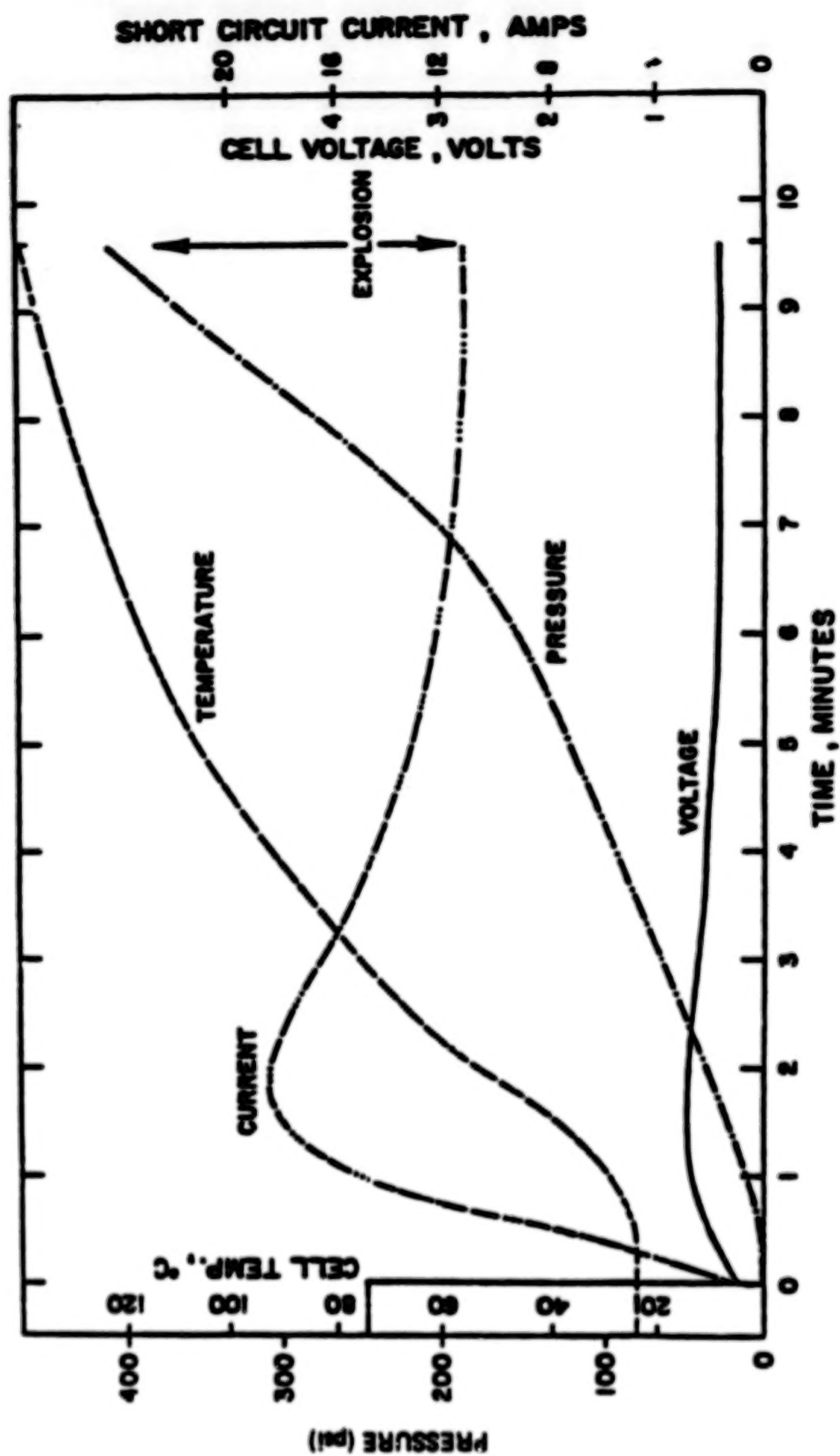


Figure 7. Pressure, Temperature, Voltage and Current During Li-SOCl₂ Cell Shorting.⁷

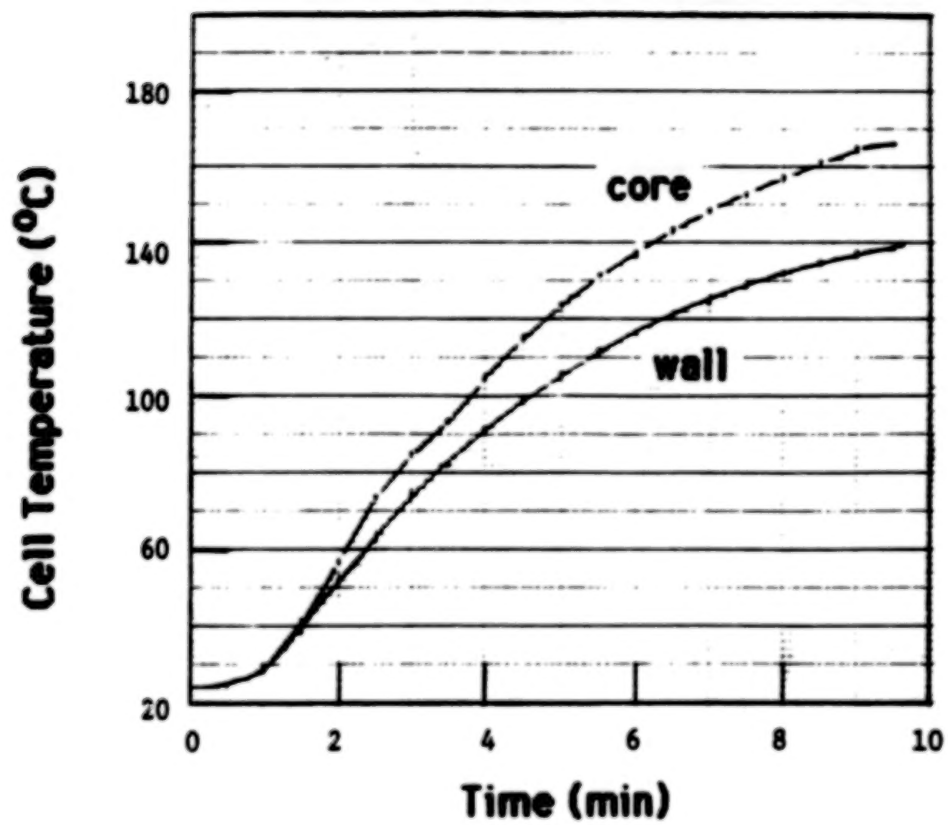


Figure 8. High discharge rate during external short circuit.

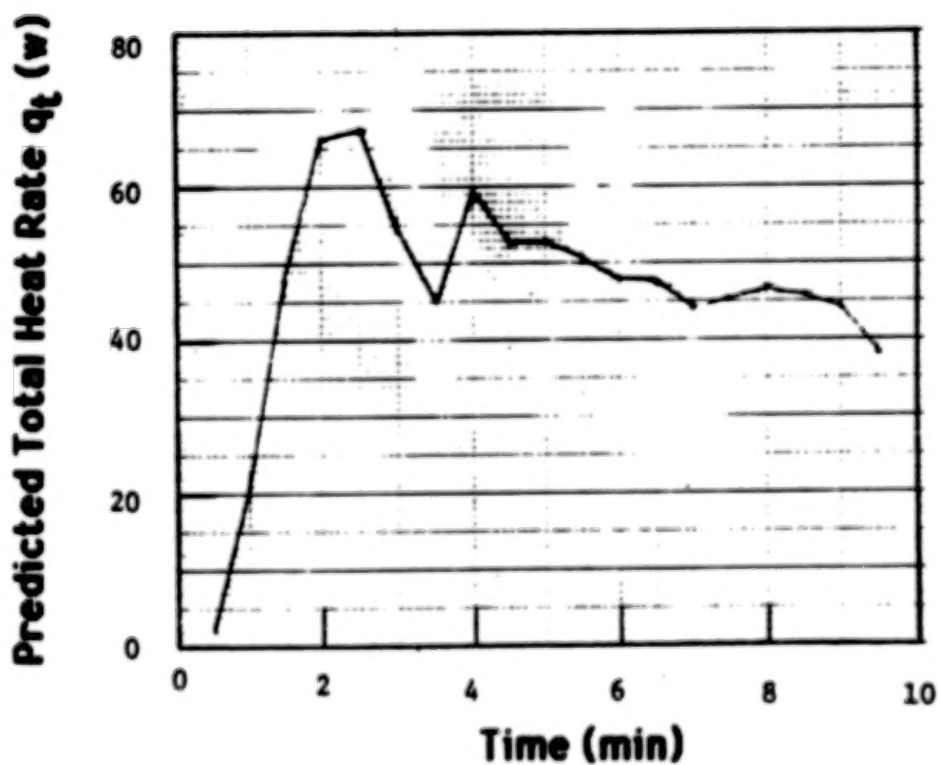
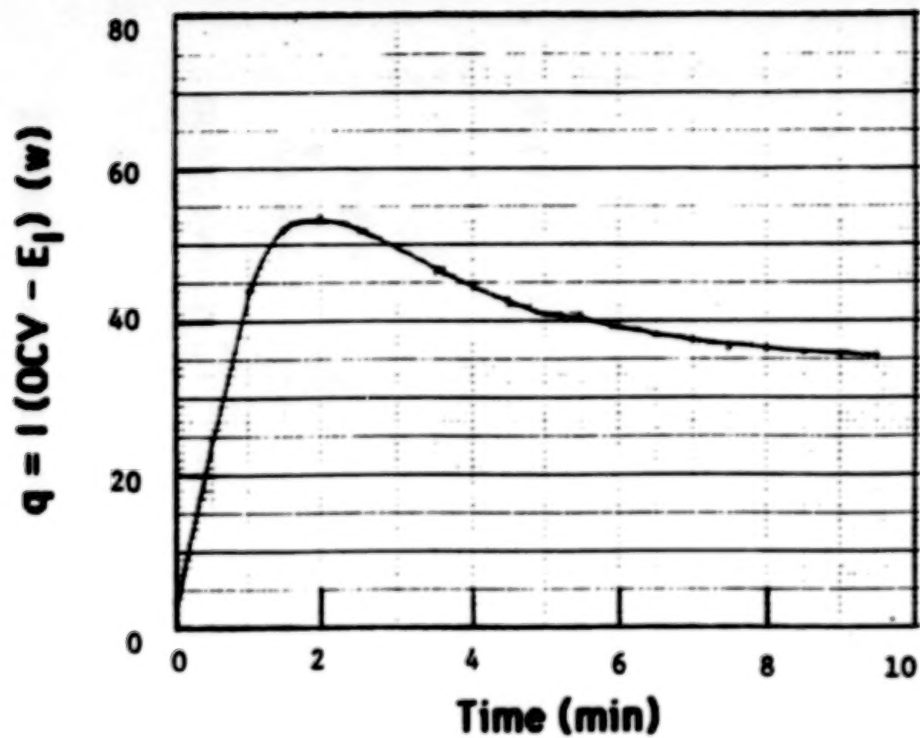


Figure 9. High discharge rate during external short circuit.

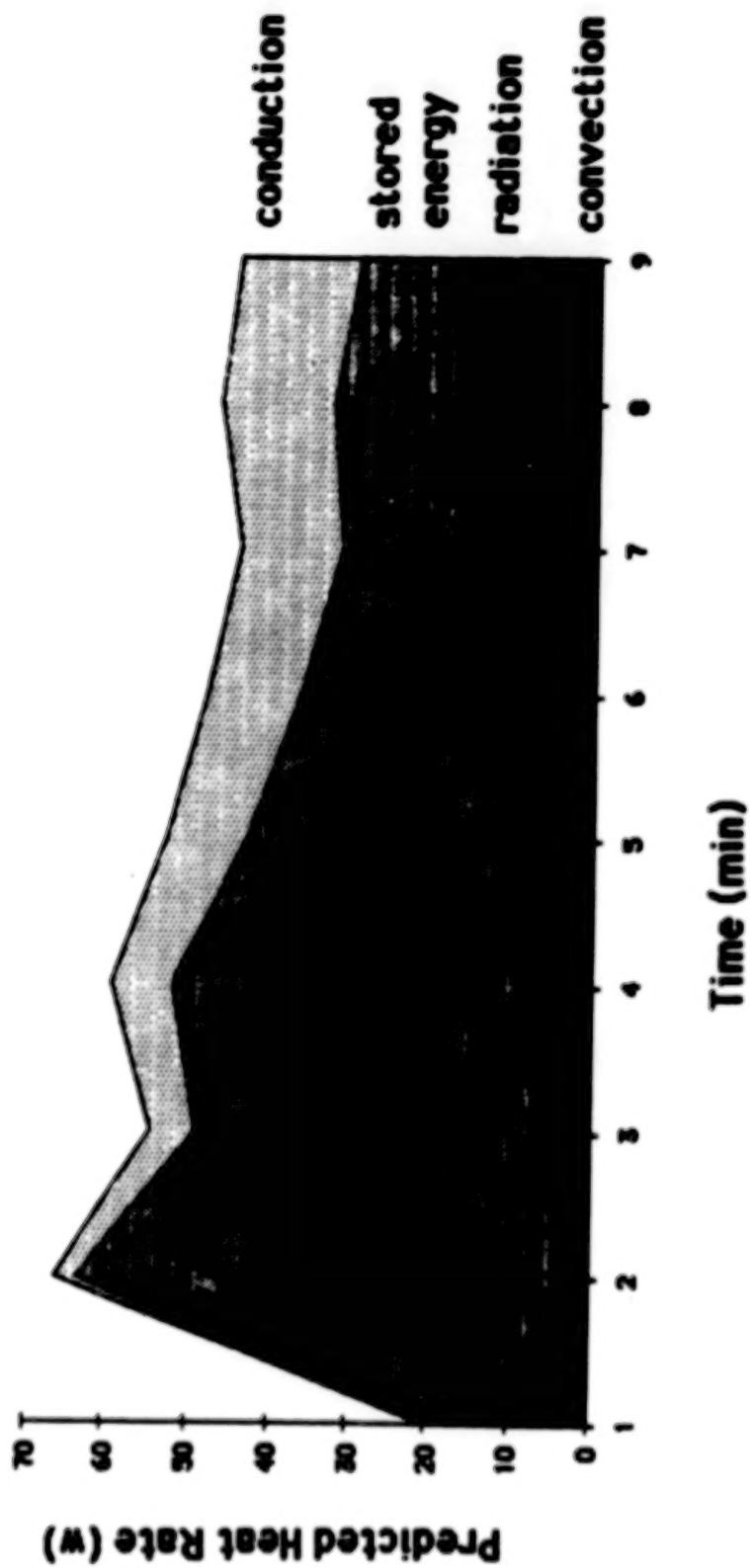


Figure 10. High discharge rate during external short circuit.

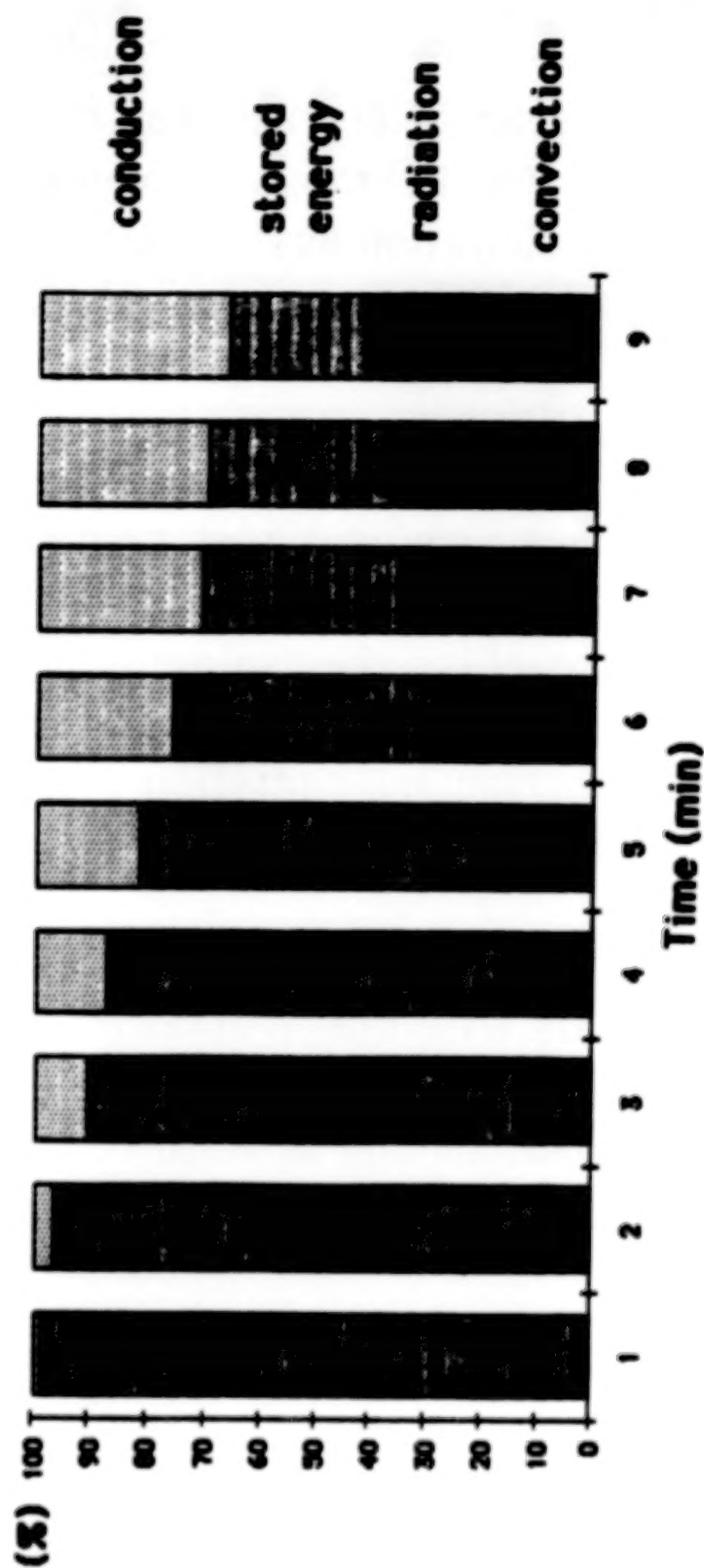


Figure 11. High discharge rate during external short circuit.

CONCLUSIONS

- o The total heat generation rate was calculated from a comprehensive thermal modeling work, including convection and radiation heat dissipation, sensible heat, heat conduction via internal thermal resistance network.**
- o Under normal discharge rate conditions, convection and radiation are dominant heat dissipation modes.**
- o However, approaching the explosion or for extremely high discharge rate cases such as external short circuits, convection and radiation dissipate less than 40% of the total heat produced.**
- o The present code is applicable for other primary cylindrical cells with minor modifications.**
- o The present methodology is valid for charging tests as well as rechargeable battery analyses.**

250AH/90A ACTIVE LITHIUM-THIONYL CHLORIDE CELL FOR CENTAUR-G APPLICATION

A. E. Zolla and D. D. Tura
Altus Corporation
San Jose, California 95112

ABSTRACT

A high rate active Li/SOCl₂ cell has been designed for use in a 28 volt, 250 amp-hour space battery system. The lithium battery is being considered as a replacement of its heavier silver-zinc counterpart on board the "Centaur-G" booster rocket which is used to launch payloads from the un-manned space vehicles.

Basically a feasibility study, this development effort is demonstrating the ability of the lithium cell to deliver up to 90 amps safely at power densities of approximately 25 watts per pound. Test data on 4 prototype units is showing an energy density of 85 watt-hours per pound and 9.0 watt-hr/in³. The cells tested demonstrated 280 to 300 amp-hours under ambient temperature test conditions using alternating continuous loads of 90, 55 and 20 amperes throughout life.

The cell is hermetically sealed in a welded stainless steel envelope of 103 in³ volume and weighs 10.9 lbs. The cell's internal impedance is a low 3.5 milliohms achieved by means of close electrode spacing, a low resistance internal bussing structure and large 3/8 inch diameter nickel pin terminals.

Data from four cells tested are presented to demonstrate the capability of Li/SOCl₂ technology for a C/3 discharge rate in active and hermetic cell units.

A simple thermal model was developed, which predicts the heat transfer characteristics and cell temperatures as a function of time and current.

DESIGN

Four cells were constructed and tested individually during this development effort. They were designed to provide slightly over 250 ampere-hours to achieve the capacity required and to have reserve capacity to guard against possible over-discharge (reverse voltage) of a cell in a multiple series circuit.

A cylindrical case configuration was chosen due to its inherent strength and ease of manufacture. The case is 4.50" O.D. and 5.06" tall. Internal to this stainless steel case, a pile construction of multiple anodes and cathodes with non-conductive but porous separator material was selected. The current collectors within these electrodes have tabs which protrude from the pile with a 120° dispersion angle between anode and cathode tabs. These anode and cathode tabs are separately brought together and welded for the electrical parallel connection to the respective electrode terminals.

8001-224

The anode disc is 4.0 inches in diameter and 0.007 inches thick. Two such discs of lithium sandwich the nickel current collector plate. Each bi-anode assembly has correspondingly 162 cm² of active surface area and a theoretical capacity of 5.94 AH.

The cathode is of similar diameter to the anode and contains 1.24 g of carbon in each disc. Two such cathodes, separated by a nickel current collector plate, form the bi-cathode assembly. Each cathode assembly supports 5.2 AH of cell reaction and therefore limits the cell's capacity delivery.

The overall cell contains a substantial excess of electrolyte which is accessible to the cathode and separators by capillary attraction.

Two minor variations of the basic design were built and tested. The first two cells (S/N 001 and 002) consisted of 57 bi-electrode pairs. The second two cells (S/N 003 and 004) were constructed with 54 bi-electrode pairs within the same cell envelope. At the 90A peak current the two designs operated at 9.7 and 10.3 mA/cm² respectively.

The latter cell design variation is preferred from the standpoint of ease of manufacture and the resultant capacity and performance still meet technical objectives.

Special emphasis was placed on the internal bussing design of the cell. It was recognized that at the intended high rates, the internal resistance must be minimal to avoid excessive internal heating, loss of voltage and internal pressure build-up. The cell was therefore designed with the largest nickel conductor cross-sectional area possible within the constraints of space available and manufacturability.

The measured voltage drop at 90 amperes across this internal bussing system is 58 millivolts, indicating 0.64 milli-ohms resistance per terminal. The sum of the two terminal assemblies is therefore 1.3 milliohms for the nickel conductors. Resistance contributions from electrochemical components raise the cell's total internal impedance to about 3.5 milliohms; an acceptable level for 90A delivery.

The bulkiness of the bussing system necessitated large terminal boxes to be located around the bussing terminations (at 120° locations around the cell). The large size allowed easier and more expedient manufacturing and assembly of the cells. These terminal housings are completely filled with electrolyte and are reservoirs for the substantial excess over the capacity requirement.

The 3/8" diameter nickel - teflon feed-thru terminals were designed specially for this cell. These were thoroughly tested for hermeticity and reproducibility in manufacture. Special care was taken in the design of welding joints in the cell case to locate the welding zones away from internal lithium. This was accomplished by "dishing" the lids on the case so that the welds are low heat butt-welds located more than 1/4" away from the internal stack. Similarly, the terminal boxes are welded to interface plates which extend from the main cell 1/2" away from lithium. In addition, a full set of heat sinks were developed to maintain the cell at low temperature during welding operations.

TESTING

The cells were equipped with pressure transducers and were further prepared for testing by attaching 7 thermocouples, and lead wires. The power leads were attached to the 3/8" nickel terminals using a clamp-connector attached to welding cable. The transducer, thermocouples, electrode potential leads and power leads were remotely connected to test instrumentation. The instrumentation sampled data every minute and a strip chart recorder continuously tracked data throughout the test. A computer was used to compile the data into tabular and graphical formats. Figure numbers 1, 2, 3 and 4 present the data graphically for serial numbers 001, 002, 003 and 004, respectively.

A summary of the test conditions for the 4 cells follows:

S/N 001 - This cell was tested on a 4.0" diameter copper block which was located on a large slab of steel. The copper block was interfaced to the cell with a layer of thermal grease. The cell was discharged 4 times with a 60 minute 90-55-20 amp constant current discharge profile (20 minutes at each level). The cell was then discharged to 2 volts at 20 amps. After a weekend at open circuit, the cell was depleted of energy on a 0.1 ohm resistor.

S/N 002 - This cell was tested on a piece of wood to create a less thermally advantageous situation than in the previous test. Also loaded 4 times with a 90-55-20 amp discharge profile, this cell was then discharged to 2 volts at 20 amps. Subsequently the cell was depleted of its energy on a 1 ohm resistor.

S/N 003 - Since this cell contains 5% less anodes and cathodes than the previous 2 cells, it operates at a slightly higher current density. This cell was, therefore, tested at conditions identical to those for S/N 002 in order to assess the differences in operation due to this current density change. The cell was tested on a wooden block with the same current profile to 2 volts as in S/N 002. On this cell, however, the 20 amp constant current discharge was continued past the 2 volt cutoff, through 0 volts into reverse voltage (about -0.1 volts) for a further 330 AH.

S/N 004 - Since the ultimate application for the cell is in space (vacuum environment), it was decided to test this cell in a near adiabatic condition to determine its behavior under this extreme situation. Both conduction and convection were precluded as far as possible with the exception of negligible conduction down the power leads. The cell was tightly wrapped in foam and placed in a covered styrofoam box tightly packed with styrofoam packing material to minimize heat loss. The cell was discharged at the same 90-55-20 amp constant current profile as its predecessors. After the third profile, however, it was determined that the cell temperature and pressure were high enough, (as expected) to abandon the fourth profile and the remainder of the test was conducted at 20 amps constant current. The cell was finally depleted of its energy on a 1 ohm resistor.

DATA SUMMARY

Table 1 includes the major data points necessary to summarize the performance of the cells. Table 2 contains detailed data on average voltages of the cells.

CELLS S/N 001 AND S/N 002 - Delivered 301 and 294 amp-hours (to 2.5 volts), respectively; well above the 250 AH goal. The energy of both cells, 973 and 956 WH were also very close. Both cells remained at very moderate temperatures and pressures throughout their respective test cycles. S/N 001 rose to a maximum case temperature of 48.9°C and a maximum pressure of 27 psig. S/N 002 achieved 58.1°C and a maximum pressure of 37 psig. The lower values for S/N 001 are clearly due to the fact that heat was conducted from the base of the cell whereas for S/N 002 it was precluded. These cells operated at 9.7 mA/cm² on the 90 amp current discharges and they both delivered high energy densities (to 2.5 volts) of about 90 watt-hours per pound.

CELLS S/N 003 AND 004 - Delivered predictably lower capacities than their predecessors due to the 5.3% reduction in carbon cathode weight. A capacity of 281.8 AH is mathematically projected and S/N 003 delivered this capacity.

Cell S/N 003 attained a pressure of only 28 psi during discharge - a very pleasing result. This cell was allowed to enter forced discharge (reverse voltage) at 20 amps, for 16+ hours after discharge was complete, in order to access the safety characteristics in this abusive condition. The cell case maintained its structural integrity and hermeticity throughout the entire reverse voltage period.

Because S/N 004, in its near adiabatic condition, operated at a much higher average temperature than S/N 003, it manifested a significantly higher average voltage.

Cell S/N 004 reached a temperature and pressure maximum of 105.1°C and 172 psig respectively during its last few minutes of constant current discharge, due to its near adiabatic state. Again, the cell maintained its structural integrity and hermeticity through-out the entire test.

The design of cells S/N 003 and 004 was validated by the test results and the resultant 85 watt-hours/ pound after 90A (at 10.3 mA/cm²) delivery exceeds the technical objectives.

THERMAL MODEL

In order to develop a grasp of the thermal operating characteristics of the cells prior to actual testing, a thermal model was developed. The model is based on a simple energy balance where the cell is assumed to be a homogenous thermal mass. The calculated heat capacity of a typical cell is 0.223 cal/g/°C. The predicted average temperature profile is determined by calculating the accumulated energy in the cell as a function of time and dividing by heat capacity and weight. Three paths for heat transfer were identified for the cells - conduction to the surface on which the cell rested, convection to air, and conduction of heat out of the cell through the nickel terminals. Heat transfer coefficients were determined for these paths, and used to formulate an overall heat transfer coefficient for the planned test conditions. The cell model is represented by Figure 5.

The integral of the three thermal transfer modes were calculated to be 1.19, 0.84, 0.84 and 0.09 watts/°C above ambient for cells tested as S/N 1, S/N 2, S/N 3 and S/N 4 respectively.

The results of solving the heat balance for each cell indicated that we could expect moderate cell temperatures for cell tests 1-3. As seen in Table #1, these predictions were quite accurate. The prediction for test number 4, the near adiabatic test, indicated a high temperature of 93.4°C at the termination of testing. Based on this information, a successful test in the adiabatic environment was predicted. As seen in Table #1, the original model is marginally less accurate at high temperatures. The original thermal model was helpful in planning the testing for this development effort. Recent refinement of the thermal model considered accelerated self discharge at elevated temperatures and this new model is useful in the design of the full 28V battery. The model credibly predicts the battery temperature and operating voltage under the various scenarios for solar and earth flux radiation and operating current.

CONCLUSION

This work has demonstrated a safe and efficient lithium thionyl chloride cell design for high capacity (250 AH) with high rate performance (C/3). The cell can deliver a sustained 1 hour at 90A and full 250 AH capacity delivery within an adiabatic environment.

The demonstrated energy density of 85 WH/LB can readily be raised to 115 WH/LB using a less conservative steel case design which is still competent for predicted internal pressures.

The developed thermal model predicts a full 9-cell battery operating safely in a space environment with the factor of two weight reduction over a silver-zinc system for un-manned space vehicle power.

This work suggests that the present high rate Li-SOCl₂ technology is ready for full system hardware development and subsequent analysis through testing.

ACKNOWLEDGEMENT

The authors express their appreciation to Ron Mikkelsen of General Dynamics - Convair Space Systems Division whose interest and support has made this work possible.

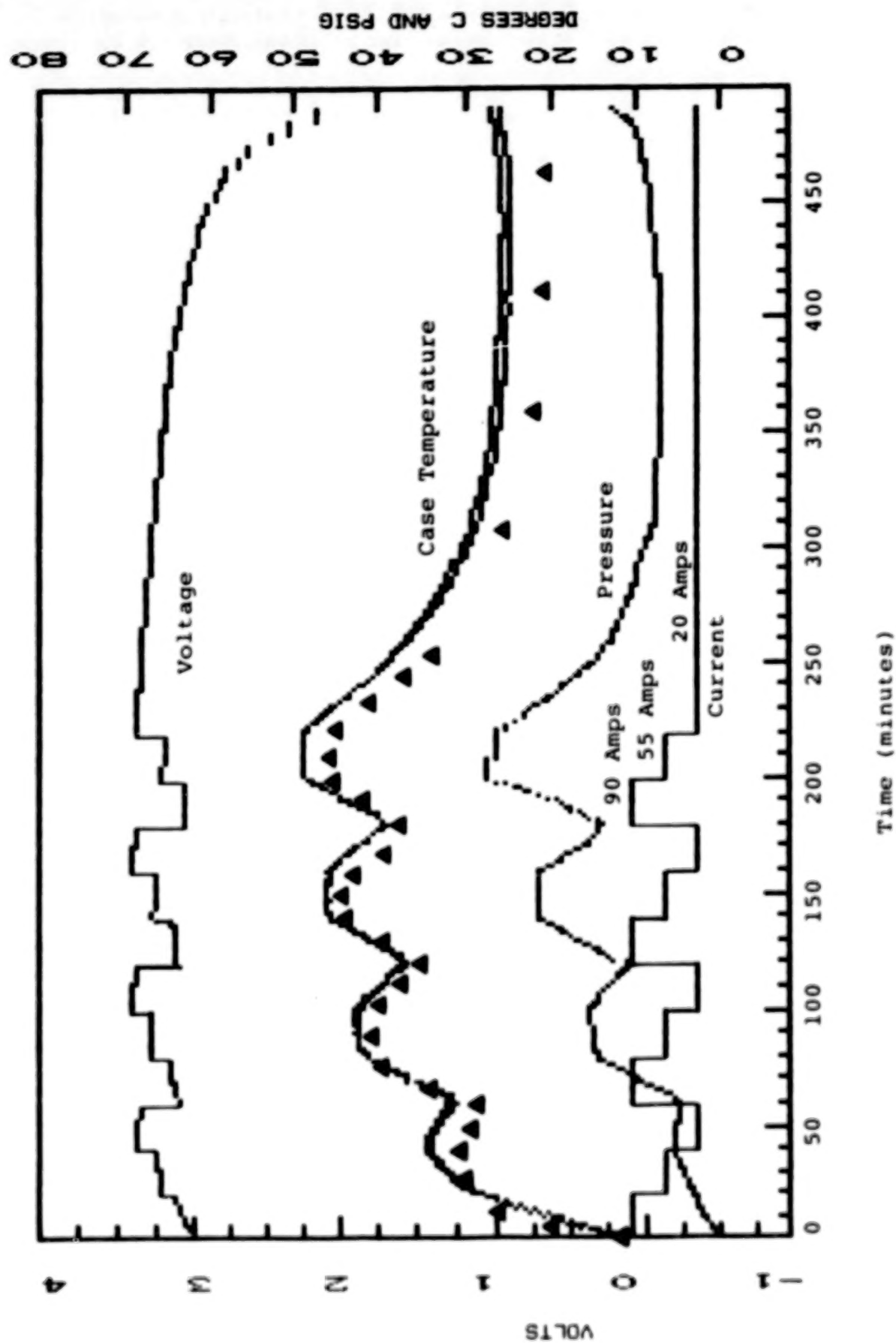
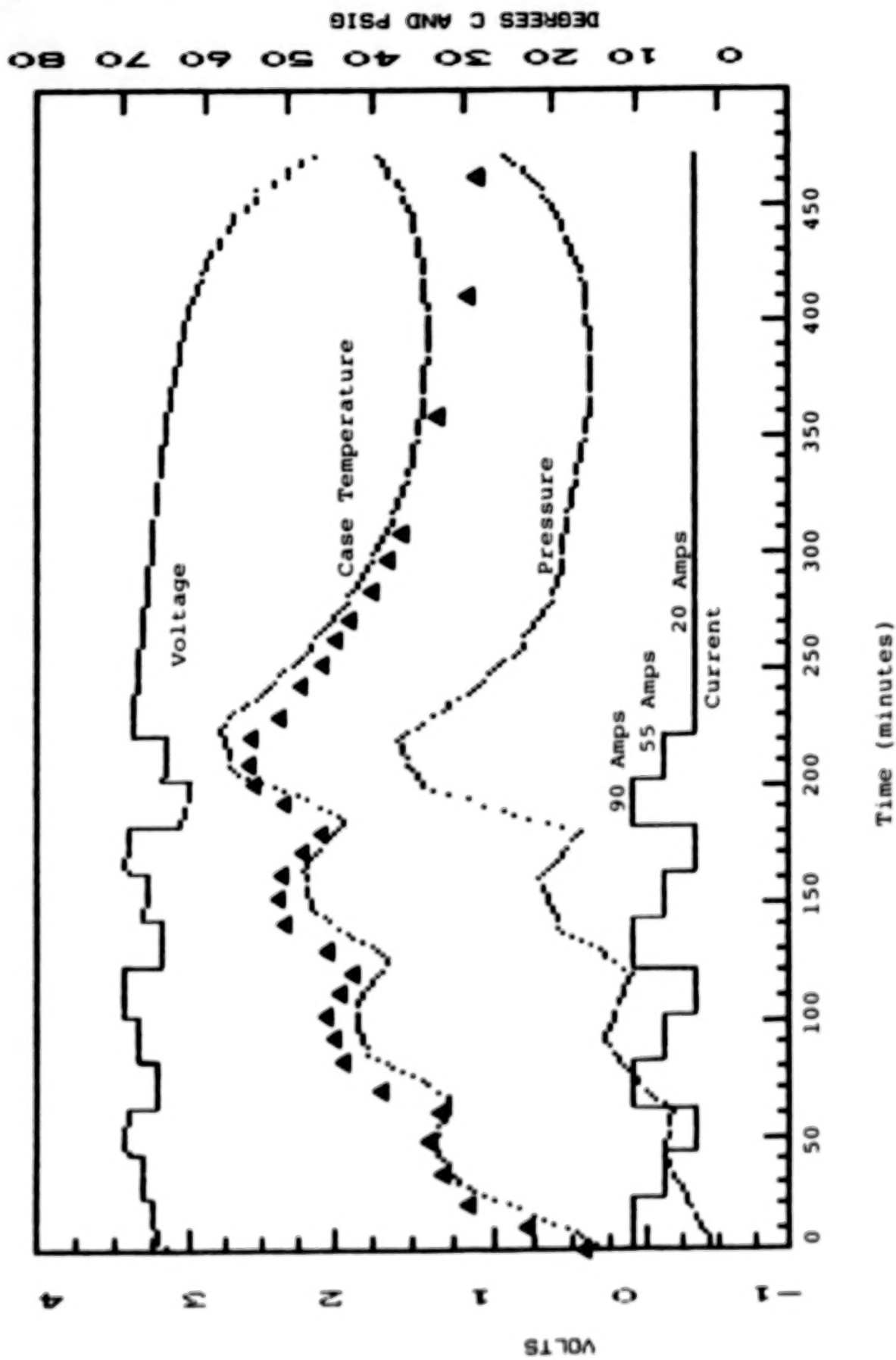
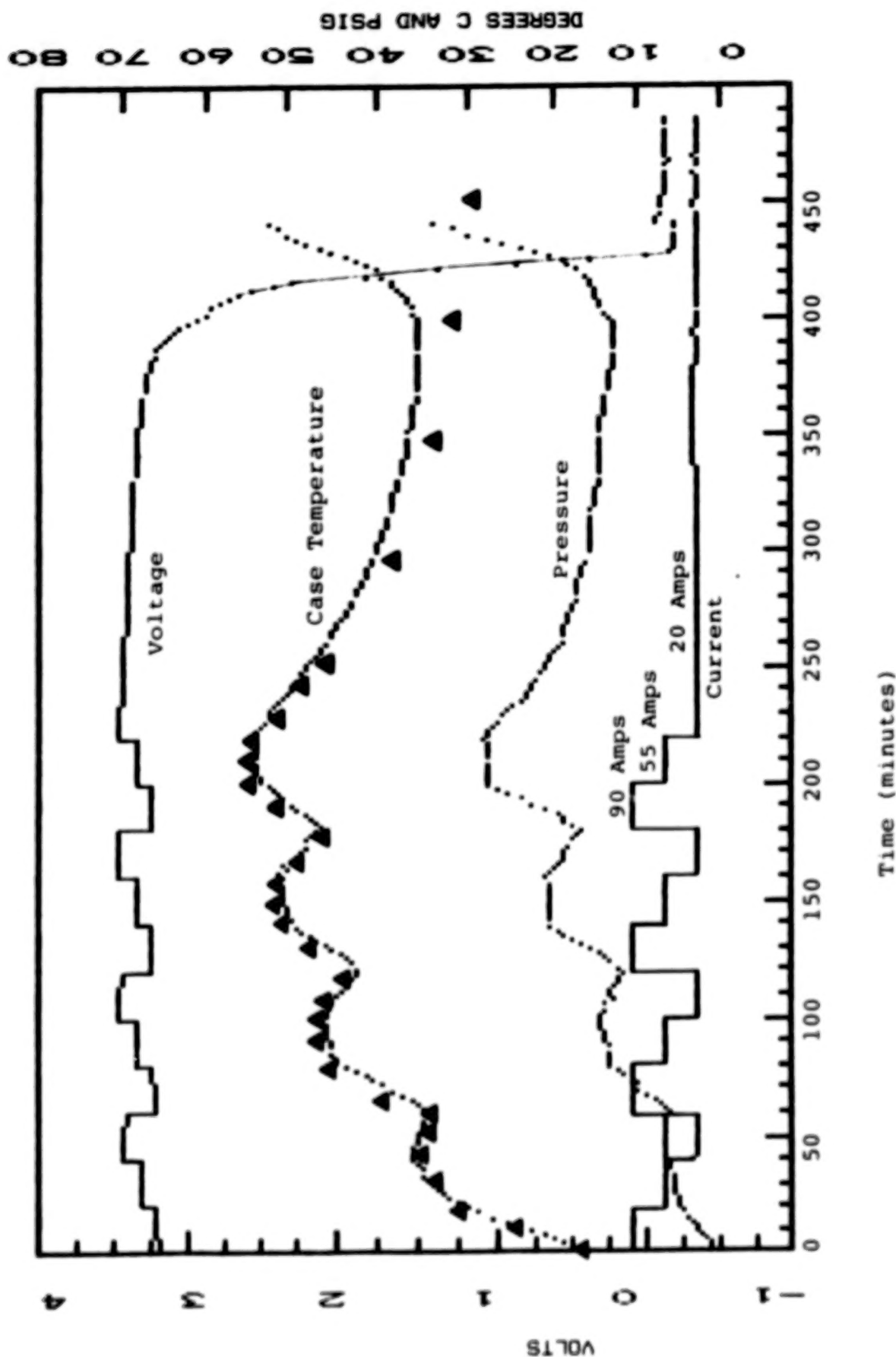


Figure 1. 250 AHr Cell (S/N 001).



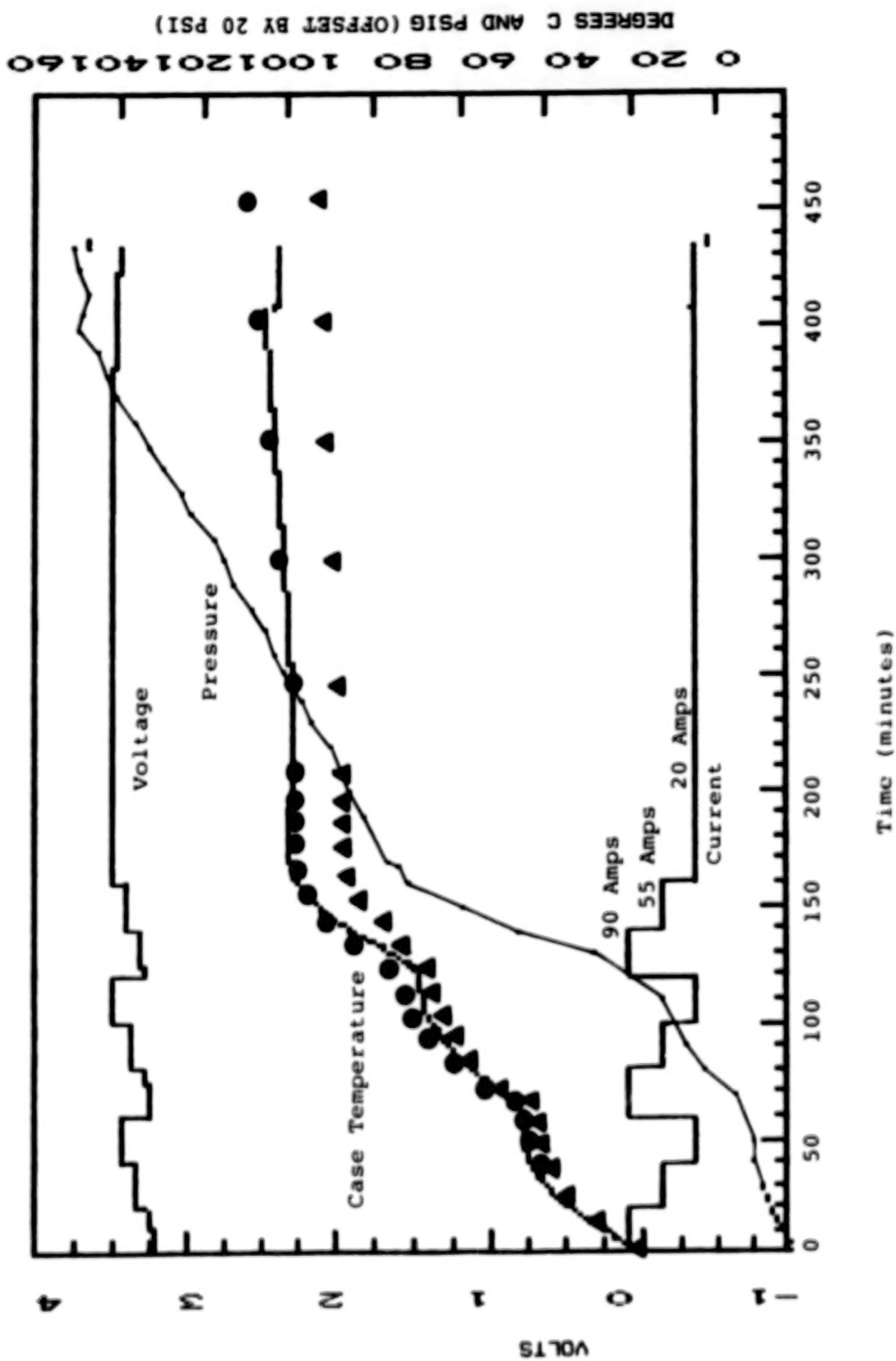
▲ Simple Thermal Model

Figure 2. 250 Ahr Cell (S/N 002).



▲ Simple Thermal Model

Figure 3. 250 AHR Cell (S/N 003).



▲ Simple Thermal Model

● Improved Thermal Model

Figure 4. 250 Ahr Cell (S/N 004).

DEGREES C AND PSIG (OFFSET BY 20 PSI)

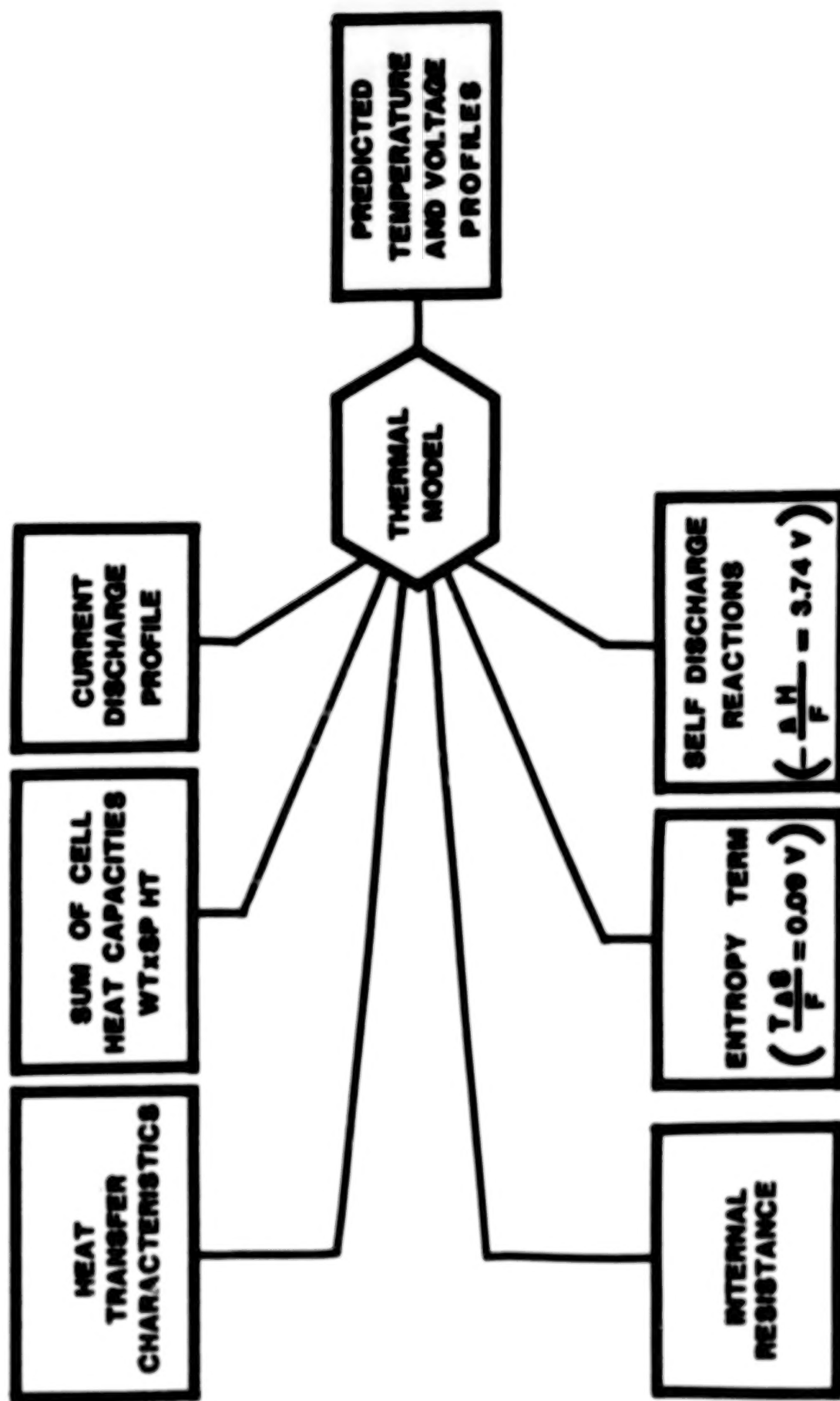


Figure 5. Thermal Model Inputs and Outputs.

Table 1.

DATA SUMMARY				
<u>SERIAL NO.</u>	<u>001</u>	<u>002</u>	<u>003</u>	<u>004</u>
CAPACITY TO 2.5 VOLTS (AHRS)	301	294	282	260
ENERGY TO 2.5 V (WHRS)	973	956	950	899
CELL WEIGHT (GRAMS)	4892	4972	4914	4969
ENERGY DENSITY TO 2.5 (WHR/LB)	90	87	88	82
INTERNAL RESIST. (M OHM)	4.6	3.7	3.3	3.2
NO. OF BI-ELECTRODE PAIRS	57	57	54	54
CASE TEMPERATURE (°C)				
LOW	11.6	15.3	16.8	19.0
AVERAGE	33.3	39.5	41.4	83.5
HIGH	48.9	58.1	53.9	105.1
PREDICTED HIGH TEMP.	45.5	54.4	54.5	93.4
PRESSURE DATA (PSIG)				
LOW	0.0	0.0	0.0	0.0
AVERAGE	11.1	17.0	14.9	92.8
HIGH	27.0	37.0	28.0	172.0

Table 2.

VOLTAGE DATA SUMMARY									
PULSE #	CURRENT (AMPS)		CELL S/N						
			1	2	3	4			
1	90	55	20	3.11	3.28	3.41	3.28	3.37	3.47
2	90	55	20	3.19	3.32	3.44	3.27	3.38	3.49
3	90	55	20	3.18	3.30	3.44	3.24	3.33	3.46
4	90	55	20	3.11	3.25	3.42	3.06	3.21	3.42
AVERAGE VOLTAGES FOR 4 PULSES									
	@ 90A			3.15			3.21		
	@ 55A			3.29			3.32		
	@ 20A			3.43			3.46		
							3.28	3.39	3.50
							3.31	3.42	3.53

**THE MOLICEL® RECHARGEABLE LITHIUM SYSTEM:
MULTICELL BATTERY ASPECTS**

D. Fouchard and J.B. Taylor

**Moli Energy Limited
3958 Myrtle Street
Burnaby, B.C. V5C 4G2**

ABSTRACT

MOLICEL® rechargeable lithium cells have been cycled in batteries using series, parallel and series/parallel connections. The individual cell voltages and branch currents were measured to understand the cell interactions. The observations have been interpreted in terms of the inherent characteristics of the Li/MoS₂ system and in terms of a singular cell failure mode. The results confirm that correctly configured multicell batteries using MOLICELs have performance characteristics comparable to those of single cells.

INTRODUCTION

The MOLICEL is based on the rechargeable couple lithium/molybdenum disulfide. It is characterized by having high rate capability, high energy density and good cycle life. The battery requirements of a large number of applications can be met by using arrays of small cells with capacities from 0.6 to 2.5 Ah. Such applications include lap computers, portable communications, consumer electronics and cameras.

The technology is by no means confined to the scale typified by these examples. Larger cells of 45 Ah have been built using an upscaling of the basic MOLICEL design. Table I gives some specifications for a number of MOLICELs.

As will be seen, there are design trade-offs in the technology. For example, capacity can be increased during manufacture at the expense of cycle life. Furthermore, the user has many options to optimize the matching of performance characteristics and demand requirements. Most of the applications mentioned have cycle life requirements ranging from 100 to 400 cycles. However, an intentional derating of the capacity by using shallow discharge can extend the cycle life to 3000 cycles.

All data given have been for single cells. The work reported here was undertaken to find out how MOLICELs performed in series connected and in series/parallel connected battery packs. In this regard, the MOLICEL system has a number of characteristics which set it apart from nickel-cadmium and lead-acid systems. Cell interactions within batteries of MOLICELs are significantly influenced by the following inherent characteristics of the Li/MoS₂ system:

- sloping voltage
- near 100% current efficiency
- large "reserve" capacity
- near perfect capacity balance.

The sloping voltage arises from the fact that the chemical potential of the cathode material varies with its state of charge. This does not occur with conventional cells which use displacement reactions. When MOLICELs are connected in parallel, the change of chemical potential with state of charge introduces a negative feedback phenomenon which tends to cancel any system imbalance. This effect works on both charge and discharge. Obviously with series connected cells, balance cannot be maintained by such a feedback mechanism.

The MOLICEL has no charge limiting mechanism comparable to the water electrolysis of a lead-acid cell or the oxygen shuttle reaction of nickel-cadmium cells. For this reason, the MOLICEL has 100% current efficiency and low heat output. There is however no mechanism for rebalancing cells within a battery pack.

A large reserve of capacity exists in MOLICELs and only a fraction of the total energy in the active materials is utilized during the standard cycling. The bulk of the normally non-utilized energy is only available below 1 volt. This ensures that a low capacity cell cycling in a series connected battery will not be driven immediately into voltage reversal on discharge.

Finally, the capacity balance of fresh MOLICEL is extremely good. This is achieved by an electrical preconditioning step at the factory which fixes the amount of active cathode material based entirely on the highly controllable parameters of current and time. As an example, in a typical sample production run, the initial capacities were found to be 0.805 Ah with a standard deviation of .017 Ah. After 100 cycles (C/10 charge, C/5 discharge, 2.4 to 1.1 V) the capacities were .639 Ah \pm .010 Ah.

From the foregoing, it would be expected that the cycling behaviour of MOLICEL multicell batteries would show certain unique characteristics. The initial capacity balance is expected to be excellent. The

maintenance of this balance depends on individual cell capacity fade rates. The effect of the inevitable imbalance on the battery performance is somewhat difficult to predict. A series of experiments was therefore undertaken to investigate the situation.

EXPERIMENTAL

Three types of experiments were carried out:

- single cell simulation of battery pack effects (fixed capacity cycling)
- cycle testing of standard, balanced battery packs
- cycle testing of deliberately imbalanced packs.

Batteries were assembled as simply as possible using shrinkable adhesive tape and spot welded nickel tabs. Cycling was carried out at constant current in gravity convection ovens. A multichannel data acquisition system recorded cell voltages and currents.

Two classes of AA size (0.6 Ah) cells were used for these tests. The first were standard MOLICELs having passed all quality control checks. The second were rejects which had failed quality control as a result of having low capacity or exhibiting a self-discharge. The test conditions for the latter were a maximum open circuit voltage loss of .062% per day over 42 days. The capacity criteria are defined earlier.

Fixed Capacity Cycling

This provides a convenient method of studying cell behaviour under conditions closely approximating those of a series connected battery pack (all applications currently envisioned will have series connected cells). Charge and discharge cut-off points in series arrays are determined by the overall voltage. Individual cells will cycle over ideal limits only if the pack remains perfectly balanced. A cell with lower capacity than the others will cycle over voltage limits which are less than ideal.

Such a 'bad' cell will simply cycle over a capacity which will be dictated by the operating capacity of the 'good' cells. Thus, cycling of a single cell under fixed capacity conditions can be used to simulate the battery environment. Tests were done at 21°C and 55°C with C/10 charge and C/3 discharge. Even reject cells could achieve more than 100 cycles when the nominal 0.6 Ah capacity was used. However, at 0.9 Ah cycling, failure occurred after less than 30 cycles.

In all cases the failure mode was the same. As can be seen from Figure 1 (for a low capacity cell) and Figure 2 (for a self-discharging cell) the voltage range over which the cells cycled increased until, at the point of failure, the lower limit reached zero volts. At this point the cells developed a permanent internal short circuit. This failure mode is totally benign and has obvious advantages insofar as the performance of series connected cells is concerned.

Cycling of Standard Balanced Batteries

Batteries were cycled using groups of 8, 12 and 16 cells drawn from standard production runs after qualification procedures. The batteries were configured as shown in Figure 3. Results are presented in Table II. The data confirm the excellent performance of MOLICELs in multicell batteries. The capacities and cycle lives of batteries up to 16 cells are very similar to these of individual cells under similar test conditions. This is true even at 60°C which is above the recommended operating limit of 55°C. The capacity imbalance is initially less than 2%. After the battery cycling at 21°C, the imbalance generally rose to about 3%. At 60°C an imbalance up to 20% was found after more than 100 cycles.

Cycling of Imbalanced Batteries

Current quality control procedures at Moli Energy reject all low capacity cells. There is however, a small but finite possibility that a self-discharging cell might not be detected and would in fact reach the customer. The imbalanced batteries were therefore tested using one deliberately planted cell which was a self-discharging, Q.C. reject.

Batteries of 4 and 8 cells were configured as shown in Figure 4.

Cycling was conducted at 55°C to accelerate the degradation process.

Type I

The individual cell voltages at the start of cycling are shown in Figure 5. The battery was initially well balanced except for the planted cell (cell 4) which cycled at lower voltage than the others. The cycle life performance of this battery was greatly degraded by the presence of the self-discharging cell. The capacity declined by 50% after only 80 cycles whereas a standard battery under similar test conditions would achieve 150 cycles. Figure 6 shows that the capacity decline is associated not only with the planted cell, but also with

another cell. The planted cell subsequently cycled at ever lower voltage and in fact was below 0.1 volts at end of discharge when the test was terminated because of almost zero pack capacity. It can be seen in Figure 6 that the second cell was also failing to recharge completely. It also cycled over a low voltage range. It is coincidental that a second cell in the pack behaved in this way although the observation does reinforce earlier statements made about the singular failure mode of MOLICELs.

Type II

Figure 7 shows a typical early cycle for this battery. It can be seen that the planted cell (cell 4) carried high currents at the end of recharge and correspondingly bore a disproportionate share of the current at the end of discharge. An internal dendrite short would be expected to produce such behaviour. At cycle 39 the battery was placed on open circuit standby. Figure 8 shows the loop current which ran for about 10 hours until the voltage had equilibrated at about 1.75 V. This is to be expected for an imbalanced parallel connected battery. All the cells are of course at the same voltage during charge. They are not however, at the same equilibrium voltage due to differing impedances and hence differing overvoltages.

The ultimate demise of this pack is shown in Figure 9. About half way through the recharge, the planted cell took the full 240 mA charge current. After going onto open circuit the battery equilibrated to 1.7 V showing that the cell did not have a "hard short". No safety hazards were associated with this failure mode.

Type III

This battery exhibited good cycle life as shown in Figure 10. the originally balanced limb remained virtually unchanged. Currents were higher in this limb at the start of discharge and higher in the imbalanced limb at the end of recharge. This is consistent with all previous observations. This can be seen in Figure 11, where the currents are plotted for both limbs but, for simplicity, only the voltages for the imbalanced limb are shown. Sporadic soft shorting occurred in one cell (cell 3) but the event was transient and the user would be unaware of this either from the standpoint of battery performance or cycle life.

CONCLUSIONS

The operation of MOLICEL rechargeable lithium cells in batteries has been found to be very satisfactory in spite of the absence of charge limiting mechanisms. The initial very good capacity balance was retained over many cycles with the result that battery performance was indistinguishable from single cell performance under similar conditions. The only exception to this was associated with the rare and singular failure mode of MOLICELs which leads to a low impedance or "soft short". This resulted in a performance penalty but no safety hazard.

The presence of a low impedance failure mode is consistent with the major findings of this study which are:

- Best results will be obtained using series connections.
- Reliability will be increased by matching cell size to capacity requirements and avoiding parallel cell connections.
- Multicell arrays will perform best if series strings are made to meet voltage needs and then parallel connection of the strings are made to meet capacity needs. Avoidance of the latter parallel connections by choice of cell size will give performance and cost advantages.

ACKNOWLEDGEMENT

Some of the work reported here was supported by the Canadian Department of National Defense, Defense Research Establishment, Ottawa.

TABLE I - CELL CHARACTERISTICS

SIZE	AA		A	BC
MODEL	06A600	06B800	51B1050	40A45000
WEIGHT g	22	24	30	1250
OPERATING VOLTAGE	2.4 to 1.3 Volts			
NOMINAL CAPACITY	0.6 Ah	0.80 Ah	1.05 Ah	45 Ah
CYCLE LIFE (TO 80% CAP)	300+	100	100	300+
OPERATING TEMP	-30°C TO +55°C			
CHARGE RETENTION	90% After 1 year at 21°C			
CHARGE RATE	C/10			

TABLE II - CYCLING OF STANDARD BALANCED PACKS

CONFIGURATION	CYCLING CONDITIONS PER CELL				NO. OF CYCLES	CAPACITY REMAINING (% OF NOMINAL)	IMBALANCE * %
	Voltage Range	Charge/Disch. mA	Temp °C				
A	2.4/1.3	80	240	21	400 400	40 50	5.3 3.0
	2.4/1.3	80	240	21			
B	2.4/1.3	80	240	21	175 225	85 80	3.0 3.5
	2.4/1.3	80	240	21			
C	2.4/1.3	60	180	21	299 293	88 71	2.9 3.3
	2.4/1.3	60	180	21			
D	2.4/1.1	60	180	21	175 175	86 89	3.3 0.5
	2.4/1.1	60	180	21			
E	2.4/1.1	60	180	60	171 138	60 62	10 20
	2.4/1.1	60	180	60			

* EXPRESSED AS STANDARD DEVIATION AS % OF MEAN VOLTAGE MEASURED AT TERMINATION OF CYCLING.

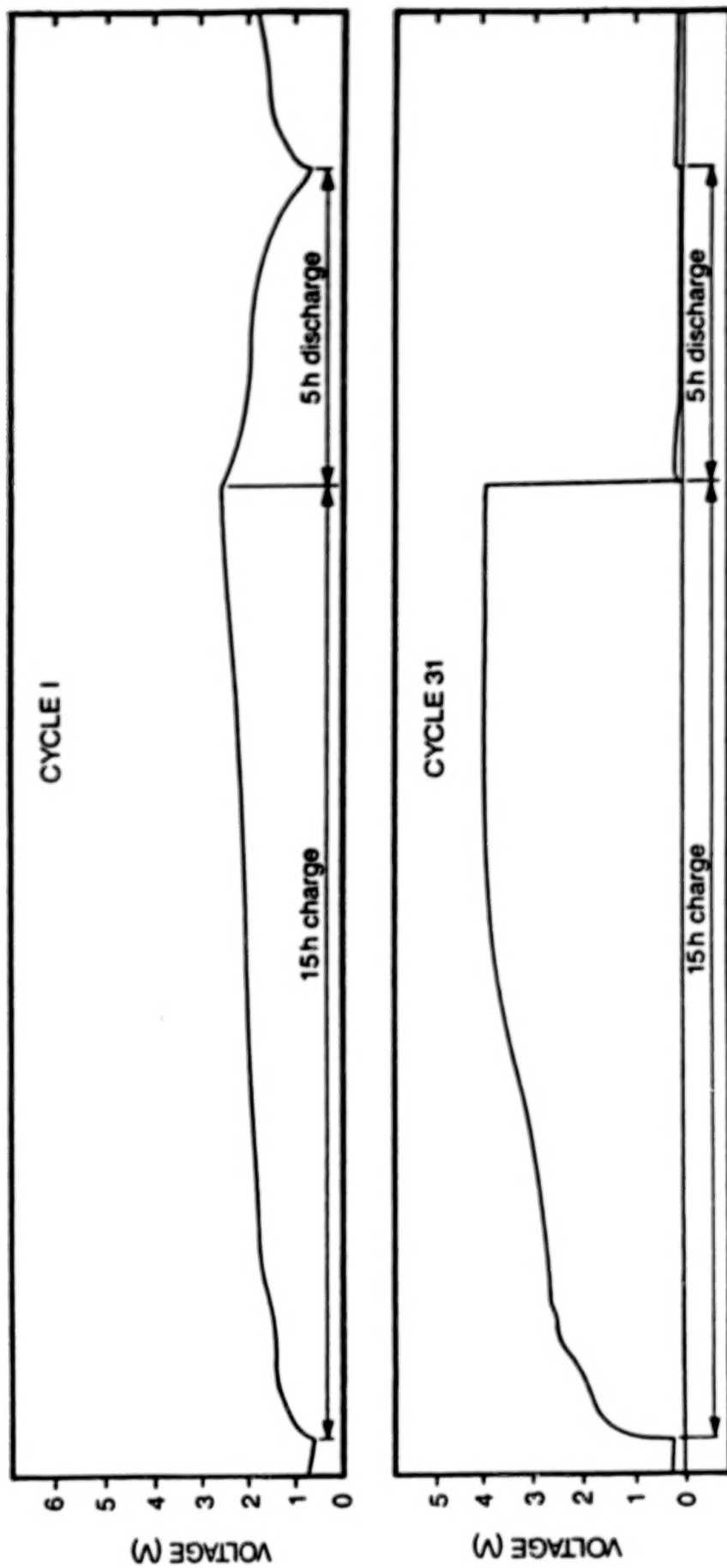


Figure 1. Fixed capacity cycling at 21°C of a MOLICEL AA cell (Q.C. reject because of low capacity). Charge current 60mA, discharge current 180 mA, fixed capacity = 0.9 Ah (150% of nominal).

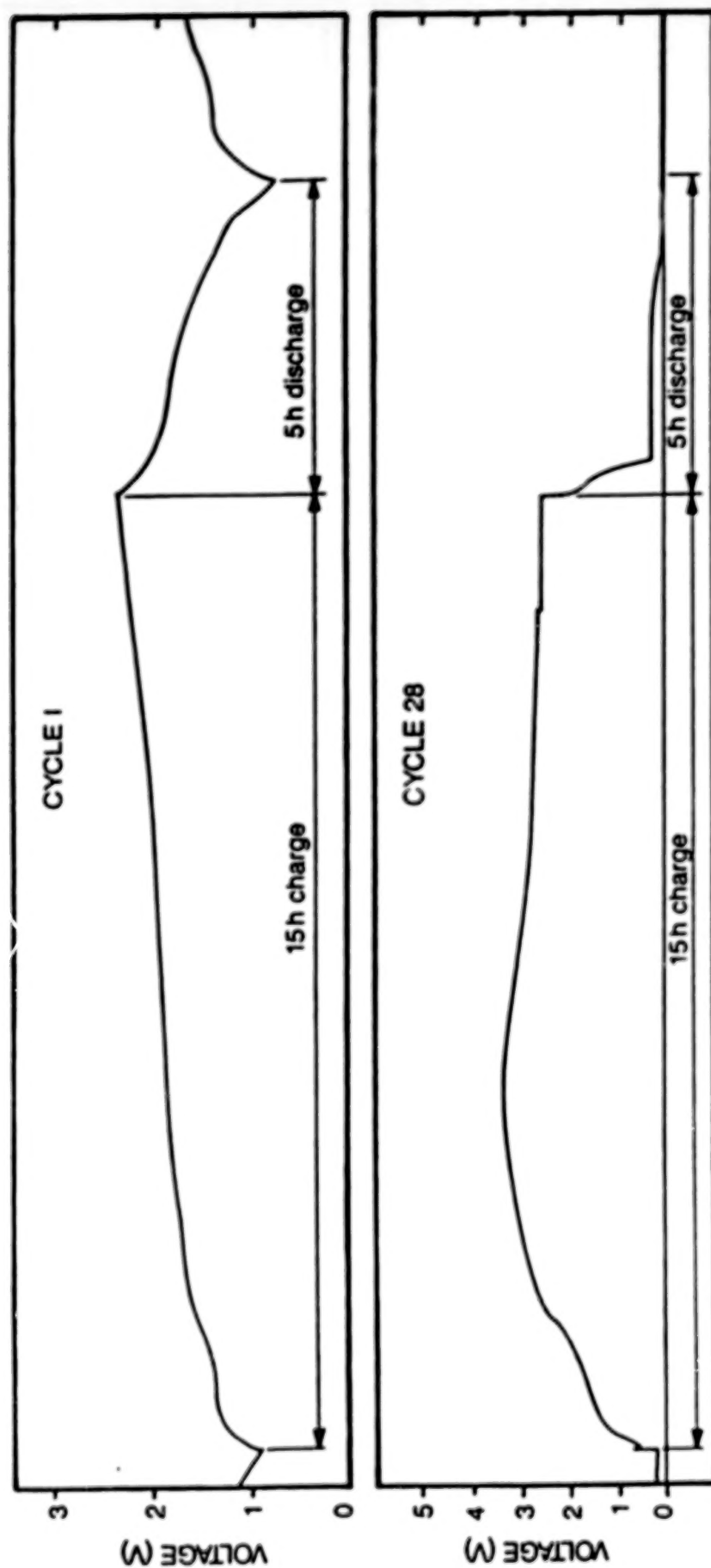


Figure 2. Fixed capacity cycling at 55°C of a MOLICEL AA cell (Q.C. reject because of self-discharge). Charge current 60 mA, discharge current 180 mA, fixed capacity = 0.9 Ah (150% of nominal).

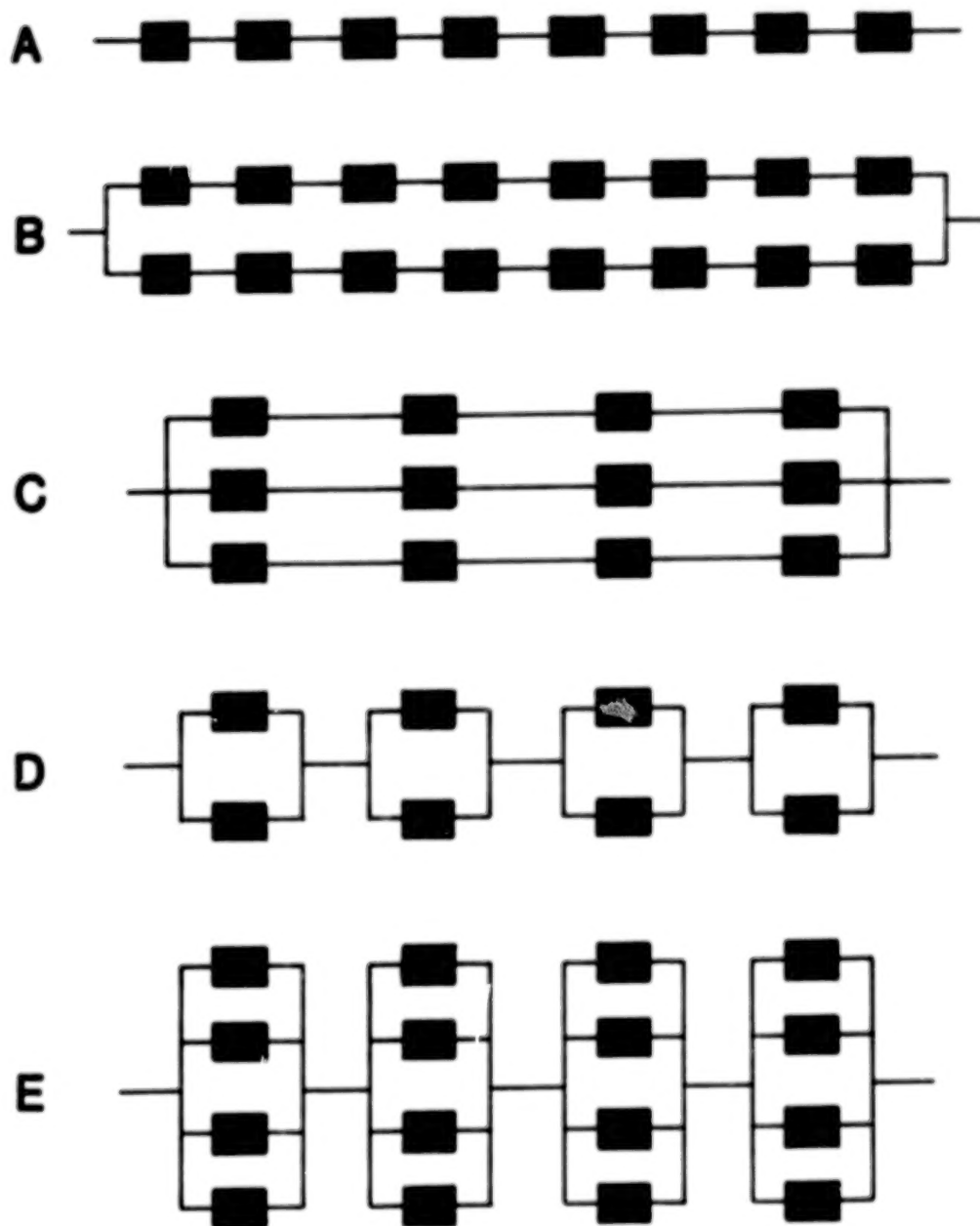


Figure 3. Battery configurations of 8, 12 and 16 cells.

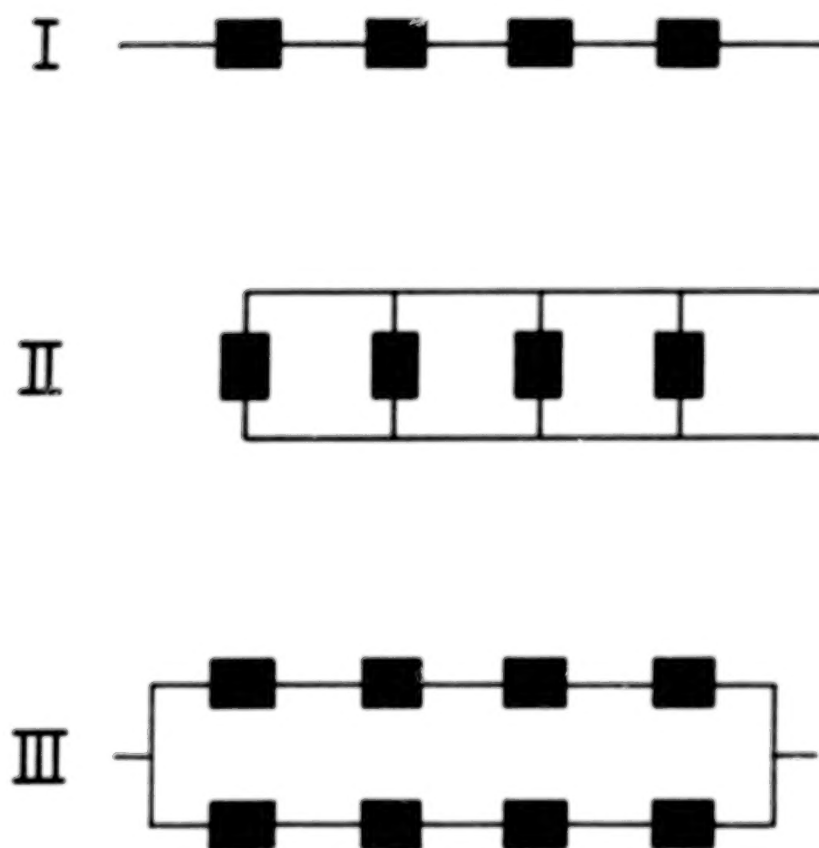


Figure 4. Battery configurations of 4 and 8 cells.

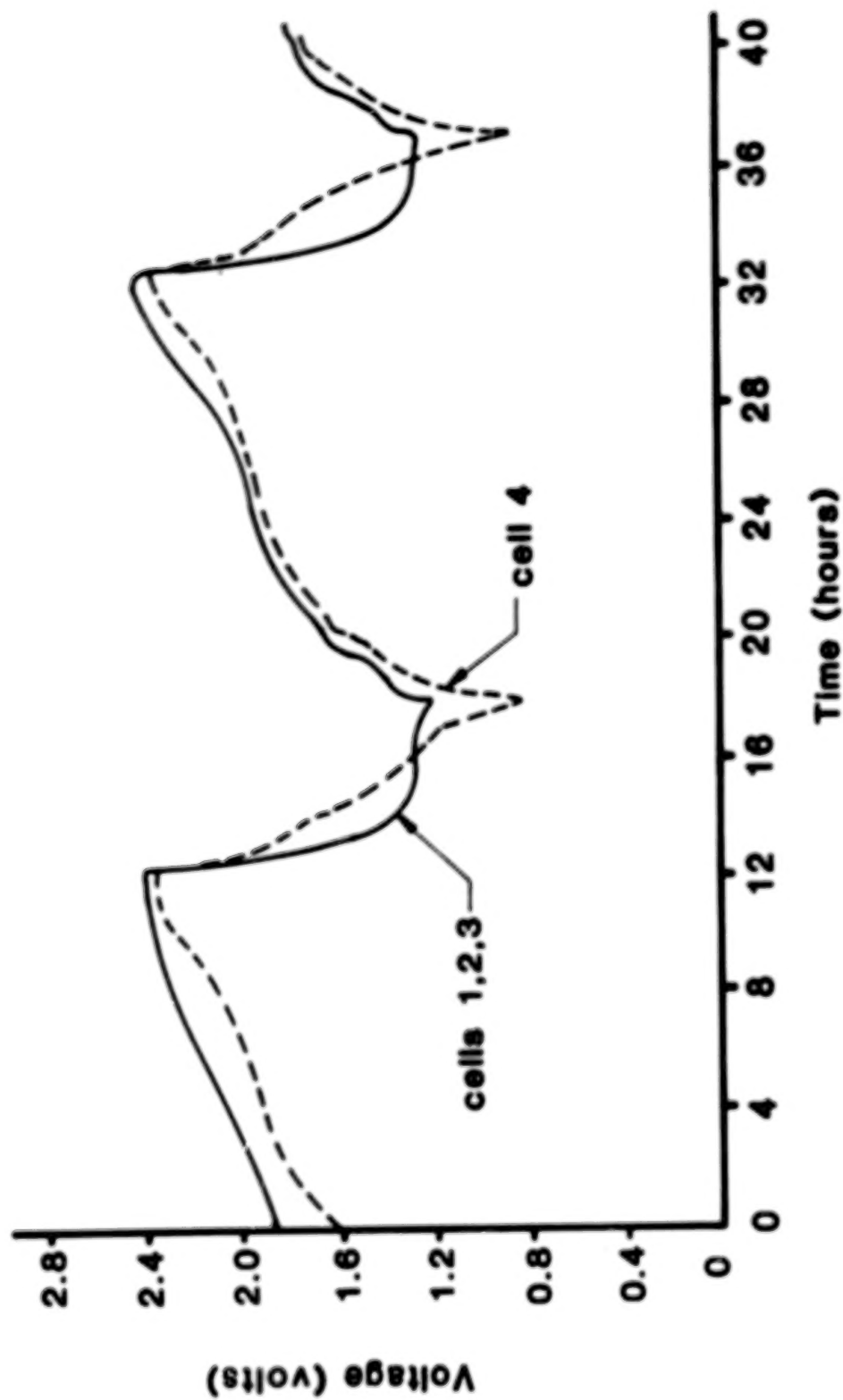


Figure 5. Individual cell voltage profiles for an imbalanced 4 cell series connected battery cycling at 55°C. Charge current 60 mA, discharge current 180 mA, limits 9.6/4.4 V. Cycles 1 and 2 shown.

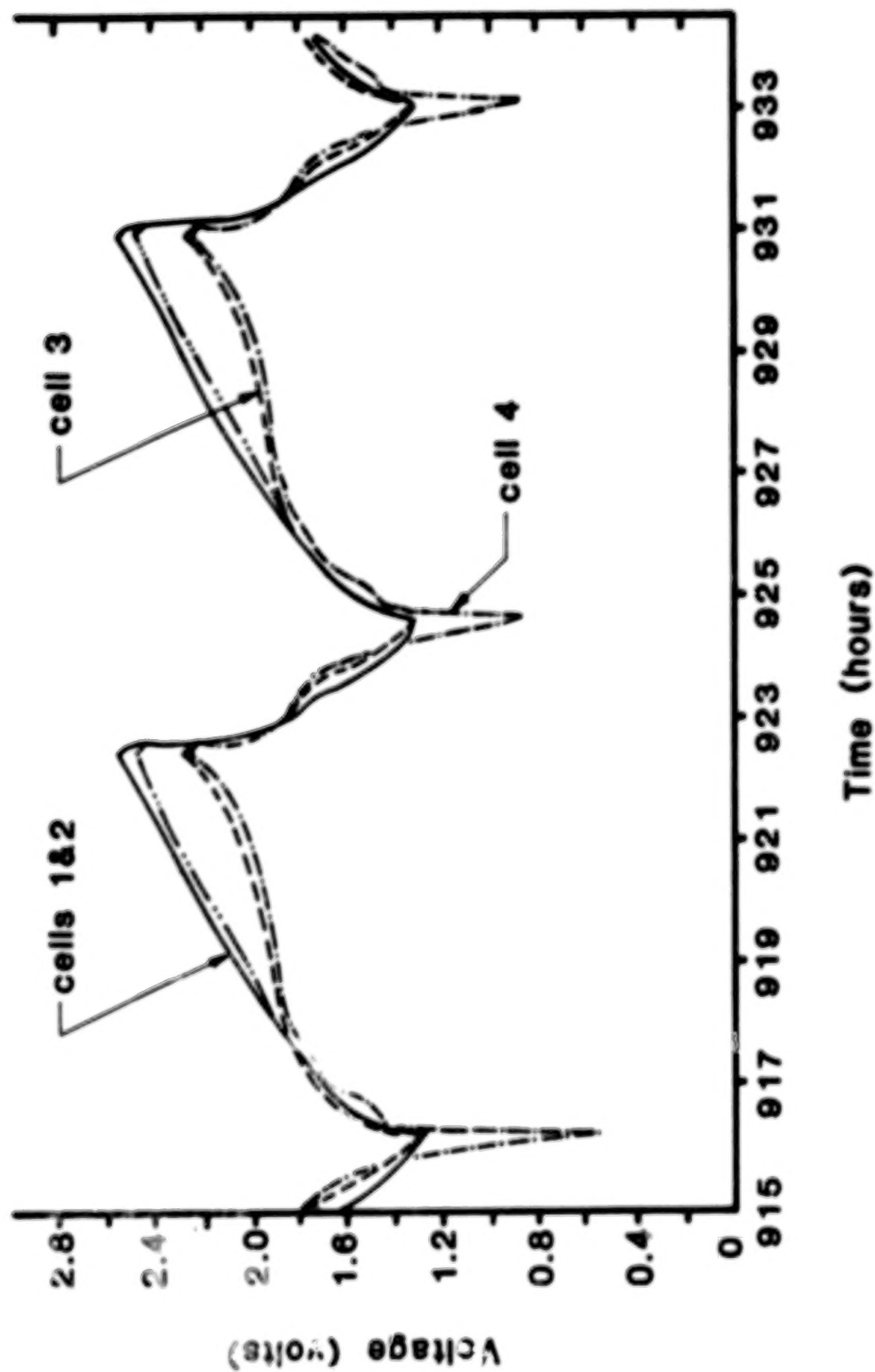


Figure 6. Individual cell voltage profiles for an imbalanced 4 cell series connected battery cycling at 55°C. Charge current 60 mA, discharge current 180 mA, limits 9.6/4.4 V. Cycles 39 and 40 shown.

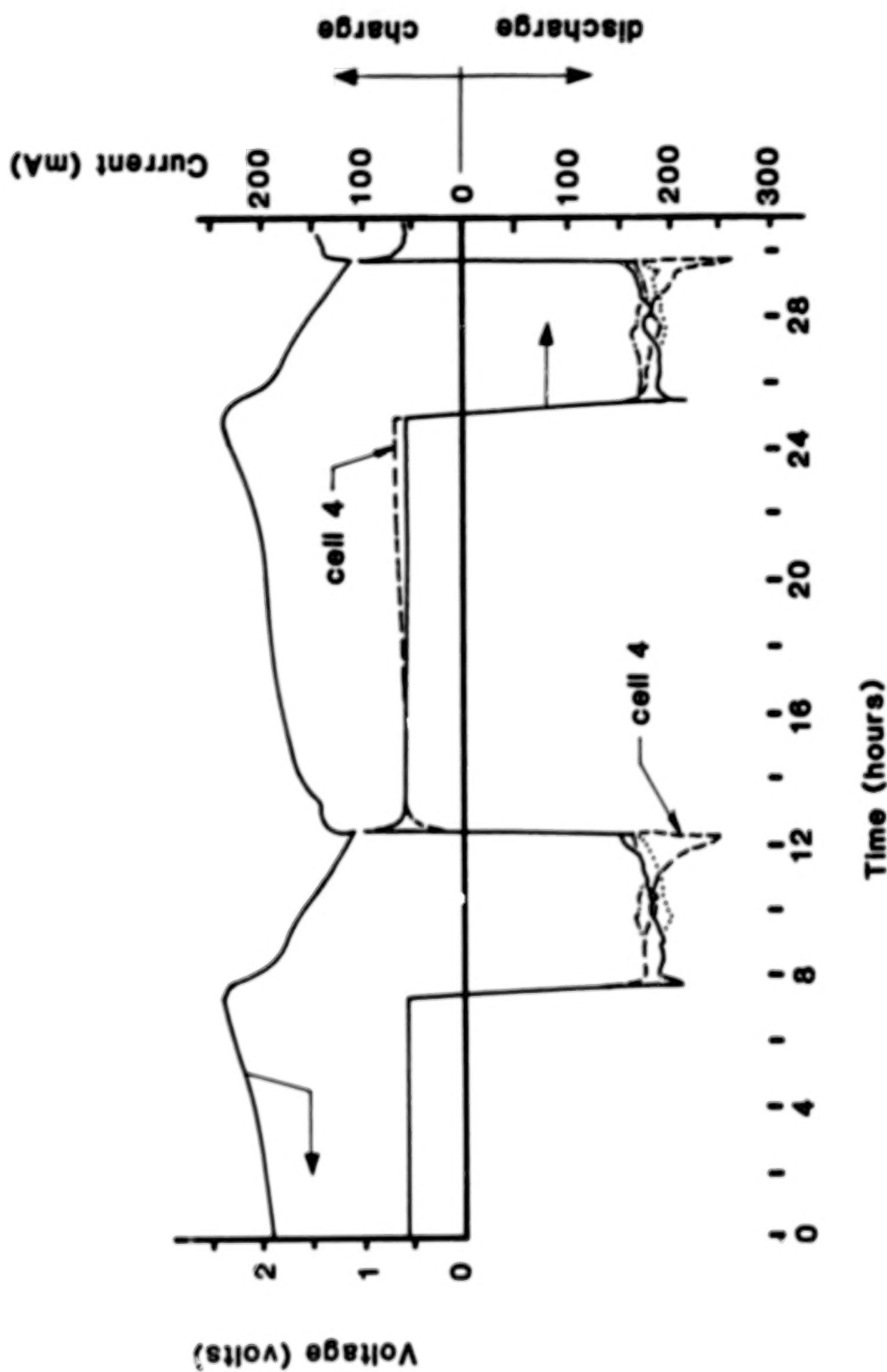


Figure 7. Individual cell current profiles and battery voltage for a 4 cell, imbalanced, parallel connected battery cycling at 55°C. 240 mA charge to 2.4 V, 720 mA discharge to 1.1 V. Cycles 1 to 2 shown.

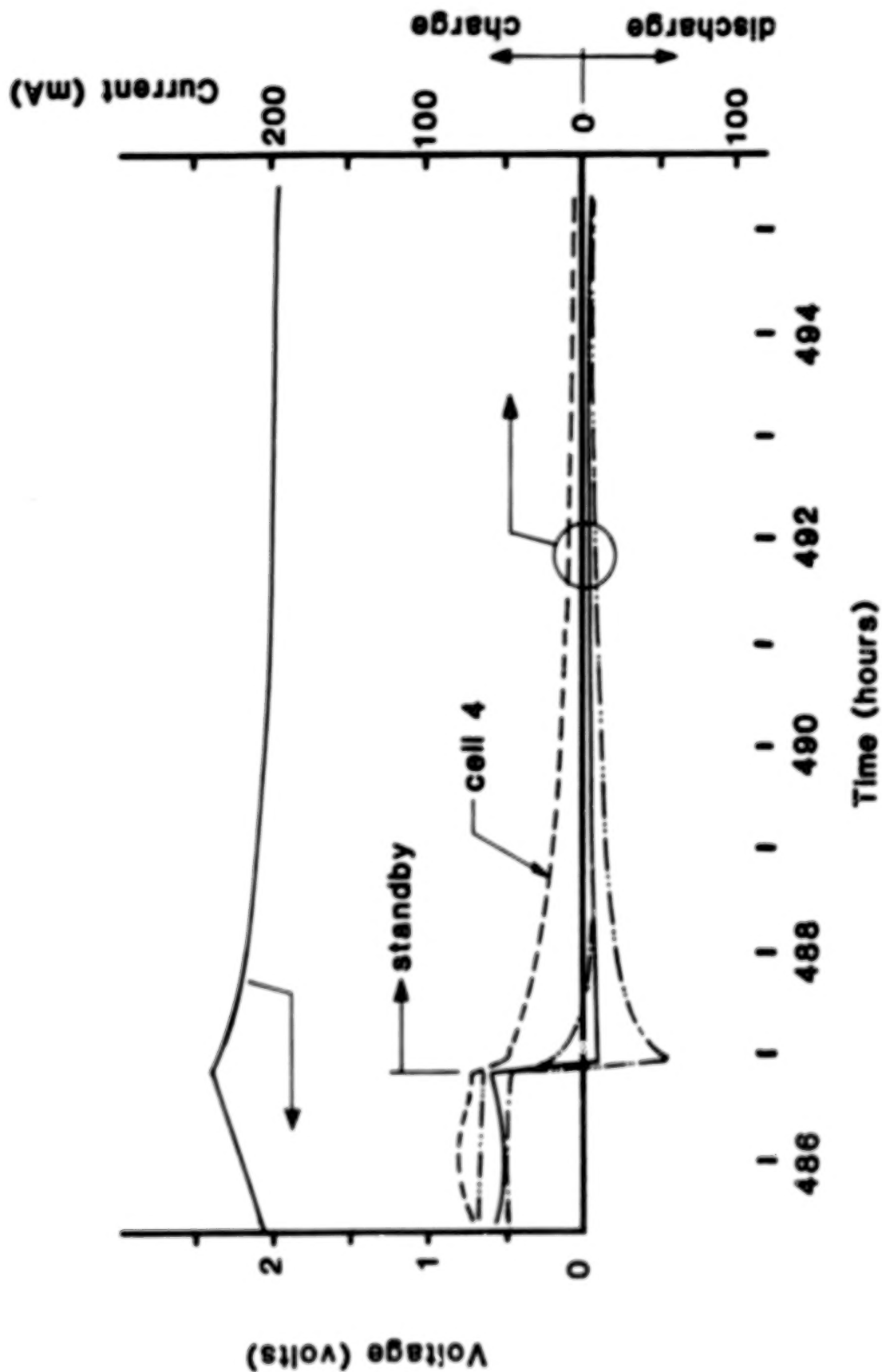


Figure 8. Individual cell current profiles and battery voltage for a 4 cell, imbalanced, parallel connected battery cycling at 55°C. 240 mA charge to 2.4 V, 720 mA discharge to 1.1 V. Cycle 39 and subsequent open circuit standby shown.

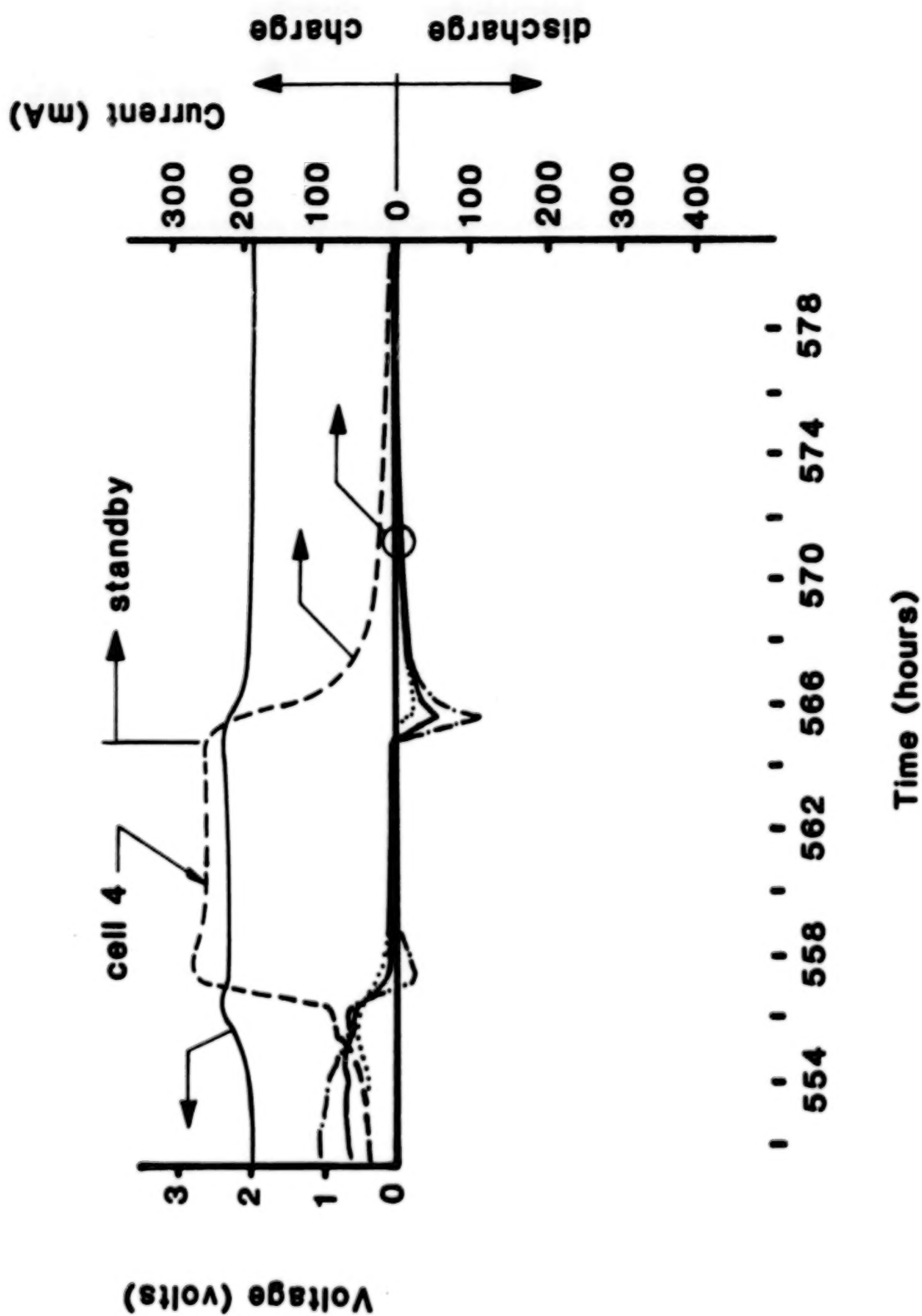


Figure 9. Individual cell current profiles and battery voltage for a 4 cell, imbalanced, parallel connected battery cycling at 55°C. 240 mA charge to 2.4 V, 720 mA discharge to 1.1 V. Cycle 45 and subsequent open circuit standby shown.

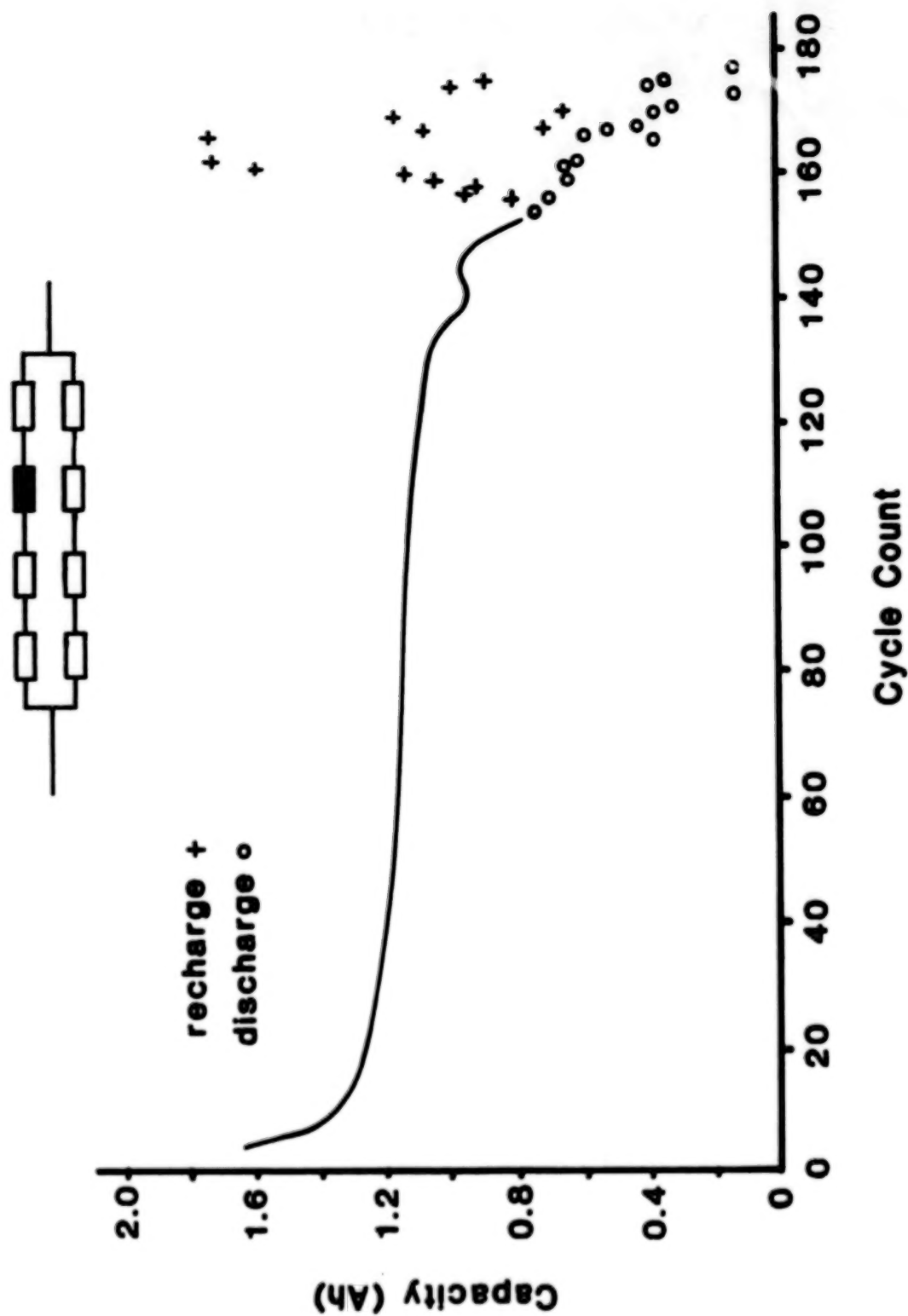


Figure 10. Cycle life plot of an imbalanced 8 cell series/parallel battery cycling at 55°C. Configuration as illustrated (self-discharging cell shown shaded). Charge current 120 mA, discharge current 360 mA, limits 9.6/4.4 V.

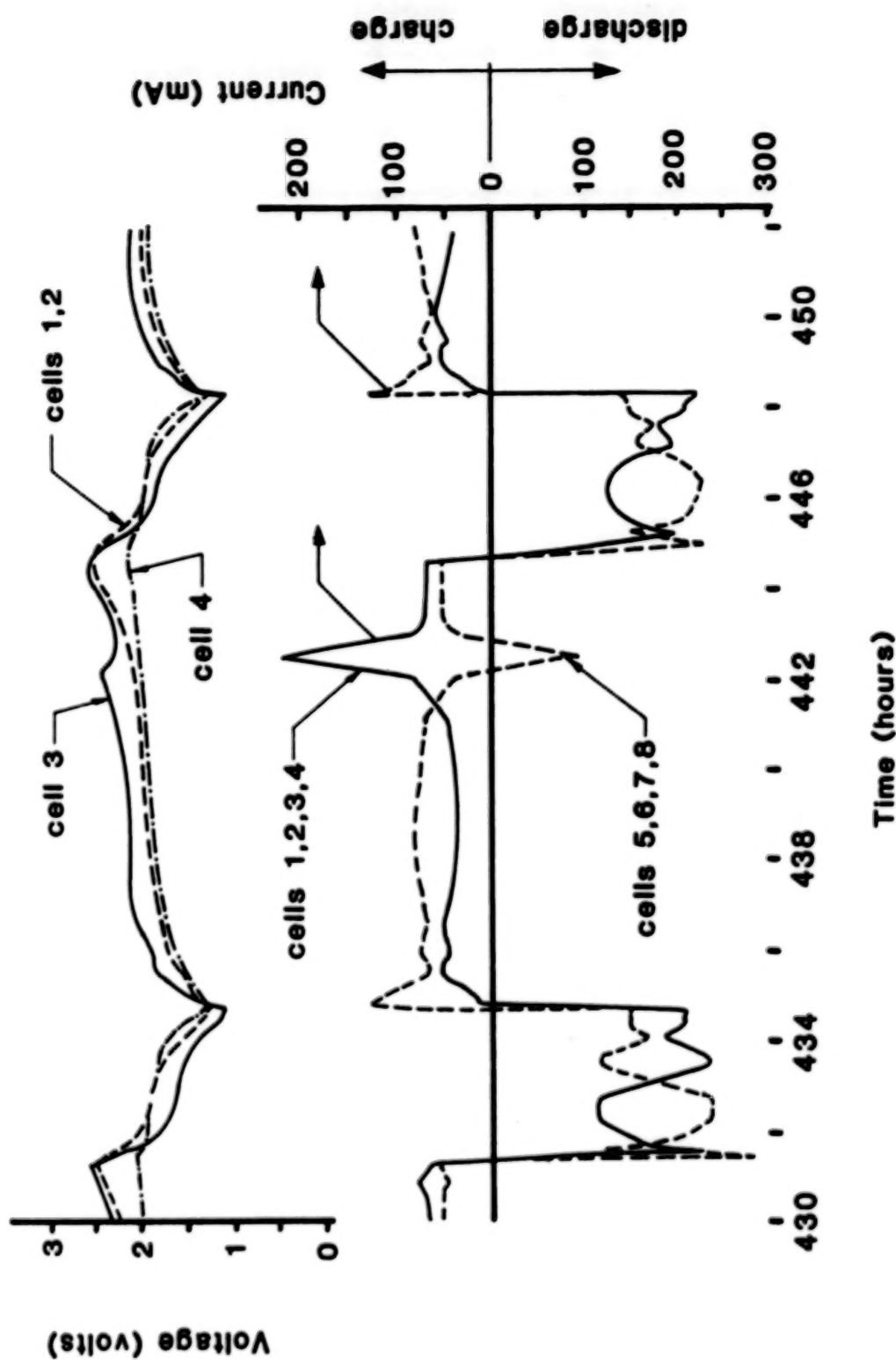


Figure 11. Individual cell voltage profiles and current branching profiles for an 8 cell series/parallel imbalanced battery cycling at 55°C. Configuration as illustrated. (Self-discharging cell shown shaded). Voltages in imbalanced string shown. 120 mA charge to 9.6 V, 360 mA discharge to 4.4 V. Cycles 26 and 27 shown.

N88-11025

Fault Tree Safety Analysis of a
Large Li/SOCl₂ Spacecraft Battery

O. Manuel Uy
R. H. Maurer

Space Reliability Group
The Johns Hopkins University
Applied Physics Laboratory
Laurel, Maryland 20707

November 1986

PRECEDING PAGE BLANK NOT FILMED

1.0 INTRODUCTION

A current spacecraft hardware program at the Johns Hopkins Applied Physics Laboratory requires an 1100 ampere-hour, 250 pound battery. This requirement can only be satisfied by a lithium chemistry battery. Several lithium chemistry systems were investigated with several manufacturers. A lithium thionyl chloride (Li/SOCl_2) F-size cell was selected.

To assess the safety hazard associated with a battery composed of eight (8) modules each containing 72 F-sized cells, a fault tree analysis was required by the program. Previous experience with lithium chemistry batteries in the ALDOT (Air Launched Deep Ocean Transponder) and SARSAT ground transmitter (Search And Rescue Satellite) programs enabled us to carry out such an analysis efficiently. Much of the initial safety hazard assessment for a single lithium chemistry cell was summarized in an internal APL report available for government agency distribution only: "ALDOT Systems Safety Analysis and the Li/SO_2 Battery," by O. M. Uy and R. H. Maurer, APL Report SOR 84084, August 1984.

This current report presents the results of the safety fault tree analysis on the eight module, 576 F cell Li/SOCl_2 battery on the spacecraft and in the integration and test environment prior to launch on the ground.

2.0 ELECTROCHEMISTRY REQUIREMENTS

The battery requirement of the satellite is for a total capacity of 1100 ampere-hours at a nominal 30 volts at 21°C and for a battery weight of less than 250 lbs. Figures 1-3 show the electrical and mechanical configuration of the battery. This translates to a specific energy density of at least 132 watt-hr/lb. A previous vendor survey for a battery requiring only 750 ampere-hours resulted in proposals which would have utilized Li/SOCl_2 , Li/SO_2 , Li/CF_x and Zn/AgO cells, with only Li/SOCl_2 complying with the energy density requirement. When the battery capacity requirement was subsequently increased from 750 to 1100 ampere-hours, the cells considered were the Li/SOCl_2 and $\text{Li/SO}_2\text{Cl}_2$. Lithium sulfuryl chloride was quickly abandoned however, because it is not as well developed as Li/SOCl_2 . Thus the electrochemical cells chosen in this program were the F-sized Li/SOCl_2 cells.

3.0 QUALITY ASSURANCE CONSIDERATIONS

In the fault tree analysis discussed later in this paper, it is shown that manufacturing defects such as internal mechanical shorts between anode and cathode or low cell capacities due to improper fill or failure of hermeticity and current leakage due to lithium diffusion through the ceramic insulator can lead to a decrease in the reliability of the battery and an increase in risk with respect to safety. It was therefore decided that a rigorous quality assurance procedure must be implemented with the cell manufacturer, with proper controls for acceptance and qualification of cell lots. We have chosen to incorporate the quality assurance documents from NASA,^{1,2} the U.S. Army³ and Navy⁴, and negotiated with the cell vendor in order to come up with specific quality assurance procedures for the

procurement of the battery, the flow-charts of which are shown in Figures 4-6. Even though these QA procedures are tailored to this program and this vendor, APL will be procuring lithium battery systems with similar specifications in the future.

4.0 SAFETY CONSIDERATIONS

Because of the high reliability and safety requirements of the program, the cells, as well as the electrical components used in the assembly of the battery, are either space or military high reliability parts. For example, the thermal fuses are 100% X-rayed and lot tested for thermal performance. There are three thermal fuses per string so that every cell in the battery is adjacent to a thermal fuse. Two blocking diodes are used in series in order to preclude charging of a cell string in the event of a single diode failure. The cells, modules and battery are subjected to random vibration and thermal environments in order to screen out workmanship defects such as weak solder or welding interconnections. Considerable attention is paid to insure that the cells used in each string and module are manufactured uniformly with respect to processes and materials. Finally, the sample cells and batteries will be subjected to overdischarge, high-rate discharge, short-circuit, heat-tape, capacity, vibration and thermal vacuum testing before the flight and spare batteries will be accepted for shipment to APL.

5.0 DEVELOPMENT OF FAULT TREE ANALYSIS

The safety fault tree for the battery module is shown in Figures 7 and 8. It has been developed applying the principles of safety fault tree analysis published in the IEEE Transactions on Reliability⁵, the Journal of the System Safety Society⁶, and the Reliability Design Handbook⁷.

In the fault tree the Top Event whose occurrence is potentially catastrophic leading to mission failure is the explosion or structural fragmentation of a battery module originated by the explosion of one or more cells in the battery pack. A single cell explosion may lead to the Top Event if the module container fails to operate as designed and relieve the overpressure condition; thus, a primary explosion may cause the Top Event. In addition, a single cell explosion may cause the Top Event to occur by creating overpressure and overtemperature conditions inside the battery pack which damage or make other neighboring batteries unstable leading to a second sympathetic explosion of such speed (less than 100 milliseconds) and force that not enough venting can occur soon enough even with the module vents functioning as designed (see Figures 7 and 8).

Basic events which either initiate the Top Event or enable it to occur are shown as ovals in the fault tree diagrams. AND gates in the tree are marked with A; OR gates with O. Intermediate and Top Events are shown as rectangles. Due to the size of the fault tree, it has been split into two figures with the intermediate event, single cell explodes, common to each main branch in Figures 7 and 8 and shown in detail in Figure 9. Figures 7 and 8 show that a single cell exploding and the failure of the module vents or a single cell exploding and the module operating nominally but with a

sympathetic secondary explosion occurring can lead to the Top Event. The assumption that has been made in the analysis is that if a single cell explodes, a secondary explosion of greater magnitude due to a multiple battery explosion will follow with some non-zero probability — here very conservatively taken as a probability equal to 1.

The basic events causing a single cell to explode are shown in Figure 9. Note that we have assumed that it is much more likely for a single cell to explode in the primary explosion scenario than for several to explode simultaneously. We would expect that a two or three cell primary explosion would occur with a frequency approximately equal to the square or cube respectively of the single cell primary explosion probability. This low probability multiple battery primary explosion is to be distinguished from a multiple battery sympathetic secondary explosion which seems to be of a fairly high probability once the unstable conditions created by the primary explosion of a single cell are in existence.

Figure 9 is the part of the fault tree showing the possible causes of single cell explosion. The branch of the tree under battery charging leads directly to an overpressure condition so quickly that the individual cell vent cannot prevent explosion from occurring. This charging condition can occur if a cell in a given string of cells, which is parallel with other strings of cells in the module, has low capacity relative to the other cells in the string and if the two diodes protecting the string both either fail shorted or have been installed backwards in any combination of these two fault conditions.

In order to make the various conditions necessary for the single cell explosion to occur more understandable we will list the ten minimum cut sets (Table 1) for all critical system states leading to the event "Single Cell Explodes" in Figure 9. The first set will be for the battery charging condition explained above.

The ten sets of basic events have been determined from literature search and discussion with experts involved with the manufacture and use of lithium batteries for both military and commercial applications. In order to determine the relative importance of the various branches in the fault tree, estimates must be made of the probability of occurrence of all basic events which are then propagated through the fault tree by addition at OR gates and multiplication at AND gates. These estimates and the rationale for their use are the subject of the next section.

After the original fault tree to estimate the module failure in the spacecraft had been developed, we also estimated the safety hazard incurred if modules were stored for one month on the ground during integration (Figure 8). The presence of an SO₂ detector lowers the risk of undetected cell or module venting and the consequent release of toxic gases in the vicinity of integration personnel to about one chance in 10,000.

Table 1

Minimum Cut Sets for Critical System States
for the Event "Single Cell Explodes"

- A. Cell Charging
- or
1. Cell Low and Diodes Installed Backwards
 2. Cell Low and Diodes Fail Shorted
 3. Cell Low and one Diode Fails and the other is installed backwards
- B. Overtemperature
1. High Ambient Temperature and Cell Vent Struck or Slow
- C. Internal Short (leading to Overtemperature)
- or
1. Seal Failure leading to shorting condition and Cell Vent Stuck or Slow
- or
2. Single Cell Shorted by external wire or conductive debris and Cell Vent Stuck or Slow
 3. Manufacturing Defects creating internal short and Cell Vent Stuck or Slow
- D. High Rate Discharge (leading to Overtemperature)
- or
1. Multi-cell Short due to external wire or debris and Thermal Fuse shorted and Thermal Switch shorted and Cell Vent Stuck or Slow
 2. One or more cells shorted to ground and Fuse shorted and Thermal Fuse shorted and Thermal Switch shorted and Cell Vent Stuck or Slow
- E. Forced Overdischarge (the rate may not be very high)
1. Cell within string with low capacity and Other cells in string with normal capacity and Thermal Fuse shorted and Thermal Switch shorted and Cell Vent Stuck or Slow

The probabilities of the fault tree basic events for a single spacecraft mission are shown in Table 2 together with comments about the rationale behind the use of the numbers. Table 3 shows the probability of an individual battery having a capacity which is 25% discharged.

It is readily seen that some of these basic event probabilities are time dependent and that some (usually related to conditions existing at the time of manufacture or to human factors) are independent of time. When the probability of module failure in storage is estimated, all time dependent basic event probabilities are multiplied by the number of hours in a month (720) rather than the 168 hour value assumed for the duration of the spacecraft mission.

The probability of failure for the diodes, gas sensors, relief valves (vents) and fuses are calculated with models and data from MIL Handbook 217D for the electronic parts⁸ and the Nonelectronic Parts Reliability Data⁹ both compiled by the Reliability Analysis Center of the Rome Air Development Center at Griffiss Air Force Base in New York. Base failure rates are taken from life test data and are usually given at a 60% confidence level from testing involving 10^5 component hours or more. These base failure rates are subsequently derated for several factors among which are

- a) the environment that the part will be used in; e.g., Airborne, Uninhabited Transport
- b) the quality level of the part, e.g. commercial or military, and the level of screening that has been applied in the part selection
- c) in some cases, the current rating of the device
- d) the application of the device, e.g. analog circuit with less than 500 mA operating current.
- e) a stress factor usually calculated as a ratio of the applied voltage or power to the rated voltage or power of the device
- f) in some cases a construction factor, e.g. hermetically sealed or metallurgically bonded.

These numbers are generally given as failures per million hours of operation which is easily transformed into a rate of failures per hour for a single unit.

Table 2

Basic Event Probabilities for Single Module

<u>Basic Event</u>	<u>Probability of Failure</u>	<u>Comment</u>	<u>Fault Tree Number</u>
1. 1N5614 diode fails short	2.73×10^{-10} per hour	MIL Handbook 217D ⁸ number times 168 hours flight time squared for two diodes per voltage string	2.10×10^{-15}
2. Diode installed incorrectly	10^{-4} per diode	Aerojet General Human Error ¹⁰ Rates Table; square of probability for single string	10^{-8}
3. Fuse or thermal fuse fails short	3.89×10^{-7}	Non-electronic parts ⁹ reliability data times 168 hours flight time times one fuse	6.54×10^{-5}
4. Battery cell shorted to ground	10^{-4} per cell	Experience with welded wire board shorts times 72 cells	7.2×10^{-3}
5. Battery cells shorted together	10^{-4} per cell	Experience with welded wire boards times 288 possible pairs to short together	2.88×10^{-2}
6. Single cell internal manufacturing defects	7×10^{-5}	Non-electronic parts ⁹ reliability data times 72 cells	5.04×10^{-3}
7. Single cell short due to conductive fragments	10^{-4} per cell	Experience with welded wire boards times 72 cells	7.2×10^{-3}

Table 2 (Continued)

Basic Event Probabilities for Single Module

Basic Event	Probability of Failure	Comment	Fault Tree Number
8. Internal short due to seal failure	1.83×10^{-6} per hour	SANDIA data ¹¹ on new cell seal times 168 hours flight times times 72 cells	2.21×10^{-2}
9. High ambient temperature	1×10^{-6}	Temperature greater than 1×10^{-6} 100°C highly unlikely in spacecraft or storage	
10. Individual cell vent stuck or slow	1×10^{-5}	Non-electronic parts data ⁹ on relief valve	1×10^{-5}
11. Explosion for unexplained reasons	1×10^{-6}	An estimate	1×10^{-6}
12. Module vents clog	5×10^{-6} per hour	Non-electronic parts data ⁹ on failure of mechanical couplings or springs times 168 hours flight time squared for two vents	7.06×10^{-7}
13. SO ₂ sensor on ground malfunctions	3.5×10^{-6}	Non-electronic parts ⁹ data on sensors in general times 720 hours per month on ground	2.52×10^{-3} /month
14. Thermal switch fails to open	10^{-4} per hour	Non-electronic parts ⁹ data on thermal switches times 168 hours flight time	1.68×10^{-2}

Table 3

Probability of Low Cell Capacity
(25% Discharged)

Coefficient of Variation, σ/\bar{x}	Standardized Normal Variate, Z	Probability of 25% Discharge	Fault Tree Number	
			Cell Charging	Forced Over-Discharge
0.09	2.78	2.7×10^{-3}	0.194	0.151

1) Calculate: $z = \frac{\text{MEAN-LOWER LIMIT}}{\text{STANDARD DEVIATION}} = \frac{\bar{x} - LL}{\sigma}$

$$= \frac{1 - LL/\bar{x}}{\sigma/\bar{x}} = \frac{1 - .75}{.09} = \frac{.25}{.09}$$

- 2) Probability found assuming a normal distribution
- 3) 72 cells in voltage strings for battery charging branch
- 4) 56 cells in position for forced overdischarge branch of fault tree
- 5) Probability of other cells in string having nominal capacity (for forced overdischarge)

$$\text{Prob} = p^8 = (1-q)^8 = 0.979$$

where q is the probability of a single cell being 25% discharged

When the mode of failure is also significant, data on the distribution of failure modes has also been used. In assessing mission reliability, whether a part fails electrically open or short may make no difference since a subsystem will often fail to function in either case. However, in assessing safety hazards it is often the case that only one failure mode presents a threat. In the case of the battery module, diodes and fuses must fail in a shorted condition for the various branches of the fault tree to be able to initiate a catastrophe. For example, 90% of the time fuses fail short or perform as if short because they are slow to open or exceed the designed current rating.

As shown in Table 2 the values used for probability of failure are multiplied by the number of hours, assumed to be 168 for the spacecraft mission, when they are time dependent and the number of parts when more than one can be independently susceptible to failure at the same time. For the storage case a separate table was not created but the numbers inserted into the fault tree (see Figure 9) have been multiplied by 720 hours representing one month of storage/integration time. Figures 10-13 show the numbers used in the respective spacecraft and storage fault trees for basic events from Table 2 and for intermediate and top events as calculated by either multiplying (AND gates) or adding (OR gates) as one proceeds up the branches of the fault tree from the bottom.

Several more comments are necessary about the basic event probabilities listed in Table 2. Mechanical basic event probabilities were assigned from data on devices which were similar in function and operation. The number on the individual cell vent being stuck or slow comes from data on pressure relief valves but is not considered to be time dependent because of the method of manufacture.

Probabilities for shorting to occur come from the authors' experience with the fabrication of welded wire boards for space hardware and soldered test boards for large designed reliability test programs.

Human factors probabilities are the most variable and the "softest" numbers in the fault trees. Values presented have been arrived at using the Aerojet General Human Error Rates Table⁶ for various common tasks plus discussions with a safety expert at the Naval Safety Center in Norfolk, Virginia¹².

Table 3 shows the probability of having an individual cell of low capacity (ampere-hours) given the coefficient of variation (the ratio of the standard deviation to the mean of the capacity for a set of samples) of the cells as manufactured. Selection of the value 0.09 is the result of discussions with the manufacturer. We defined battery low as being a 25% discharged condition even though testing has most often concentrated on 50% discharged cells. Thus, if the coefficient of variation of the lithium-thionyl chloride cells is 0.09, a 25% discharge state is 2.78 standard

deviations from the mean with a probability of occurrence of 2.7×10^{-3} . This last number comes from any table of probabilities for standardized normal variates assuming a normal distribution for cell capacities.

The probability of an individual cell being 25% discharged (CELL LOW in the fault trees) is then multiplied by the number of cells in the module battery pack. Thus, "Fault Tree Numbers" presented in Table 3 are entered as CELL LOW in calculating the frequency of occurrence of the Top Event of the fault tree. In addition, (see Cell Charging branch) the probability for one diode being incorrectly installed is 10^{-4} ; for two to be simultaneously incorrectly installed is 10^{-8} . Actually, if one diode were inserted backwards, the second one might also have a high probability of being inserted in a like manner; however, a polarity check has been specified in the fabrication process. The probability of this polarity check failing has been judged to be the same order of magnitude as installing a diode backwards. Thus, we maintain the 10^{-8} value.

Some logic implicit in the fault trees will now be explained. Once we have determined the probability for anyone of 72 independent cells having low capacity or being shorted to ground or being internally shorted, we must be careful not to overestimate the probability of protective devices such as diodes, fuses or cell vents failing at the same time to enable the cell failure to cause cell explosion. That is, any of 72 cells can have low capacity or be internally shorted which is why the single cell probabilities are multiplied by 72 in some cases in Table 1. However, once a single battery cell has low capacity or is internally shorted, it is only the vent for that cell or the diodes for that cell's string or the fuse associated with that cell that can simultaneously fail enabling single cell explosion to occur. The failure of other vents, diodes, fuses, etc. not associated with the cell in question would not enable the top event of single cell explosion to occur. Therefore, the probabilities of failure for protective devices such as diodes, fuses, cell vents, etc. are not multiplied by the total number of such components in the battery module (see Table 2).

Table 3 also contains a column showing values for the Forced Overdischarge branch of the fault trees. For this phenomena cells at the end of strings are not included because voltage reversal cannot occur unless both cell terminals are connected to neighboring cells in a series circuit. Only the seven interior cells in the voltage strings - a total of 56 cells - can experience this failure mode. Together with a single cell having low capacity, the remaining cells in the same string must have nominal capacities. The probability for nominal cell capacity in this case is $p^8 = (1-q)^8$ where q is the probability of one interior cell having low capacity.

In Table 2 the probability of failure from an Internal Short due to cell Seal Failure is given as 1.83×10^{-6} per hour, which, when multiplied by the 168 hour flight time in the spacecraft and 72 cells in the battery pack yields 2.21×10^{-2} for the spacecraft fault tree (see Figure 12). For the storage fault tree (see Figure 13), however, we do not multiply by the 720

hours in a month. The shorting due to seal failure is a self-limiting process in that as a crack in the seal becomes larger with time, there is less capacity in the cell to supply the greater current that can now flow. The Seal Failure Internal Short is a very slow physical mechanism and consideration of both individual cell capacity and the level of current necessary for heating lead us to conclude that such an internal short must take place over a period of roughly 100-200 hours to generate heat fast enough to create an OVERTEMPERATURE condition. For the Storage Fault Tree the Seal Failure basic event probability has also been multiplied by 168 instead of 720 hours.

7.0 USE OF THE FAULT TREE

Two points must be emphasized at the outset of this discussion: A) we have assumed that Failure of the battery module initiated by the explosion of a single cell is equivalent to damage to the spacecraft; B) the main usefulness of the fault trees and the purpose for which they are most valuable is determining the relative importance of the various branches of the fault tree and the sensitivity of the Top Event occurrence frequency to significant changes in any of the basic event probabilities. The fault tree will show which factors are most important to be improved or closely controlled in order to make the Top Event frequency as low as possible within the limits of practicality.

The "hardness" or absolute accuracy in many of the probabilities presented in Figures 10-13 can be argued at some length. Thus, instead of taking a given Top Event probability as a gospel value it is better to state that if we relax stringent limits on quality control and don't do a good job in the battery module design, our Top Event hazard probability may be as great as 10^{-2} for the mission; while, conversely, if we do the best possible job of quality control on components, and cells and do a good job on the module design, our Top Event hazard probability may be as low as 10^{-6} per module, essentially that for explosion for unexplained reasons.

Likewise, the probability for an undetected Single Cell Venting (Figure 11) during one month's Storage/Integration is reduced from 3.43×10^{-2} to 8.63×10^{-5} per module by the use of an on-site SO_2 detector during integration. The probability of a single cell venting is calculated from Figure 13 with the basic event Cell Vent Stuck or Slow probability set equal to one (the cell vents as it is supposed to; no explosion occurs, but gases are released from the battery module).

8.0 CONCLUSIONS

The analysis has shown that with the right combination of blocking diodes, electrical fuses, thermal fuses, thermal switches, cell balance, cell vents and battery module vents the probability of a single cell or a 72-cell module exploding can be reduced to 10^{-6} , essentially the probability due to explosion for unexplained reasons. This one chance in a million value for the module is quite conservative since we have assumed (see Figure 10) that if a

single cell explodes, then one or more additional cells will also explode in a sympathetic secondary reaction even though the module vents operatenominally. This certainty of an uncontrollable secondary explosion seems to us to be the only reasonable assumption based on the present dearth of data for battery modules of the present design and for cells of Li/SOCl_2 chemistry.

For one month of integration and test of the spacecraft on the ground the probability of module failure is 10^{-6} (Figure 11) as stated above. Of equal importance we have considered the possibility of a cell venting (the cell vent operates correctly in Figure 13 and the 10^{-5} probability of the cell vent being stuck or slow is replaced by 0.99999) and releasing toxic gases that may injure personnel. The probability of a cell venting has been calculated as 3.43×10^{-2} in Figure 13. We can reduce the probability of personnel exposure by the use of a sulfur dioxide monitor in line with the module vent manifold. An audible alarm will be triggered whenever the concentration of SO_2 exceeds 1 ppm in the manifold. The left side of Figure 11 shows that this reduces the probability of an undetected toxic gas release to 8.63×10^{-5} per battery module or about 7×10^{-4} for the complete spacecraft battery.

ACKNOWLEDGMENT

The authors would like to acknowledge the help of R. M. Sullivan, F. J. Porter, and P. Leigh of the APL Space Department, R. F. Bis and J. A. Barnes of NSWC, K. Hill of Patrick AFB, C. Berger, M. Brundage and E. Reiss of Army LABCOM at Fort Monmouth, J. B. Trout and B. J. Bragg of NASA Johnson Space Center, and R. Murphy of the Advanced Battery Group.

"Figure 3 not received for publication."

References:

1. NASA-JSC Report No. EP5-83-025, "Specification for Acceptance and Lot Certification Testing of Li/BCX Cells and Batteries for Delivery to NASA, Johnson Space Center," 8 September 1983.
2. NASA-JSC Doc. No. TTA-T-2P137, "Test Procedure for Receiving Inspection and Vibration Testing of Pre-certified Li/BCX Cells," 12 January 1984.
3. MIL-B-49461(ER), "Military Specification - Batteries, Non-Rechargeable, Lithium Thionyl Chloride," 3 March 1986.
4. NAVSEANOTE 9310, "Responsibilities and Procedures for the Naval Lithium Battery Safety Program," 11 June 1985.
5. C. Dunlinson and H. Lambert, IEEE Trans. Rel. R-32, 52 (1983).
6. N. Piccinini, et. al, J. Sep. Safety Soc. 18, 28 (1982).
7. R. T. Anderson, Reliability Design Handbook No. RDH376, Reliability Analysis Center, RADC-GAFB, NY (1976).
8. Reliability Prediction of Electronic Equipment, MIL-HDBK-217D, 15 January 1982.
9. R. G. Arno, Nonelectronic Parts Reliability Data, NPRD-2, RADC-GAFB, NY (1981).
10. L. E. Rackley, Proc. Sys. Anal. Tech. Conf., Washington, D. C., June 21, 1984, p. 117.
11. S. C. Levy, SAND 79-1383, Sandia Laboratories, Albuquerque, NM., March 1980.
12. C. Stewart, Naval Safety Center, Norfolk, VA., Private Communication.

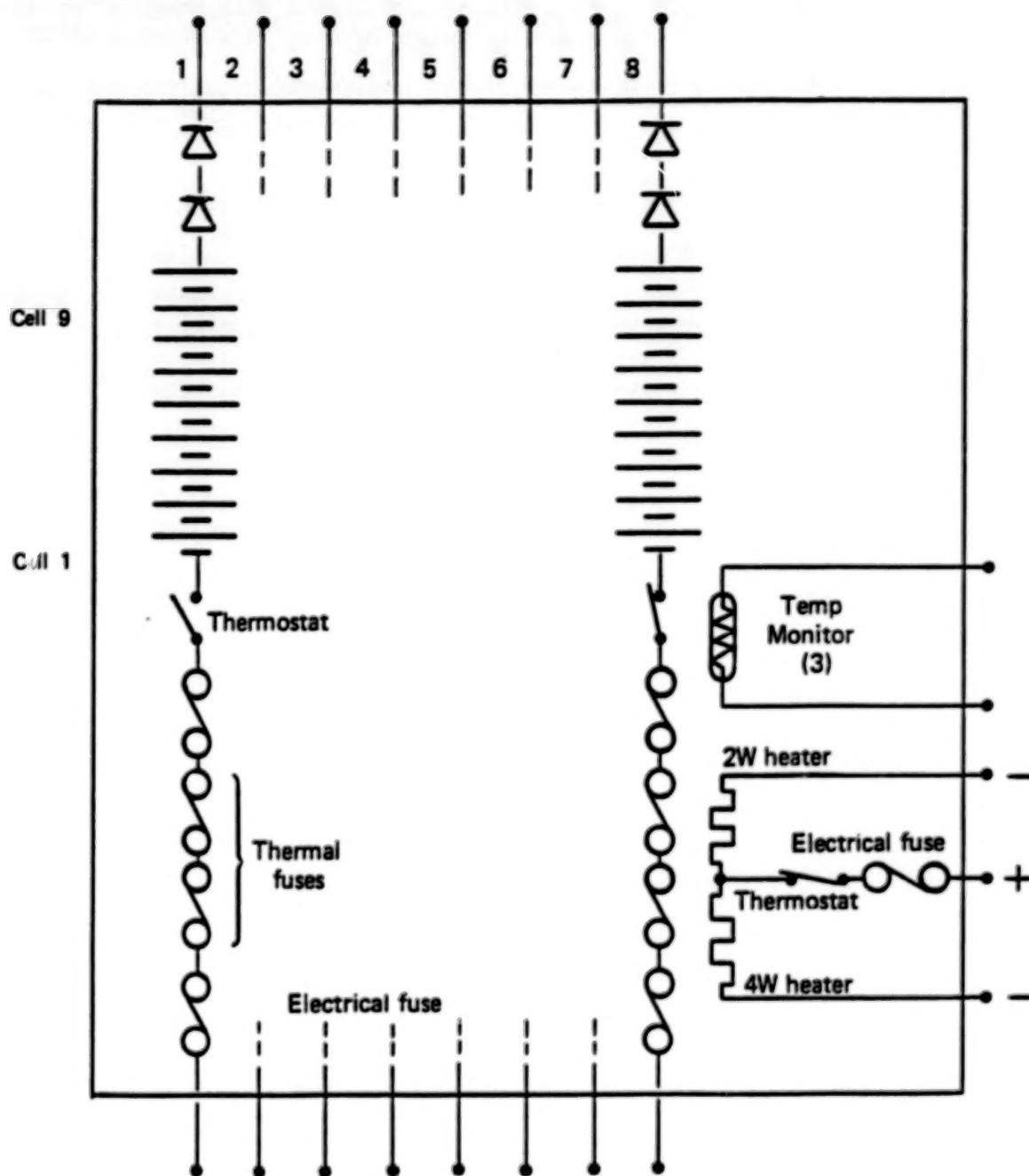


Figure 1. Module circuit configuration.

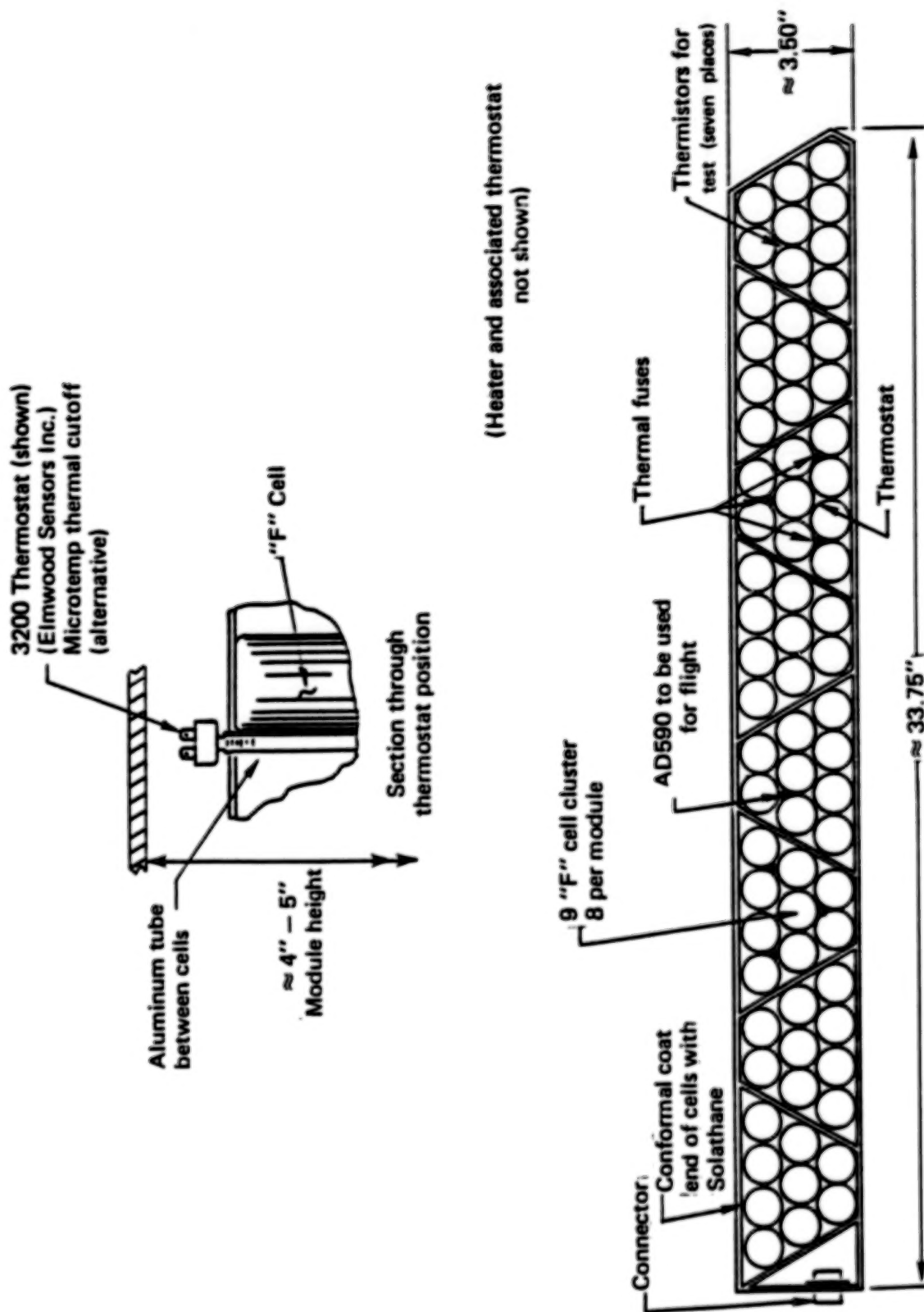


Figure 2. Module configuration.

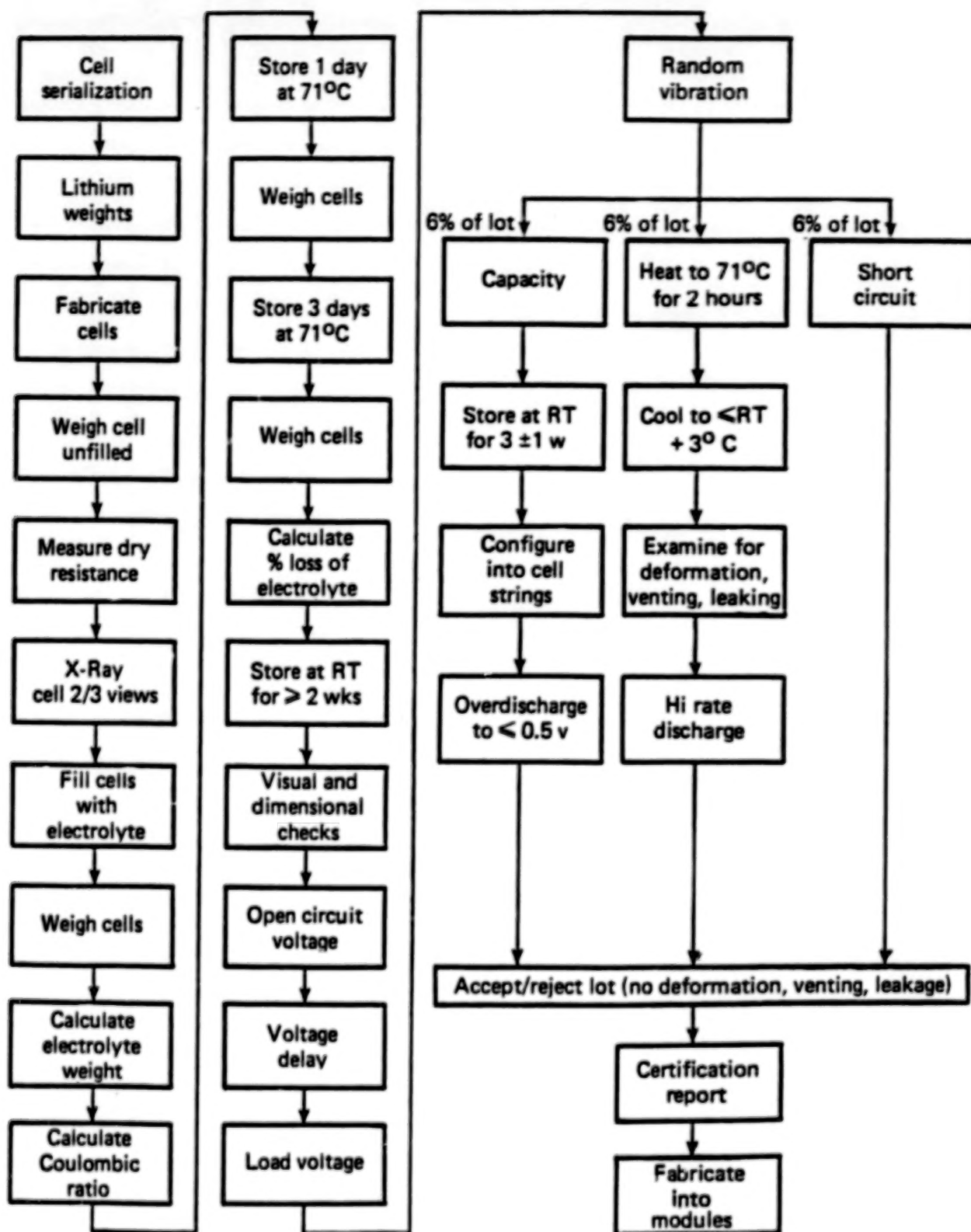


Figure 4. Cell fabrication and test flow.

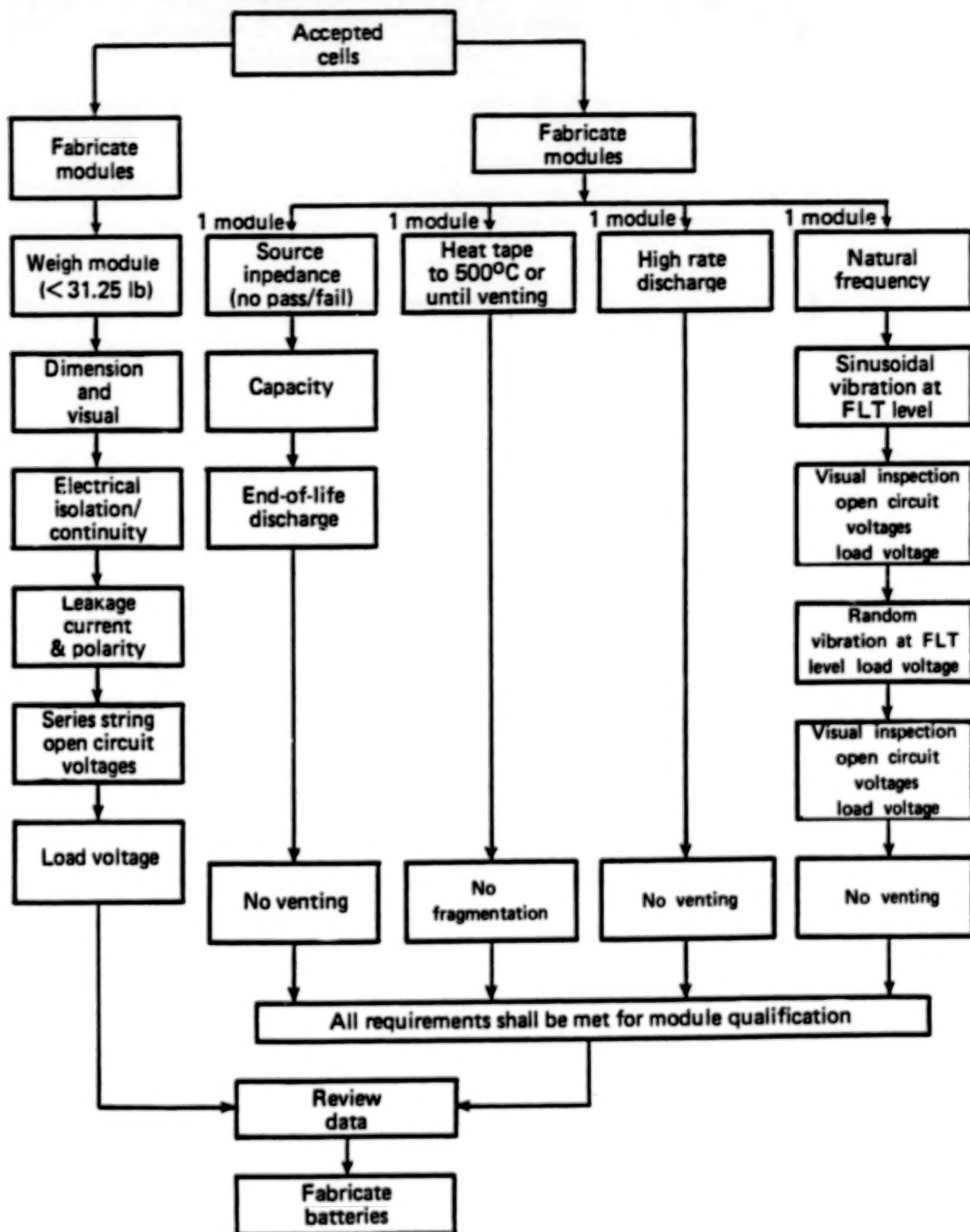


Figure 5. Module fabrication and test flow.

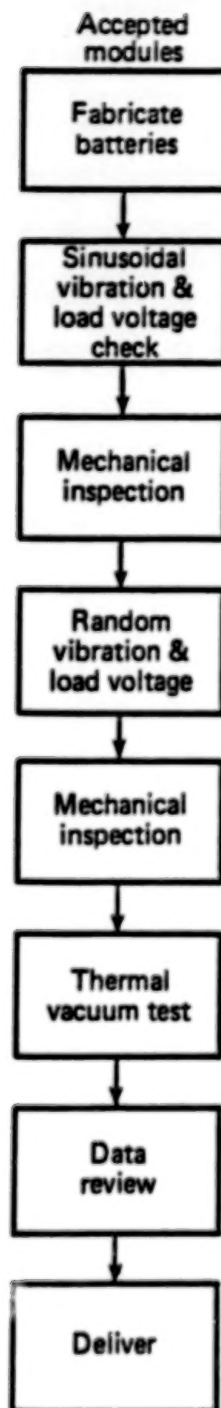


Figure 6. Battery fabrication and test flow.

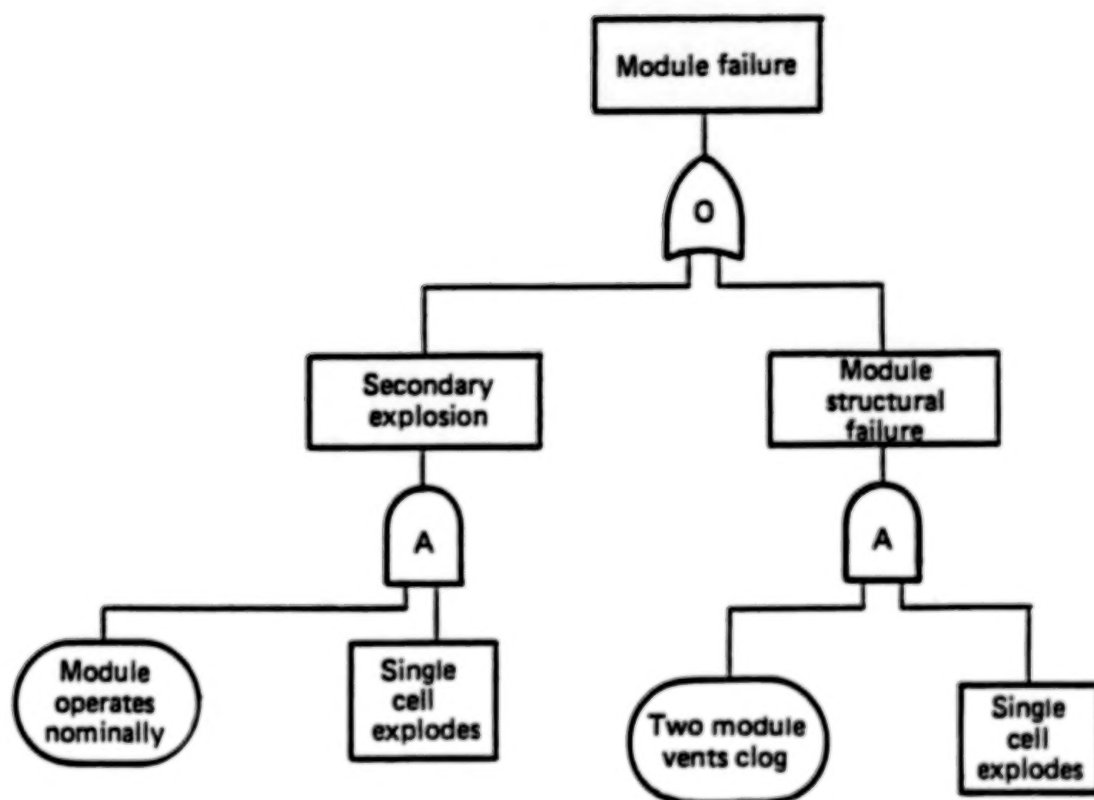


Figure 7. Battery module safety fault tree for spacecraft.

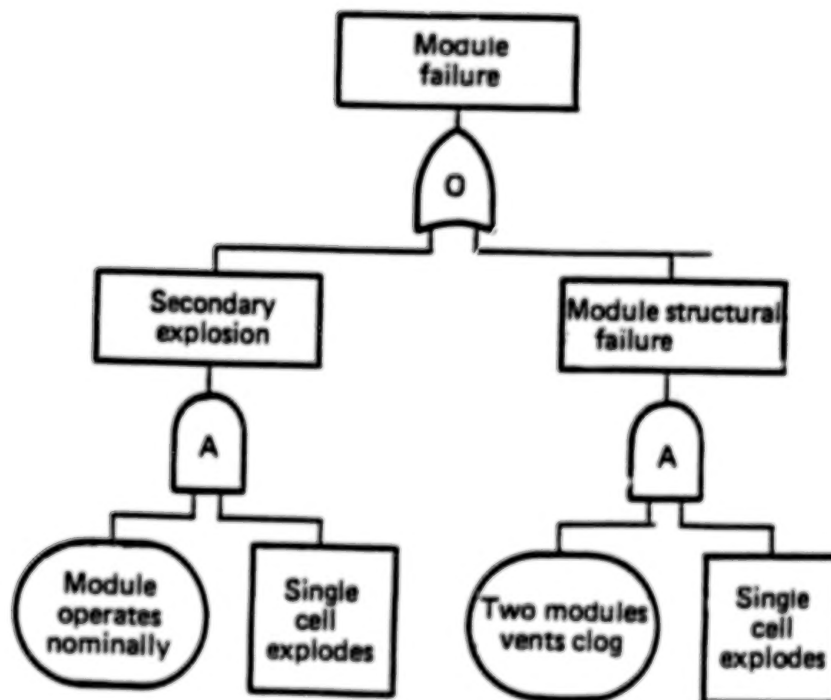
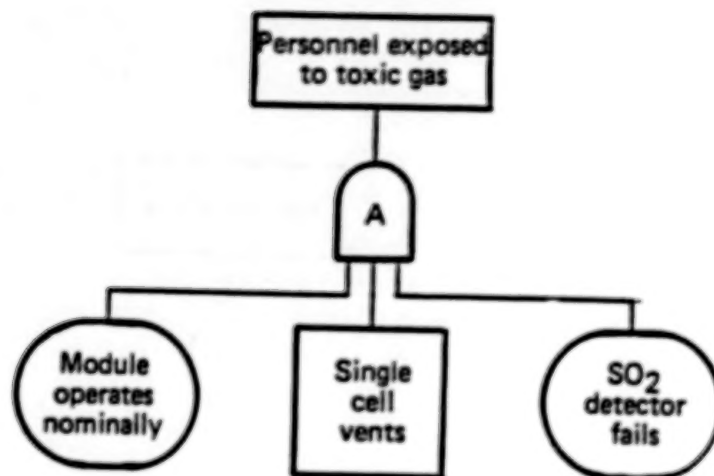


Figure 8. Battery module safety fault tree for ground integration.

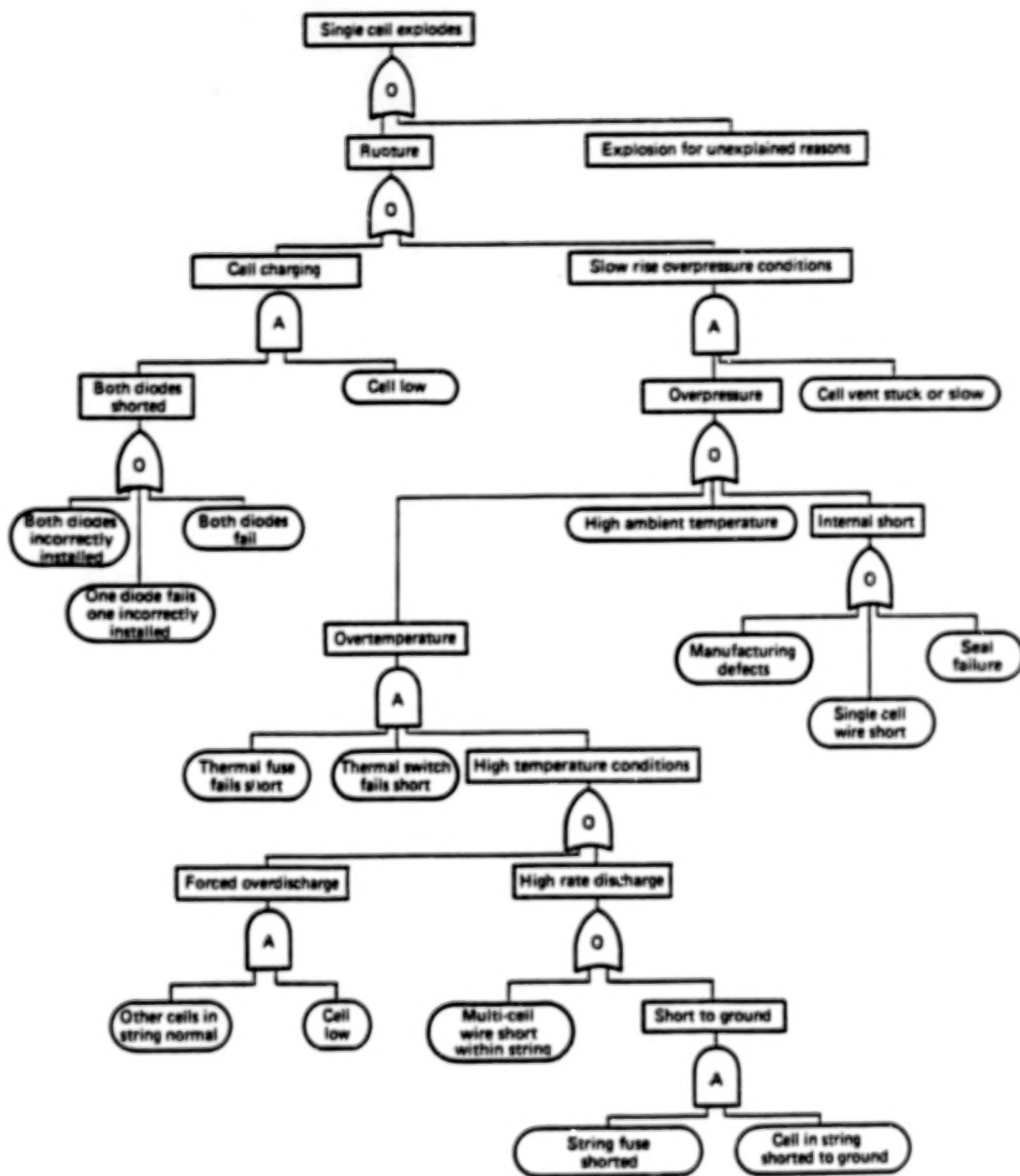


Figure 9. LiSOCl_2 single cell safety fault tree.

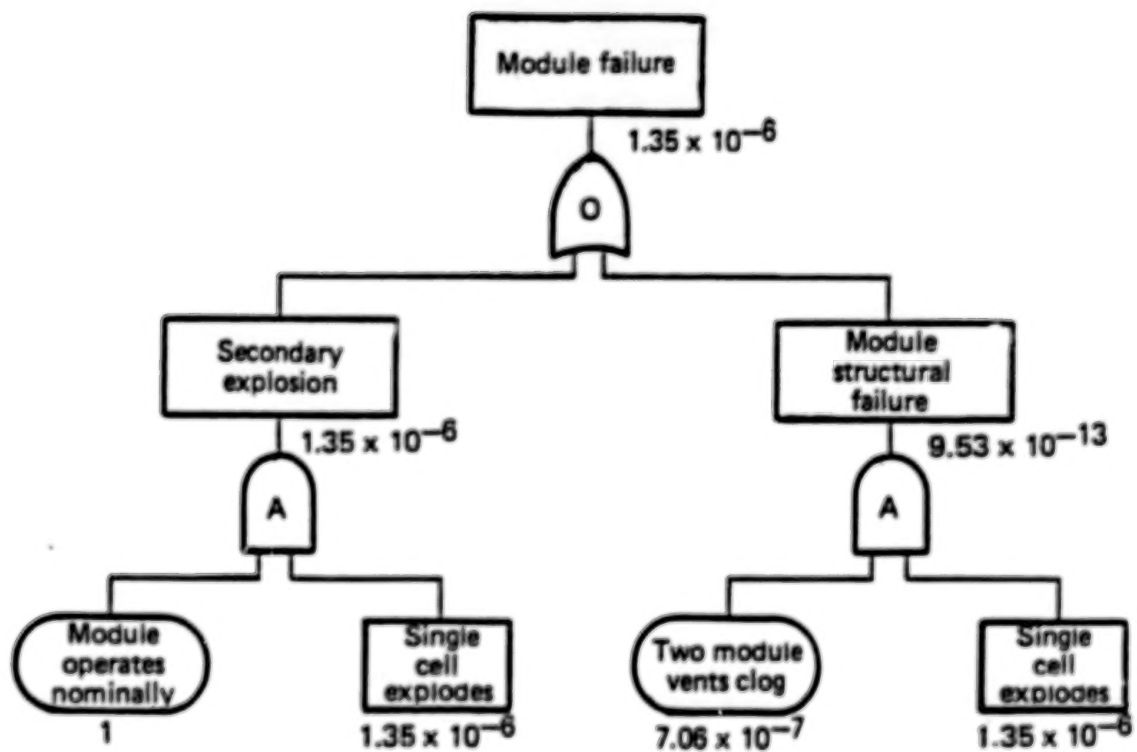


Figure 10. Battery module safety fault tree for spacecraft.

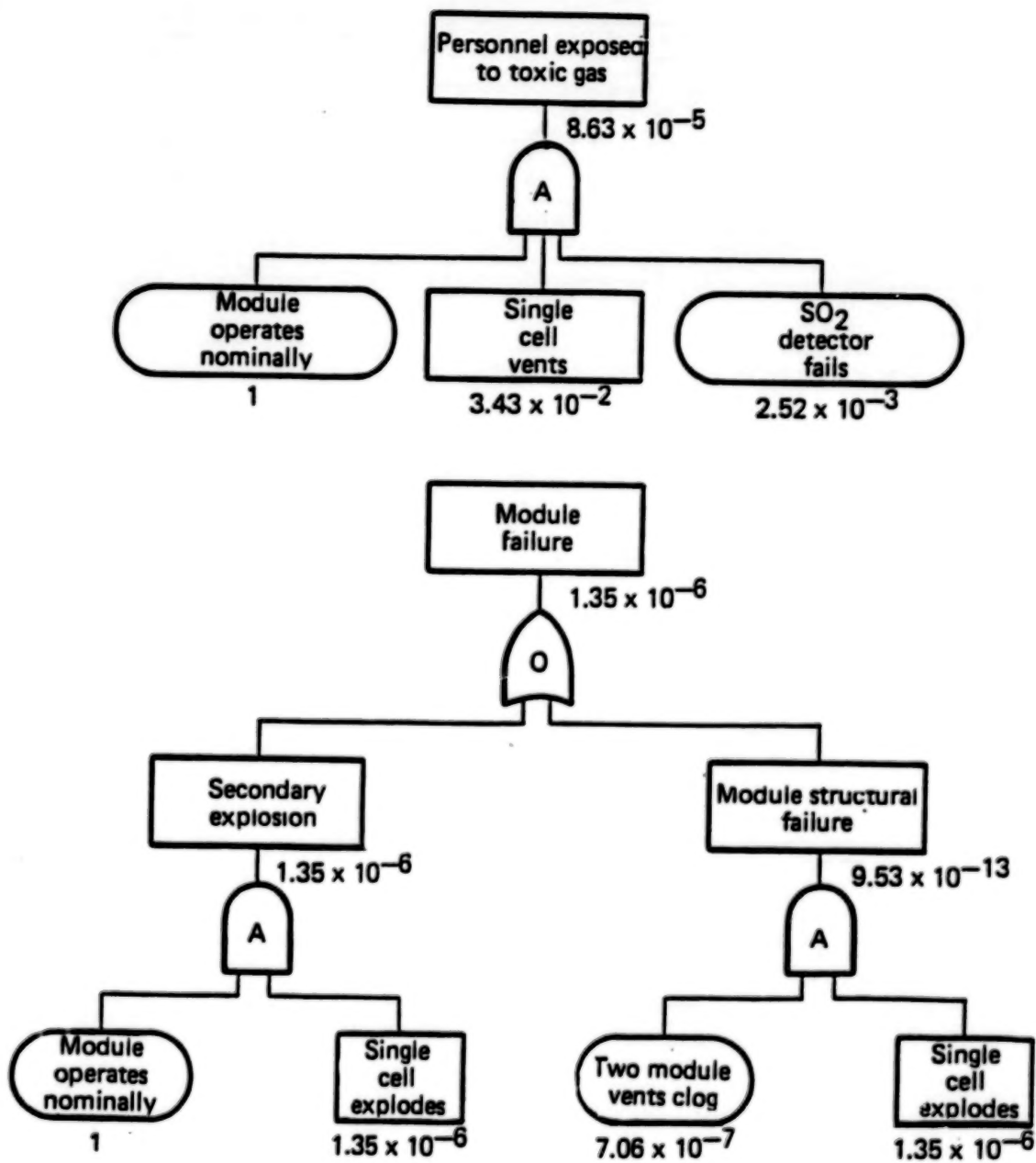


Figure 11. Battery module safety fault trees for ground integration.

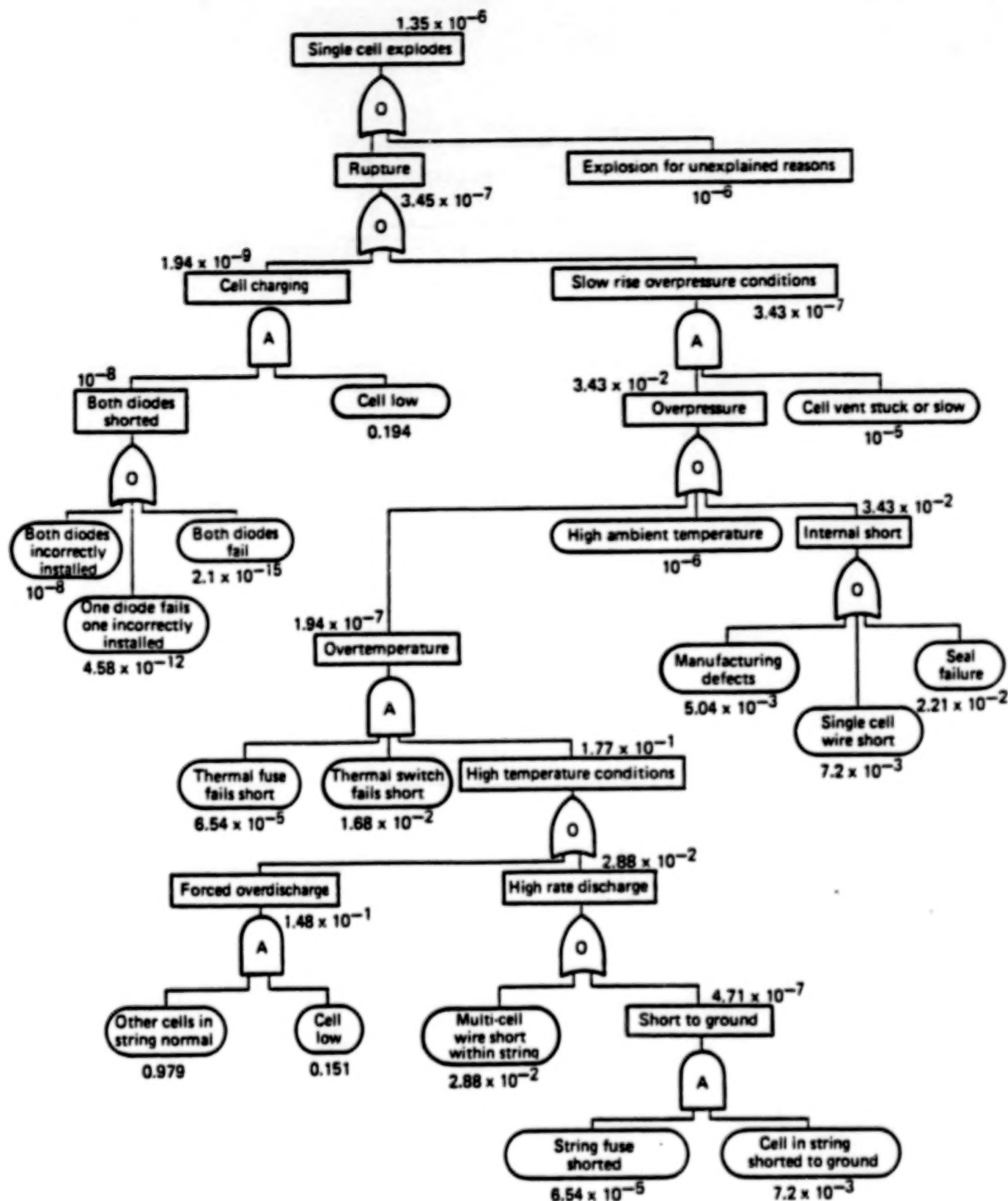


Figure 12. LiSOC1_2 single cell safety fault tree for spacecraft.

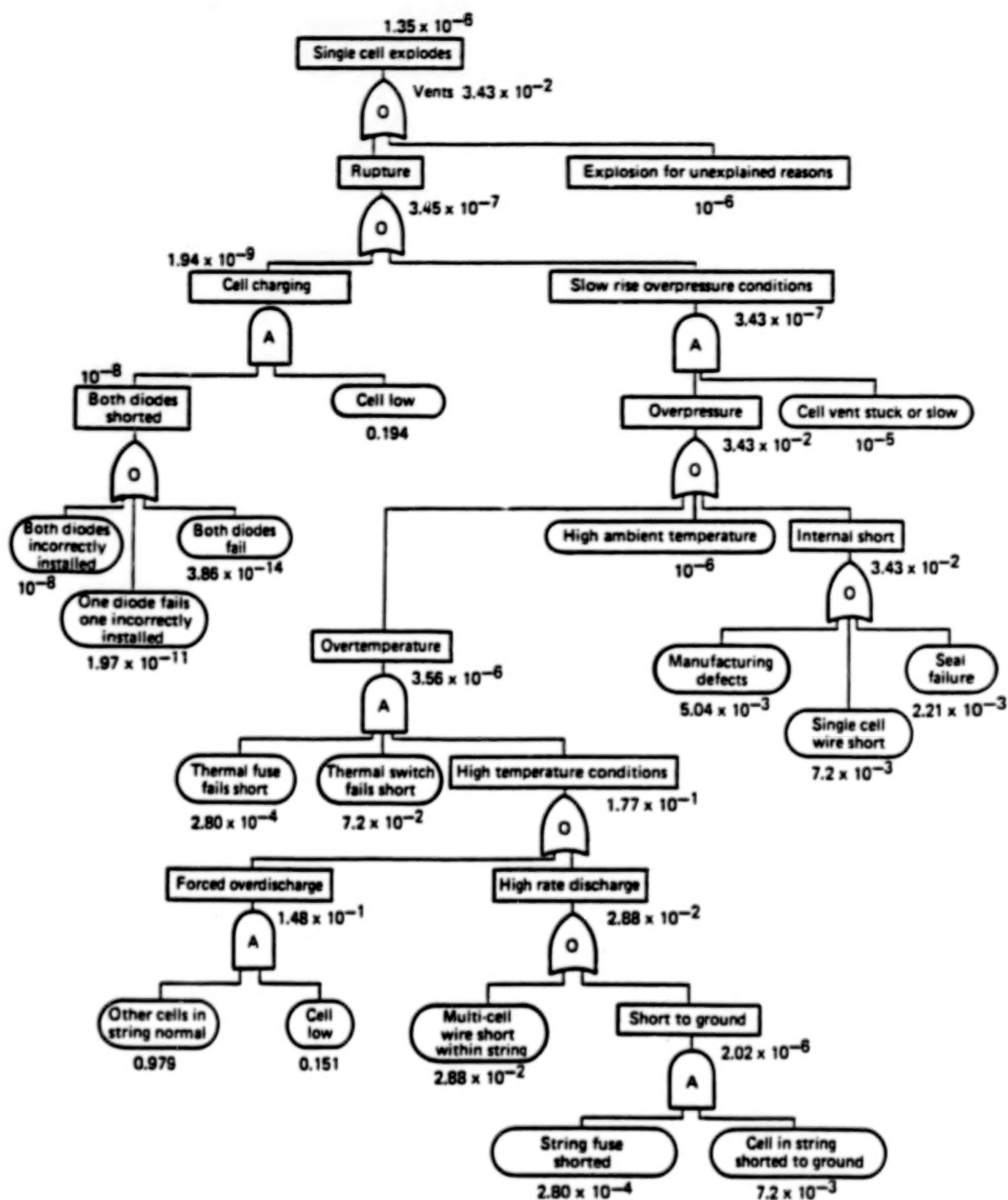


Figure 13. LiSOCl_2 single cell safety fault tree for storage of 1 month.

CHEMICAL ANALYSIS OF CHARGED Li-SO₂ CELLS

S. SUBBARAO, D. LAWSON, H. FRANK, and G. HALPERT

Jet Propulsion Laboratory, California Institute of Technology,
4800 Oak Grove Drive, Pasadena, CA 91109 (USA)

J. BARNES and R. BIS

Naval Surface Weapons Center, Silver Spring, MD 20903-5000 (USA)

1. Introduction

For some time the Navy has been concerned about the hazards associated with charging of lithium/sulfur dioxide cells. This concern is based on earlier verbal reports and also exploratory investigations both of which indicated that charging of these cells can result in explosion.

Based on these initial inputs the Navy deemed it important to examine the charging of these cells in greater detail. For this reason the Navy initiated a joint program with the Jet Propulsion Laboratory to study the charging of these cells.

Initial focus of this program was to confirm that charging can indeed result in explosions and thereby constitute a significant safety problem. Results of this initial effort clearly demonstrated that cells do indeed explode on charge and that charging does indeed constitute a real and severe safety problem. These conclusions were based on numerous experimentally demonstrated explosions of sonobuoy cells that had been partially discharged and stored prior to charge at high rates [1,2].

Subsequent efforts of this program were focused on determination of the causes for the observed explosions. In particular, it was desired to resolve two major issues. The first of these was to determine if the explosions were

02011-88

influenced by the type and size of cell and also its operating conditions. The second was to determine the most likely chemical processes that are involved and could explain the origin of the explosions.

A report is in preparation on results of investigations dealing with the impact of cell type and size as well as charge conditions on the explosions (3). Therein it will be shown that the occurrence of explosions is rate dependent and appears to be generic for lithium/sulfur dioxide cells.

This paper describes results of the second effort to identify the chemical reactions involved in and responsible for the observed behaviors.

2. Experimental

Two types of cells were employed in this investigation. The first consisted of the commercial spiral wound, high rate cells described previously [1,2]. The second was a laboratory type cell installed in a glass assembly. This section contains a brief description of these cells as well as the procedures employed in handling and disassembling them for analyses. The analytical methods were the same for both types and are also described herein.

The commercial cells were Duracell type LO30SH with the cylindrical configuration and contained spiral wound electrodes. The cells were hermetically sealed in steel cans, and were carbon limited in design; rated capacity of these was 4.2 amp-hr at the C/2 discharge rate.

The lab cells consisted of small parallel plate electrodes immersed in a commercial SO₂ solvent/electrolyte mix. These components were housed in sealed laboratory glass hardware. The electrode assembly consisted of two outer lithium electrodes that sandwiched one inner carbon electrode. Lengths, widths, and thicknesses of the two lithium electrodes were 0.5 in., 0.5 in., and 0.018 in. respectively. Corresponding dimensions of the carbon electrode were 0.5 in., 0.5 in., and 0.033 in. Relative sizes of the two electrodes were selected so that the cells would be carbon limited, like the commercial cells, and capacities were 100 mah. The solvent/electrolyte contained 7% lithium bromide, 23% acetonitrile, and 70% sulfur dioxide by weight.

Both the lab and commercial cells were operated in a similar manner in this investigation. The operation typically consisted of first discharging them 20%, then letting them stand, and then placing them on charge. Operating current densities were the same for both types, and specifics are shown in Table I. The cells were disassembled in the fresh, discharged, and charged conditions.

The lab cells provided a great deal of versatility to this investigation and permitted controlled and visual operations not possible with the commercial cells. With the glass hardware it was possible to observe the electrodes and color changes in the solution as described herein.

Disassembly of the commercial cells in the charged condition was not treated lightly in that this is a potentially hazardous operation. For this reason, the following procedures were devised and used in disassembly of these cells in the charged condition.

These operations should only be done in proper facilities because the Li-SO₂ cells may detonate during the process. It is important that each new or modified type of cell be x-rayed so that the operator will not cut through the electrode structures during the disassembly operation.

- A. The cell is charged to some given point prior to venting or detonation. If the cell vents it is best to continue the charging to detonation which usually occurs in less than a minute after venting.
- B. Stop the charging current and remotely and quickly quench the cell with liquid argon (-189°C: 84°K). Liquid nitrogen is not used for this purpose because it can react with lithium metal if the cell vents or detonates and create added safety problems.
- C. When the frozen cell voltage drops to near zero for a period of 30 minutes, the fill tube of the cell is then opened by an operator using proper protective gear. Care should be used that the filling tube orifice is open and will allow the passage of gases and liquids.

- D. The frozen cell is stored in a pumped vacuum chamber, (less than 10mm), with the open fill tube pointing in a downward position for 2 or more days. The voltage of the cell should be 20 millivolts or less at this point. Any static electrical charge applied at this point to the cell terminal may cause the cell to detonate.
- E. The cell is cut open in a dry argon atmosphere, and components are stored in an argon gas environment. Care should be taken in this operation in that the cell stack is quite active as evidenced by some crackling noises that originate at the anode. Also the anode materials appear to be sensitive to any form of static electrical energy.

Because of the much smaller amounts of active materials in the lab cells, the disassembly of these in the charged condition was not deemed as hazardous as that of the commercial cells. For this reason the disassembly of these was carried out with customary precautions and equipment for laboratory operations (safety glasses, face shield, etc.). In order to avoid contamination, the cells were disassembled in a dry room instead of a glove bag as above. Components were removed and processed into samples.

The analytical techniques employed were the same for samples of lab and hardware cells. These techniques consisted of ultraviolet (UV) visible, Fourier Transform Infrared (FTIR) spectroscopic analyses, as well as Scanning Electron Microscopy (SEM), and Energy Dispersive Spectroscopy (EDS).

3. Experimental Results

The lithium anode of the undischarged, discharged, and discharged-then-charged cells were markedly different in their behavior and physical appearance even though their chemical analyses were similar. SEM pictures of the three types of electrodes are shown in Figures 1 and 2. The undischarged and discharged lithium electrodes were both coated with crystalline platelets. The lithium electrodes which had been partially discharged and then charged were quite different in appearance. They were covered with rough, dull gray, non-adherent deposits which appeared to be composed of fine filaments or dendrites when studied by SEM. Upon removal from a cell and subsequent drying, these

lithium electrodes were found to be very reactive. Also these charged lithium electrodes, particularly those from commercial cells, were found to sputter and yield cracking sounds when cut with a scissors or hit with a hammer. Finally the charged lithium electrodes that were freshly removed from a cell were observed to burn when exposed to dry air. No similar behavior was observed with uncharged electrodes.

Diffuse reflectance FTIR spectroscopy [4] was used to study the surface films on the three types of lithium electrodes. This technique was chosen to minimize disturbance of the anode-surface films. As is clear from Figure 3, the surfaces were chemically similar. The major component was $\text{Li}_2\text{S}_2\text{O}_4$ (peaks at 1075, 1025, and 910 cm^{-1}) with traces of Li_2SO_3 or Li_2SO_4 (peaks at 975 and 655 cm^{-1}). Peaks in the 1150 - 1250 cm^{-1} region are assigned to traces of lithium polythionates [5,6].

The deposit/film on the lithium electrode was examined by EDS and found to contain Li, S, and O in the ratio of approximately 2:2:4. This result supports the assignment of $\text{Li}_2\text{S}_2\text{O}_4$.

The carbon cathodes were examined in a similar manner to that described above. Upon removal from the cells, these cathodes were quite benign and did not sputter and crack like the lithium electrodes. Diffuse reflectance FTIR measurements were made on the carbon cathodes from fresh, discharged, and charged cells. Spectra for each of these cathodes were found to be quite similar and are shown in Figure 4. The peaks are assigned to $\text{Li}_2\text{S}_2\text{O}_4$ (1043, 1027, and 921 cm^{-1}) [7]. These results indicate that $\text{Li}_2\text{S}_2\text{O}_4$ is the predominant species in all three types of cells (the smaller peaks at 1237 cm^{-1} are attributed to traces of polythionates). This finding is not unexpected in the case of the discharged cells in that $\text{Li}_2\text{S}_2\text{O}_4$ has been reported as the end product of the cell reaction. The presence of some $\text{Li}_2\text{S}_2\text{O}_4$ in the fresh cell may be attributed to short duration test discharges applied by the cell or sonobuoy manufacturer before delivery of the units.

Figure 5 illustrates the effect of charging on the aluminum grid current collectors of the carbon cathodes. Shown therein are the grids from three cells subjected to varying amounts of charge. The grids on the left designated

as "discharged" were from cells that received no charge. These appear quite smooth. The grids in the middle designated as "discharged and charged" were from cells that were discharged 20% of capacity and then recharged back to full capacity. These appear to be slightly corroded. The grids on the right designated as "charged excessively" were from previously discharged cells that were charged approximately 300% of capacity. Comparison of these grids indicates that charging causes corrosion which is dependent upon the amount of applied charge. The corrosion is believed to be caused by bromine (Br_2) which is formed by oxidation of bromide ions at the carbon electrodes during charge.

The laboratory cells were used in another series of runs to examine the time-dependence of cell open circuit voltage after charging. The procedure consisted of charging both fresh and partially discharged cells and then terminating charge and monitoring cell voltages. Results, shown in Figure 6, reveal a difference in the voltage behavior of the two types. At the start of the stand period, both cell voltages were noted to be near 3.6 volts. After a few minutes, the voltage of the partially discharged cell was noted to decline to 3.0 volts while voltage of the fresh cell remained at 3.6 volts. Color changes were also noted for the solvent/electrolyte of these cells. After the start of charging, the color of both solutions changed from colorless to a dull red. After termination of charge, the solution of the fresh cell remained red while the color of the partially discharged cell began to fade. The fading of the latter solution occurred after a few minutes of standing and corresponded to the decline of cell voltage.

These results were attributed to the formation of bromine during charge and subsequent rapid reaction of the Br_2 with $\text{Li}_2\text{S}_2\text{O}_4$ in the case of the partially discharged cell. Support for the formation of bromine is given by the observed voltage of 3.6 volts which corresponds to that of the $\text{Li}-\text{Br}_2$ couple and also the reddish color which is associated with bromine. Support for the reaction of bromine with $\text{Li}_2\text{S}_2\text{O}_4$ is based on favorable thermodynamics, the known reaction of the two, and the intimate contact of these two at the carbon electrode during charge. The persistence of the red color in the solution of the fresh cell is explained by the absence of significant amounts of $\text{Li}_2\text{S}_2\text{O}_4$ in that this cell was not discharged. Finally it should be pointed out that after about 10 hrs the solution color in the freshly charged cells had

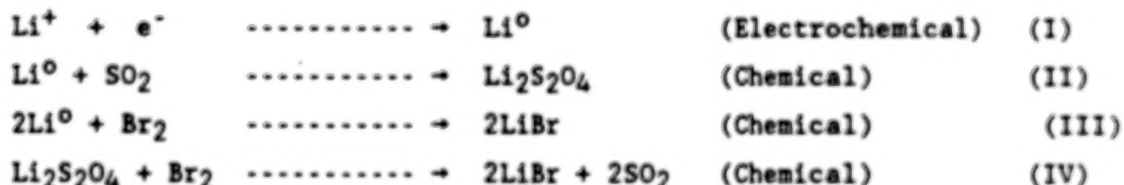
faded and cell voltage returned to 3.0 volts. This observation is explained by the slow diffusion of bromine to the lithium electrode and consumption of bromine by the Li-Br₂ reaction.

6. Conclusion

The finely divided particles on the surface of the lithium electrodes after charging are believed to be comprised of a mixture of Li₂S₂O₄ (as shown by FTIR & EDS) and metallic lithium. The Li₂S₂O₄ may be in the form of a layer that encapsulates the lithium. This mixture would be expected to form as freshly reduced lithium reacts with SO₂ in the electrolyte.

The pyrophoric behavior of the charged lithium electrodes is attributed to the reaction between the Li and Li₂S₂O₄. Support for this explanation is based on the work of Kilroy who showed that the mixture of these two reacts quite readily and exothermically [8]. The rapid and highly exothermal nature of the reaction for these particular samples is attributed to the fact that the mixture is very finely divided.

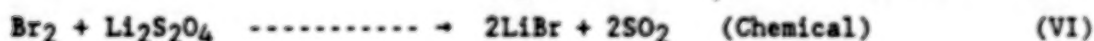
Based on our experimental observations the following reactions are deemed possible at the lithium electrode during charge:



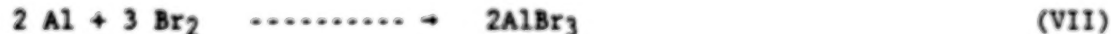
Equations I-IV give reactions at the lithium electrode. Equation I describes the predominant electrochemical reaction which is the reduction of lithium ions to form lithium metal. Equations II and III give two overall chemical reactions in which the lithium can be consumed. Equation II gives the reaction for oxidation of the lithium by the SO₂ which is part of the solvent/electrolyte. Equation III gives the reaction for oxidation of the lithium by Br₂ which diffuses from the cathode, where it is formed, to the anode. Equation IV describes another chemical reaction of the evolved Br₂. This consists of oxidation of the Li₂S₂O₄ film on the anode. In a partially

discharged cell, Equations III and IV will be relatively minor in that most of the Br_2 will be consumed by reaction with $\text{Li}_2\text{S}_2\text{O}_4$ at the carbon electrode.

Equations V and VI give reactions at the carbon electrode. Equation V describes the predominant electrochemical reaction; the oxidation of Br^- ion in the electrolyte to form elemental Br_2 as suggested above. Equation VI represents the chemical oxidation of $\text{Li}_2\text{S}_2\text{O}_4$ by the Br_2 . The only difference between this and Equation IV is that in Equation VI the $\text{Li}_2\text{S}_2\text{O}_4$ is on the carbon electrode where the Br_2 is formed and there is no diffusion required for contact of the two.



Equations VII and VIII give reactions at the aluminum grid portion of the carbon electrode. Equation VII describes the oxidation of the grid by the evolved Br_2 . Equation VIII represents the subsequent chemical reaction of AlBr_3 with Br^- from the electrolyte to form AlBr_4^- ion.



Results suggest that the explosion which can occur when a lithium/sulfur dioxide cell is charged may result from a combination of events. First, very reactive lithium metal, in the form of high-surface area dendrites, is deposited on the lithium electrode. This metal then reacts with the SO_2 in the electrolyte to cover each dendrite with a layer of $\text{Li}_2\text{S}_2\text{O}_4$. An explosion may then be caused by a run-away reaction involving the finely divided particles of lithium, $\text{Li}_2\text{S}_2\text{O}_4$, SO_2 , and other cell components. This run-away reaction can be initiated in a variety of ways. It is believed that in a high-rate charging experiment, the reaction is most likely initiated by thermal means. The required initiation temperatures are produced by the heat released from a variety of reactions including those between Li and SO_2 , Br_2 and $\text{Li}_2\text{S}_2\text{O}_4$, as well as Li and Br_2 , and Al and Br_2 . Additional heating is caused by the cells' resistance to the flow of current (I^2R heating). Monitoring of cell

temperature during charging and theoretical studies of cell heat balance (calculations involving heat added, heat lost, and cell heat capacity) support this hypothesis for "normal" charging.

Although the thermal explanation for initiation is quite straightforward and can account for most of the observed behaviors, it should be pointed out that other possible explanations exist. For example, the explosions can sometimes occur in charged cells by application of a physical blow. In this case the initiation could be attributed to mechanical shock.

It is the goal of this study to gain a quantitative understanding of the relationship between charging and subsequent hazardous reactions or explosions of lithium/sulfur dioxide cells. Some progress has been made in reaching this goal in the work described herein and additional results of electrical tests to be reported in a forthcoming document [3]. Although results to date have not been shown to be entirely reproducible, the variations which can and do occur are most likely related to differences in cell design and history. Until this matter is completely resolved there remains a degree of uncertainty between "probably safe" and "clearly dangerous" cells under conditions of charging. For this reason, extreme care should be taken to avoid charging lithium/sulfur dioxide cells.

TABLE I. EXPERIMENTAL CONDITIONS FOR CELL TESTS

Analyzed electrodes from lab and commercial cells in 3 states

- Undischarged
- Discharged 20%
- Discharged 20% and then charged

Conditions for discharge/charge

<u>Parameter</u>	<u>Lab Cell</u>	<u>Commercial Cell</u>
Discharge current	10 mA	66 mA
Discharge duration	2 hrs.	24 hrs.
Discharge output	20 mAh (20% DOD)	1.6 Ah (20% DOD)
Charge current	100 mA (20 mA/cm ²)	10 A (20 mA/cm ²)
Charge duration	8 - 15 min.	8 - 15 min.

References

1. "Safety of Lithium-Sulfur Dioxide Batteries Under Pulsed Load Profiles," Lawson, D.D. and Frank, H. Interim Report No. JPL D-2126, May 4, 1984.
2. "Safety Hazards Associated with the Charging of Lithium/Sulfur Dioxide Cells," Frank, H., Halpert, G., and Lawson, D. (Jet Propulsion Lab), Barnes, J. and Bis, F. (Naval Surface Weapons Center), Journal of Power Sources, 18, pp 89-99, (1986).
3. "Safety of Lithium-Sulfur Dioxide Batteries Under Pulsed Load Profiles," final report in progress, April 1987.
4. "The Analysis of Lithium Anode Surface Films in the Lithium-Sulfur Dioxide Cell Using Diffuse Reflectance Fourier Transform Spectroscopy," Anderson, M., Spectroscopy, 2, No. 2, pp 54-58 (1987).
5. "Characterization of Reactions and Products of the Discharge and Forced Overdischarge of Li/SO₂ Cells," Rupich, M. W., Pitts, L., and Abraham, K.M., J. Electrochemical Society, 129, No. 9, pp 1857-1861, (1981).
6. "Reactions at the Anode During Storage of Partially Discharged Li/SO₂ Cells," Abraham, K.M. and Pitts, L., Accelerated Brief Communication, J. Electrochemical Society, 130, No. 7, pp 1618-1620, (1983).
7. "Chemical Reactions in Lithium Sulfur Dioxide Cells Discharged at High Rates and Temperatures," Bowden, W.L., Chow, L. Demoth, D.L. and Holmes, R.W., J. Electrochemical Society, 131, No. 2, pp 229-234, (1984.)
8. "Investigation of Li/SO₂ Cell Hazards II Thermal Decomposition Studies of Discharge Products," Kilroy, W. P., J. Electrochemical Society, 132, No. 5, pp 998-1005, (1985).

ORIGINAL PAGE IS
OF POOR QUALITY



FRESH



DISCHARGED



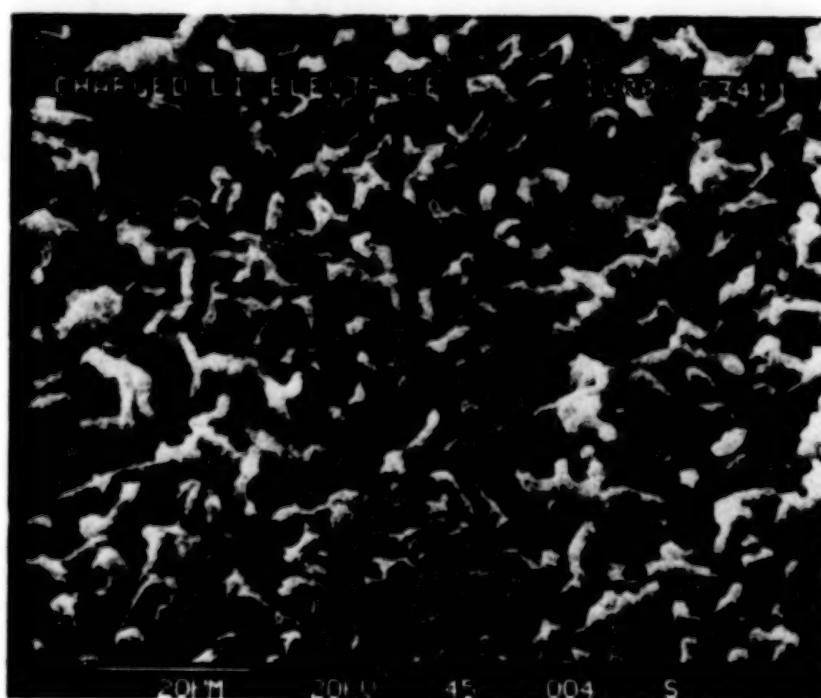
DISCHARGED
AND CHARGED

Figure 1. Sem of Lithium Electrodes 1.

ORIGINAL PAGE IS
OF POOR QUALITY



CHARGED (200X)



CHARGED (1000X)

Figure 2. Sem of Lithium Electrodes II.

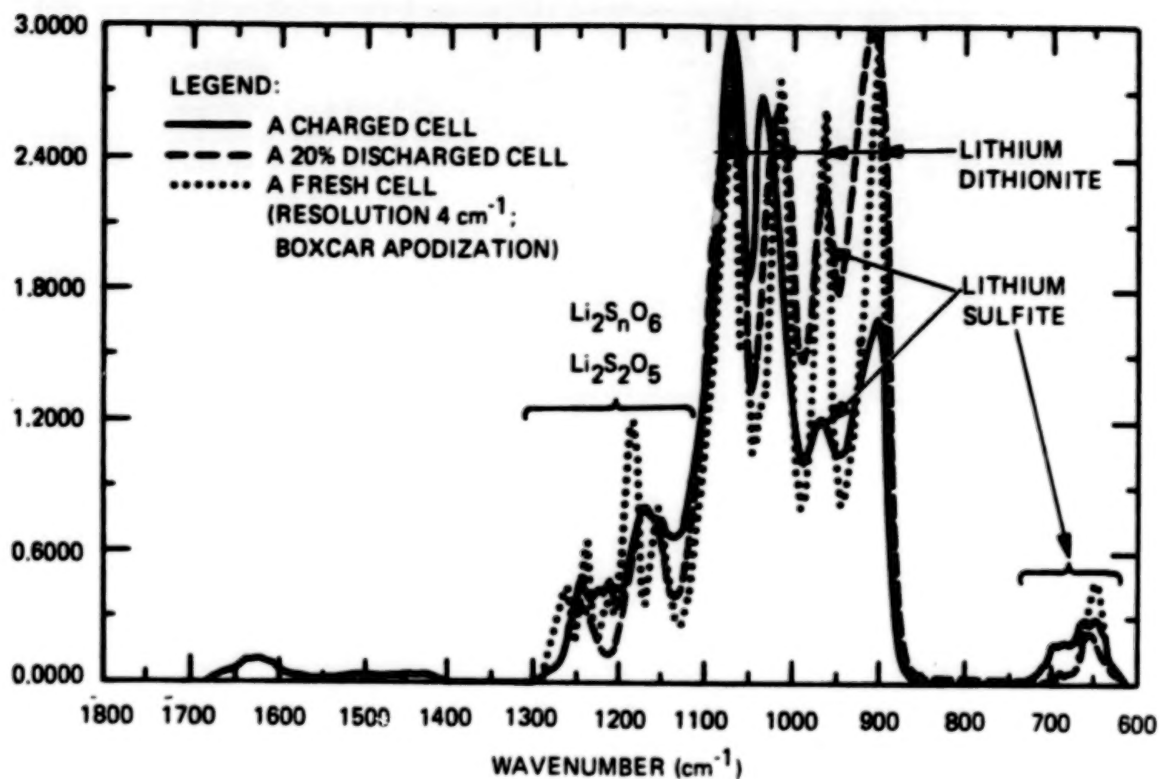


Figure 3. Infrared Spectra of Lithium Electrodes.

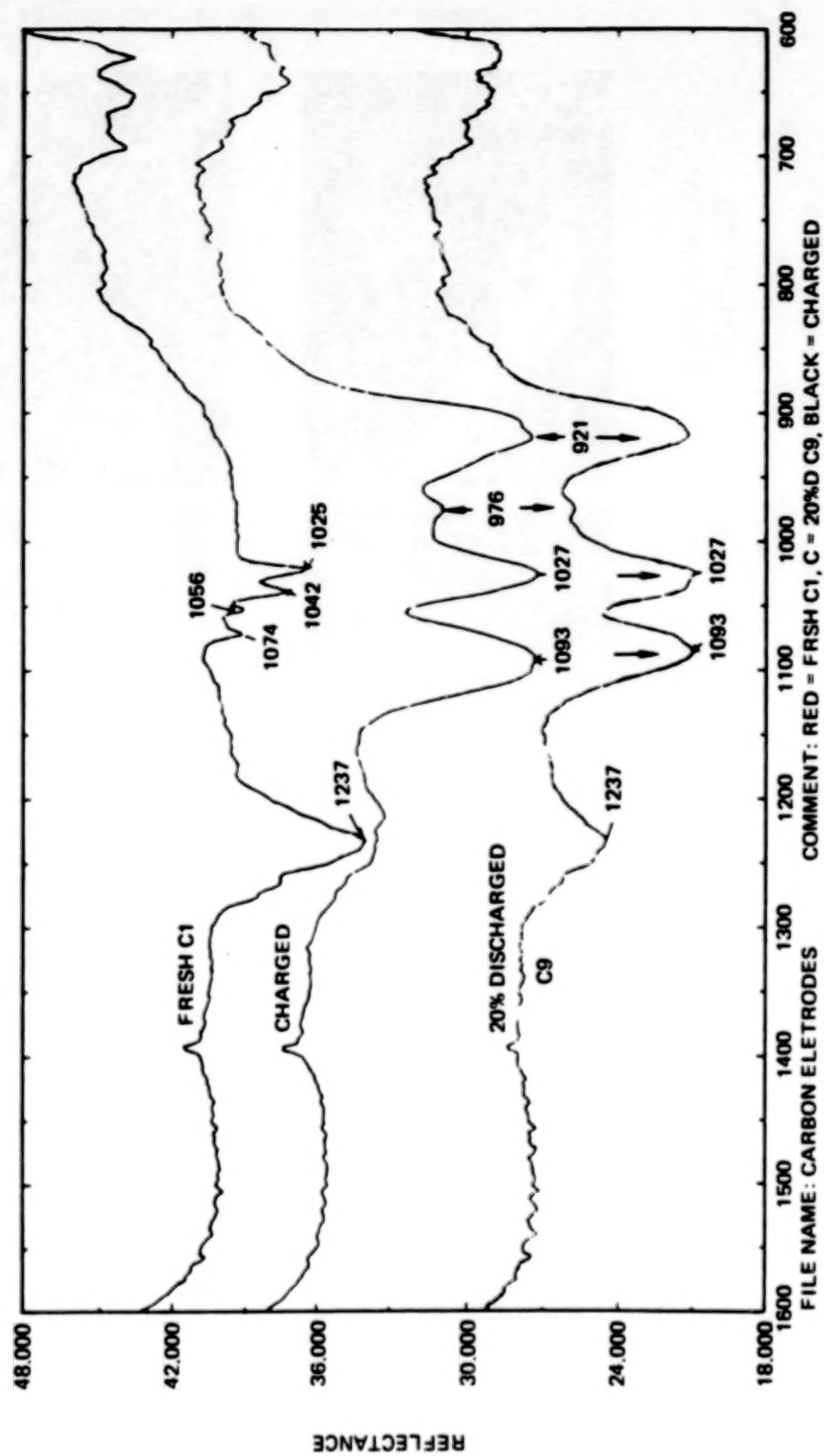


Figure 4. Infrared Spectra of Carbon Cathodes.

DISCHARGED



350X

DISCHARGED
AND
CHARGED



CHARGED
EXCESSIVELY



50X



Figure 5. Effect of Charge on Aluminum Cathode Grid.

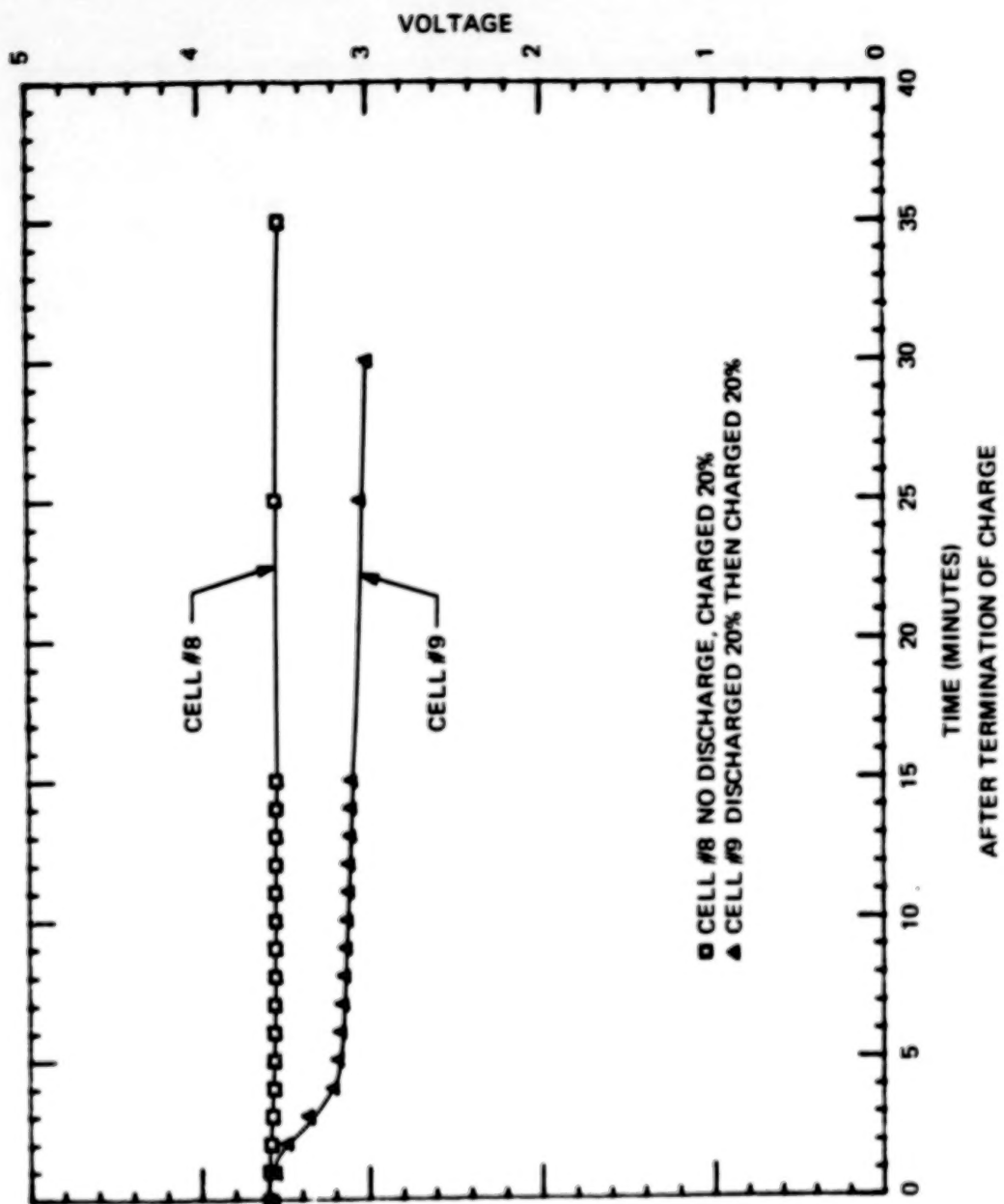


Figure 6. Voltage Decay After Charging.

SESSION II

NICKEL-HYDROGEN TECHNOLOGY

Chairman: L. Thaller, NASA/LeRC

PRECEDING PAGE BLANK NOT FILMED

BATTERY DEVELOPMENT AND TESTING AT ESA

Jean Verniolle
Energy Storage Section
European Space Research and Technology Center
European Space Agency

ABSTRACT

The principal activities of the Energy Storage Section of the Space Research & Technology Center (ESTEC) of the European Space Agency are presented. Nickel-hydrogen and fuel cell systems development are reported. The European Space Battery Test Center (ESBTC) facilities are briefly described along with the current test programs and results obtained.

INTRODUCTION

Whereas nickel-cadmium batteries have been used for the vast majority of past ESA spacecrafts, the enormous diversification in energy storage requirements for future missions such as COLUMBUS (the European contribution to the US space station), HERMES (the European Space Transportation Vehicle) and deep space scientific missions, has led to a rapid increase in development activities for new energy storage systems.

The majority of test programs in the ESBTC involves nickel-cadmium batteries but the situation will change as prototype hardware from the new system developments is delivered for evaluation.

ESA BATTERY DEVELOPMENT ACTIVITIES

The main activities are summarised in Table 1. Nickel-hydrogen and fuel cell systems development will be described in more detail.

The growing interest in deep space missions has led to studies of suitable primary power sources. Work has started on the adaptation of lithium sulfur dioxide cells for such applications.

The high energy density prospects, coupled with encouraging lifetime and reliability data, brought ESA to start feasibility studies on using sodium-sulphur batteries for various types of mission.

Ni-H2 IPV CELL DEVELOPMENT FOR GEOSTATIONARY APPLICATIONS.

ESA is providing support in certain area to the Ni-H2 individual pressure vessel (IPV) cell development for GEO applications headed by the French national space center (CNES) under a substantial Research and Development program with SAFT.

The key features of the Ni-H2 cell developed by CNES are presented in Table 2 and figure 1. The cell, which operates at a maximum pressure of 75 bars and covers the capacity range 30-50 Ah is notable for the one-piece sleeve. This is an integral part of the mechanical cell design contributing to the high safety factor of 4. The sleeve is of course an integral part of the cell thermal design as well. This sleeve concept also offers a small mass saving over the conventional split-sleeve design.

The nickel electrodes are fabricated by the aqueous electrochemical impregnation process, the reproductibility of which has been improved by greater control of the impregnation bath parameters. Individual electrode capacity is 1.90 Ah at 20°C in flooded KOH which gives a value of 0.146 Ah/g and 0.044 Ah/cm². The 50 Ah cell has an energy density of 50 Wh/Kg and a volumetric energy density of 70 Wh/l.

ESA has been in charge of the development of a thermal model of the cell-sleeve assembly. A 59-node computer model (SINDA program) has been developed by Aerospatiale and indicates that a 5°C maximum temperature gradient between cell stack and inside pressure vessel will exist during 70 % D.O.D geostationary cycle conditions with a recharge factor of 1.2. A thermal vacuum test will be carried out to validate this result.

This test is part of a large CNES validation test program on the 50 Ah cell, due to be completed by December 1987. The final step will be a qualification program to be finished in mid 1988.

GEO Ni-H2 BATTERY ENGINEERING MODEL DEVELOPMENT.

The geometry of nickel-hydrogen cells requires that careful consideration be given to thermal and structural battery design. Furthermore due the volumetric energy density disadvantage compared to Ni-Cd, particular attention is required to maximise the packing density of the cells into the battery assembly. Finally, the battery mass to total cell mass ratio has to be kept as low as possible.

ESA has a development contract with BRITISH AEROSPACE (U.K) and SAFT (F) for the manufacture and testing of a battery engineering model designed to a European communication spacecraft specification. The design concept is presented in figure 2. The cells are bounded to an Al thermal sleeve (either of a split or one piece concept) mounted

via a flange to a light support base plate to the opposite side of which is mounted a thin radiator plate. A cavity is provided in the thickness of the base plate so that the cell, with its terminals positioned downwards partially projects into it. Protection by-pass diode circuitry using the base plate as heat sink is provided for each cell. This packaging concept couples good thermal design with a very short harness length. The design accommodates SAFT 81 mm diameter cells in the 40-50 Ah range.

Ni-H₂ CPV DEVELOPMENT FOR LEO APPLICATIONS

ESA secondary batteries for current LEO spacecrafts such as ERS-1 and EURECA are based on Ni-Cd technology. Qualified cells up to 40 Ah are now available in Europe. Nevertheless a 50% saving in battery mass might be expected if nickel-hydrogen cells were used instead.

ESA Ni-H₂ technology development for LEO applications is primarily driven by the COLUMBUS project where power levels in the range of 5 Kw to 20 Kw are required. An investigation of alternative Ni-H₂ technologies (IPV, CPV, Bipolar) that could satisfy COLUMBUS needs was performed by HARWELL (U.K) (1) and led to a preference of Ni-H₂ CPV (Common Pressure Vessel) cell option.

A contract for the design and validation of a complete 80V, 3.3Kw CPV Ni-H₂ battery module including integral active thermal management and with a lifetime requirement of 18000 to 30000 cycles, was awarded to MARCONI SPACE SYSTEM (U.K) with HARWELL (U.K) as a subcontractor.

An initial design trade-off study led to the selection of a battery based on a spherical, 50 Ah dual-stack CPV cell. The cell design is shown in figure 3a. The final choice had been between this concept and a more conventional cylindrical 2-stack CPV design (figure 4a).

Both cells operate at 40 bar maximum with an Inconel 718 pressure vessel and incorporate LEO and CPV design requirements. Concentric current collectors are used, which in conjunction with the end plates fully contain each stack. This containment is mandatory to avoid any electrolyte bridging or electrolytic corrosion of the pressure vessel. Water transfer, caused by migration of free oxygen, is controlled by recombining any oxygen within the cell from which it was produced. The electrode expansion during cycling is accommodated by a system of Belleville washers. The stacks include electrolyte reservoirs. A good thermal link is provided between the two stacks in order to have isothermal stacks and the stack thermal design is such as to maintain a temperature difference between the stack and the pressure vessel at less than 8 deg.C.

The geometrical difference between the two designs arises from a radical change of the thermal design (figures 3b, 4b). In the cylindrical design the stack is cooled at its outer periphery, via a hydrogen gap, through the pressure vessel wall to the thermal sleeve. In the spherical design the stack is cooled via an insulated central support tube, itself supported on a thermally conductive pillar. The rest of the pressure vessel can then be designed to the lightest possible geometry. Although the cooled contact area is smaller than in the conventional design, it is possible to provide a much better thermal contact with the stack. This thermal and mechanical design uses electrodes of a larger diameter (120 mm as opposed to 84 mm selected for the cylindrical cell).

Another feature of the spherical design is that the 2 contained stacks are independent units which greatly simplifies the cell assembly. The stacks are supported to the central Inconel tube, which also acts as a tie rod, via the positive inner current collector and the series connection is performed by connecting the inner collector of one stack to the outer collector of the other one as opposed to the cylindrical design where the central tie rod forms the series connection.

The expected energy density for both optimised designs is around 43 Wh/Kg (including the sleeve).

The two cell designs lend themselves to rather different battery packaging schemes:

- Cylindrical design

The cell is centrally mounted by a short thermal sleeve, itself coupled to a mounting plate incorporating a fluid loop or heat pipes.

- Spherical design

The cells are mounted on either side of a support plate by means of a mounting flange at the base of the thermal pillar. The plate is formed in two halves sandwiching an active cooling loop or heat pipes.

Thermal analysis of the cell and of the mounting plate for both designs at 40% DOD indicates that in order to maintain a maximum cell stack temperature of 20 deg.C, a mounting surface temperature of 5.7 deg.C is required for the spherical CPV which then shows an inside maximal thermal gradient of 6.2 deg.C whereas the figures for the cylindrical gives 7.7 deg.C and 5.3 deg.C.

The volumetric energy density is of course lower for the spherical CPV cell (32 Wh/l against 45 Wh/l) but the overall battery volume is about the same for both battery modules because of the lower foot print area of the spherical CPV on the supporting plate, which still leaves room for protection diode circuitry.

FCS AND RFCS PRE-DEVELOPMENT

For a manned re-entry vehicle such as HERMES, with mission durations up to 28 days, a primary Fuel Cell System (FCS) is the only realistic choice of power source.

Of the electrochemical secondary power sources that can be considered for longer term high power applications in LEO (such as COLUMBUS AOC (Advance Orbital Configuration), a Regenerative Fuel Cell System (RFCS) appears to be a promising choice. This system consists of a O₂-H₂ fuel cells to provide energy to the spacecraft during eclipse periods and of an electrolyser which regenerates the O₂ and H₂ reactants during sunlight periods by electrolysis of the water produced by the fuel cells.

ESA is presently running pre-development studies for both applications. It is intended that the fuel cell system chosen for HERMES will also be used in the RFCS. Design requirements are presented in table 3.

The different Fuel Cell Systems under consideration are alkaline (with mobile or immobile KOH electrolyte) or acid (with Solid Polymer Electrolyte [SPE]).

For the regenerative fuel cell system design trade-off studies of these different fuel cell options, coupled with electrolyser and ancillary mechanical sub-systems (gas-liquid separators, reactant storage technologies, pumps) are presently underway. One of the RFCS concepts proposed by DORNIER is presented in figure 5. This design is based on a mobile KOH system which is representative of the state of the art in Europe. The KOH electrolyte loop participates in the thermal management of both fuel cell and electrolyser and a gas/electrolyte separator is necessary. The reactant gases are stored in pressure tanks provided with electrical heaters to prevent condensation of water.

The main steps in both FCS and RFCS development are as follows:

- Selection of system concept: KOH (mobile-immobile); SPE
- System design trade-offs
- Optimization of the water removal system
- Development of reliable separators for space
- Optimisation of heat rejection concepts
- Selection and testing of materials
- Optimisation of system architecture
- Acquisition of lifetime data.

TABLE 1: MAIN ESA ELECTROCHEMICAL POWER SOURCES DEVELOPMENT PROGRAMS

ITEM	TYPE	DEVELOPMENT	APPLICATIONS	PRIME/SUB CONTRACTORS
Ni-H ₂	GEO	30-50 Ah IPV + ONE PIECE SLEEVE	TELECOM. SATELLITES	SAFT/AEROSPATIALE (F) UNDER CNES MANAGEMENT
		40-50 Ah BATTERY E.M.	TELECOM. SATELLITES	BAe (UK)/SAFT (F) ELECTRONIK CENTRALEN (DK)
Ni-H ₂	LEO	50 Ah CPV 80 V. 3.3 KW BATTERY MODULE	COLUMBUS IOC	MARCONI/HARWELL (UK)
RFCS	LEO	TRADE-OFF DESIGN STUDIES KOH (MOBILE- IMMOBILE) SPE	20 KW MODULE COLUMBUS AOC	DORNIER SYSTEM (D)
PCS	VEHICLE		4 KW MODULE HERMES	
Li PRIMARY	DEEP SPACE PROBES	10 Ah D-SIZE CELL 8 YEARS SHELF LIFE C/4 RATE	TITAN PROBE (CASSINI)	BTC VENTURE (UK)
Na/S	LEO	EVALUATION	BASIC DEVELOPMENT	TO BE CHOSEN
	GEO			

TABLE 2 : CNES-SAFT Ni-H₂ CELL KEY FEATURES.

MECHANICAL	ELECTROCHEMICAL
<p>Pressure vessel: Thin walled 81 mm in diameter with 2 hemispherical end caps</p> <p>Material: Inconel 718 heat treated</p> <p>Stack: Back to back circular with flats supported on a central tie rod and two rigid end plates. Belleville washers to accommodate stack expansion</p> <p>Terminals: Ceramic feedthrough with Ni plated braze. Both located at one end cap</p> <p>Filling Tube: 45 deg. off-set</p> <p>Hydrogen pressure: 5/ P/ 75bars</p> <p>Sleeve: One piece Light Al alloy</p> <p>Safety factor: 4 at for cell+sleeve 2.5 mini. for cell only</p>	<p>Positive electrode: Nickel plated perforated steel substrate. Ni(OH)₂ electrochemically impregnated on sintered Ni powder</p> <p>Negative electrode: Expanded Ni grid substrate Porous layer of active C with Pt catalyst. Hydrophobic porous PTFE</p> <p>Separator: Non woven polyamide felt extending to vessel wall</p> <p>Gas screen: Woven nylon</p> <p>Electrolyte: KOH 7.3 N</p>

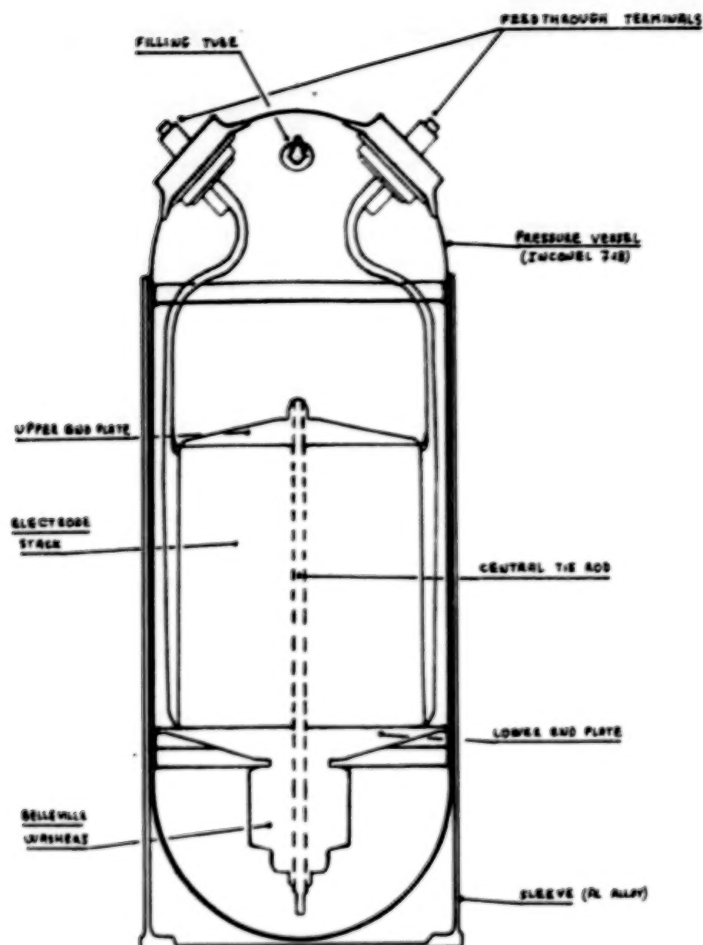


Figure 1. CNES-SAFT 50 Ah Ni-H₂ Cell.

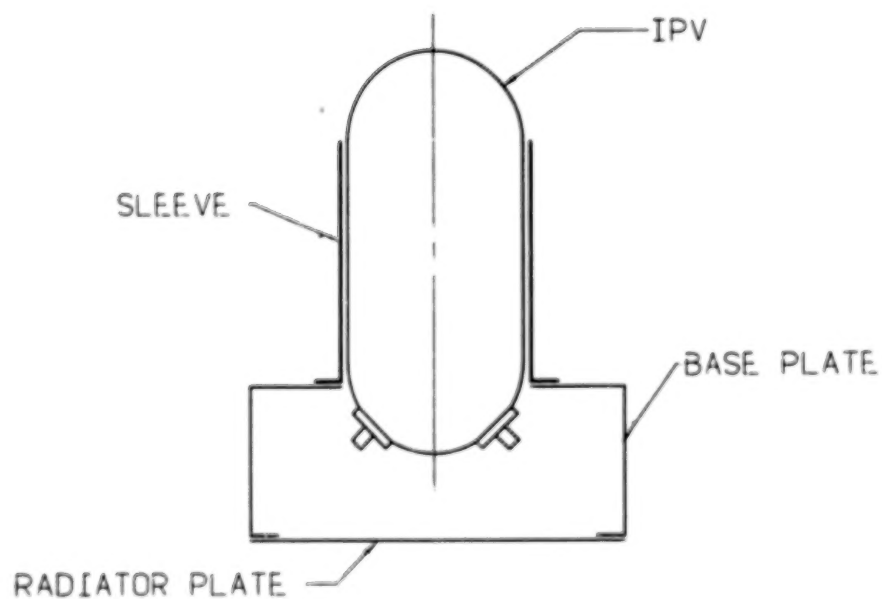


Figure 2. Ni-H₂ Battery Design Concept.

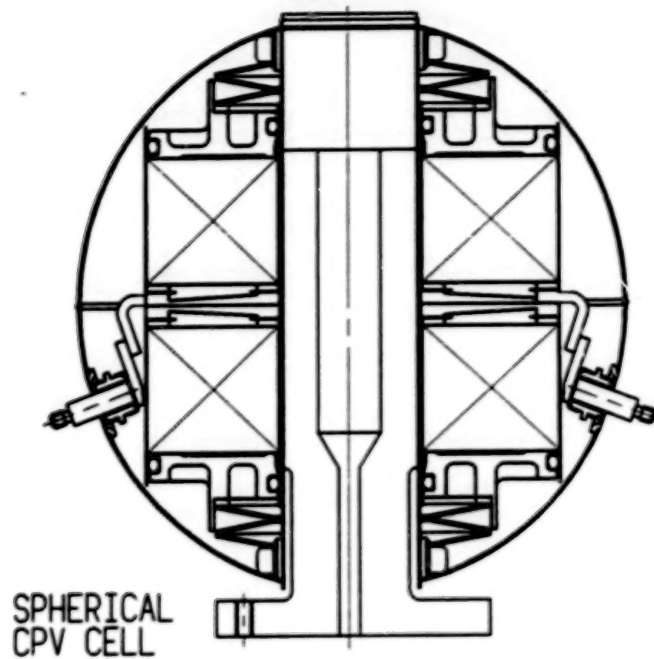


Figure 3a. Spherical CPV Cell Design.

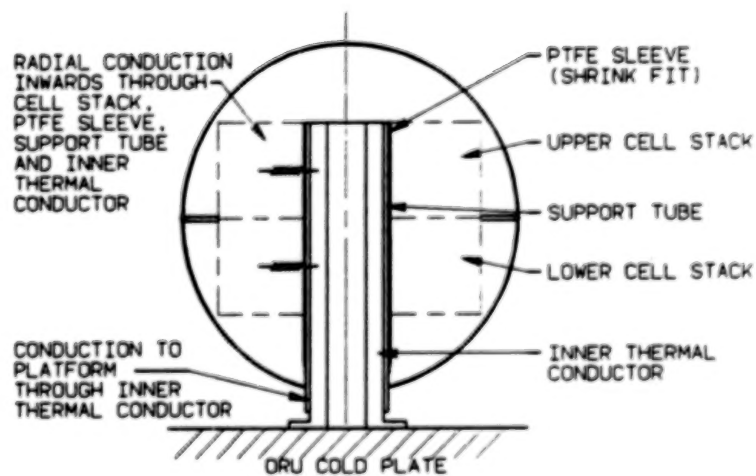


Figure 3b. Spherical Cell Thermal Design Concept.

CYLINDRICAL
CPV CELL

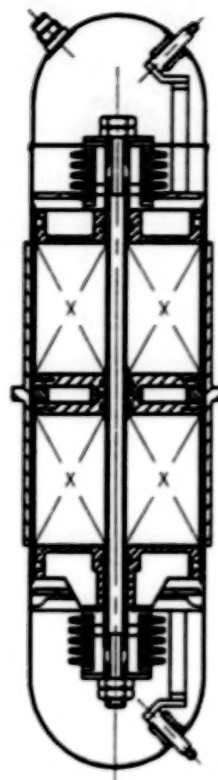
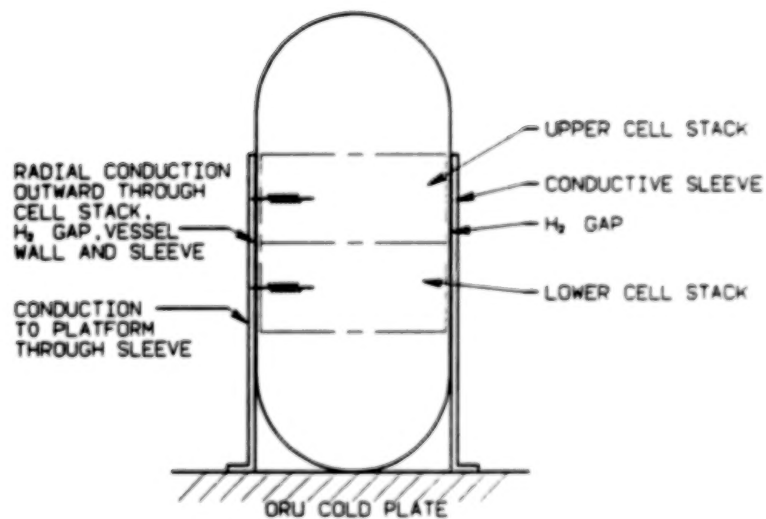


Figure 4a. Cylindrical CPV Cell Design.



CONVENTIONAL CELL STACK THERMAL DESIGN

Figure 4b. Cylindrical Cell Thermal Design Concept.

ORIGINAL PAGE IS
OF POOR QUALITY

TABLE 3: COMPARISON OF MAIN DESIGN REQUIREMENTS

	HERMES	COLUMBUS AOC
AVERAGE POWER LEVEL	4 kW	20 kW
VOLTAGE LEVEL	85-135 VDC	150 VDC
MISSION DURATION	11 (28) DAYS	5 YEARS
OPERATING TIME BETWEEN MAINTENANCE	30 DAYS max.	90 DAYS min.
ORBITAL REPLACEMENT UNIT	NO	YES
OPERATION DURING LAUNCH	YES	NO
REACTANT STORAGE	CRYOGENIC	PRESSURE TANK
GAS/LIQUID SEPARATOR	YES	YES

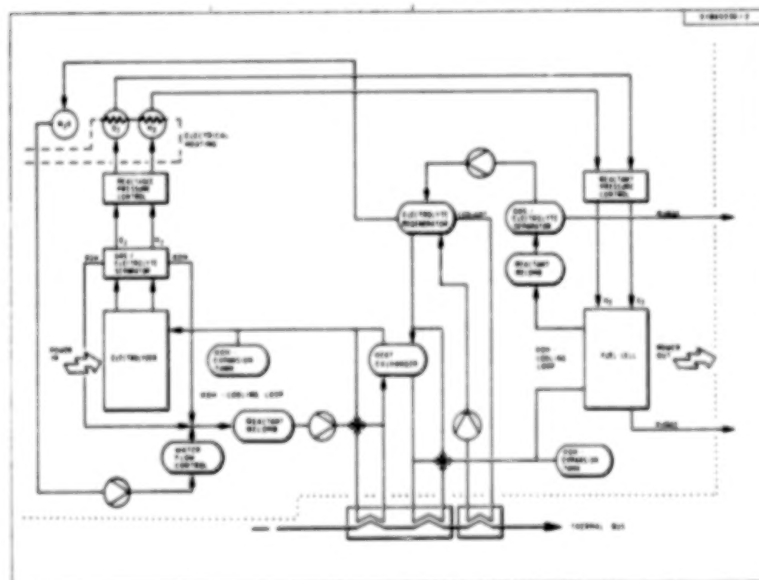


Figure 5. Mobile KOH RFCS.

ESTEC BATTERY TEST ACTIVITIES

The main test activities are presented in table 4. These include battery lifetime tests, product comparisons, battery management evaluations and support to spacecraft projects. All these tests are performed at ESTEC in the European Space Battery Test Center.

In addition to these tests, experimental cell thermal studies are carried out under contract.

EUROPEAN SPACE BATTERY TEST CENTER (ESBTC)

Commissioned in 1978, the ESBTC is a large automated test facility designed to monitor up to 100 test stations, with a total capability of 2000 measurement channels (2). The overall ESBTC test control, data acquisition and data processing systems are presented in figure 6. This is based on a dual DEC PDP 11-45 computer which provides test control and data recording on all active test stations.

Measurement channels are scanned as a minimum every 57 seconds. Raw test data are accumulated on magnetic tapes (day tapes) and sent in parallel to an HP-1000F computer dedicated to data processing. Recent data (up to 3 weeks) are stored on large individual disk files rapidly accessible for checking test progress. Periodic data transfer to magnetic tapes is performed for archiving.

In order to obtain the higher level of system flexibility of the system as well as test sophistication now required, the 'centralised' system is in the process of being gradually replaced by a 'decentralised' system. As indicated in figure 6, each test station will be under direct control of a dedicated microcomputer and have its own data acquisition unit. The link to the HP1000F system will be conserved, allowing this machine to continue to be used for fast processing and archiving of large data files.

Ni-Cd LEO LIFETIME ASSESSMENT

The relative lack of lifetime data for Ni-Cd batteries under LEO conditions led ESA and CNES to initiate a joint five-year test program called ELAN. The program, started in June 1985, includes battery cycling at different depths of discharge and at different temperatures carried out at the ESBTC, along with destructive analysis of failed cells carried out under contract at an independent laboratory. The batteries are 12-cell assemblies specially designed to be thermally representative of a real spacecraft battery but to enable removal of individual cells in case of failure.

The matrix of the cycling program, including the test conditions are presented in figure 7a. Figure 7b shows a typical battery cycling profile which derives from the French SPOT earth observation program. A 35 mn discharge is performed in two different constant current steps and a 65 mn charge starting at a constant current is terminated at a temperature-compensated constant voltage (tapering technique) which is selectable among 16 different levels to provide control of the recharge factor K.

Figure 8 gives the end of discharge (EODC) cell voltages (based on battery voltages) at the end of the second discharge as a function of the number of cycles. Cycling of 40 Ah cells has just begun and therefore is not mentioned. The arrows indicate when reconditioning was performed along with the determined capacities. As of October 1986, up to 7000 cycles have been completed. As expected, for a given temperature the end of discharge voltage decreases with time, this being more pronounced at high DOD and high temperature. In the case of the 40% DOD test at 5 deg.C a voltage stabilisation is apparent which may be due to reaching a second plateau voltage.

The effect of the reconditioning is visible by comparison of the results from the 2 batteries at 15 deg.C and 20 % DOD. One can see that the voltage for the reconditioned battery is the same as that for the battery at 5 deg. C. This reconditioning has also resulted in the cell voltage remaining at a higher value throughout the cycling. The capacity remains constant as well. It seems that for 25 deg. C. conditions the voltage decay with cycling is more pronounced than at the 3 lower temperature levels investigated.

The test on the G.E cells has just started and the highest values observed remain in the internal resistance difference with the SAFT cells, coupled as well with a lowest DOD (18 %).

TEMPERATURE DERIVATIVE TECHNIQUE EVALUATION TEST

Battery lifetime is strongly dependant on the battery management scheme employed. End of charge termination is particularly important in order to minimize overcharge. The comparative study of different charge control methods is of particular interest for LEO applications where high charge rates are necessary, and a new charge control technique developed at ESTEC and recently awarded a patent(3) is under evaluation at the ESBTC.

This method, called Temperature Derivative Technique (TDT) has been described in more detail in previous publications (4,5). Briefly, charge is terminated when the temperature of specially positioned thermistors passes through a minimum (which precedes the onset of the thermal dissipation at end of charge). This technique makes use of thermal properties fundamental to the cell reactions and reduces in general the amount of overcharge experienced by the cells compared to the more conventional voltage taper charge control method. The

avoidance of taper charge decreases significantly the size of the solar array required for battery charging.

The TDT has been tested under LEO conditions on 3 parallel-connected batteries, each of 14 SAFT 35 Ah cells and having its own TDT detector. The cycling profile consists of a 3-step discharge giving a DOD of 26.7%, and the charge is terminated when the first of the three detectors is activated. The batteries are mounted on a cold plate set at 15°C.

Up to now 16000 cycles have been achieved and encouraging results obtained. Figure 9 gives some of the battery parameters at 500 cycle intervals. Due to some aged electronic equipment dedicated to this test a number of test hardware failure have occurred. These explain the abnormal values in the upper right plot.

The test results show that the 3 batteries present the same behaviour during the course of the cycling. Cell EOCH (end of charge) voltages are nearly identical and cell EODC voltages are within 2%. A slight (5%) difference in K factor values is noticeable. The DOD values were within 3%. The battery temperature differences (up to 1.1 deg.C) are not judged significant. It should be noted that the cells were not matched nor are of space-grade.

The evolution of the test parameters during the 16000 cycles is quite remarkable. The average EODC cell voltages after a period of instability showed a slow downward trend interrupted around cycle 9500 by a change in DOD. The overall decrease is very low, EODC cell voltages varying from 1.22 volts at cycle 500 to 1.17 at cycle 15670. In comparison the ELAN battery at 30% DOD and 15 deg.C, for which the discharge rate is less severe already gives at cycle 5500 an EODC cell voltage value of 1.07 volts. The EOCH cell voltages show a sharp increase during the first 2000 cycles from 1.41 volts to 1.47 volts, followed by a gradual stabilisation around 1.49-1.5 volts. This shows some correlation with the K factor behaviour. The marked rise for cycle 9500 in the temperature plots results from changes in the set temperature of the cold plate.

These results confirm the interest and advantage of that charge technique which provides battery charging under steady conditions and consequently may be expected to limit the battery degradation over extended cycling. The battery temperature is reproducible. In this paralleled batteries test, thermal balance is also maintained between the batteries. Balanced electrical performances are then observed as opposed to previously reported results on a similar test using a tapering method (5).

METAL-HYDROGEN LEO TEST

In an initial investigation of nickel hydrogen cells for future LEO applications, ESTEC has initiated a test to evaluate and compare cells from SAFT and from DAUG (Deutsche Automobil Gesellschaft). Neither design is optimised for this application. In addition a parallel test is in progress using SAFT Ag-H₂ cells.

The test matrix and preliminary results are presented in table 5. All cells are cycled at 40% DOD and a comparison of their behaviour with and without charge tapering will be made.

MARECS ACCELERATED GEO TEST

This test was initiated in 1981 in support of the ESA MARECS (Maritime European Communication Satellite) program, which requires a battery lifetime of 10 years at 57% (max) DOD. It is an accelerated GEO cycling test using 12-cells batteries, one of SAFT VO 21 S3 cells (coming from the MARECS B1 flight production batch) and the other one using General Electric 22 Ah cells.

The test program is presented in figure 10 along with a typical EODC and EOCB battery voltage evolution through one eclipse season. For the first 8 eclipses, battery charging was terminated when a pre-set charge time was reached, to achieve recharge factor of 1.05, or when a voltage limit of 1.49 V per cell was reached. Later it was noticed that the tendency of the batteries was to accept more charge during the second half of the eclipse period. The K factor was then set to 1.10 in order to favor charge termination due to the voltage setting and to allow the natural tendency of an increase in the K factor. In orbit solar array degradation was simulated from the 4 th season by a gradual decrease of the charge current. The solstice simulation period is reduced to 45 days so as to simulate the 10 years of operation in half the time. Battery capacity determination and battery reconditioning are performed prior to the eclipse period. The initial capacities were 26.1 Ah (average) for SAFT cells and 23.36 for the G.E cells

Both batteries are now in their 20 th season, and maintain good performance. Figure 11 shows some battery parameters through the 19 completed seasons. Except for the battery voltages at the end of the reconditioning, the trend in the parameters is the same for both batteries. The plot showing the minimum EODC cell voltages (which occurs during period 5 or 6) indicates a marked degradation up to season 6 followed by stabilisation with a tendency towards improvement noticeable from season 10 where the K factor setting was modified from 1.05 to 1.10. There exists a reproducible voltage difference between the two batteries arising from a internal resistance difference of about 2 milliohms. At season 19 the minimum cell voltages are 1.168 for SAFT cells and 1.19 for G.E cells. No battery

capacity data is available for seasons 1 to 5. Nevertheless the plot indicates no sign of capacity degradation.

Since reconditioning is stopped as soon as the first cell reaches 0.1 volts, the battery voltage at the end of the reconditioning gives information about the matching of the cells in the battery assembly. Both types of cells were initially matched within 3% in capacity. A high battery voltage indicates a larger deviation in voltage amongst the 12 cells at the end of the C/100 discharge. For the SAFT cells one can observe a rapid increase in the deviation followed by a stabilization. For the G.E cells this deviation was reduced at the beginning but has increased somewhat since.

Ni-Cd HIGH DOD GEO LIFETIME ASSESSMENT.

Useful Ni-Cd battery energy density for GEO spacecrafts are usually about 20 Wh/Kg. This results from a limitation of the battery DOD to a maximum value of 60%, chosen conservatively to meet lifetime requirements.

From Marecs test and in flight data it appears that higher DOD values may be used. ESTEC has initiated an accelerated test program on three spare ECS-1 (European Communication Satellite) battery models (28 SAFT 18 Ah cells) on a cold at 3 deg.C. The test sequence is identical to that of the MARECS test, except that the maximum DOD's are respectively 100%, 90% and 70% of nameplate capacity.

Results for the first 5 seasons are presented in figure 12. The degradation of the minimum end of discharge cell voltage is low and if trend remains linear one would expect to achieve 20 seasons above a minimum cell voltage of 1 volt.

THERMAL CHARACTERISATION OF SPACE BATTERY CELLS

The thermal design of batteries becomes particularly important in LEO spacecrafts because of the strong negative impact of increased temperature on lifetime. In order that the necessary cell-level thermal data is available for use in battery design a flow calorimeter has been developed under ESA contract by ElektronikCentralen (DK). Figure 13 shows the calorimeter version adapted to high capacity cells. Complete cells are cycled totally immersed in the calorimeter and the results deconvoluted to remove effects due to non-ideality of the calorimeter. In the case of nickel-cadmium cells, measurements have also been made of the thermal conductivity along the X and Y cell directions and of the thermal capacity at various states of charge. This data has been used to establish a dynamic thermal model of the cells.

As an example figure 14 shows the instantaneous heat transfer across the surface of a SAFT 40 Ah Ni-Cd cell during a LEO cycle at 40% DOD. Similar heat transfer characterisations have also been performed on SAFT Ni-H₂ cells during GEO cycles and on SAFT Ag-H₂ cells during LEO cycles (figures 15 and 16).

ACKNOWLEDGEMENTS

My acknowledgements are addressed to G. Dudley and all the other ESTEC members who provided me with help in preparing this presentation.

REFERENCES

- 1 ESA-CR(P)-2106-VOL-2
- 2 G.J Dudley, F. Baron : Space Battery Testing in ESTEC
ESA BULLETIN No.48, November 1986
- 3 ESA Patent/1.2/MM/6838 (H.J Spruijt)
- 4 H.J Spruijt: Temperature Derivative Technique.
Proc. 16th. Power Electronic Specialists Conference,
Toulouse (France), June 24-28, 1985, ed. ESA SP-300, pp.107-121.
- 5 F. Baron : LEO life testing with different charge control.
The 1984 Goddard Space Flight Center Battery Workshop, ed., NASA
CP-2385, pp.343-367

TABLE 4: PRESENT ESBTC MAIN TEST ACTIVITIES

TEST	TYPE	BATTERY	CONFIGURATION	OBJECTIVES
ELAN	LEO	Ni-Cd (SAFT)	20 BATTERIES 12 CELL ASSEMBLY ON COLD PLATE	JOINT ESA-CNES LIFETIME ASSESSMENT PROGRAM COUPLED WITH DESTRUCTIVE FAILURE ANALYSIS
X-80	LEO	Ni-Cd (SAFT)	1 BATTERY 14 CELL ASSEMBLY IN TEMPERATURE CONTROLLED CHAMBER	LIFETIME ASSESSMENT 22500 CYCLES COMPLETED AT 23% D.O.D EODC CELL VOLTAGE STILL ABOVE 1 VOLT
TDT	LEO	Ni-Cd (SAFT)	3 PARALLEL BATTERIES 14 CELL ASSEMBLY ON COLD PLATE	NEW CHARGE CONTROL METHOD EVALUATION
ERS-1	LEO	Ni-Cd (SAFT)	1 BATTERY 12 CELL ASSEMBLY ON COLD PLATE	BATTERY MANAGEMENT ASSESSMENT FOR ERS-1 PROJECT
METAL-H ₂	LEO	Ni-H ₂ (SAFT) Ni-H ₂ (DAUC) Ag-H ₂ (SAFT)	3 BATTERIES 2 CELL ASSEMBLY MOUNTED ON CHASSIS PLACED IN TEMPERATURE CONTROLLED CHAMBER	LIFETIME ASSESSMENT PRODUCT COMPARISON
MARECS	ACC.GEO	Ni-Cd (SAFT) Ni-Cd (G.E.)	2 BATTERIES 12 CELL ASSEMBLY IN TEMPERATURE CONTROLLED CHAMBER	SUPPORT TO SPACECRAFT LIFETIME ASSESSMENT PRODUCT COMPARISON
ECS	ACC.GEO	Ni-Cd (SAFT)	3 EX-FLIGHT MODELS 28 CELL ASSEMBLY ON COLD PLATE	HIGH D.O.D LIFETIME ASSESSMENT
OTS	REAL TIME GEO	Ni-Cd (SAFT)	1 BATTERY 2-14 CELLS MODULES IN SERIE IN TWO DIFFERENT CHAMBERS	REAL LIFETIME FLIGHT SIMULATION

TABLE 5: METAL-HYDROGEN LEO TEST MATRIX

manufact.	DAUG	DAUG	SAFT	SAFT	SAFT	SAFT
type	Ni-H ₂	Ni-H ₂	Ni-H ₂	Ni-H ₂	Ag-H ₂	Ag-H ₂
nom. capacity (Ah)	40	40	42	42	26	26
charge current (A)	(20)	16.6	(21)	17.3	(13)	10.4
charge technic	tap.		tap.		tap.	
disch. current (A)	25.6	25.6	26.8	26.8	16.6	16.6
DOD (X)	40	40	40	40	40	40
cycles completed	2000	2000	1900	2050	1850	1900
k-fact.	1.04	1.04	1.04	1.03	1.01	1.01
efficiency (X)	80	80	82	78	72	72
heat diss.	3.0	3.0	2.8	3.5	2.9	2.9
VBeoc (V)	3.0	3.2	3.0	3.2	3.4	3.5
VBeod (V)	2.3	2.3	2.4	2.3	2.1	2.1
Peoc (bar)	52	57	58	63	60	50
Peod (bar)	38	42	43	50	40	20
TCeoc (deg C)	11.5	10.5	11	11	50	40
TCeod (deg C)	14	14	12	12	30	10
Test parameters:	charge period : 60 min disch. period : 37 min 30 sec mean base plate temp. : 10 - 11 deg.C. each test with two cells in series					

ORIGINAL PAGE IS
OF POOR QUALITY

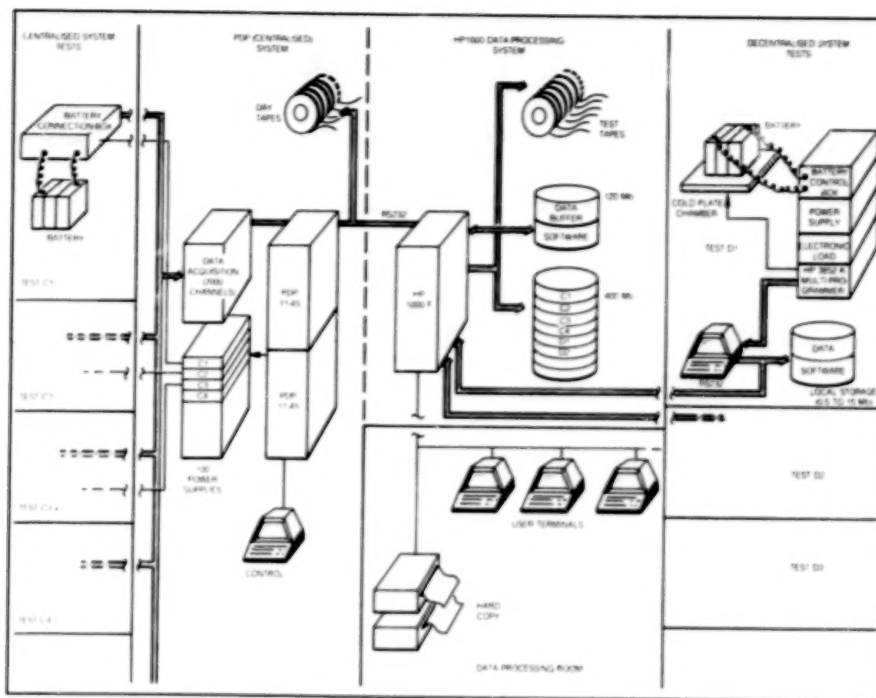


Figure 6. ESBTC Configuration.

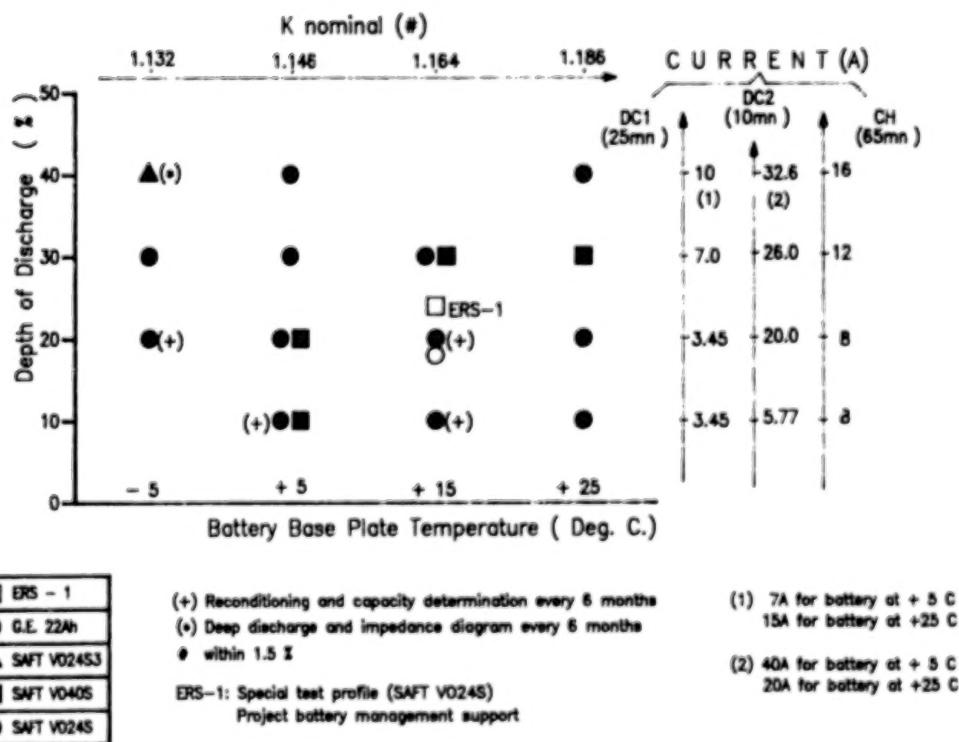


Figure 7a. ESA-CNES Elan Program.

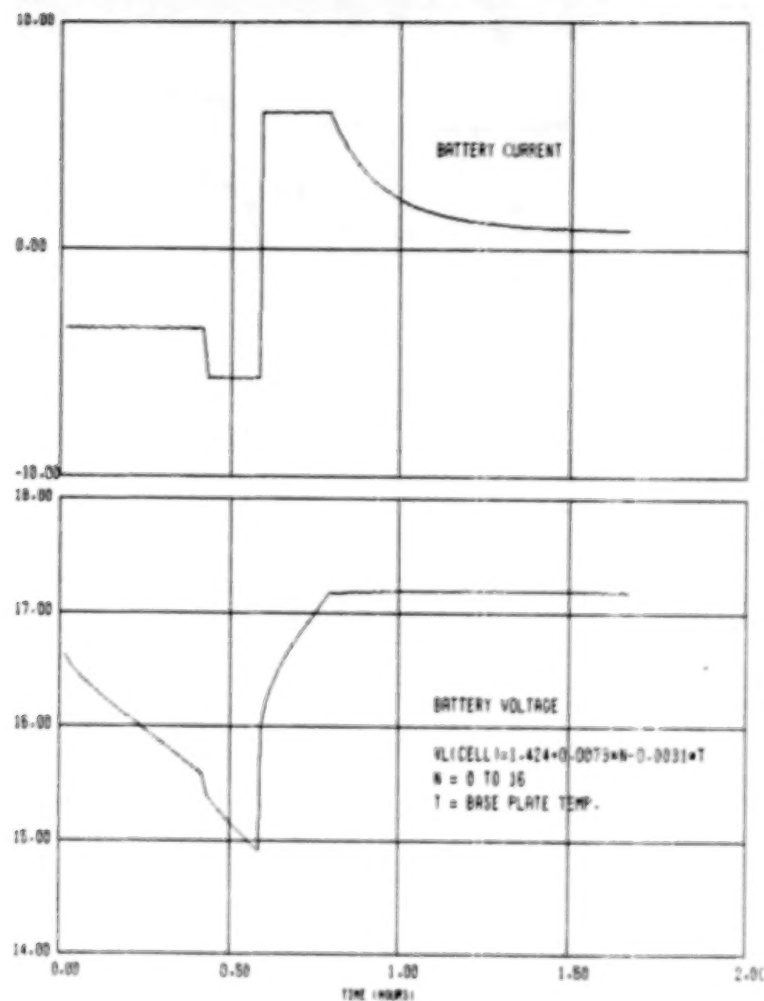


Figure 7b. Typical Elan Cycle Profile.

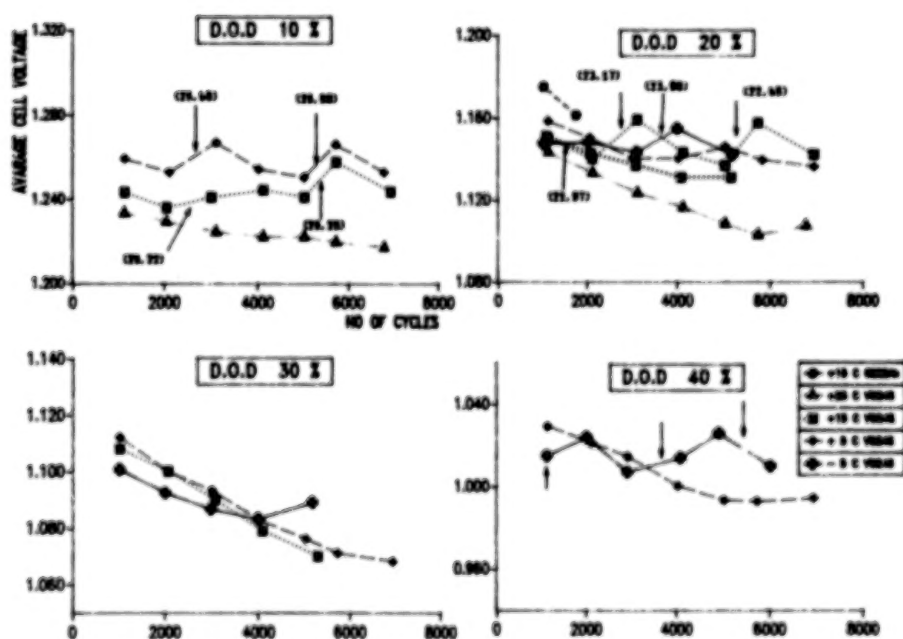


Figure 8. Elan: EODC Average Min. Cell Voltage/No. of Cycles.

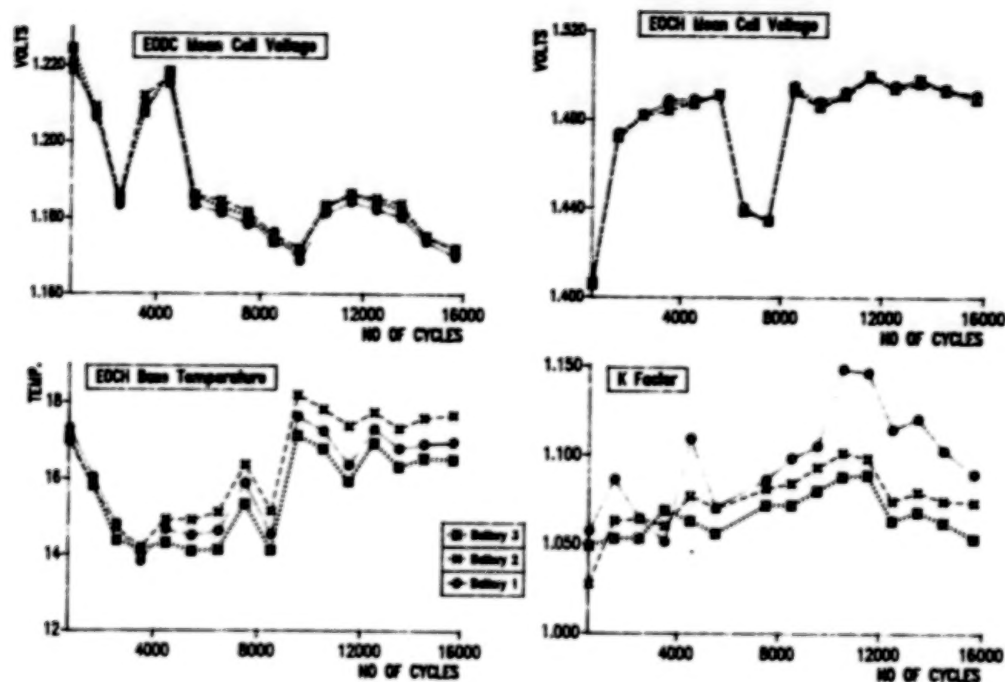


Figure 9. TDT Test Results.

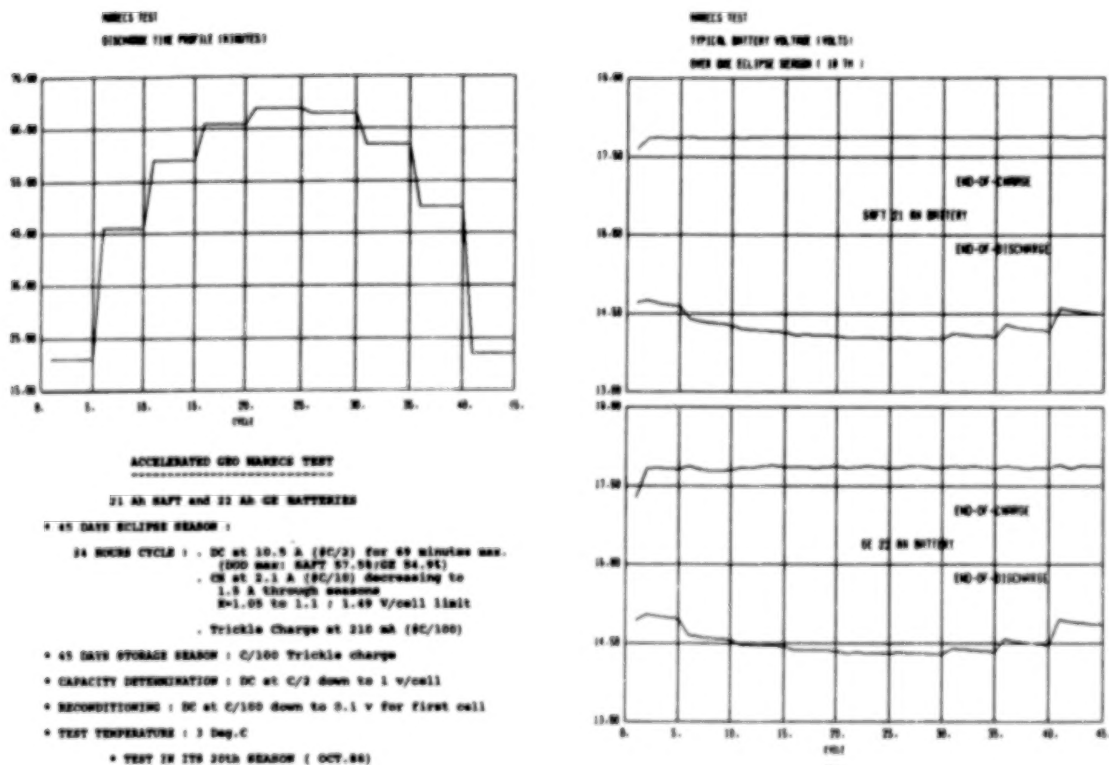


Figure 10. Marecs Test Profile.

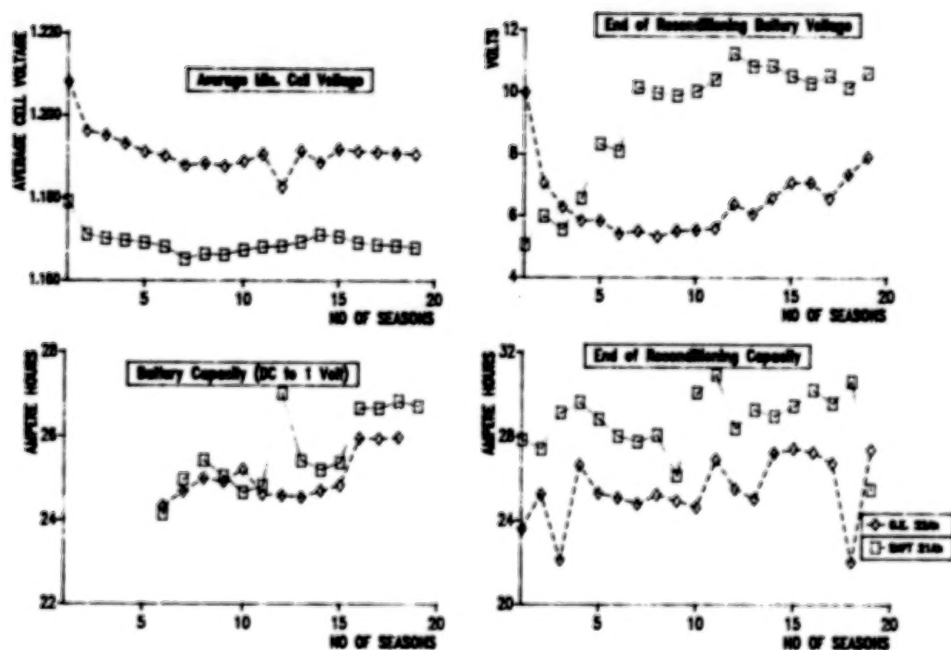


Figure 11. Marecs Test: Parameters Evolution Through 19 Seasons.

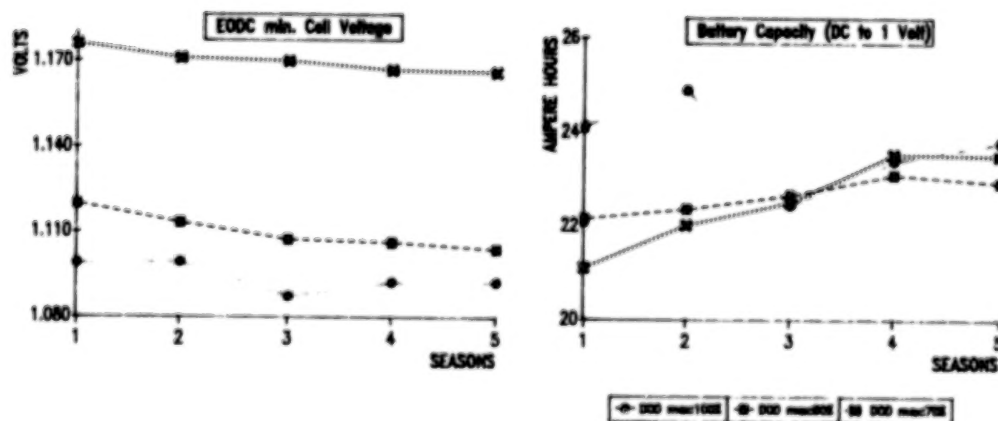


Figure 12. Ni-Cd High DOD Test Results.

ORIGINAL PAGE IS
OF POOR QUALITY

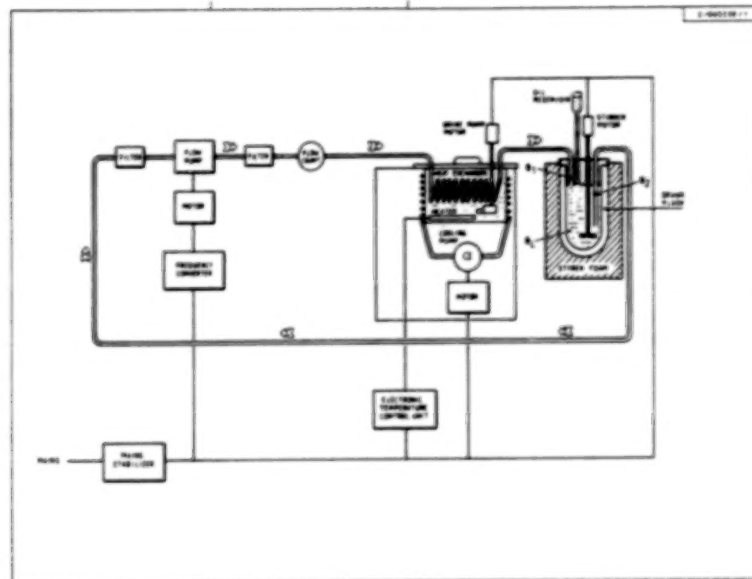


Figure 13. Schema of the Flow Calorimeter.

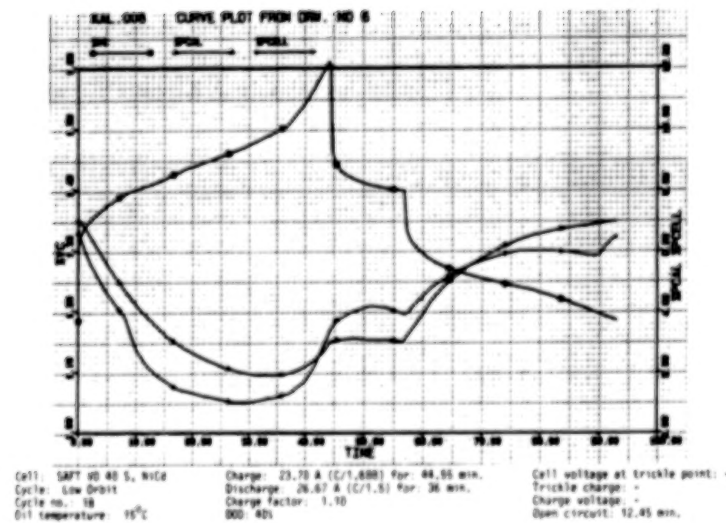


Figure 14. 40 Ah Ni-Cd Cell Heat Dissipation During a LEO Cycle at 40% DOD.

ORIGINAL PAGE IS
OF POOR QUALITY

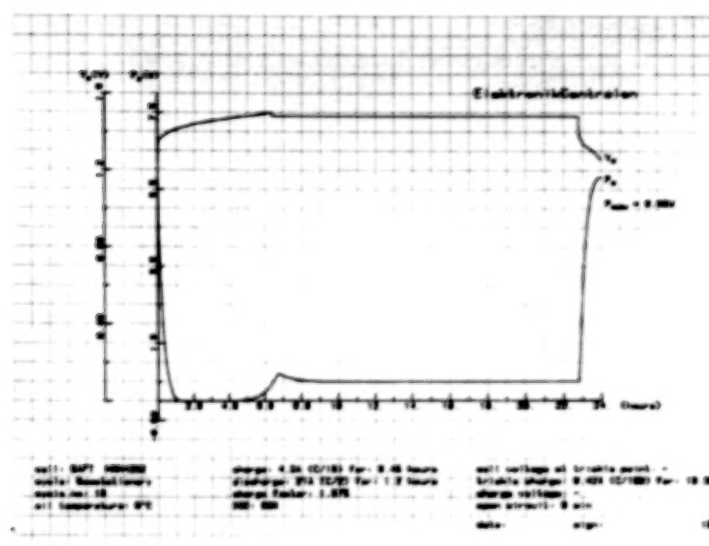


Figure 15. 42 Ah Ni-H₂ Cell Heat Dissipation During a GEO Cycle at 60% DOD.

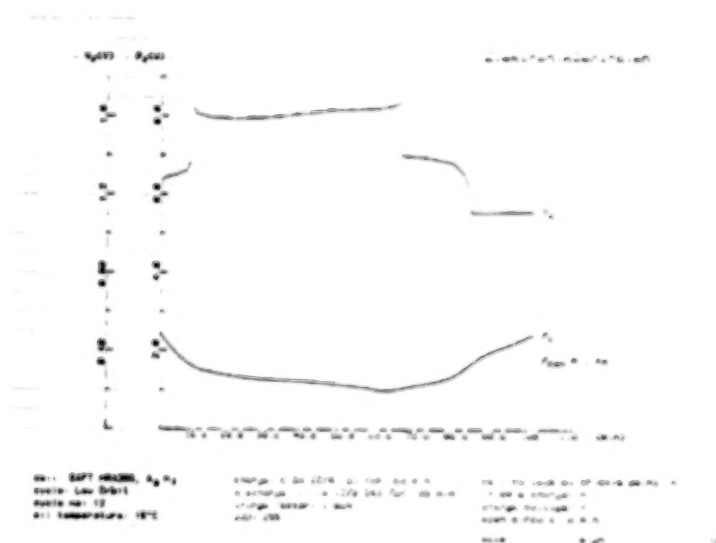


Figure 16. 26 Ah Ag-H₂ Cell Heat Dissipation During a LEO Cycle at 25% DOD.

N88-11028

Nickel Hydrogen Low Earth Orbit
Test Program Update and Status

Paper to be presented at the
1986 NASA/GSFC Battery Workshop

November 18-19, 1986

C. C. Badcock and S. W. Donley
The Aerospace Corporation
P. O. Box 92957
Los Angeles, CA 90009

A. B. Felts and R. L. Haag
Naval Weapons Support Center
Crane, IN 47522

PRECEDING PAGE BLANK NOT FILMED

ABSTRACT

This document describes the current status of Nickel Hydrogen (NiH_2) testing ongoing at NWSC, Crane IN, and The Aerospace Corporation, El Segundo CA. The objective of this testing is to develop a database for NiH_2 battery use in Low Earth Orbit (LEO) and support applications in Medium Altitude Orbit (MAO). Individual pressure vessel-type cells are being tested. A minimum of 200 cells (3 1/2 in diameter and 4 1/2 in diameter cells) are included in the test, from four U.S. vendors. As of this date (Nov. 18, 1986) approximately 60 cells have completed preliminary testing (acceptance, characterization, and environmental testing) and have gone into life cycling.

INTRODUCTION

In the Spring of 1984 a survey of life testing status and results for NiH_2 cells was performed.¹ Data were either available or would be available within the next two to three years to support the use of NiH_2 batteries in high orbits requiring up to 3000 cycles at maximum depths of discharge of up to 80% with a high level of demonstrated reliability and confidence. Calendar life on orbit in excess of ten years was anticipated. It was suggested that optimum performance would be achieved when the temperature of operation was at less than 15 deg. C and the amount of overcharge was minimized while maintaining an adequate state of charge.

On the other hand, the data available to support the use of NiH_2 batteries in low earth (LEO) and mid altitude orbits (MAO) are deficient. The extent of the data base consists of mixtures of technologies and several generations of LEO cell designs. Cells have been tested under extreme conditions with less regard for the limitations of these cells than is normally applied to space-type secondary cells. However, small samples of the most recently built cells when tested under severe conditions (90 m cycle, 80% DOD, 1.4 C discharge, 0.8 C charge, 105% charge return ratio, 23 ± 4 deg. C) have consistently given 10,000 cycles before failure occurred. This suggests that the cells have the capability to surpass the performance of present state-of-the-art NiCd cells in LEO applications. Presently, design variations among NiH_2 cells are beginning to stabilize and future changes are expected to be incremental. Testing to establish reliability and performance appears to be practical at this time.

NiH₂ cells must significantly outperform NiCd cells or they would be disadvantageous to use because of their greater specific volume, higher present unit cost, and the risks inherent in any new design. This increase in performance can be in life and/or usable energy density. Present NiCd batteries used under near-optimum conditions offer 14 - 18,000 cycles at 20 - 25% DOD and 25 - 30,000 cycles at 7 - 14% DOD depending on specific conditions of load profile, power system requirements, and environment with high reliability and confidence. NiH₂ cells must demonstrate significant increases over these numbers if they are to be the next generation of LEO batteries. This life test will demonstrate the performance capabilities of state-of-the-art NiH₂ cells in low earth orbit, and in addition will support their use in mid altitude orbit; and, will provide a database, when combined with other relevant life test data and with program specific testing, that will permit an estimate of reliability at an appropriate confidence level.

Objectives and Goals

The NiH₂ cell life test has the following objectives²:

1. Demonstrate NiH₂ performance in LEO applications and support use in MAO at levels superior to current NiCd capabilities.
2. Develop a statistically significant NiH₂ battery cell database.
3. Disseminate the test data and results in a timely fashion.
4. Demonstrate NiH₂ cell performance in pulse applications.
5. Demonstrate that the Manufacturing Technology Program (MANTECH) cells are capable of performing in high orbit as well as LEO.

It is the intent to test cells from all viable vendors in sufficient numbers to provide a comparison and to establish a statistically significant database with a sufficiently high confidence level. A minimum of 155 3.5 in diameter and 45 4.5 in diameter cells are included in the test plan. Additional cells will be added as the need is demonstrated. Approximately equal numbers of cells from four U.S. vendors (GEBBD, Eagle Picher, Yardney, and HAC) are to be tested in so far as schedule and funding permit.

The goals of these tests are to demonstrate at least 30,000 cycles at 40% DOD and at least 20,000 cycles at 60% DOD in LEO and at least 5000 cycles at

80% DOD in MAO or high orbit. The 40% DOD cycle goal is greater than present NiCd cells can expect to achieve at three years of planned life. A small number of cells (5 from each vendor) will be tested at 25% DOD to provide correlation with present NiCd testing and life data bases. It must be emphasized that cells could fail to reach desired goals, e.g. 60% DOD and 5 years, and still perform significantly better than present state-of-the-art NiCd cells.

A second goal is to establish a minimum reliability of 90% with a confidence level of at least 80% for the goals stated above. This goal requires an additional year of testing beyond the goal periods, if one assumes the improbable condition that none of the groups of ten cells can be statistically combined.

Reports are issued when significant milestones are reached and at regular periods. Each major milestone, e.g. completion of acceptance testing, results in a brief report. The progress of the test shall be reported in an "Annual Report of Cycle Life Testing" from NWSC Crane and will, in addition, be summarized at least once a year and presented in an appropriate forum (of which this is the second). The detailed data will remain available after completion of the test for access by qualified organizations.

Test Plan

The test plan consists of acceptance and pre-life testing (including environmental testing), characterization testing, life testing, and failure and end-of-test analyses. Cell manufacturing specifications, testing procedures, and failure analysis procedure have been fully documented, except for end-of-test analysis which is in preparation.

All the packs in the test will be 10-cell packs except for those (LEO 25% DOD and some 4.5 in. packs) that are meant mainly to correlate with other data bases. The standard sample size of 10 was chosen by a method based on the two-parameter Weibull failure distribution function as a compromise between the high cost of a large sample size and the statistical uncertainties of a small sample size.

Acceptance Testing: Acceptance testing is conducted at NWSC. All cells of the same type and from the same vendor are tested in a single series string whenever practicable. The following tests are performed on all cells:

1. Visual inspection, weight, and dimensions (diameter and length).
2. Indicator leak test (at beginning and end of testing).
3. Conditioning capacity (10°C, repeat until two cycles agree within 2% in capacity).
4. Standard Capacities at -5°, 10°, and 20°C.
5. Impedance at 50% state of charge and 20°C.
6. Overcharge voltage and pressure stability (when available) at 0°C.
7. Capacity loss upon charged stand at 10°C for 72 hours.

The ampere-hour and watt-hour capacities of the cells are reported to 1.20, 1.15, 1.10, 1.05, 1.00, and 0.5 V. at the standard discharge rate (a C rate is used to correlate with the rates used in testing). All temperatures refer to the midpoint along the cell cylinder on the thermal flange.

A 20% sample of the cells of each type (at least two cells) and from each vendor are subjected to random vibration testing at levels 6 dB higher than the highest level anticipated in any application. The cells that are vibrated will be distributed throughout the test packs to determine any long-term effects of vibration.

Characterization Testing: These tests are performed to determine the required charge characteristics. A group of 5 are cells of each type and from each vendor are tested to determine charge efficiencies at selected rates and temperatures. These data along with acceptance data are used to initiate charge control for life testing.

Life Testing: Life testing will be performed using a nominal 90 minute orbit with a 30 min. eclipse period and a 60 min. sun period. Testing will be performed at -5° and 10°C with the latter temperature being baseline. In a corporate program-oriented test at Martin-Marietta Aerospace, 20°C is being used for a group of cells.³ We choose not to duplicate this condition. The charge control method is ampere-hour integration (recharge fraction control). This method is flexible and particularly easy to integrate into a digital control system. In the LEO testing, control is accomplished by

changing the charge returned under a fixed depth of discharge until the following parameters are minimized:

1. The decrease in the end of discharge voltage.
2. The increase in the end of charge voltage (high rate and trickle).
3. The recharge fraction (both watt-hour and ampere-hour).

A limit of a 112% charge return is established to permit the setting of charge rate capability (charge returns of this size are not anticipated during testing.) The charge sequence for LEO will be to return 100% of the charge at the required rate followed by C/5 charging for the remainder of the charge period. The high charge rate is adjusted to set the charge control parameters. A similar approach will be used in MAO but the high charge rate and the final charge rates will be lower. Trickle charge, which is used only in emergencies, will be at C/80 or lower.

Reconditioning is not planned for the cells in LEO testing. MAO testing may require reconditioning to maintain adequate efficiency. No capacity discharges will be performed.

Failure is defined as a voltage of less than 0.50 V at the end of the prescribed discharge or a voltage greater than 1.75 V during any portion of the charge. Data for other end-of-useful-life criteria will be available. Upon being declared a failure, the affected cell will be removed from the test pack and subjected to a repeat of at least part of the acceptance test within 180 days of failure. The cell will then be dispositioned for further failure analysis.

The schedule given on Figure 1 shows the proposed plan. It is hoped that the test will continue until the majority of the cells in each pack have failed.

Special Testing: The general test will employ continuous constant discharges. However, the applications requiring pulsed high rate discharge within the envelope of the planned DODs are sufficiently prevalent to make the correlation of such results with the general life test important. A small group of cells will be placed on life test in a pulse discharge regime at maximum rates of approximately 5C. Cells will be acceptance tested at the

testing organization and sent to The Aerospace Corporation Battery Evaluation Laboratory for the special testing.

RESULTS AND STATUS

The full test matrix of cells expected to be tested is shown in Table 1. The total number of cells of all types and from all vendors is 275, of which 210 are 3.5 in diameter cells and 65 are 4.5 in diameter. Numbers and types of cells currently on hand or committed are shown in Table 2. Some cells manufactured in or prior to 1985 were found initially to have insufficient capacity. These have been subjected to a LEO cycling regime in order to increase their capacities to the minimum level required, namely 50 Ah for 3.5 in diameter cells. In all cases the capacities of affected cells have been recovered in this way, although requiring more than 400 LEO cycles in some cases. Newly manufactured cells have not exhibited this characteristic.

It is estimated that by the date of delivery of this paper 57 3.5 in diameter cells will be undergoing life cycling. The remainder of the 3.5 in cells on hand at this time, numbering 46 cells, will be undergoing pre-life testing for a total of 103 3.5 in diameter cells. Also, by this date 21 4.5 in diameter cells will have been received and will be in preparation for testing. Additionally, 45-3.5 in diameter cells, and 20-4.5 in diameter cells are on order and are to be received during FY 1987, so that by the end of FY 1987 189 cells should be undergoing testing in both LEO and MAO regimes.

We expect to have completed acceptance, characterization, and environmental testing on all 103 cells that are on hand at Crane by the end of January 1987. These cells will enter life testing as soon as pack assignments can be made but no later than the completion of all pre-life testing. Twenty-one high rate 4.5 inch diameter cells are expected in the last quarter of 1986. These will enter prelife testing as soon as the equipment is available (January 1987).

REFERENCES

1. C. C. Badcock and M. J. Milden, Nickel Hydrogen Battery Cell Testing Data Base: An Industry and Government Survey, Space Division/Air Force Systems Command, No. SD-TR-85-88, Dec. 31, 1985.
2. C. C. Badcock, Nickel-Hydrogen Low Earth Orbit Test Program, paper presented the 1985 NASA/GSFC Battery Workshop, Greenbelt, MD, Nov. 29, 1985.
3. J. K. McDermott, Low-Earth-Orbit Testing of Nickel-Hydrogen Cells, paper presented at the 21st Intersociety Energy Conversion Engineering Conference, Aug. 25-29, 1986.

Table 1. NiH₂ LOW EARTH ORBIT LIFE TEST

TEST MATRIX

ORBIT	DOD	MFR	3.5" DIA. CELLS		4.5" DIA. CELLS		TOTAL CELLS		
			TEMPERATURE 100C	TEMPERATURE -50C	TEMPERATURE 100C	TEMPERATURE 100C	3.5"	4.5"	
LEO	25	YARD	5				5		
		EP	5				5		
		GEBBD	5				5		
		HAC	5				5		
	40	YARD	10	10			20		
		EP	10Z	10A	10		20	10	
		GEBBD	10	10			20		
		HAC	10		10		10	10	
	60	YARD	10	10	10		10	10	
		EP	10Z, 10A	10Z			30		
		GEBBD	10		10		10	10	
		HAC	10	10			20		
MAO	80	YARD	10				10		
		EP	10			10*	10	10	
		GEBBD	10			10*	10	10	
		HAC	10				10		
SPECIAL TESTS		2 or 3, 3.5" cells and 1+ 4.5" cell from each manufacturer						10	5
		TOTAL CELLS						210	65

Table 2.

NiH₂ LOW EARTH ORBIT LIFE TEST

CELLS COMMITTED TO THE TEST

<u>MANUFACTURER</u>	<u>SIZE/CAPACITY</u>	<u>QUANTITY</u>	<u>DATE AVAILABLE</u>
YARDNEY	3.5"/50	31 (ZA)	Now
EAGLE PICHER	3.5"/50	24 (A)	Now
		33 (Z)	Now
EAGLE PICHER (CS)	4.5"/100	8 (Z)	12/86
	4.5"/130	10 (Z)	4/87
GE BBD	3.5"/50	15 (Z)	Now
	3.5"/50	15 (Z)	8/87
	4.5"/100	8 (Z)	12/86
	4.5"/130	10 (Z)	4/87
HUGHES	3.5"/50	30 (Z)	8/87
	4.5"/100	5 (Z)	12/86

TOTAL 3.5" CELLS.....	148
TOTAL 4.5" "LEO" CELLS.....	21
TOTAL 4.5" "HEO" CELLS.....	20

NIH2 LIFE TEST SCHEDULE SCHEDULE

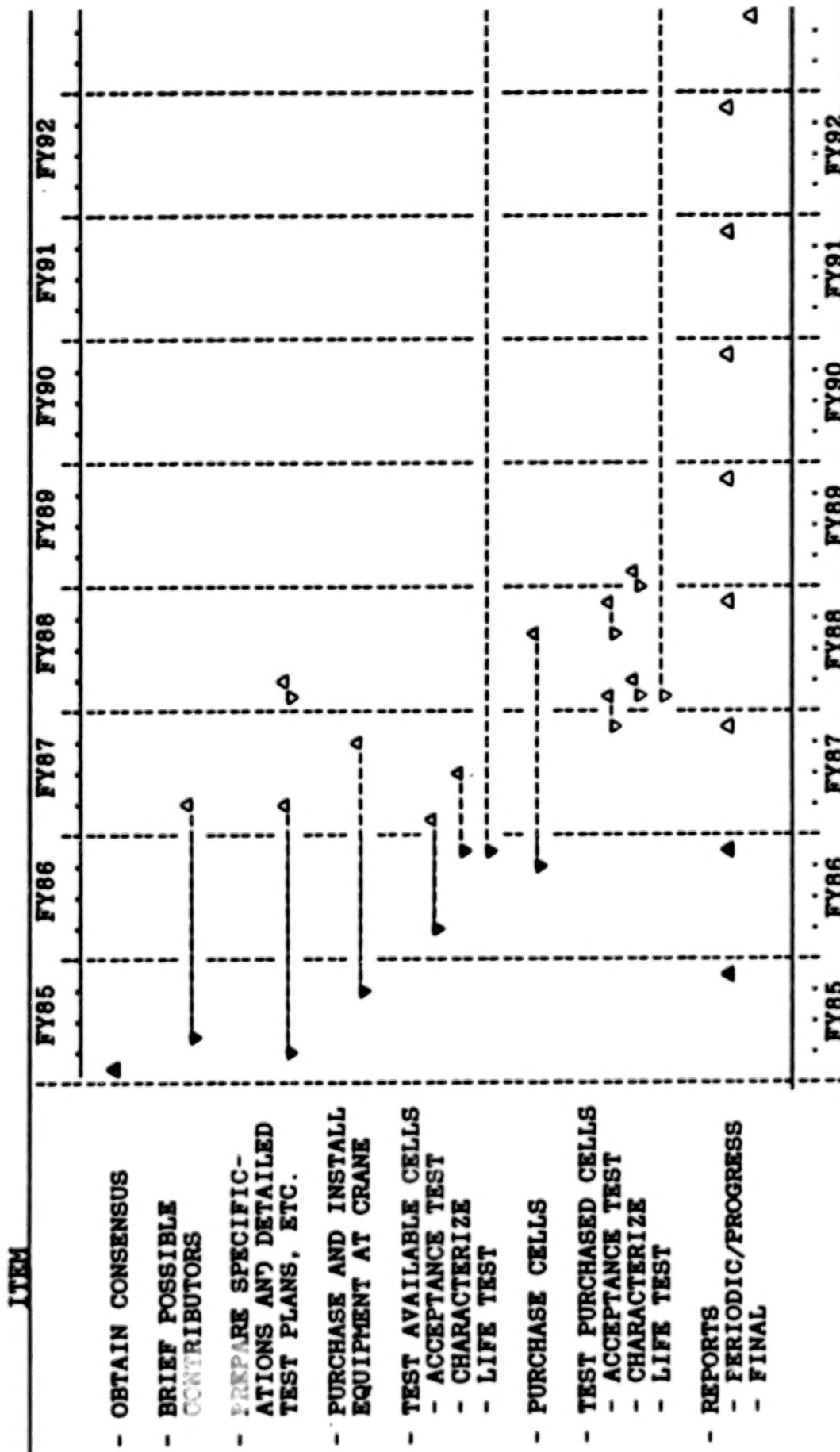


Figure 1.

Nickel Hydrogen Low Earth Orbit Test Program: Update and Status

C. C. BADCOCK AND S. W. DONLEY

**THE AEROSPACE CORPORATION
LOS ANGELES, CA 90009**

A. B. FELTS AND R. L. HAAG

**NAVAL WEAPONS SUPPORT CENTER
CRANE, IN 47522**

FOR PRESENTATION AT

**THE 1986 NASA/GSFC BATTERY WORKSHOP
GREENBELT, MARYLAND
NOVEMBER 18, 1986**

NiH₂ Low Earth Orbit Life Test

● OBJECTIVES

- DEMONSTRATE NiH₂ PERFORMANCE IN LEO
- SUPPORT MID-ALTITUDE ORBIT OPERATION
- RELATE LARGER DIAMETER CELLS TO DATA BASE
- DEVELOP A STATISTICALLY SIGNIFICANT DATA BASE
- PROJECT BATTERY RELIABILITIES
- SUPPORT OTHER TESTING DATA
- PROVIDE UNIFORM, COMPARABLE DATA
- INCORPORATE OTHER DATA BASES
- DIRECT COMPARISON OF MANUFACTURERS' CELLS

● GOALS

- DEMONSTRATE A MINIMUM CYCLE LIFE
- 30,000 CYCLES AT 40% DOD
- 20,000 CYCLES AT 60% DOD
- 5,000 CYCLES AT 80% DOD (MAO orbit)
- ACHIEVE A MINIMUM RELIABILITY
- 90% RELIABILITY AT AN 80% CONFIDENCE LIMIT

NiH₂ LEO Life Test

ORGANIZATION AND APPROACH

● ORGANIZATION

- PROGRAM MANAGEMENT BY AFSTC
- NWSC/Crane TO PERFORM ACCEPTANCE, CHARACTERIZATION, AND LIFE TESTING
 - DOD NATIONAL TEST FACILITY FOR BATTERIES AND CELLS
- AEROSPACE TO PROVIDE TECHNICAL SUPPORT
 - PREPARE DOCUMENTATION AND ASSIST IN REPORTING RESULTS
 - PERFORM SPECIALIZED TESTING
- AFWAL/POOC TO SUPPORT PROGRAM
 - PROVIDE PREVIOUSLY PURCHASED CELLS AND PURCHASE SERVICES FOR FIRST CELLS PURCHASED (FY86)

● APPROACH

- TEST CELLS UNDER LEO AND MAO REGIMES (majority in LEO)
 - LIMIT VARIABLES TO INCREASE STATISTICAL SIGNIFICANCE
 - TEST UNDER MOST BENIGN, ACHIEVABLE CONDITIONS
 - TEST CELLS FROM ALL VIABLE U.S. MANUFACTURERS
 - TEST 3.5 AND 4.5 INCH DIAMETER CELLS

NiH₂ Low Earth Orbit Life Test

TEST PARAMETERS

- TEST - 80% OF THE CELLS UNDER LEO CONDITIONS
 - 16 CYCLES/DAY: 30m DISCHARGE/60m CHARGE
 - MAO TESTING AT 6 HOURS/CYCLE
- DEPTH OF DISCHARGE BASED ON ACTUAL MINIMUM/PACK
 - LEO
 - 25% (correlation with NiCd only)
 - 40% IS THE CONSERVATIVE GOAL
 - 60% IS THE DESIRED GOAL
 - MAO
 - 80% WILL PERMIT BOL DESIGNS AT 70 + %
- TEMPERATURE
 - LEO TESTING AT 10°C AND - 5°C (± 4°C)
 - MAO TESTING AT 10°C ONLY
- CHARGE CONTROL MINIMIZES RECHARGE FRACTION
 - MINIMIZE PARAMETERS
 - DECREASE IN EODV
 - INCREASE IN EOCV
 - WH AND AH RECHARGE FRACTION

NiH₂ Low Earth Orbit Life Test

STATISTICAL CONSIDERATIONS

- **DEMONSTRATE STATISTICAL SIGNIFICANCE IN TESTING**
 - **TRADE-OFF TEST TIME AND NUMBER OF CELLS AGAINST OTHER GOALS**
- **MINIMUM CREDIBLE TEST MATRIX CHOSEN AS BEST COMPROMISE**
 - **LONGER TEST TIME WITHOUT FAILURE CAN INCREASE SIGNIFICANCE**
 - **COMBINING TEST PACKS FROM DIFFERENT CONDITIONS AND/OR MANUFACTURERS CAN INCREASE SIGNIFICANCE**
- **LONGER TEST TIME IS MOST EFFECTIVE DIRECTION FOR RELIABILITY**
 - **5 YEAR APPLICATION, TESTING WITH NO FAILURES**
 - **10 CELLS: TEST TIME = 5 YEARS, CL = 0.8, R = 86.3%**
 - **20 CELLS: TEST TIME = 5 YEARS, CL = 0.8, R = 92.6%**
 - **10 CELLS: TEST TIME = 8 YEARS, CL = 0.8, R = 97.8%**

NiH₂ Low Earth Orbit Life Test **TEST MATRIX**

ORBIT	DOD %	MFR	3.5 in. dia CELLS TEMPERATURE		4.5 in. dia CELLS TEMPERATURE	TOTAL CELLS	
			10°C	-5°C		3.5 in.	4.5 in.
LEO	25	YARD	5			5	
		EP	5			5	
		GEBBD	5			5	
		HAC	5			5	
	40	YARD	10	10		20	
		EP	10Z	10A	10	20	10
		GEBBD	10	10		20	
		HAC	20		10	10	10
	60	YARD	10	10	10	10	10
		EP	10Z, 10A	10Z		30	
MAO	80	GEBBD	10		10	10	10
		HAC	10			20	
		YARD	10	10		10	
		EP	10		10*	10	10
		GEBBD	10		10*	10	10
		HAC	10			10	

SPECIAL TESTS 2 OR 3, 3.5 in. CELLS AND 1 + 4.5 in. CELL
 FROM EACH MANUFACTURER

10	5
TOTAL CELLS	210
	65

NiH₂ LEO Life Test **CELL ACQUISITION STATUS**

MANUFACTURER	SIZE/CAPACITY	QUANTITY	DATE AVAILABLE
YARDNEY	3.0 in./50	31 (ZA)	NOW
EAGLE-PICHER (JOP)	3.5 in./50	24 (A)	NOW
		33 (Z)	NOW
EAGLE-PICHER (CS)	4.5 in./100	8 (Z)	12/86
	4.5 in./130	10 (Z)	04/87
GENERAL ELECTRIC BBD	3.5 in./50	15 (Z)	NOW
	3.5 in./50	15 (Z)	08/87
	4.5 in./100	8 (Z)	12/86
	4.5 in./130	10 (Z)	04/87
HUGHES AIRCRAFT	3.5 in./50	30 (Z)	08/87
	4.5 in./100	5 (Z)	12/86

	TOTAL CELLS ACQUIRED	TOTAL CELLS TO BE PURCHASED
3.5 in. LEO	148	62
4.5 in. LEO	21	24
4.5 in. GEO	20	

NiH₂ LEO Life Test

PROGRAM PLAN

• DOCUMENTATION

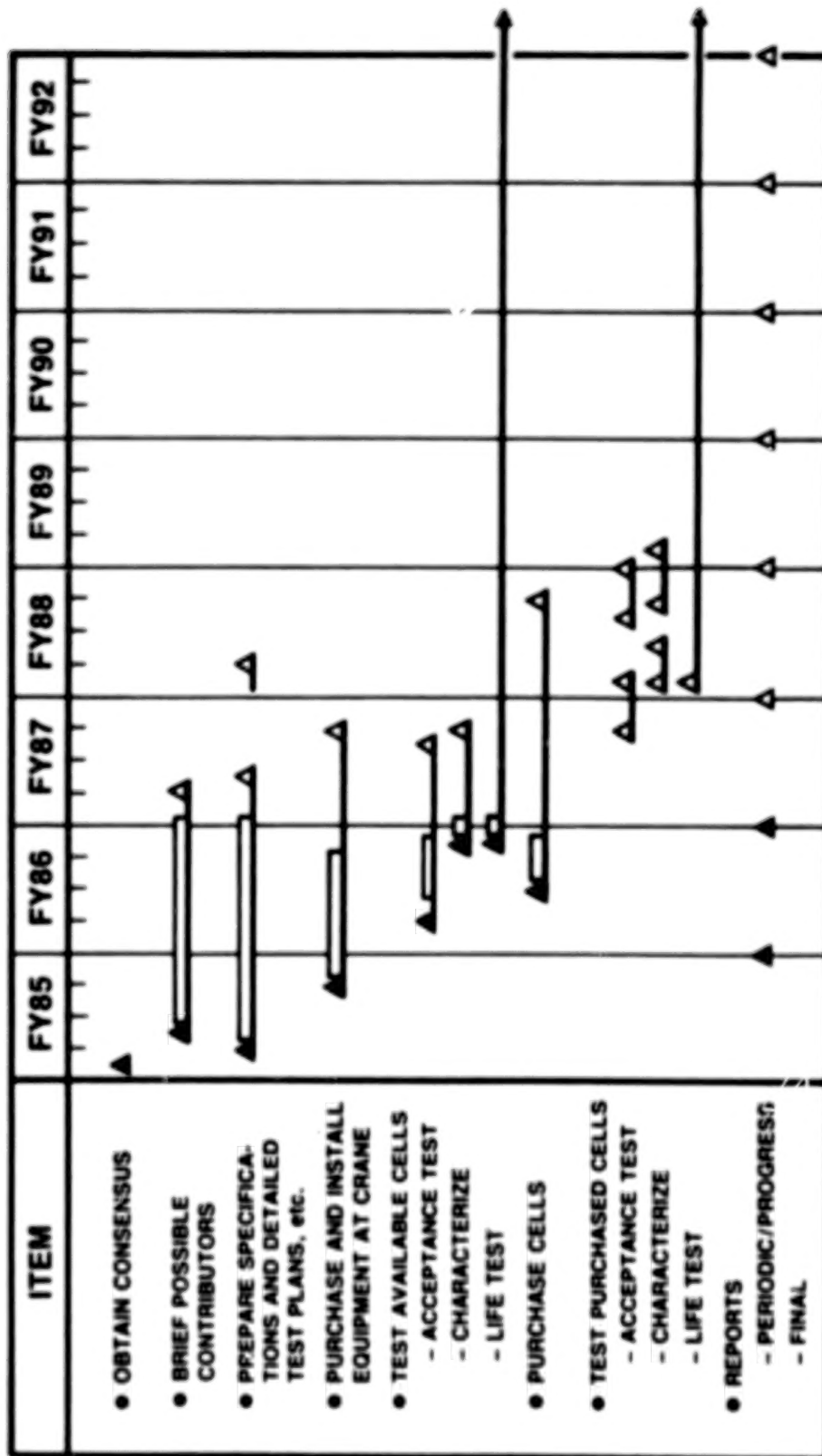
- TEST PLAN (revision 5 in preparation)
- STATISTICAL SUPPLEMENT (complete)
- SPECIFICATION, INCLUDES ACCEPTANCE TEST (50 Ah complete)
- CHARACTERIZATION PROCEDURE AND PLAN (complete)
- SPECIAL TEST PROCEDURE (complete, not issued)
- LIFE TEST PROCEDURE (in review)
- FAILURE ANALYSIS PROCEDURE
- ANNUAL STATUS AND MILESTONE REPORTS (FY85 and FY86 issued)

• TESTING

- EQUIPMENT (most purchased in FY85)
- RECEIVE AND ACCEPTANCE TEST CELLS (20% environmentally tested)
- CHARACTERIZE 5 CELLS OF EACH DESIGN/VENDOR (non-destructive)
- LIFE CYCLE TEST CELL PACKS
 - CYCLE UNTIL ~ 50% OF CELLS FAIL IN EACH PACK TO ESTABLISH FAILURE DISTRIBUTION

NiH₂ LEO Life Test

SCHEDULE



Special Testing at Aerospace

- SCOPE OF TEST
 - 10 - 3-1/2 INCH DIAMETER CELLS
 - 5 - 4-1/2 INCH DIAMETER CELLS
- PURPOSE OF TEST
 - VERIFY LIFE CAPABILITY OF NiH_2 CELLS IN A LEO ORBIT.
REGIME CONTAINING HIGH RATE (5C) PULSES
- TEST SCENARIO
 - ACCEPTANCE AND CHARACTERIZATION TESTING AT CRANE
 - LIFE TESTING AT AEROSPACE — DURATION 3-5 YEARS FROM START
- TEST STATUS
 - SPECIAL HARDWARE AND SOFTWARE DESIGNED AND
IN CONSTRUCTION
 - PRELIMINARY SYSTEM CHECK-OUT END OF NOVEMBER, 1986
 - LIFE TEST START DATE — ON RECEIPT OF CELLS

NiH₂ LEO Life Test

SUMMARY

- **NiH₂ BATTERIES HAVE THE CAPABILITY TO OPERATE AT MUCH HIGHER ENERGY DENSITIES THAN NiCd BATTERIES**
 - **GREATEST ADVANTAGE IS IN LEO APPLICATIONS**
 - **CELL CAN BE SCALED TO LARGE CAPACITIES**
- **PROGRAM NEEDED TO ESTABLISH BASELINE DATA FOR ORBITAL USE OF NiH₂ CELLS IN LEO AND MAO**
 - **CORRELATE DESIGNS AND SIZES IN DATA BASE**
- **LIFE TEST PROGRAM ESTABLISHED TO PROVIDE REQUIRED DATA**
 - **LONG TERM TEST TO ESTABLISH LIFE**
 - **COORDINATE WITH OTHER LIFE TEST PROGRAMS**
 - **USE ALL DATA TO COMPLETE DATA BASE**
 - **NEED ADDITIONAL FUNDING TO COMPLETE PROGRAM AS PRESENTLY CONFIGURED**
 - **MODIFY PLAN TO CONFORM TO FUNDING BY MID-1987**
- **LIFE EVALUATION AND LONG TERM PERFORMANCE DATA WILL BEGIN TO BE AVAILABLE BY 1990**

N88-11029

ADVANCES IN NICKEL HYDROGEN TECHNOLOGY

AT

YARDNEY BATTERY DIVISION

A PRESENTATION BY

J. G. BENTLEY AND A. M. HALL

TO THE

1986 GODDARD BATTERY WORKSHOP

AT

NASA GODDARD SPACE FLIGHT CENTER

18 NOVEMBER 1986

INTRODUCTION

This presentation outlines the current major activities in nickel hydrogen technology being addressed at Yardney Battery Division. It covers five basic topics:

1. An update on life cycle testing of ManTech 50 AH NiH_2 cells in LEO regime.
2. An overview of the Air Force/Industry briefing on the Yardney ManTech program.
3. Nickel electrode process upgrading.
4. 4 1/2" cell development.
5. Bipolar NiH_2 battery development.

1. UPDATE ON LIFE CYCLE TESTING OF MANTECH 50AH NiH_2 CELLS IN LEO REGIME

A year ago at the 1985 Goddard Workshop Yardney reported in a short informal briefing on the effort to date in LEO regime life cycle testing on Yardney ManTech cells which were the prototypical output of Phase II of the ManTech Program (Fig. 1). This depicted the testing of two cells to 5000 cycles at 80% depth of discharge including, in the first 1000 cycles, efforts to optimize charge/discharge ratios and fine tune the computerized test and data acquisition systems. The consensus among several of those in the NiH_2 technological community at that point was that the 80% DOD was overly rigorous and unrealistic.

Therefore, when we restarted cycle testing we did so at 60% Depth of Discharge. Also, by this time we were delivering cells to customers representing the final configuration coming out of the ManTech Program, that is to say, Phase III cells. These vary from the prototype Phase II cells only in areas of mechanical design. The number, type, and arrangement of electrochemical elements remained unchanged. We added one of these Phase III cells to the test group as we restarted testing.

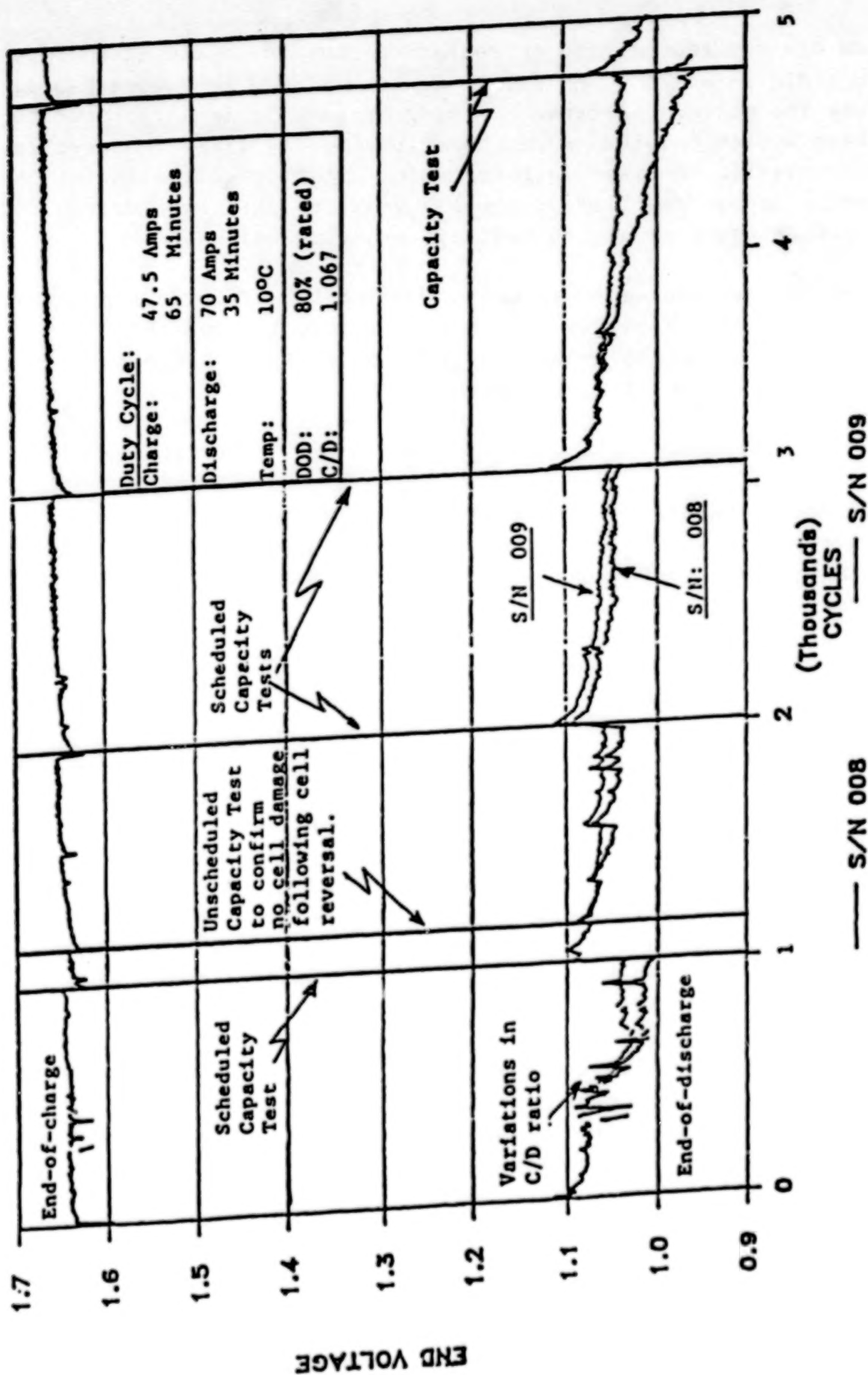


Figure 1. YNH-50-1 Cells (5-Apr-84 to 24-May-85).

We did not recondition or recharacterize the cells t 6000 cycles but did so at 7000 and 8000. As can be seen in Figure 2 cell 008 was the poorer performer of the group. This is attributed to test system problems encountered during the first 5000 cycles. In addition to power failures which interrupted testing at the most inopportune times the cells were at least once driven into reversal as a result of test system malfunctions.

Testing has proceeded to about 8900 cycles of which approximately 8800 cycles are represented here. During the current recharacterization we have decided to explore some other characteristics of these cells.

One of these was cell impedance at various temperatures and states of charge (Figure 3). It is of interest that at 0°C impedance values converged and as temperature is increased charged cells have a greater impedance while discharged ones exhibit less impedance. It should be noted that these values were taken at 40 Hz.

A second peripheral investigation was in regard to what is sometimes referred to as the "double knee phenomenon" which cells exhibit during discharge. The three ManTech test cells had been maintained for a sustained period (10-14 days) at less than 10 mV and were then charged at a C/10 rate for 20 hours and discharged. The first discharge was at C/25 and exhibited no "double knee" phenomenon (Figure 4). Repeating the same test 3 days later exhibited a genesis of the phenomenon (Figure 5). A retest at a C/10 rate discharge shows a slightly more pronounced display (Figure 6). A repeat of the test at a discharge rate of C/2 exhibits a more substantive but less pronounced characteristic (Figure 7). Finally, at a C rate discharge the differentiation of the two "knees" has almost disappeared (Figure 8). These characteristics illustrate an inherent dependency of the positive electrode active nickel structure on prior cycle history and rate of discharge. We are continuing to evaluate this phenomenon relative to cell performance.

Additionally, radiographic examinations were made to determine positive plate growth. Less than .002"/plate was noted on cells S/N 008 and 009 in the first 5000 cycles. No measurable growth was discerned in the subsequent 3800 cycles.

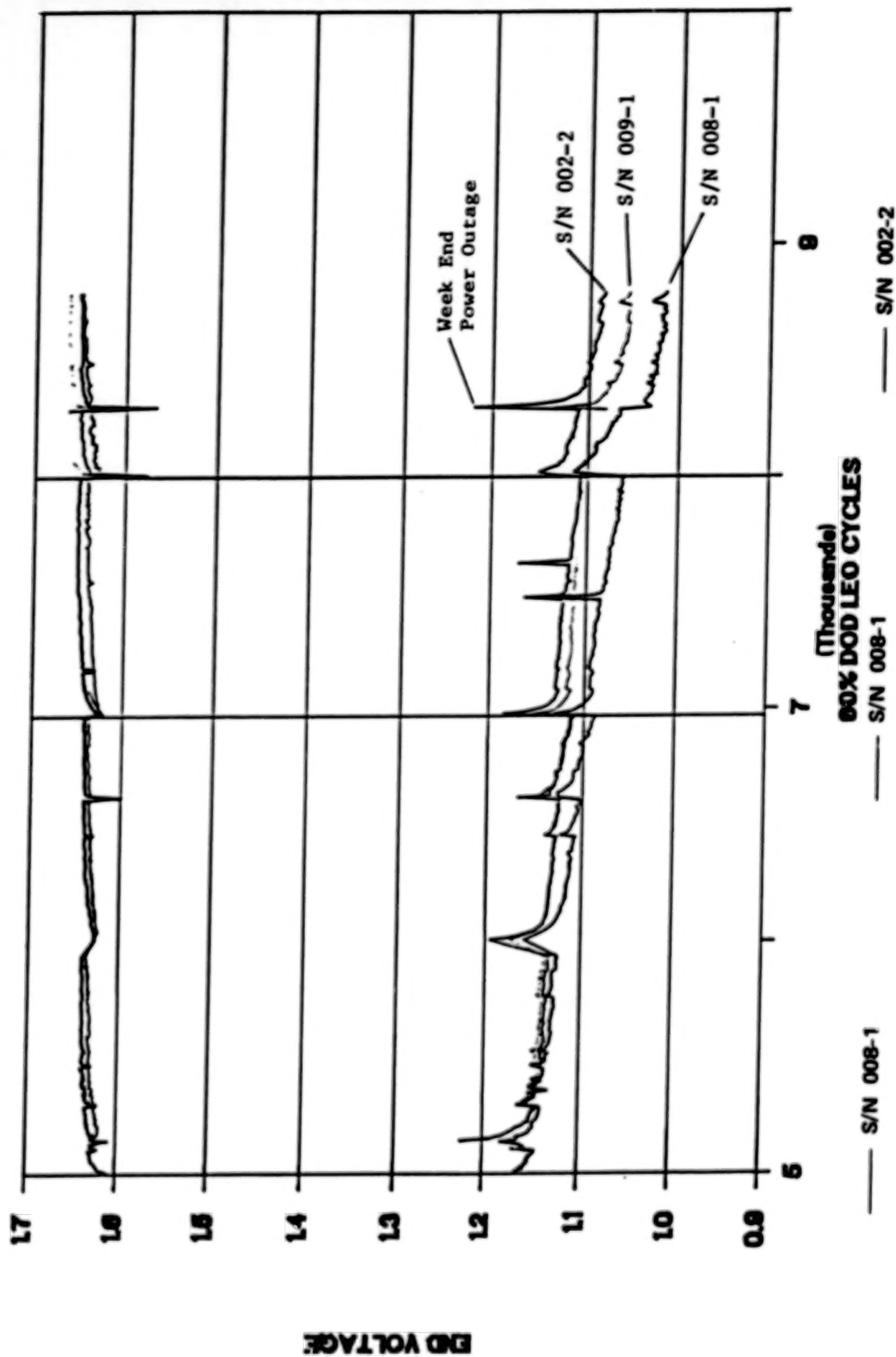
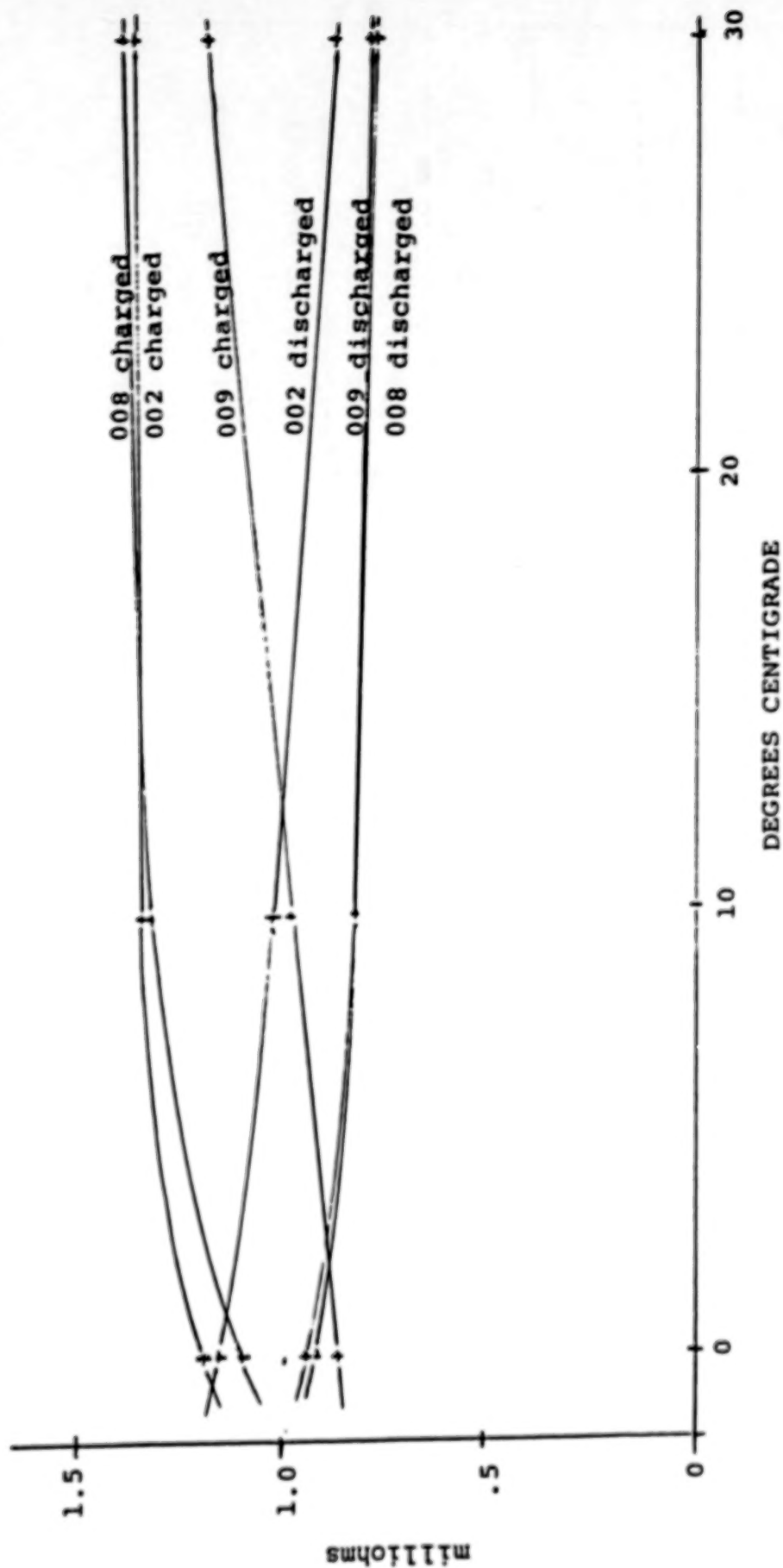


Figure 2. YNH-50 Cells (22-Sep-86).



Cells 008 and 009 after 9000 LEO cycles (5K @ 80% and 4K @ 60% DoD).
 Cell 002 after 4000 LEO cycles @ 60% DoD.
 Measurements made with a Keithley Model 503 milliohmmeter at 40 Hz.

Figure 3. Impedance of NiH_2 Cells at Various Temperatures when Fully Charged and Fully Discharged.

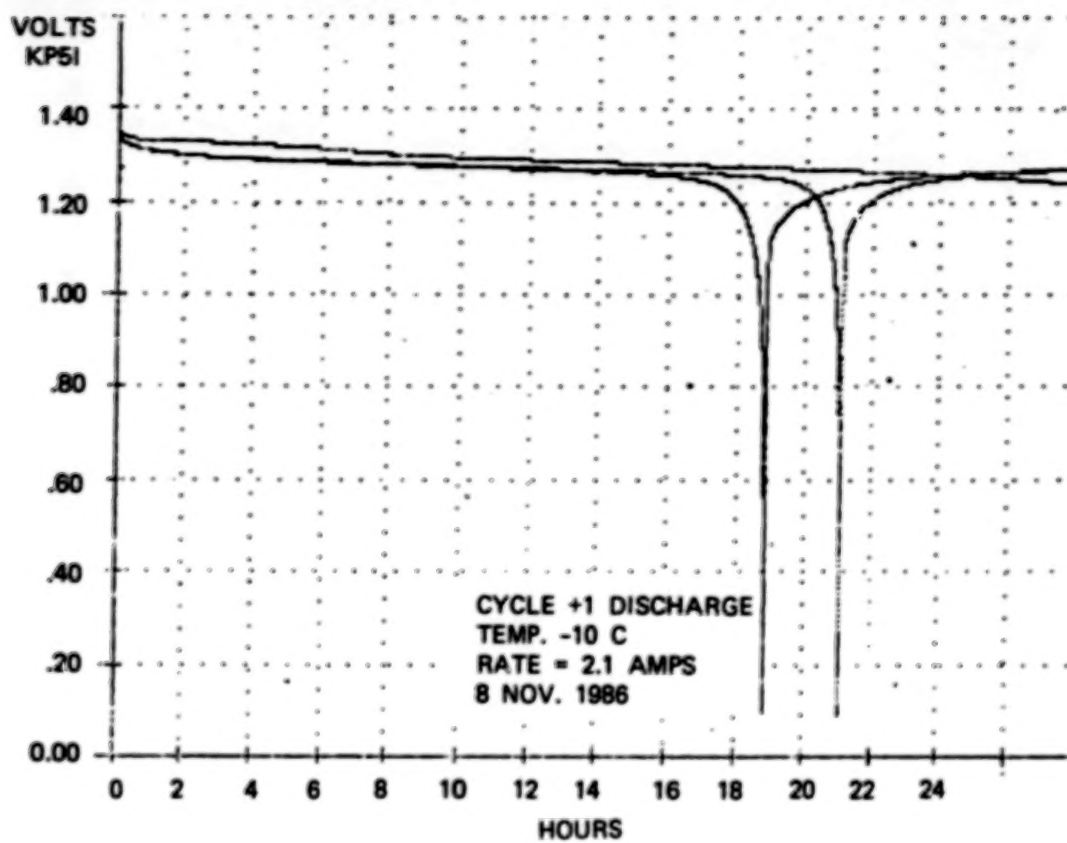


Figure 4.

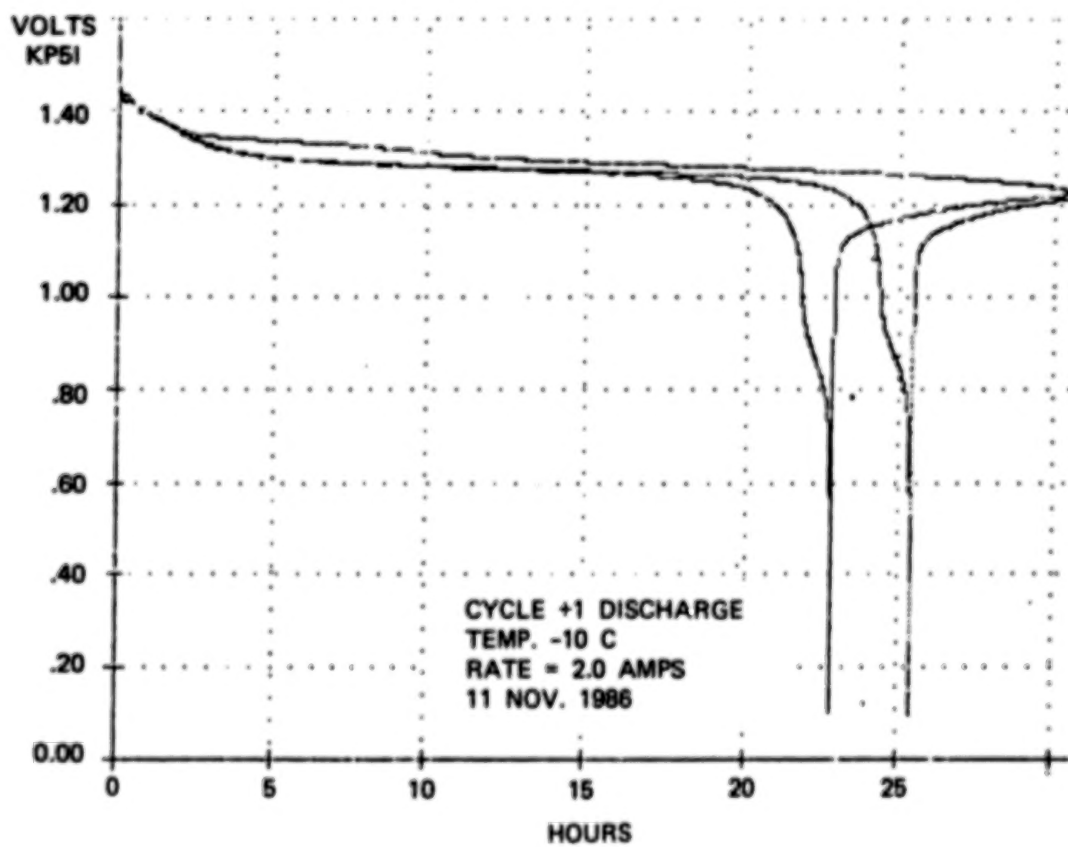


Figure 5.

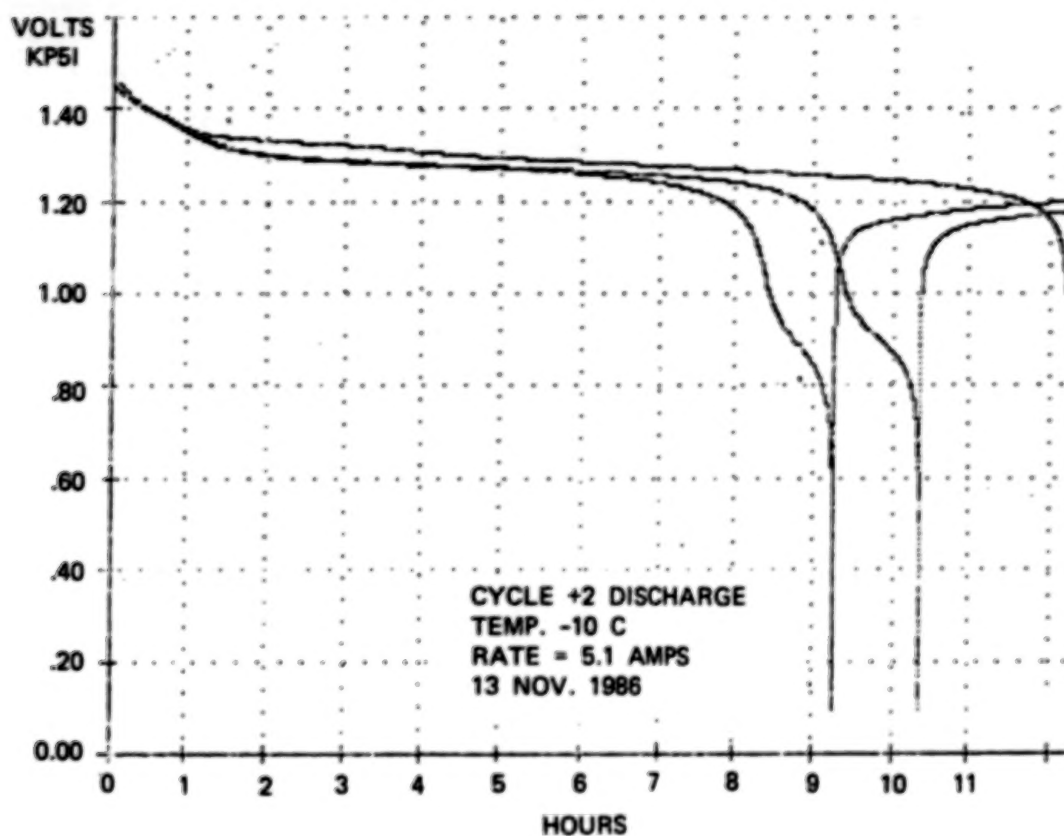


Figure 6.

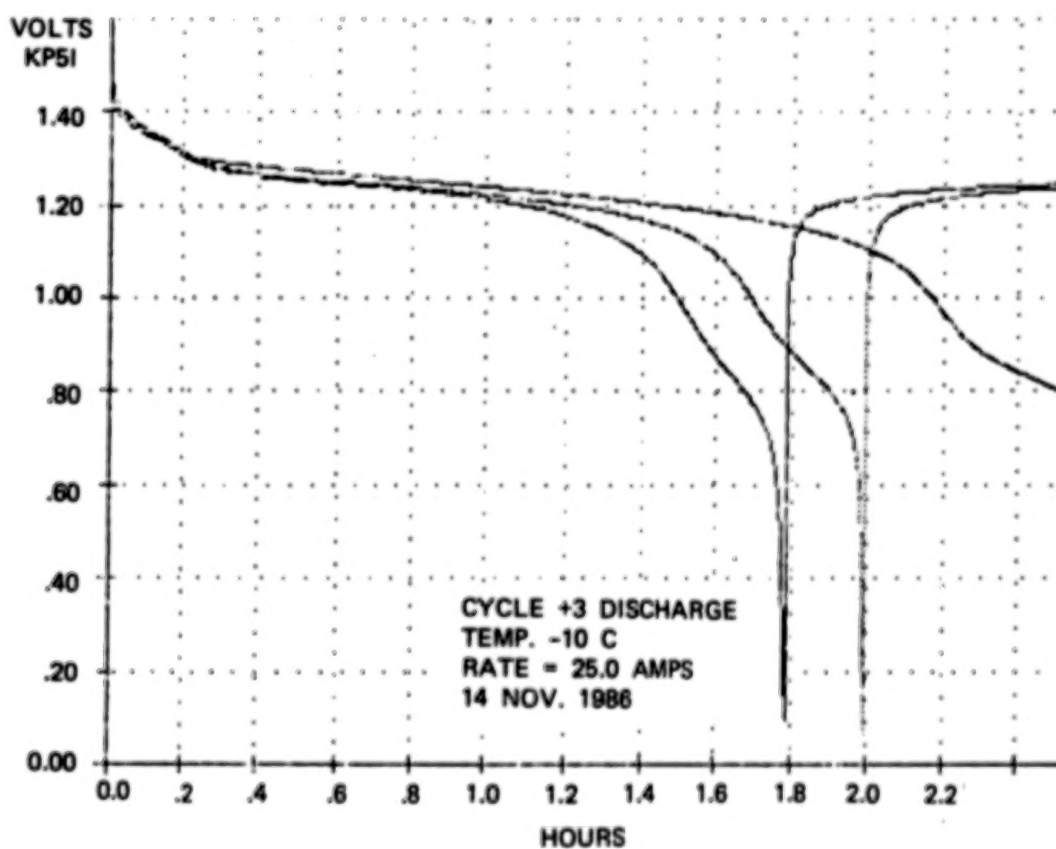


Figure 7.

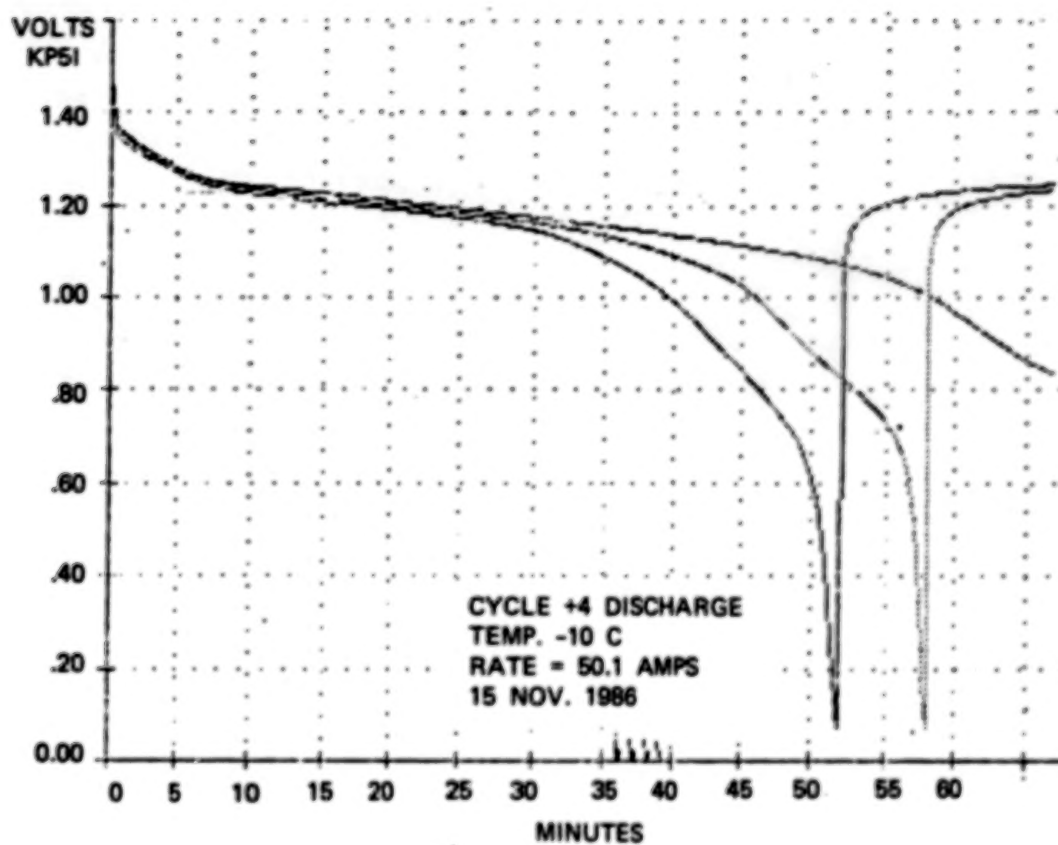


Figure 8.

2. OVERVIEW OF THE AIR FORCE/INDUSTRY BRIEFING ON THE YARDNEY/MANTECH PROGRAM

As some of you are aware we are at this time completing our contract with Wright Patterson Materials Lab for the application of manufacturing technology to the baseline Air Force 3 1/2", 50 AH cell. While the ITAR regulations prevent an in-depth technical discourse in this forum we can give a very brief overview of the project.

This program, initiated in 1981, while encountering several problematical delays, has resulted in a number of technical break-throughs, including the reduction in platinum loading of the negative without loss of performance, the improvement in structural accommodation to plate growth and, most importantly, a reduction in price from the baseline cell of from 30 to 50% or more depending on production lot size.

In addition to the prototype cells coming out of the program and being tested at Yardney we have delivered cells to the Wright Patterson Materials Lab, and to Don Warnock's group at Wright Patterson both of which cell lots are now on test at the Naval Weapons Support Center, Crane, Indiana. Additional cell lots in the Phase III configuration have been produced for other customers as well.

3. NICKEL ELECTRODE PROCESS UPGRADING

Within Yardney's new dedicated NiH_2 manufacturing facility a substantial effort has been directed at nickel positive manufacturing techniques. The Yardney positive process includes a wet slurry-type plaque which is sintered in a reducing atmosphere and electrochemical impregnated (EI) by the Pell Blossom process. New plaque pulling, sintering and EI equipment are providing superior control of those phases of the operation.

These efforts are now providing positive plates which meet stringent requirements of thickness growth and blistering when subjected to a 200 cycle high rate stress test. This test consists of 10 C charge for 12 minutes and a 10 C discharge for 8 minutes at room temperature. Criteria for acceptance are a maximum of 3 mil thickness growth and less than 3% of the plate area blistered for the standard 31 and 35 mil thick electrodes.

4. 4 1/2" CELL DEVELOPMENT

In May of 1985 Yardney embarked on a cooperative effort with Ford Aerospace Corporation to develop a 4 1/2 inch diameter nickel-hydrogen cell with a nominal rating of at least 220 AH in a LEO regime. The design is a tandem stack, floating core type, typical of Yardney's 3 1/2 inch Air Force arrangement, but incorporating wall wick recombination and back-to-back electrodes. Mechanically the structure is a 35% scale-up variant of 3 1/2 inch components employed in the ManTech and Air Force cells. The program was somewhat accelerated in order to produce light-weight cells for performance evaluation in less than six months. Figure 9 identifies some of the improved design features employed in this cell.

A series of characterization tests were carried out on five of these cells to determine the effect of temperature between 0 and 36°C. The temperature was controlled by fluid transfer in manifolded sleeves clamped to the cylindrical section of each pressure vessel. These temperature trials, which were conducted as the first cycles, demonstrated that the best capacity is at 10°C for an average value of 243 AH. After 150 LEO cycles this early capacity increased to an average value of 259 AH above 1.0 volts.

Figure 10 illustrates the end of charge and discharge voltage trends for this initial cycle series. Continued life testing is now being planned for several of these cells.

Figure 11 shows the characteristic curves of voltage for the rating cycle of all five cells. Figures 12 and 13 indicate the consistency of discharge performance between cells from the 5th to the 150th cycle.

In early 1986 Yardney responded to customer interest to produce 100 AH LEO regime, 4 1/2 inch diameter cells. This design also employs a tandem stack, floating core; however, the stack elements are arranged in a conventional recirculating sequence. The pressure vessel wall is coated with zirconium oxide in the common Air Force practice, and no platinum catalyst is incorporated for wall recombination. Assembly of the first 100AH

CELL DESIGN FEATURES
YARDNEY 4 1/2" MODEL YNH-HRWTS220

- 4 1/2" DIA. CYL. x 18 3/8 LOA
- MANTECH/MILSTAR GROWTH VARIANT(1.35 SCALE-UP)
- BACK-TO-BACK ELECTRODES (.031" MANTECH THICKNESS)
- ZIRCAR AND ASBESTOS SEPARATOR
- WELL 'NG w/MINIMAL "WIDTH"
- SIMPLIFIED CENTER SUPPORT PLATE
- BELLEVILLE SPRING STROKE MAXIMIZED
- RECOMBINATION & MAJOR HEAT SOURCE ON WALLS
- ANTI-TWIST TERMINAL

Figure 9.

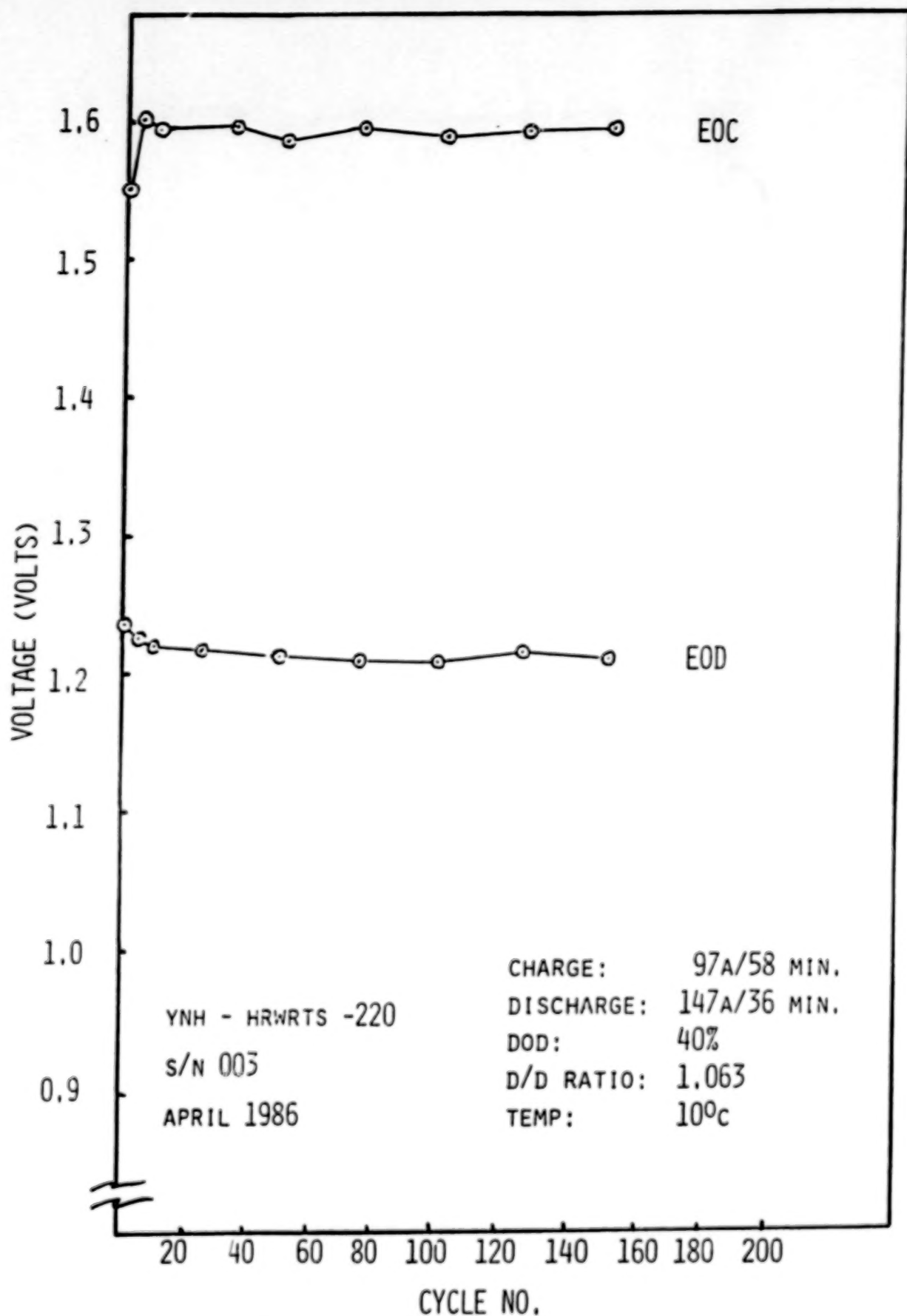


Figure 10. LEO Life Cycle Data Summary.

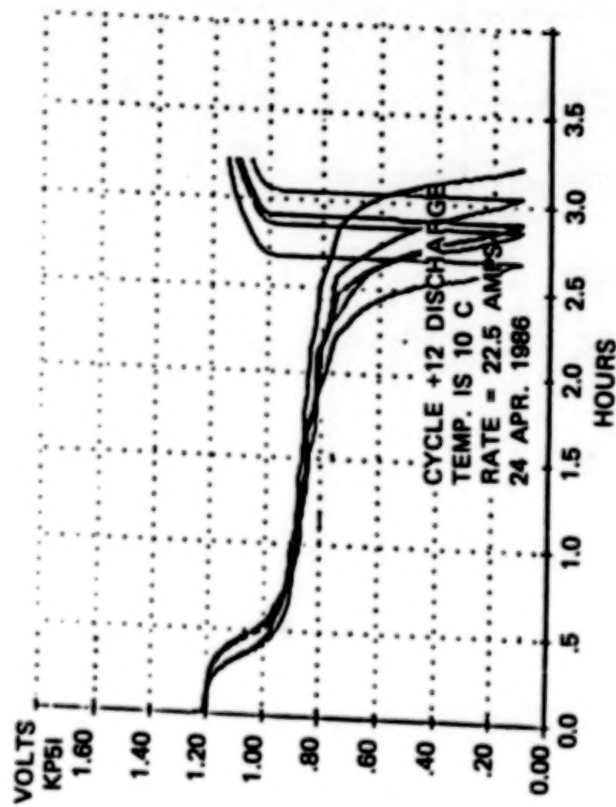
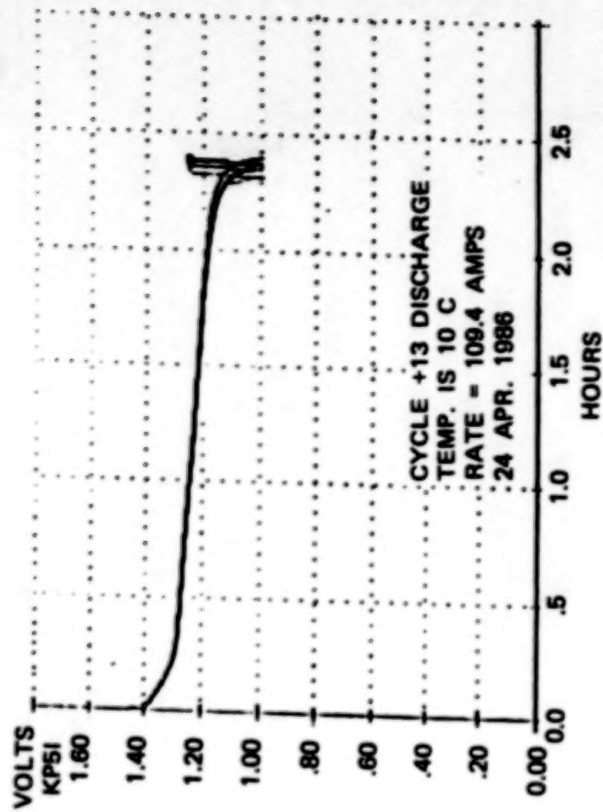
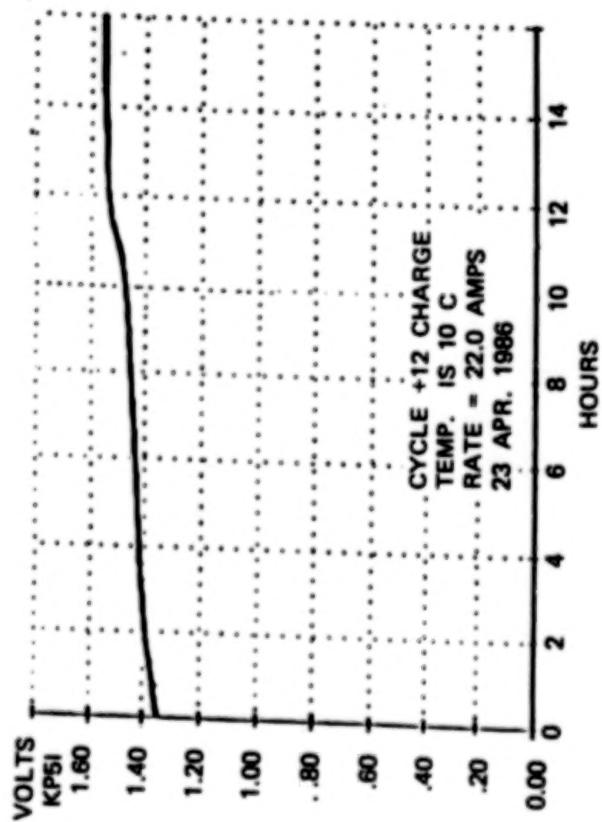


Figure 11.

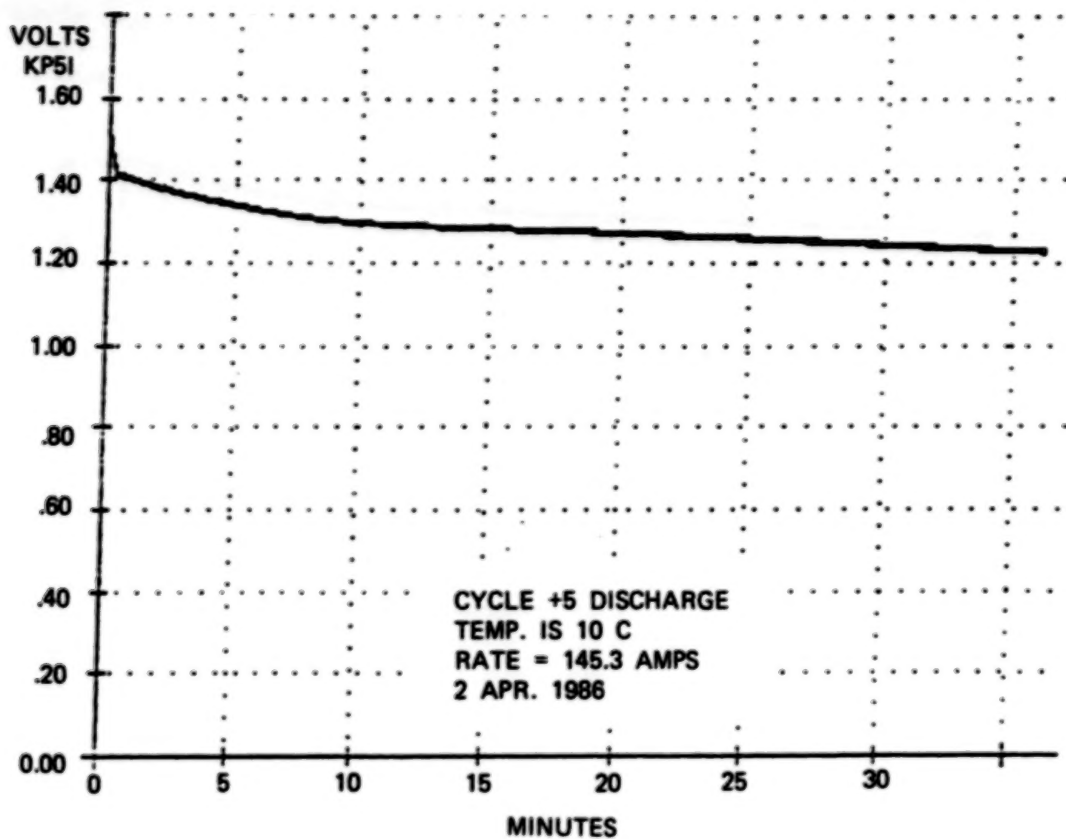


Figure 12.

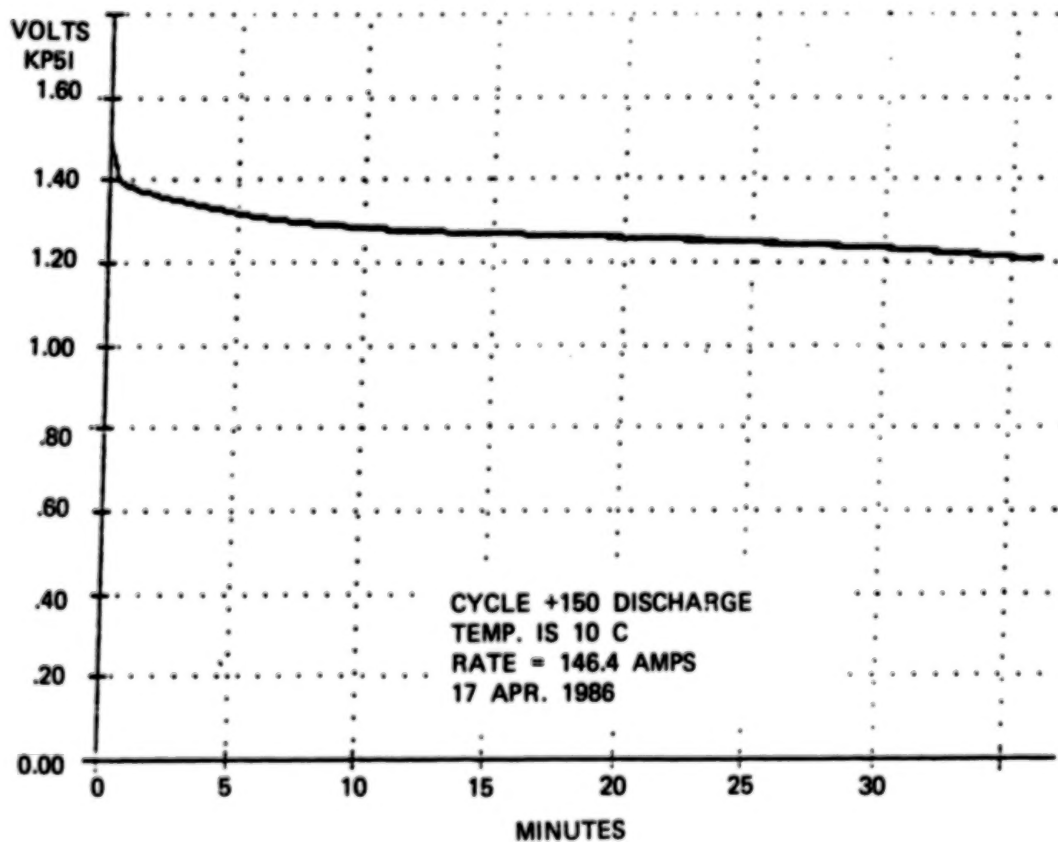


Figure 13.

units is currently underway and characterizations tests are scheduled for December 1986.

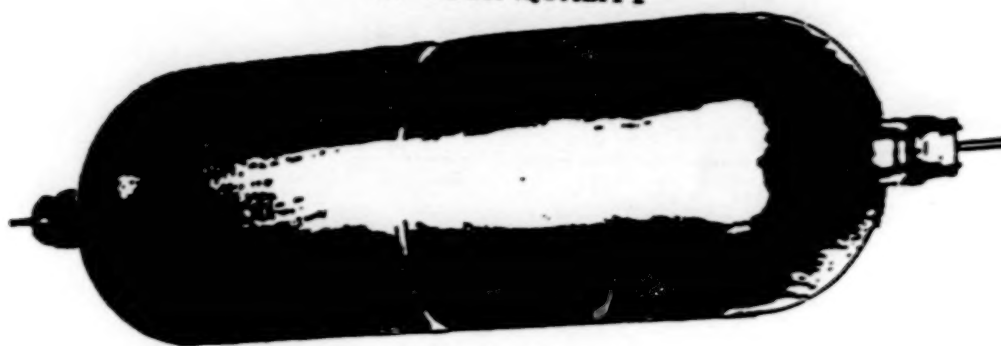
Figure 14 depicts the relative size of 50 and 70 AH 3 1/2" cells and 100 and 220 AH 4 1/2" cells.

5. BIPOLAR ACTIVITIES

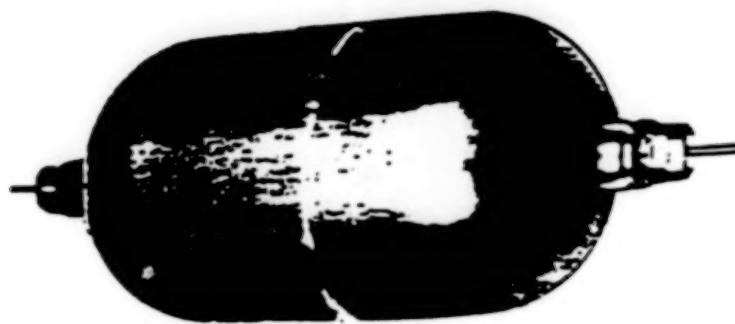
Yardney is in the third year of development regarding a 75 AH bipolar experimental battery for space applications. This NASA program is organized to evaluate a baseline design and its variants. Ford Aerospace Corporation is the prime contractor and Yardney has responsibility for the stack development. The design is inherently modular in nature, lending itself to high capacities and voltages depending on cell stack arrangement within a common pressure vessel. The program objectives include development of thick electrodes and evaluation of designs for heat removal within a context of simplicity and consequent ease of manufacturability.

The basic electrode is .080 inches thick with an area of 4 x 16 inches. Three such electrodes are ganged together in individual frames on a common "bi-polar" heat conducting plate at each cell level. A model was built early in the program to represent a full-scale section only one-sixth in length, with electrodes 4 x 8 inches. Thermal path lengths and mechanical details remained the same for the model as for the prototype size. Figure 15 shows the 10-cell model manufactured by Yardney with the cooling plates in place. This model was characterized for capacity at approximately 10°C by charging and discharging at various combinations of rates. These results are shown in the form of a carpet plot on Figure 16. It can be seen that capacity to 1.0 volts varies in a continuous manner with best results relating to optimum charge rates between C/2 and C for discharges between C/4 and 2C, respectively. After the characterization series, LEO cycles were run at 80% and 60% DOD for a total of approximately 380 cycles. The model was then torn down and inspected. In general, the cells appeared in good condition with the exception of one shorted cell attributed to the mechanical design. Figure 17 illustrates the first 75 AH stack built to this design for thermal and performance evaluation in a specially designed pressure vessel at Ford Aerospace Corporation.

ORIGINAL PAGE IS
OF POOR QUALITY

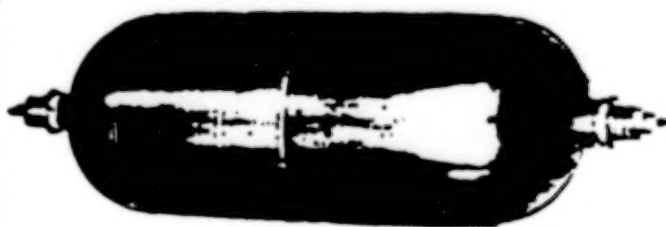


YHII-HRTSWR220-1

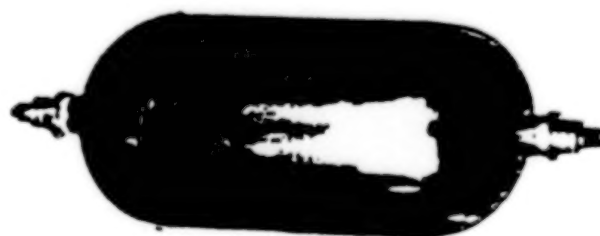


YHII-HRTS100-1

YHII-HRTS70-1



YHII-HRTS70-1



YHII-HR50-2

Figure 14.

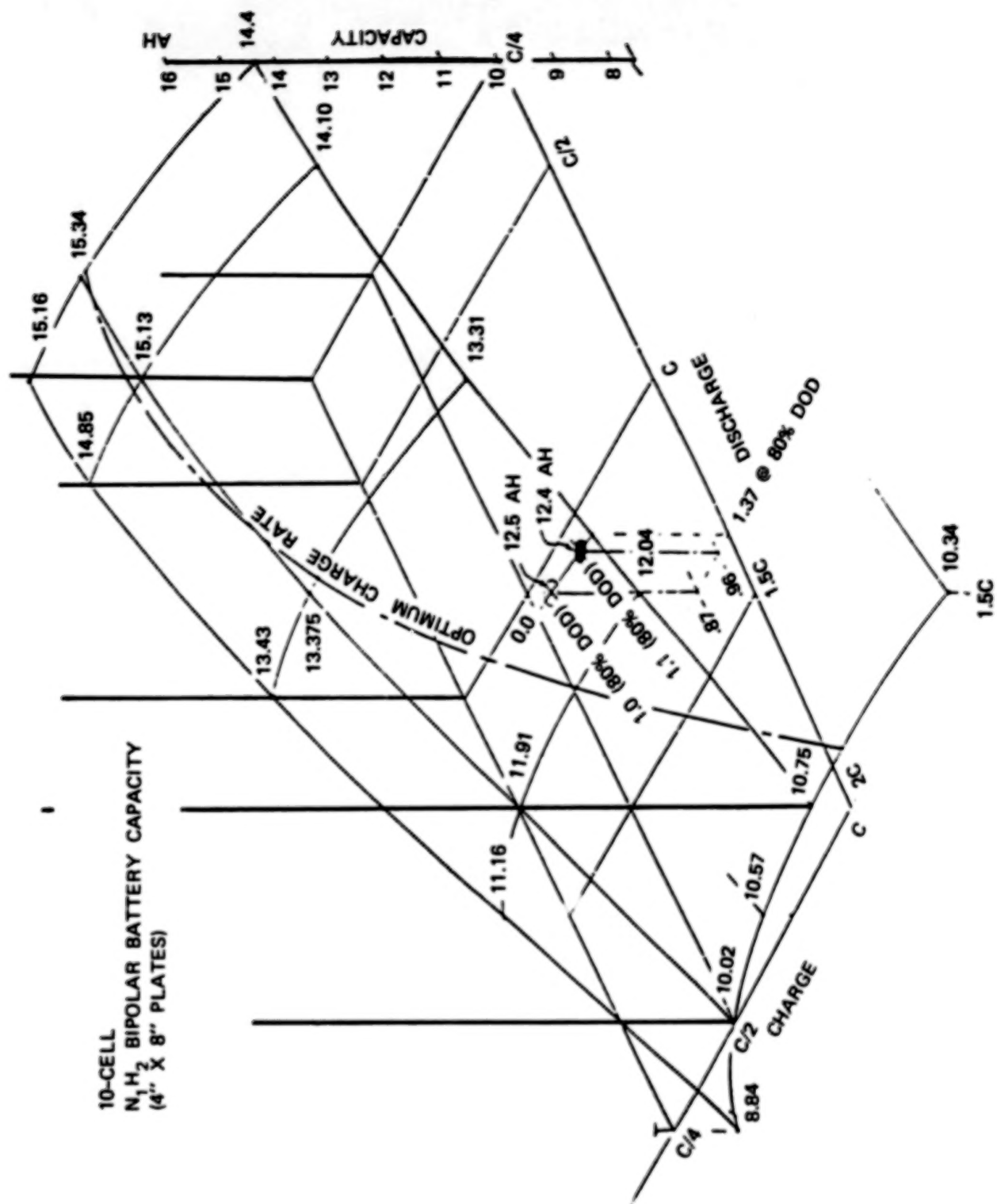


Figure 15.

ORIGINAL PAGE IS
OF POOR QUALITY



Figure 16.

ORIGINAL PAGE IS
OF POOR QUALITY



Figure 17. 75 AH NiH₂ Battery.

FAILURE ANALYSIS OF A 3.5 INCH, 50 AMPERE-HOUR
NICKEL-HYDROGEN CELL

KENNETH H. FUHR
MARTIN MARIETTA DENVER AEROSPACE
DENVER, COLORADO

Abstract

The 3.5 inch, 50 ampere-hour nickel-hydrogen cell was on a Low Earth Orbit (LEO) test regime and was being cycled at 10°C and 60% depth of discharge. At cycle number 511 the Automatic Control and Data Acquisition System (ACDAS) terminated the test when the end of discharge voltage dropped below the 1.00 volt cutoff. Upon removal of the stack assembly from the pressure vessel, portions of the zircar separator were found to be completely missing. Upon further examination portions of both the positive and negative plates were found to be missing from its substrate and several gas screens were damaged due to excessive heat which caused fusing. The postulated cause of failure is free electrolyte in the cell which caused oxygen channelization resulting in localized recombination which degraded the stack components leading to a short.

Introduction

The subject nickel-hydrogen cell was manufactured according to the Hughes-Airforce specifications with the recirculating electrode stack design using two layers of zircar separators. The cell is 3.5 inches in diameter and is rated at 50 ampere-hours.

The cell was mounted to a cold plate by means of an aluminum collar and the cold plate was oriented inside an environmental chamber such that the cell was being tested in the horizontal position. The test chamber was kept at 10°C and the cold plate was also cooled to 10°C with circulating chilled water.

The cell was on a LEO test regime consisting of 55 minutes charge time, and 35 minutes discharge time and was being tested to a 60% depth of discharge. Cycling was controlled automatically on the ACDAS to permit unattended operation. During the charge phase of cycle #509 the cell voltage began deviating from the other test cells by 80 millivolts. During discharge on cycle #511 the cell voltage dropped below the 1.00 volt cutoff and the ACDAS terminated the test. The cell was removed from the test fixture and an insulation resistance test between mounting collar and pressure vessel was performed and found to be greater than one megaohm. The internal impedance was found to be 1.10 milliohms compared to the initial impedance of 1.15 milliohms.

08011-887

A reconditioning charge of 5.0 amps was applied for 16 hours during which time the maximum voltage recorded was 1.397 volts. Upon termination of the charge, the open circuit voltage was monitored and found to decay to 1.0 volt over a three hour period. A one ohm resistor was placed across the terminals for twenty-four hours to completely discharge the cell. After this time a shorting wire was placed across the terminals until the failure analysis could be performed.

Failure Analysis Results

The shorting wire was removed and the voltage was monitored for possible signs of recovery of which there was none. The cell was placed in a nitrogen glove box and the fill tube was cut off. The cell was inverted in order to allow free electrolyte to drain. Approximately 2-3 milliliters of electrolyte were collected. The cell was orientated with fill tube up and evacuated and allowed to back fill with nitrogen. This procedure was repeated for a total of four cycles in order to remove residual hydrogen gas. The vacuum line was again attached to the cell and it was evacuated and inverted to remove any remaining electrolyte. An additional 2-3 milliliters were obtained. The cell was then mounted in a lathe and a high speed motor with a Norton A364 reinforced carborundum wheel attached to the motor shaft was mounted on the tool post of the lathe. The pressure vessel was opened by cutting through the walls on the cylinder side of the girth weld making sure penetration of the cutoff wheel was deep enough to cut through the inside weld ring. The terminal hardware was removed and the dome end of the cylinder was removed. The edges of the cylinder were deburred and the cutoff area was thoroughly cleaned to remove cutting debris.

Upon removal of the plate stack from the pressure vessel, a large dark area was clearly visible (Figure 1) beginning at positive plate (counting from positive terminal end) number 15 and continuing to approximately positive plate number 38 with the major damaged area occurring from plate 15 to plate 31 (Figure 2). Detailed examination of the plate stack assembly revealed the complete absence of separator material. Active material was noted to be missing from both the positive and negative substrate (Figures 3 & 4). Shorting of adjacent positive and negative plates was found in these areas. Portions of the gas screens from this area were found to be missing and the edges of the missing area appeared to be burned or fused together (Figure 5). Examination of the separator material also revealed portions of it to be missing, (Figure 6).

Conclusions

The cause of failure is hypothesized to be free electrolyte collecting in the bottom of the stack when the cells were being tested in the horizontal position. This excessive electrolyte in turn results in oxygen channelization causing localized recombination. The localized recombination results in hot spots and "popping" which destroys the separator and plates. The popping causes plate material to be dislodged from the substrate which in turn caused the plate to plate short.

ORIGINAL PAGE IS
OF POOR QUALITY

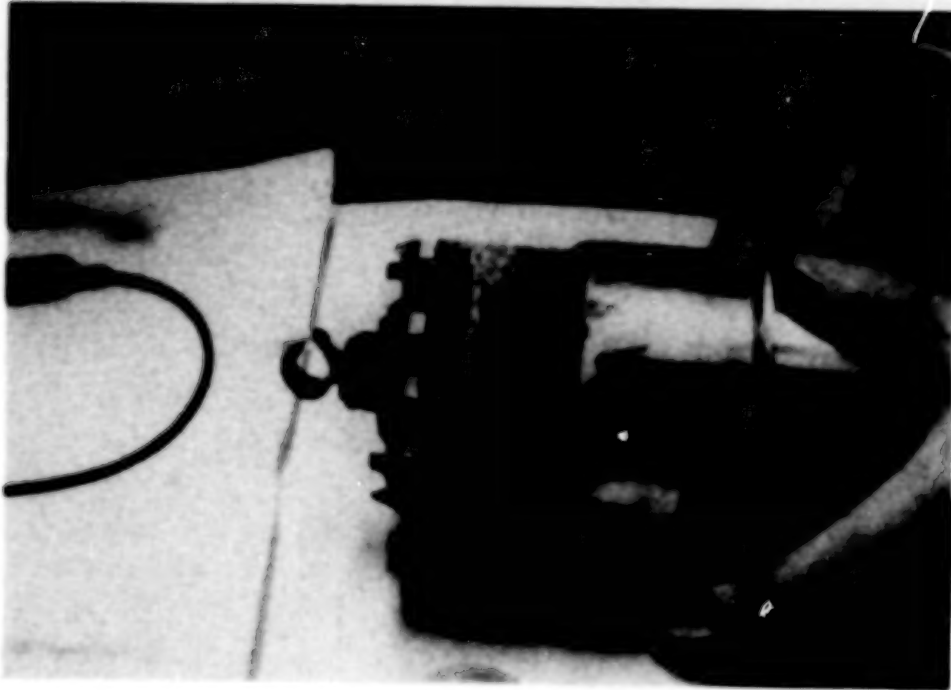


Figure 1.

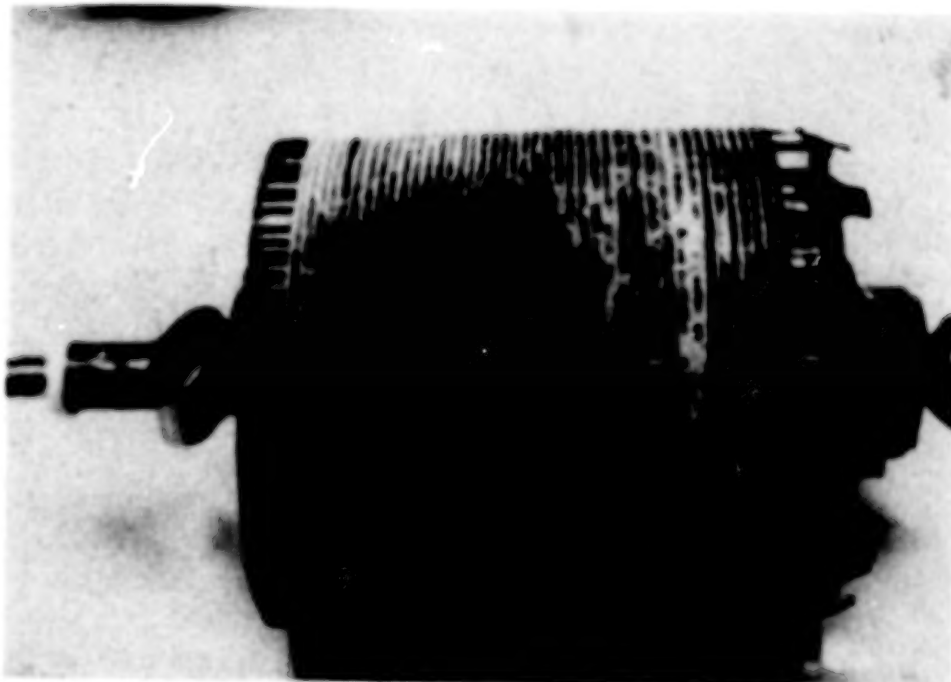


Figure 2.

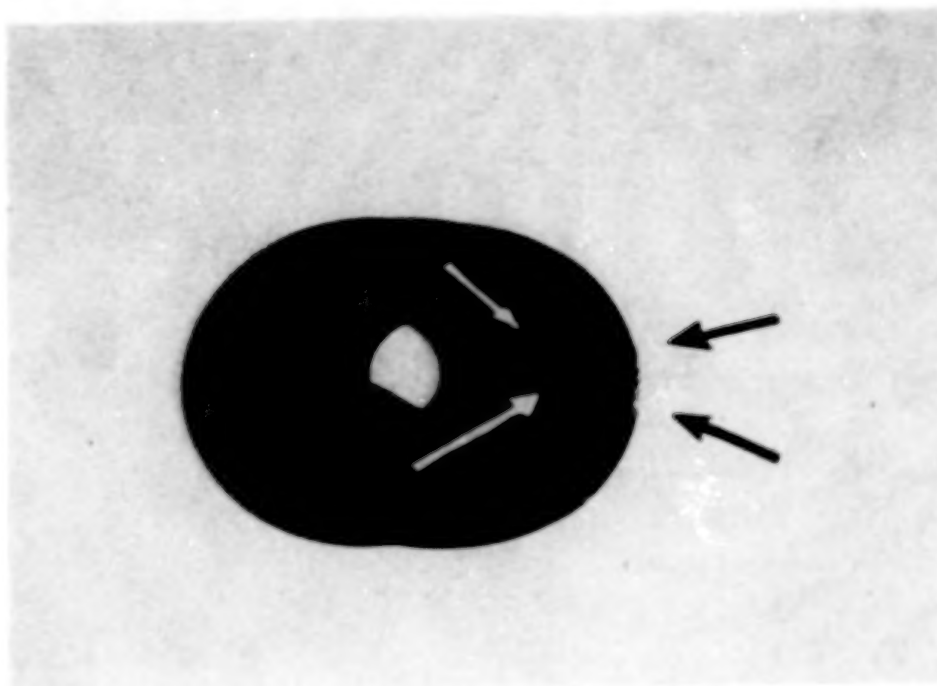


Figure 3.

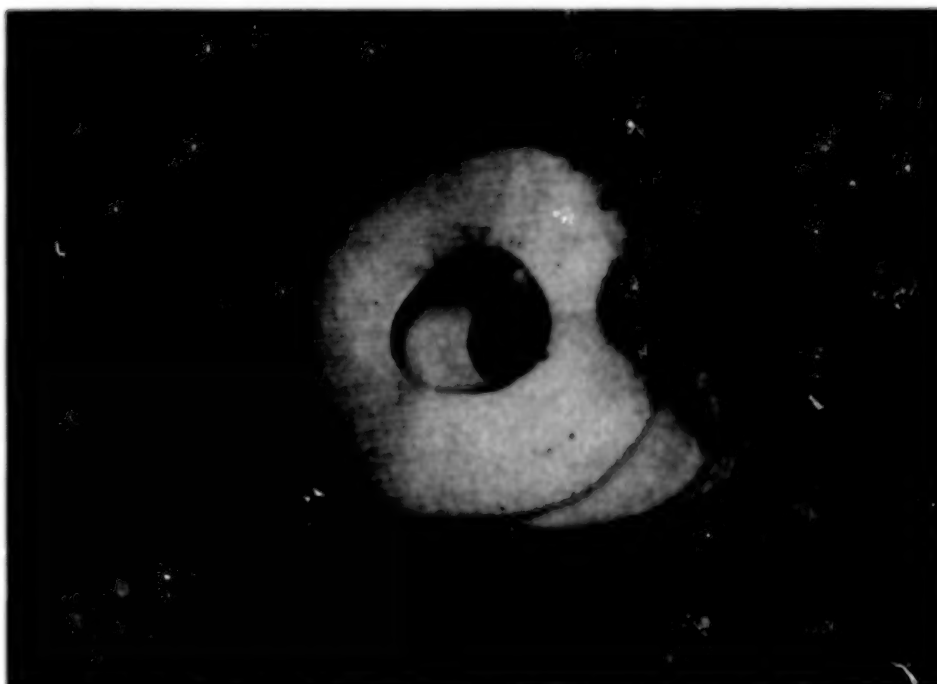


Figure 4.

ORIGINAL PAGE IS
OF POOR QUALITY

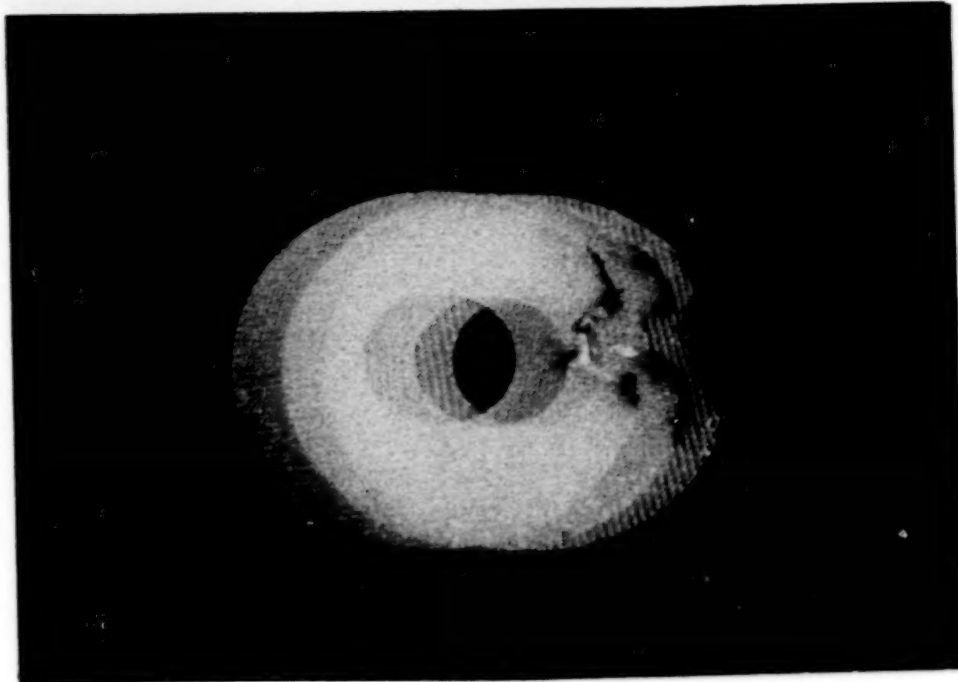


Figure 5.

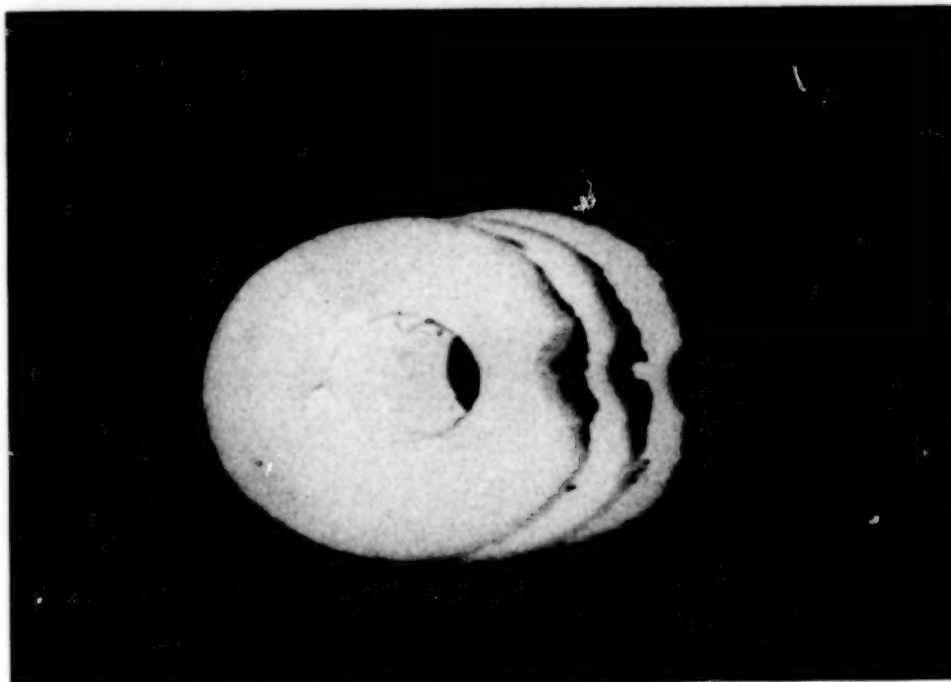


Figure 6.

Grace DAKASEP Alkaline Battery Separator

R. T. Giovannoni, J. T. Lundquist
W. R. Grace & Company, Research Division
7379 Route 32, Columbia, MD 21044

and

W. M. Choi^{*}
W. R. Grace & Company, Polyfibron Division
62 Whittemore Avenue
Cambridge, MA 02140

The Grace DAKASEP separator was originally developed as a wicking layer for nickel-zinc alkaline batteries. DAKASEP is a filled non-woven separator which is flexible and heat sealable. Through modification of formulation and processing variables, products with a variety of properties can be produced. Variations of DAKASEP have been tested in Ni-H₂, Ni-Zn, Ni-Cd and primary alkaline batteries with good results.

Table I shows properties of DAKASEP which are optimized for Hg-Zn primary batteries. This separator has high tensile strength, 12 micron average pore size, relatively low porosity at 46-48% and consequently moderately high resistivity. Versions have been produced with greater than 70% porosity and resistivities in 33 wt% KOH as low as 3 ohm cm.

Performance data for Hg-Zn E-1 size cells containing DAKASEP with properties shown in Table I are more reproducible than data obtained with a competitive polypropylene non-woven separator. In addition, utilization of active material is in general considerably improved.

^{*} Person to whom inquiries about DAKASEP should be addressed.

PRECEDING PAGE BLANK NOT FILMED

Table I

GRACE DAKASEP Alkaline Battery Separator Characteristics*

<u>Production Run Number</u>	<u>47</u>	<u>48</u>
Ream Weight (pounds/3000 ft ²)	74.2	71.7
Thickness (mils)	11.5	11.5
Tensile strength (pounds/in ²)	1260	1190
Tensile (pounds/in)	14.5	13.7
Maximum pore size (micron)	21.1	21.1
Average pore size (micron)	12.0	12.2
Porosity (volume percent)	46	48
Wetout time (sec in 33% KOH)	<3	<3
Resistivity (ohm cm)	15.0	14.8

*Note that properties of DAKASEP can be tailored to customer specifications.

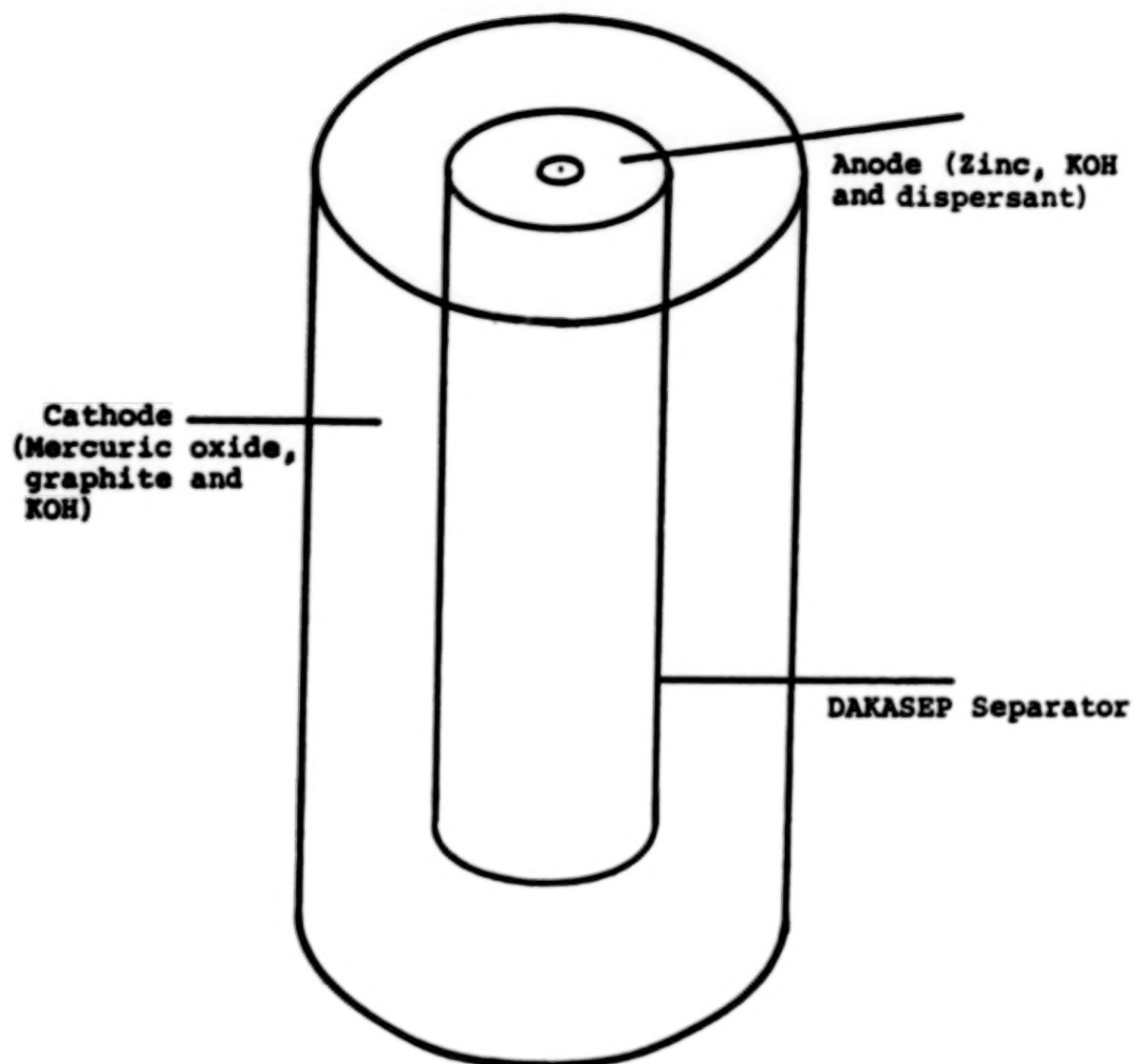
GRACE DAKASEP Alkaline Battery Separator Development

- Grace has developed a separator for alkaline batteries.
- DAKASEP is a filled non-woven (flexible and heat sealable) separator.
- Properties of DAKASEP can be tailored to battery manufacturers specifications.
- Variations of DAKASEP have been tested in Ni-H₂, Ni-Zn, Ni-Cd and primary alkaline batteries with promising results.

<u>Production Run Number</u>	<u>47</u>	<u>48</u>
Ream Weight (pounds/3000 ft ²)	74.2	71.7
Thickness (mils)	11.5	11.5
Tensile strength (pounds/in ²)	1260	1190
Tensile (pounds/in)	14.5	13.7
Maximum pore size (micron)	21.1	21.1
Average pore size (micron)	12.0	12.2
Porosity (volume percent)	46	48
Wetout time (sec in 33% KOH)	<3	<3
Resistivity (ohm cm)	15.0	14.8

* Note that properties of DAKASEP can be tailored to customer specifications.

Figure 1. GRACE DAKASEP Alkaline Battery Separator Characteristics.*



Schematic Representation of a
Hg - Zn Cell

Figure 2.

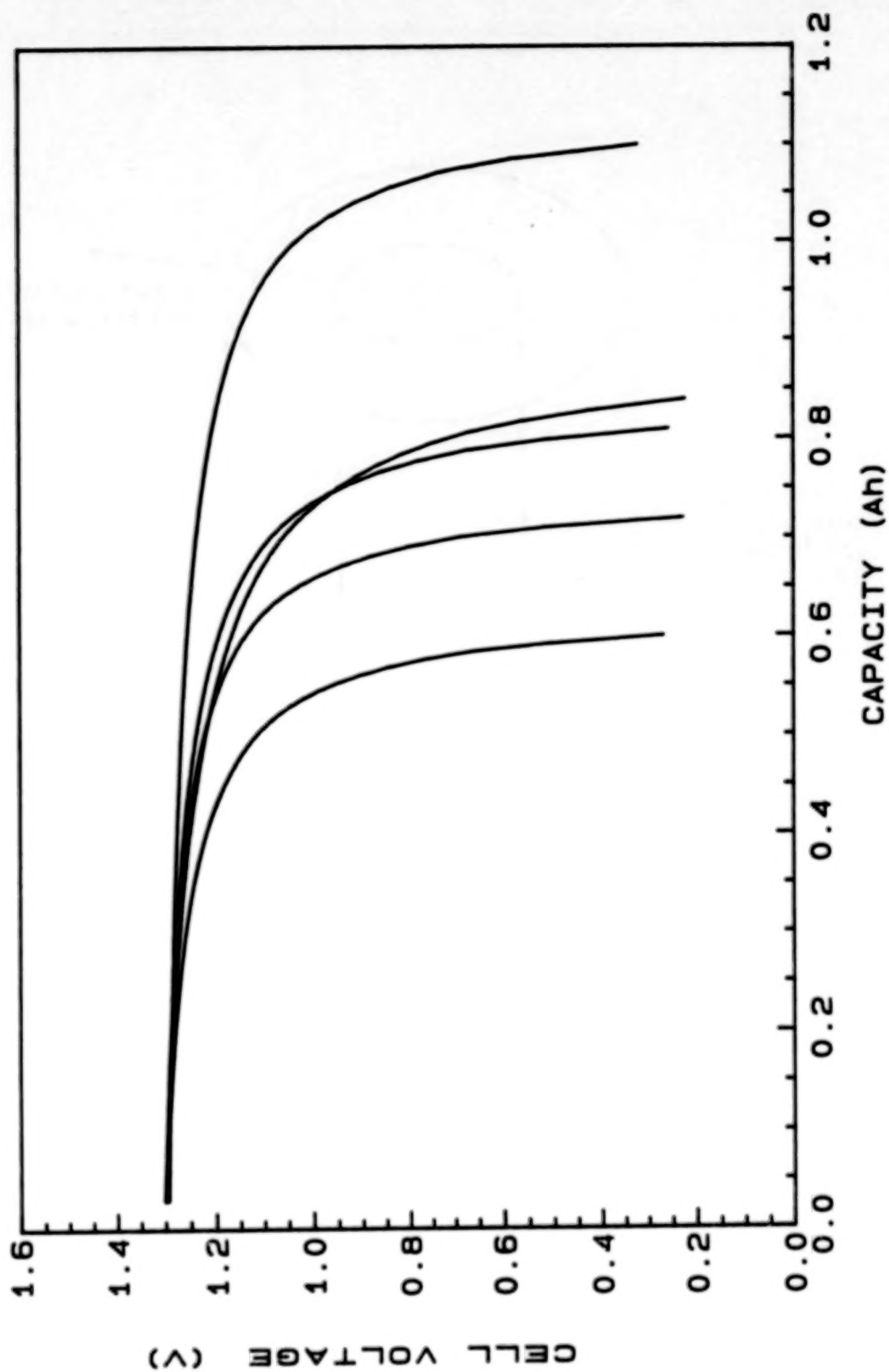


Figure 3. Performance of E-1-Size HG/ZN Cells ($R = 35 \text{ OHM}$); Competitive Separator (Polypropylene Nonwoven).

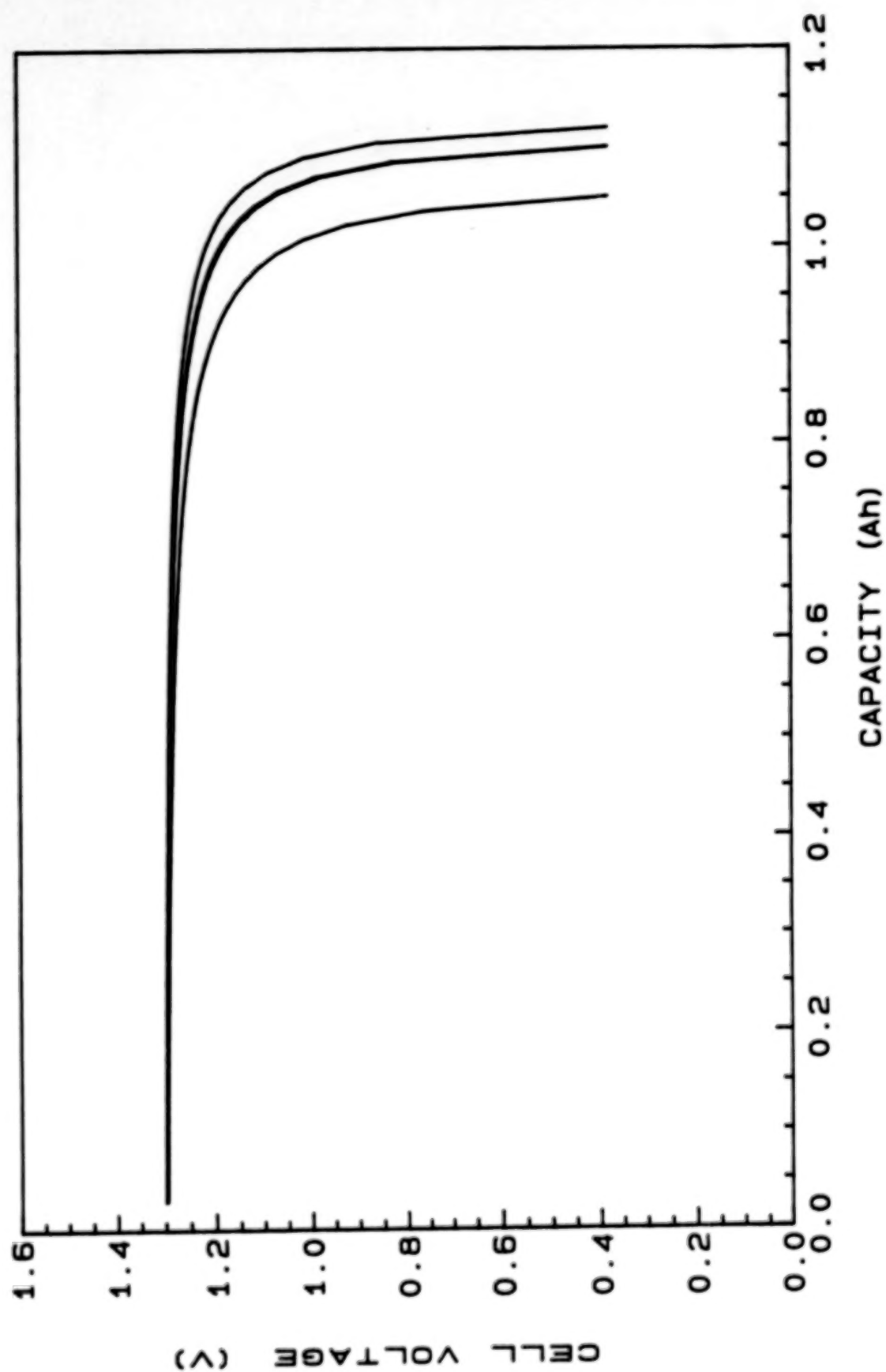


Figure 4. Performance of E-1-Size HG/ZN Cells ($R = 35 \text{ OHM}$); Grace DAKASEP Separator.

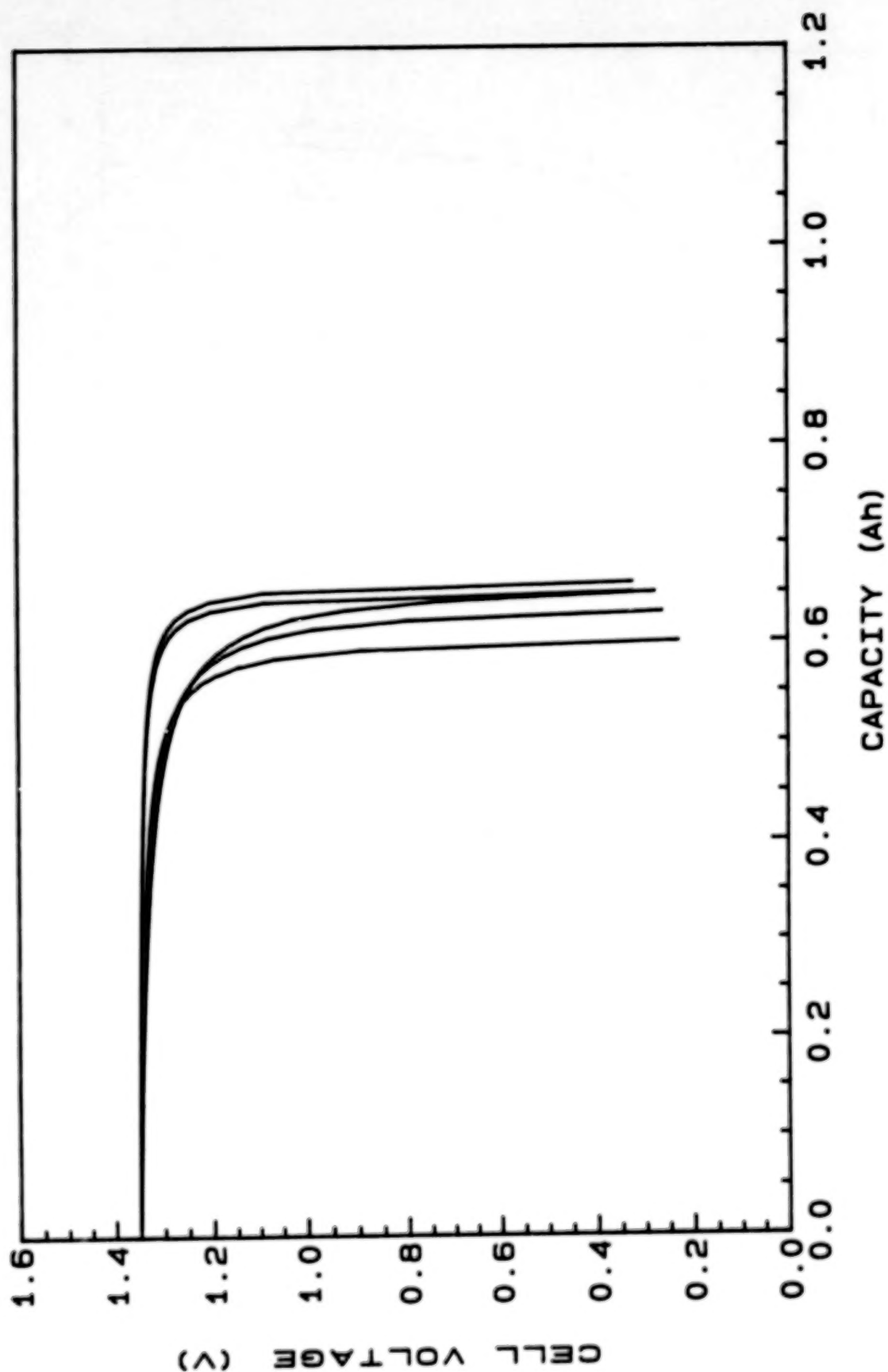


Figure 5. Performance of E-1-Size HG/ZN Cells ($R = 15 \text{ OHM}$); Grace DAKASEP Separator.

SESSION III

SIMULATED ORBITAL CYCLING & FLIGHT EXPERIENCE

Chairman: T. Yi, NASA/GSFC

Sérgio Ricardo Azevedo Ferreira

Space Segment Division

EMBRATEL

Rio de Janeiro, Brasil

ABSTRACT

A description of the anomalies encountered during ground preparation for launch and in-orbit operation of Brasilsat A2 batteries is given.

Processes used during recovery of these batteries and the improvement on main parameters are discussed, covering many cycles of reconditionnings and behaviour during SEPTEMBER/86 eclipse charge/discharge cycles.

INTRODUCTION

Brasilsat A2 is a HS-376 Spacecraft that uses 2 NiCd batteries. They were formed from cells that came from two different lots under GE fabrication/inspection procedures.

These cells were activated in October 1984 because initial planning had A2 launch scheduled for August 1985. This date was delayed to March 1986 when was finally launched from KOUROU (French Guiana).

During the tests at the manufacturer, no anomalies were reported with the lots and, the capacities and mass values measured, were all compatible with the size of the cells. Also agreed with the numbers seen in A1 cells.

Based on the HUGHES criteria (higher capacities/lower masses) the cells were selected and some additional testing were carried out which showed no strange behaviour.

In January 1985, the cells were assembled in packs at KANATA (SPAR facility) and the first reconditionning at this level was made (march 1985), showing good results in terms of capacity and cell voltages. After that, followed a 2 month period at ambient temperature mounted on the S/C for the mass-properties.

Right after that, the batteries had their F.A.T. (june/85) which presented good results, comparable with the ones previously seen.

From June until October/85, the packs went to cold storage and then, had two reconditionning cycles at 20° C and 10° C as preparation for the launch campaign. During these cycles, no abnormal values were registered, assuring that no degradations were caused due to the storage, except for the failure in the final "retention test" of one cell in battery 1. A similar test was performed (10 min of boost charge + 24 hours stand) and all cells passed. The failure was considered not too serious, because the cell voltage was below but close to the minimum required value (MIN = 1.15V and cell voltage at 1.065 Volts).

CAMPAIGN (FIRST PHASE)

The packs were then shipped to the launch site (KOUROU) and as they arrived (MID-OCTOBER), an initial 40 hours charge at C/20 (1.2 Amps) was initiated. For this charge a few air conditioners/fans were used in order to maintain pack temperatures at low values (24° C) even after reaching ROLLOVER. During the charge, it was noticed that 3 cells didn't have a ROLLOVER. But this phenomena was explained by the fact that the cells were all placed at extremes of the packs thus, having a more efficient cooling effect, that forced the cells temperature down. Consequently, the cell voltages remained at their PEAK values.

After this initial charge, the batteries were kept on a weekly TOP-UP regime (charge at C/10 until PEAK + 30 min). In the beginning of the first TOP-UP (31/OCT/85) it was observed that cell # 17 on battery 1 had a voltage about 12 mV (2 bits on 1W) below the whole group. This difference persisted throughout the charge. The subsequent TOP-UP's (NOV 8th and 14th) showed the same behaviour, making believe that this particular cell had a higher self-discharge current when left on open circuit.

With the postponement of the launch date to FEB/86, it had been decided a break on the campaign, leaving the batteries discharge/shorted and mounted on the S/C, due to the period of storage (10 weeks) and to minimize the handling.

Thus, a discharge happened on NOV.14th and a small decrease in measured capacities was observed (Table 1). Cell # 17 on battery 1 was the lowest cell, confirming the suppositions.

PHASE	BATTERY 1	BATTERY 2
KANATA	26.13	26.65
14.11.85	25.95	26.13
24.01.86	24.45	25.01
28.01.86	24.83	25.20
29.01.86	24.45	25.01

TABLE 1 - Capacity Variation

NOTE: Values in Amp. hours

The storage period finished on JAN 22nd, when batteries were charged for 40 hours at C/20. The maximum voltage values recorded during this charge, revealed an increase of about 18 mV (3 bits) as shown in Table 2.

PHASE	BATTERY 1	BATTERY 2	TEMPERATURE
OCT 25th	1.459 V	1.453 V	- 23 C
JAN 22nd	1.477 V	1.474 V	- 22 C

TABLE 2 - Maximum cell voltages(at 1.2 Amps)

As per Hughes recommendation, 3 extra cycles were performed on these batteries. A summary of these cycles is given in Table 1, which shows a reduction in capacity values of - 6% compared to the NOV 14th discharge. The charges at C/10 had to be interrupted because of high cell voltage problems (exceeding the VxI curve), causing shifts on the limiting curve and reduction on the rates in order to complete the charges. Table 3 shows a comparison of the maximum cell voltages in two charges at C/10, before and after the storage.

PHASE	BATTERY 1	BATTERY 2	TEMPERATURE
F.A.T.	1.489 V	1.481 V	- 20 C
JAN 27th	* 1.508 V	* 1.506 V	- 21 C

TABLE 3 - Maximum cell voltages (at 2.4 Amps)

* Charge aborted

From the end of January until the launch day (March 28th) the batteries experienced 3 different management procedures. Initially, we started with the traditional TOP-UP (C/10; once a week) that was accumulating too much time in open-circuit stand, aggravating the spread on cell voltages (specially on battery 1) and, not bringing any significant improvement on the high voltage problem.

On March 11th the rate was changed to a Trickle charge (\approx C/50), which was applied daily for about 10 to 15 hours (limited by maximum temperature allowed = 29.4°C). The result was a better equalization of the cells at end-of-charge, although the other mentioned anomalies remained unchanged.

IN-ORBIT BEHAVIOUR

After launch, in the initial transfer orbits, the stop charge criteria used didn't allow batteries to reach the ROLLOVER thus, hiding the high voltage problem. A few hours after the panel was deployed, the Trickle charge was turned ON. The pack temperatures were around 10°C and in less than 2 hours many cells had exceeded the limit (Table 4), causing the interruption of the charge.

PACK ($^{\circ}\text{C}$) TEMP.	5	6	7	8	9	10	11	12	13	14	15
MAXIMUM VOLTAGE (V) TRICKLE	1.484	1.482	1.480	1.478	1.476	1.474	1.472	1.470	1.469	1.467	1.465
MAX. VOLT. AT C/10	1.539	1.537	1.534	1.531	1.529	1.526	1.524	1.521	1.519	1.516	1.514

TABLE 4 - Charge Limit

For the last 15 days of eclipse in this season, the recharge management was:

- Charge at (M+I) or C/20 until limit is reached (Table 4);
- Try once a day a Trickle charge;
- Leave in open-circuit for the rest of the day.

This procedure was enough to support these discharges.

RECONDITIONING CYCLES

The proposed "solution" for the problems was to have the batteries reconditioned a few times (Table 5), until it accepted the trickle charge without exceeding any limit

BAT	1st CYCLE	2nd CYCLE	3rd CYCLE	4th CYCLE
1	April 21st	May 21st	May 26th	June 1st
2	May 5th	May 12th	-	-

TABLE 5 - RECONDITIONING SCHEDULE

Battery 1

In the first cycle (April 21st), the results obtained showed a highly reduced capacity (Table 6), probably due to cell # 17. During the charge, at about 105% of the removed capacity, cell 32 exceeded the C/20 limit. This battery maintained its behaviour on Trickle, although showed some improvement.

TABLE 6 - Capacity Evolution

CYCLE	** EXPECTED VALUES	1	2	3	4
BAT 1	- 29.00	24.18	23.77	26.93	26.76
BAT 2	- 29.58	* 26.94	27.70	-	-

* Values in AH

** 111% of the FAT values

The second cycle occurred only on May 21st, after the two reconditionnings on battery # 2, before which it had been maintained by a 2 trickle charge tries per day routine. This one month period, removed the small improvements caused by the first cycle.

The results showed a further reduction in capacity and the charge (C/20) stopped at 103% return, with higher average cell voltage.

Other two cycles were performed, and the capacity suffered a big increase (~ 3 AH). The cell voltages had a smaller spread at ROLLOVER, with a reduction on the rise rate (mV/min). The Trickle charge was applied without problems, although the C/20 rate still had to be interrupted (at ~ 104% return).

Battery 2

It was first cycled on May 5th, also presenting a large reduction in capacity (Table 6) and having to stop the charge prematurely (~ 107%), because of cell # 20 excessive voltage. Trickle charge was still forcing the cells to go above limits. The second cycle (May 12th), showed a 0.76 AH increase in capacity. Although still having the (M+T) charge aborted at 106% return, the trickle charge was fairly well accepted by the cells.

A smaller charge rate (~ 0.2 Amps) was used between the reconditionning cycles, and proved to have helped a lot on equalizing the cells before the subsequent discharge, decreasing significantly the spread, without making the cell voltages go above to limits.

AUGUST RECONDITIONNING PERFORMANCE

During the August/86 reconditionning, a relevant enhancement was verified in all parameters. The capacities increased almost to the expected values (Table 7) and the cells could be charged at the C/20 rate without exceeding significantly the limits (maximum 3 mV = 1/2 bit). These improvements were probably caused by the long period in the trickle charge rate, that helped equalizing the state of charge of the cells and breaking the "big crystals" formed in the overcharge protection region of the plates, called as responsible for the high voltage anomaly.

BAT	CAPACITY (AH)	MAX. CELL VOLT.	TEMPERATURE	LIMIT
1	27.91	1.534 V	.8 ° C	1.531 V
2	28.85	1.512 V	8 ° C	1.531 V

TABLE 7 - August/86 Reconditionning

The September/86 eclipse season, demonstrated how healthier these batteries are now, showing values very comparable with the ones achieved by the Satellite A1 batteries. Although the average cell peak voltage is still above the normal (A1) values by about 30 to 40 mV, we've got confidence that with the next 4 month period of continuous trickle charge, the performance in the following season (March/87) will show even better results.

CONCLUSION

It has been presented the sequence of events occurred with the Brasilsat A2 batteries . The long short-circuited in ambient stand period seems to have been the main reason for the major anomalies encountered in the operation of these units. Although it didn't take too long for the problems to arise, the process of removing this uncomfortable behaviour, has been predicted as an arduous and long period. Up to now, a number of reconditioning cycles have been applied with significant improvements in performance. At least, now we can be sure that no permanent degradation occurred, and the life of these batteries shall not be affected.

INTERNATIONAL ULTRAVIOLET EXPLORER (IUE)
SPACECRAFT BATTERY PERFORMANCE UPDATE

SMITH E. TILLER
NASA/GODDARD SPACE FLIGHT CENTER
CODE 711
GREENBELT, MARYLAND 20771

SUMMARY

January 26, 1987 marks the ninth inflight anniversary of the IUE spacecraft, launched into an eccentric synchronous orbit on January 26, 1978. The orbital path has subjected the spacecraft to 18 solar eclipse seasons since launch. Nine years of inflight operations culminate a major milestone for battery support to a spacecraft, which is well in excess of the initial 3-year design life.

Figure 1, provides a brief outline of events, power system characteristics, and papers presented at previous Battery Workshops. In 1978 and 1979, the papers presented describe the IUE battery and cell characteristics and highlight the spacecraft power system design properties. The last paper listed provides an update of battery performance through 1983. Battery cell design characteristics are listed in figure 2 providing pertinent background information relative to the data presented in this paper. It should be especially noted that the battery cells were manufactured utilizing Pellon 2505 separator, and that the negative plates were teflonated to level 1 standards. A second major design characteristic outlined is the light loading of the P.Q. plate with a design goal to reduce plate loading by 10 percent over previous designs. A design goal was also established to increase the quantity of KOH to 4cc/rated ampere-hour. The data listed in figure 3 is the results obtained during cell manufacturing. This data shows the increase in electrolyte (31

percent KOH) and light plate loading resulted in a level of 4.17cc/rated ampere-hour for a 6 ampere-hour nickel-cadmium cell. Figure 4 provides a brief summary of the original battery design parameters. The maximum discharge current level of 4 amps/battery to an 80 percent depth-of-discharge (DOD) limit was the initial design criteria. The DOD limit was decreased to 60-70 percent following eclipse season number 2 to extend battery life as long as possible without unduly limiting spacecraft operations during the eclipse seasons. The objective of this paper is to update battery performance from 1983 through 1986.

CONFIGURATION

The battery photograph presented in figure 5 is typical of the two 6 ampere-hour nickel-cadmium batteries aboard the IUE spacecraft. Each battery contains 16 regular cells and 1 signal electrode cell used to provide charge control in the main battery charger system. The power control system encompasses direct-energy-transfer (DET) of bus power during spacecraft operations. Each battery is diode coupled to the main bus via a boost regulator providing 28 volts of regulated power.

INTRODUCTION

The 6 ampere-hour batteries provide full power for spacecraft operations during the 14 to 77-minute shadow periods of the bi-annual eclipse season which last from 23 to 25 days each. Battery power is also provided wherever the main bus requirement exceed the solar array output during the sun solstice seasons when the spacecraft beta angle is below 0° or greater than 130° .

FLIGHT PERFORMANCE

During the eclipse season shadow periods, battery recharging is accomplished utilizing the spacecraft main charger control system augmented by a low rate trickle charge system. Both operations are depicted in figure 6--the main chargers are operating between elapsed time hours 6 through 16--with the low rate chargers operating from hour 16 to the completion of the 24th hour of the depicted eclipse day. It should also be noted that data previously presented including figure 6 show the batteries are being commanded to a low rate charge (approx. 0.1 amps) at hour 16 because the main charger for battery 2 fails to taper the charge current to the 0.1 amp design level. The charge scheme depicted has been used during all previous recharge operations due to the third electrode sensitivity anomaly.

Telemetry data received during eclipse season 2 indicated that the battery discharge voltage recorded at the peak of the eclipse season (day 17) decreased from 20.25 volts during eclipse season 1, to 19.92 volts at the peak of eclipse season 2. Power conservation measures were implemented to limit the maximum battery discharge to the 4 amp per battery design level. Directives were also initiated to turn off non-critical spacecraft loads when either battery exceeded 50 percent DOD. Data plotted for eclipse season 12 and 18 in figure 7 shows that the action taken reduced battery discharge from a 76.7 percent level for eclipse season 2 to approximately 62 percent for eclipse seasons 12 and 18. Figure 8 provides additional support which shows that the reduction in spacecraft power usage is also conducive in reducing battery DOD during the eclipse season shadow periods.

Immediately after launch, the spacecraft telemetry data indicated that battery 05 was approximately 8°C warmer than battery 06. Data analyzed during eclipse seasons 1 through 9 gave indications that the operational life of battery 05 may be shortened by the warmer temperature delta. However, data plotted for eclipse seasons 10 through 18 indicate that the battery DOD may be the predominate factor in cell degradation. The temperature delta between the batteries appears to be the controlling factors in load sharing, i.e., battery 06 (approx. 23°C) provided more power than battery 05 (approx 15°C) during the peak discharge periods for eclipse seasons 1-9. A switch in load sharing occurred during eclipse season 10 where battery 05 started providing more power than battery 06, supporting the theory that the battery DOD may be the predominate degradation factor. Additional data is shown in figure 10 indicating that battery discharge current is directly proportional to the DOD data previously shown in figure 9.

Figure 11 is a composite data plot of 10 cells on test at NWSC, Crane, Indiana. Discharge cell voltages were plotted versus ampere-hour during a capacity test at the peak of eclipse season 19. It should be noted that the cells are being tested in a simulated synchronous orbit at 10°C to 80 percent DOD. The recharge profile was modified prior to eclipse season 13 to simulate the recharge scheme utilized to recharge the spacecraft batteries. The data demonstrates that the test cells discharge voltages track in a close pattern and that cell capacity exceeds 6 ampere-hours after 18-1/2 simulated eclipse seasons.

CONCLUSIONS

The IUE battery cell performance is excellent--with exception of the third electrode anomaly and temperature delta between batteries. Data indicates that battery DOD may be more critical to extend battery life than small operational temperature deltas between batteries. It is predicted that several additional years of battery life may be obtained by a reduction in operational battery DOD.

INTERNATIONAL ULTRAVIOLET EXPLORER

● LAUNCH DATE:.....	JANUARY 26, 1978
● ORBIT:.....	ECCENTRIC SYNCHRONOUS
● POWER SYSTEM:.....	DIRECT ENERGY TRANSFER
● BATTERIES:.....	TWO 6 AMPERE HOUR NICKEL--CADMIUM
● BATTERY CHARGE CONTROL:.....	THIRD ELECTRODE
	VOLTAGE TAPER
	CURRENT LIMIT
● CELL MANUFACTURER:.....	GENERAL ELECTRIC
● PREVIOUS BATTERY WORKSHOP PAPERS:	
- IUE FLIGHT PERFORMANCE	1978
- UPDATE OF THE IUE BATTERY.....	1979
- PERFORMANCE OF THE IUE BATTERIES.....	1983
	AFTER 70 MONTHS

Figure 1.

IUE CELL DESIGN (6 Ah NiCd)

- GENERAL ELECTRIC CELL
- DUAL, NICKEL-BRAZE, CERAMIC-TO-METAL SEALS
- PELLON 2505 SEPARATOR
- TEFLONATION OF NEGATIVE PLATE, LEVEL 1
- CARBONATE REDUCTION PROCESS
- P.Q PLATE WITH LIGHT LOADING
GOAL: 10% REDUCTION IN LOADING
- HIGHER QUANTITY OF KOH
GOAL: 4cc/RATED Ah

Figure 2.

CELL MANUFACTURING DATA (6 Ah NiCd)

•	LOADING-POSITIVE AVERAGE.....	12.72 gm/dm ²
	NEGATIVE AVERAGE.....	16.2 gm/dm ²
•	THEORETICAL CAPACITY-POSITIVE.....	10.13 Ah
	NEGATIVE.....	18.19 Ah
•	FLOODED CELL TESTS-POSITIVE AVERAGE.....	7.81 Ah
	(ECT) NEGATIVE AVERAGE.....	14.48 Ah
•	NEGATIVE/POSITIVE RATIO.....	1.85:1
•	PRECHARGE SET (BY O ₂ VENTING).....	2.84 Ah
•	ELECTROLYTE (31% KOH).....	4.17 cc/ Rated Ah
•	SEPARATOR SET OUT TIME (AVERAGE).....	39 Sec

Figure 3.

PERTINENT BATTERY DESIGN PARAMETERS

• AVAILABLE POWER TO SPACECRAFT.82 WATTS/BATTERY
• MAXIMUM DISCHARGE CURRENT.4 AMPS/BATTERY
• DEPTH-OF-DISCHARGE80 PERCENT
• ECLIPSE PERIODBI-ANNUAL (23-25 DAYS EACH)
• WEIGHT	5.8 Kg/BATTERY
• SIZE280 CUBIC INCHES/BATTERY

Figure 4.

ORIGINAL PAGE IS
OF POOR QUALITY



Figure 5.

24 HOUR BATTERY RECHARGE CHARACTERISTICS FOR DAY 243, AUGUST 31, 1966

IUE SHADOW SEASON #18

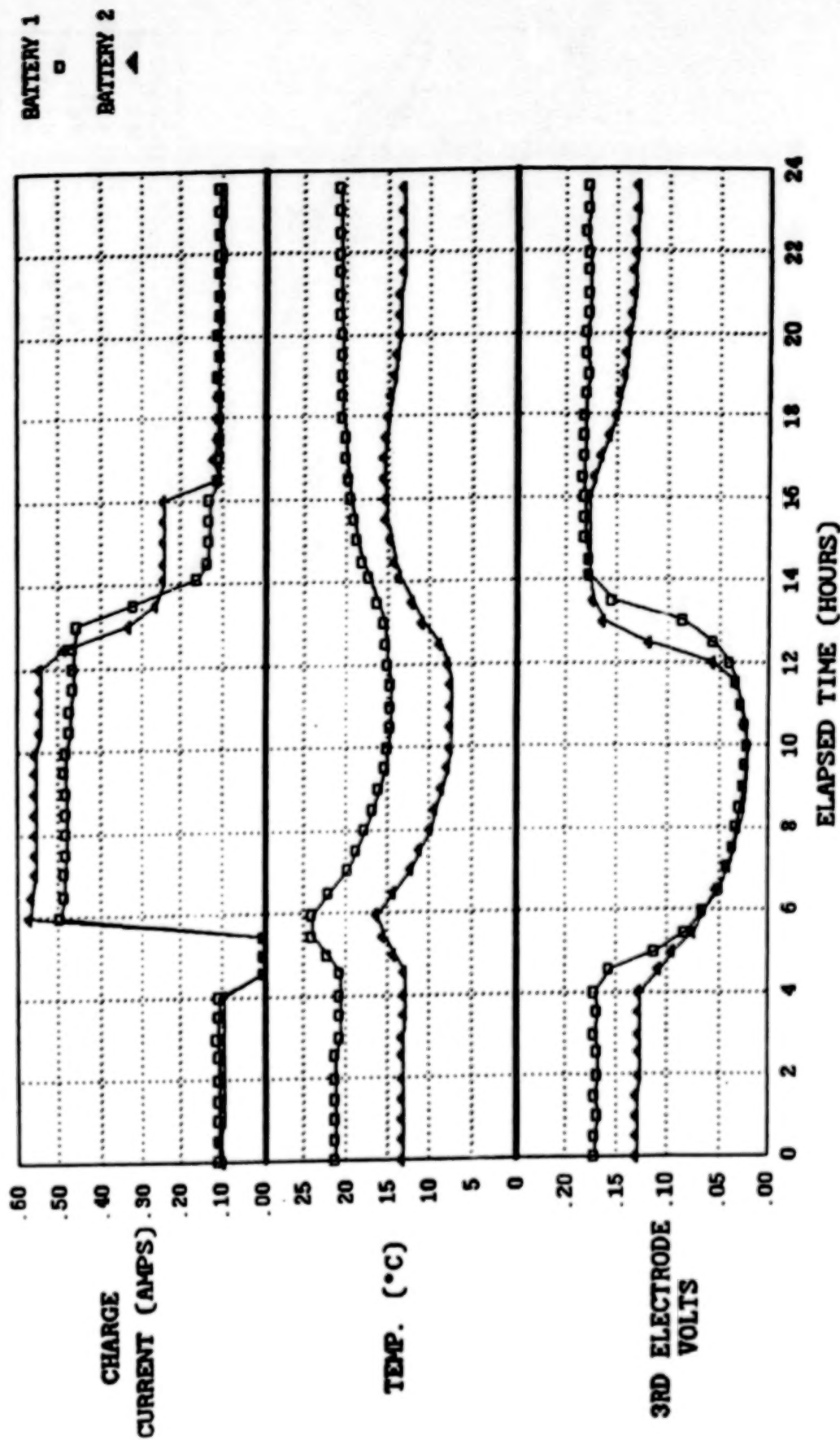


Figure 6.

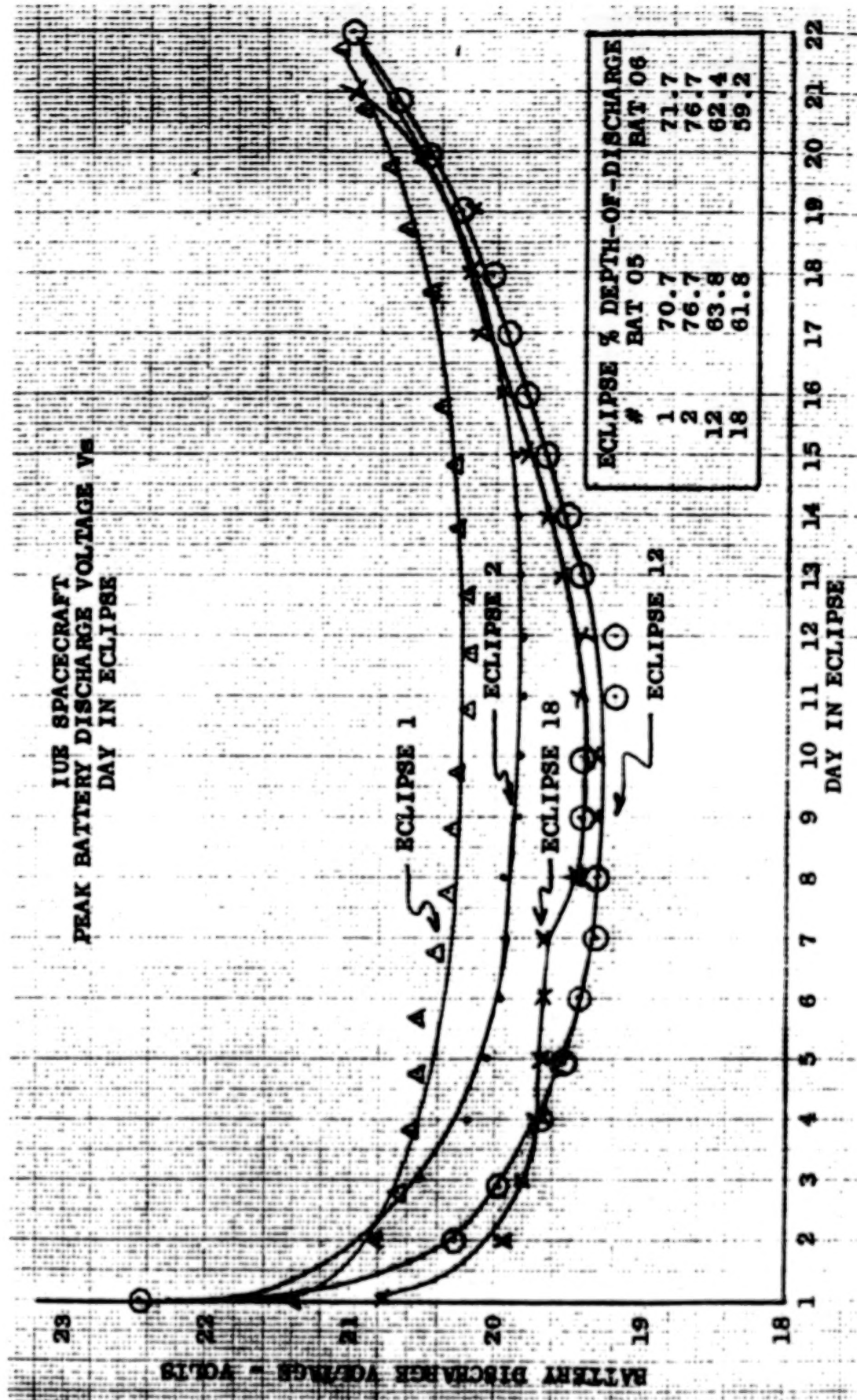


Figure 7.

IUE SPACECRAFT
BATTERY DISCHARGE VOLTAGE
ECLIPSE SEASONS 2, 12 & 18

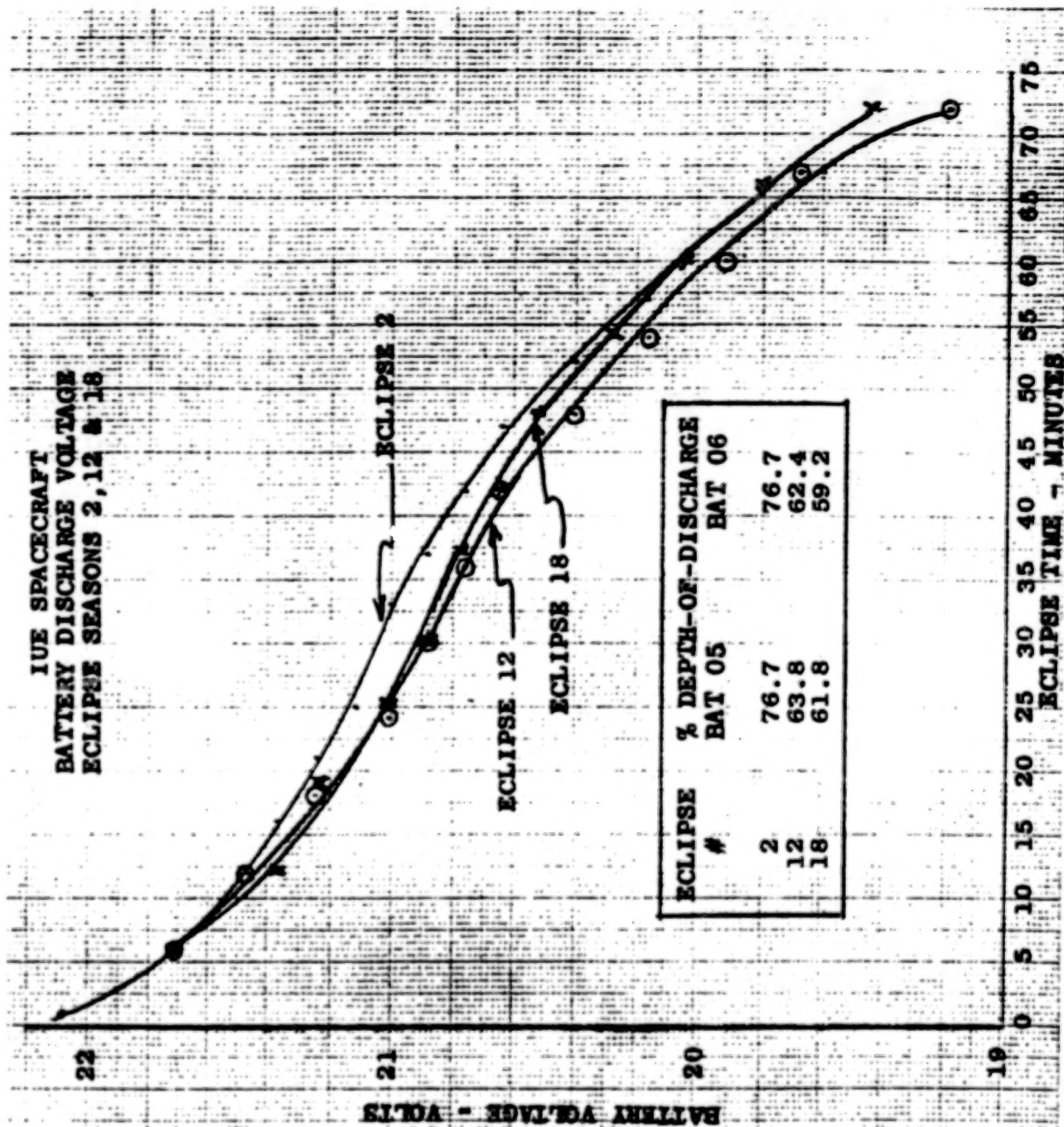


Figure 8.

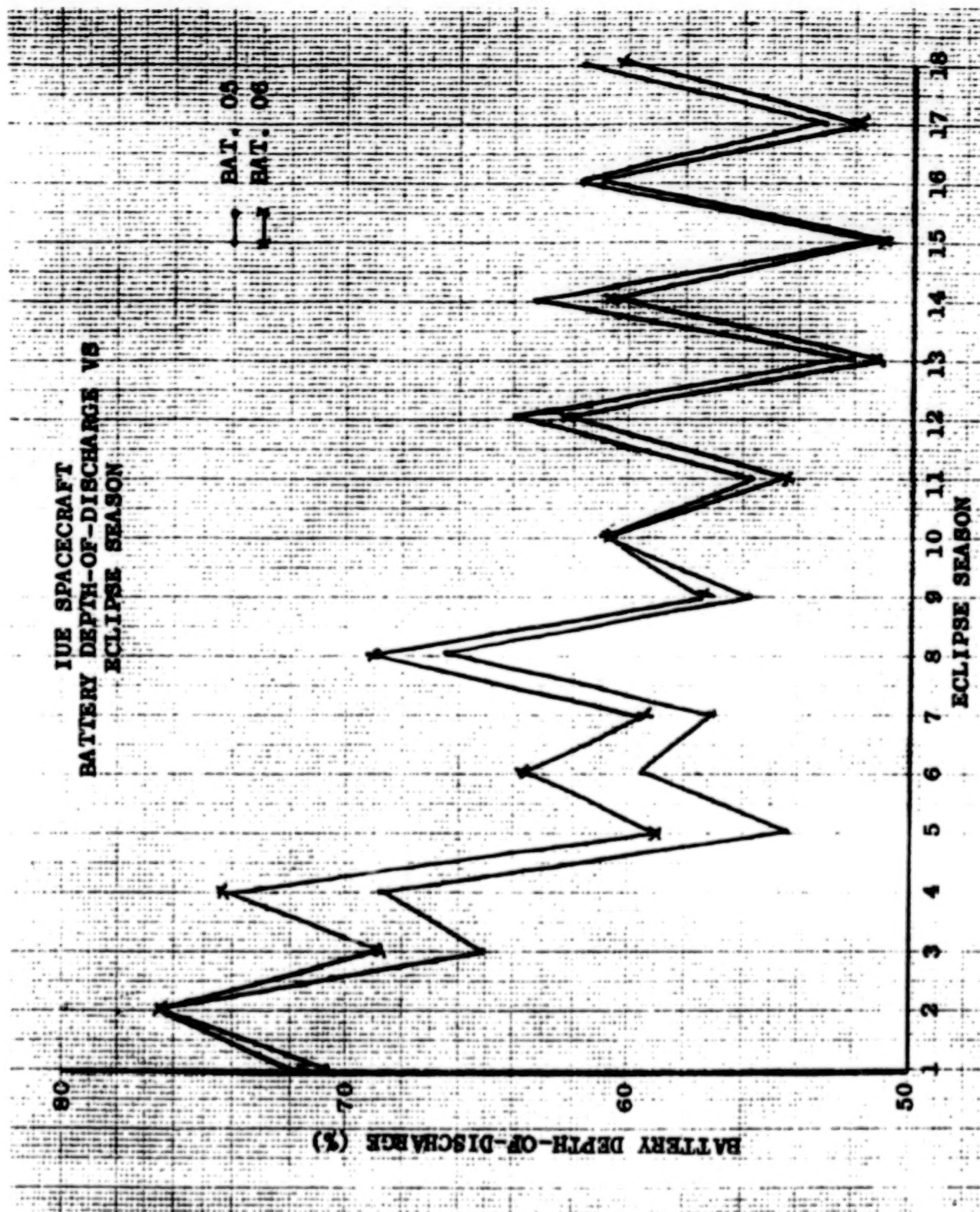


Figure 9.

ORIGINAL PAGE IS
OF POOR QUALITY

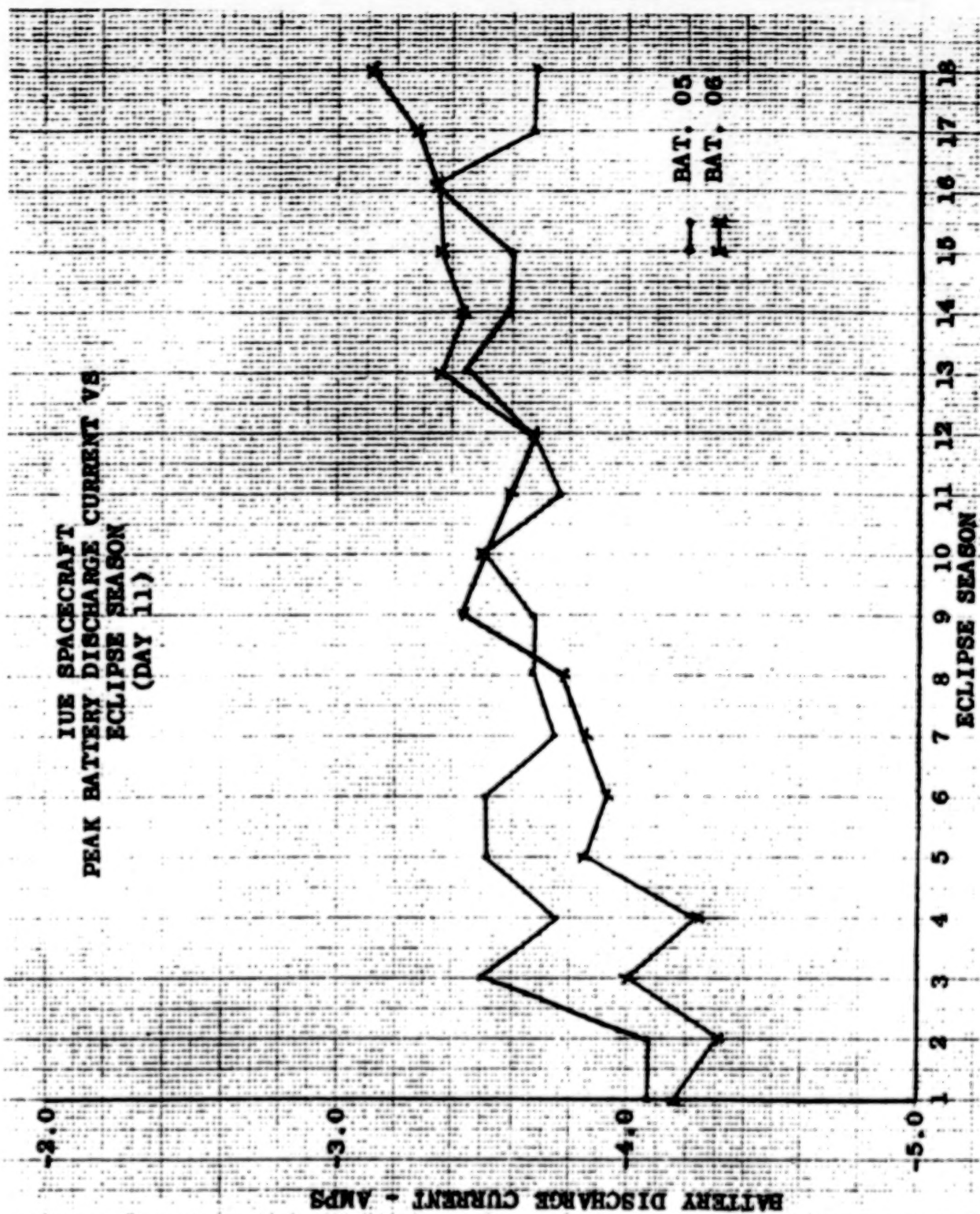


Figure 10.

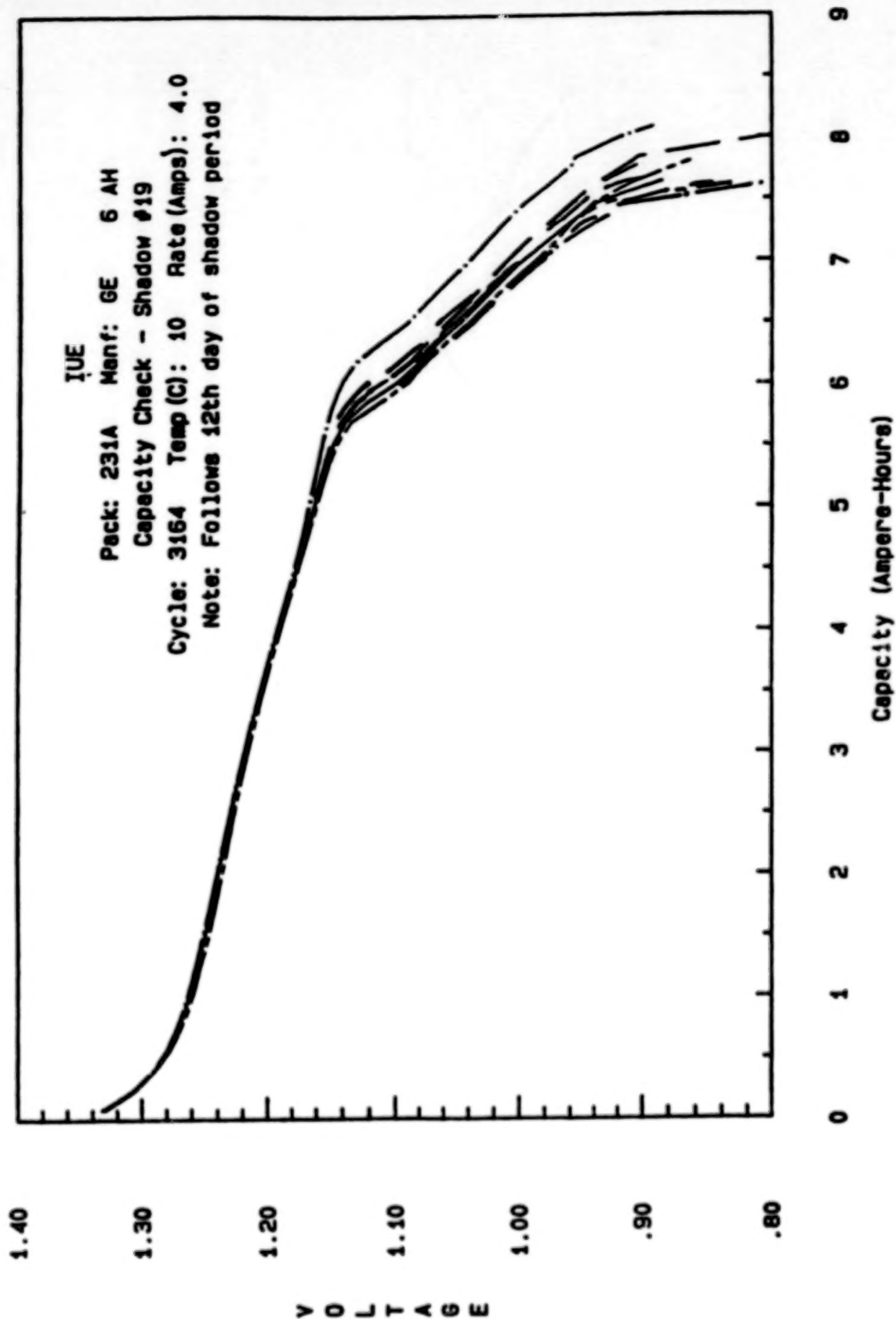


Figure 11.

**EARTH RADIATION BUDGET SATELLITE (ERBS)
ORBITING PROFILES AND Ni-Cd USE**

MARLON L. ENCISO

Space Power Applications Branch, Code 711

NASA/Goddard Space Flight Center

Greenbelt, MD 20771 (U.S.A.)

Summary

The Earth Radiation Budget Satellite (ERBS) is one of the more recently launched satellites of the Goddard Space Flight Center. This paper presents the flight data of the two 50 Ah NASA standard batteries that are being flown on the ERBS. Trend characteristics of the batteries were collected over a period of two years. The parameters that were trended are; the battery end-of-discharge voltage, time in peak power track, and time in constant current mode. All were plotted versus mission elapsed time. The slopes exhibited by the trended parameters indicate no adverse trends that would signify any appreciable degradation in the batteries.

Introduction

The succeeding paragraphs provide a brief background of the ERBS orbital regime and power system configuration in the normal operating mode.

The ERBS was launched on Oct. 5, 1984 from the Space Shuttle Challenger to a 600 km circular orbit with an inclination of 57 degrees from the equator. This orbital configuration gives ERBS a 97-minute orbital period and occasional periods of full-sunlit orbits.

The ERBS power system has a peak power tracker, a constant current trickle charge mode (C/50), and an on-line ampere-hour integrator. These components together with the VT limiting capability controls the charging of the two batteries connected in parallel. The batteries share a common load. Charge control is dependent on the hotter battery, which is battery number 1. These batteries are charged to 32.12 volts (1.46 v/cell), equivalent to the Goddard VT6 at an average temperature of 9 degrees C. The average depth of discharge the batteries are subjected to is 10%.

Shown in Figure 1 is a typical single orbit power profile of the ERBS. As shown, as soon as the solar arrays see sunlight the peak power track takes over and charges the batteries until the voltage reaches the selected VT setting. From here the voltage limiting mode of charging takes place as indicated by the taper charge until the ampere hour integrator indicates 100 % SOC. The batteries are then charged at the constant current mode equivalent to a C/50 charge rate. Figure 2 shows the orbital power profile

ORIGINAL PAGE IS
OF POOR QUALITY

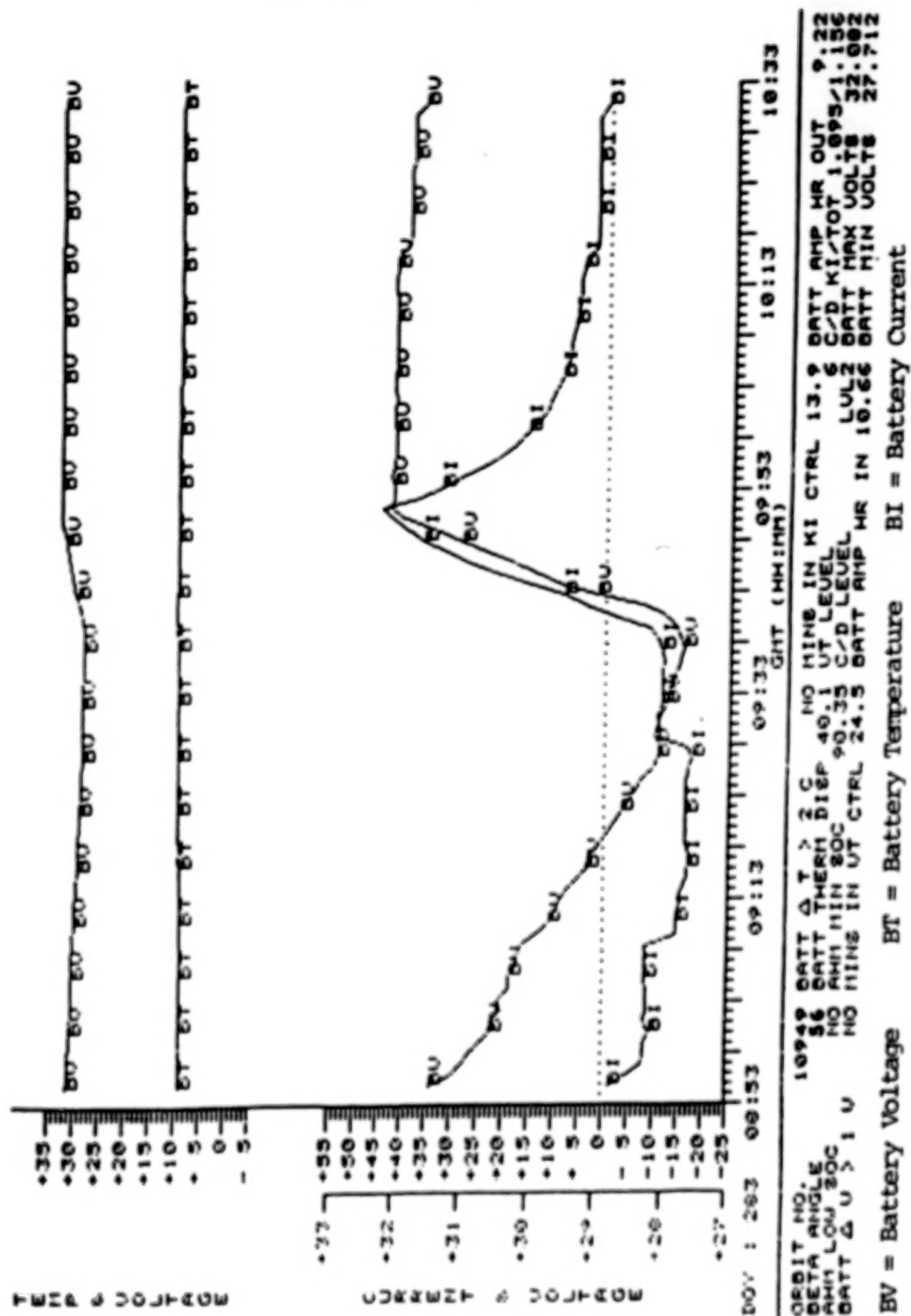


Figure 1. ERBS Orbital Power Profile.

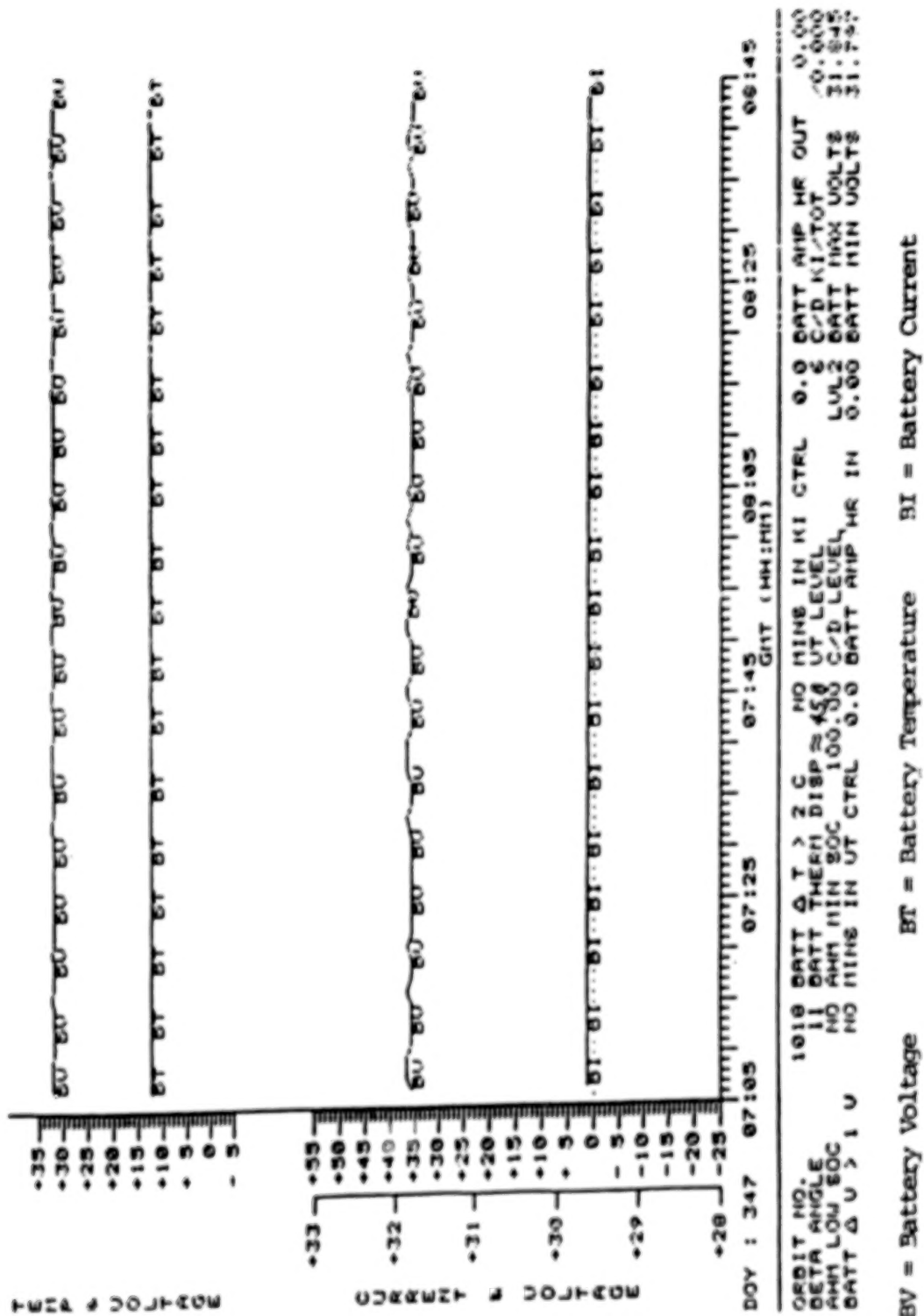


Figure 2. ERBS Orbital Power Profile.

when the spacecraft is in full-sun. Notice that the batteries remain at a constant current charge and the temperature is about 4 - 5 degrees over the orbital average of 9 degrees C.

Flight Data Presentation

For the purpose of providing consistency in the data used in trending the selected battery parameters, a similar orbit comparison technique was used. Data from sun angles 45 and 90 degrees were selected due to their outright availability and for no other reasons. Although, data from the 90 degree sun angle region, which happens to be the worst case eclipse period, gives a more representative end-of-discharge voltage. All the data used for the trending were taken from the orbital power profiles ran for the selected sun angles.

Figures 3 and 4 show the Time in Peak Power Tracking and Time in Constant Current Charge respectively. Both parameters were plotted versus mission elapsed time. Pertinent spacecraft configuration and load conditions for all the data used in both figures as well as Figure 5 are as follows:

Sun angle : 45 +/- 5 degrees

Minimum State of Charge : 93 +/-0.5%

Loads : No power amplifier usage

Current at End-of-Discharge : 12 +/- 2 amps.

Sun angle : 90 +/- 2.5 degrees

Minimum State of Charge : 91 +/-1%

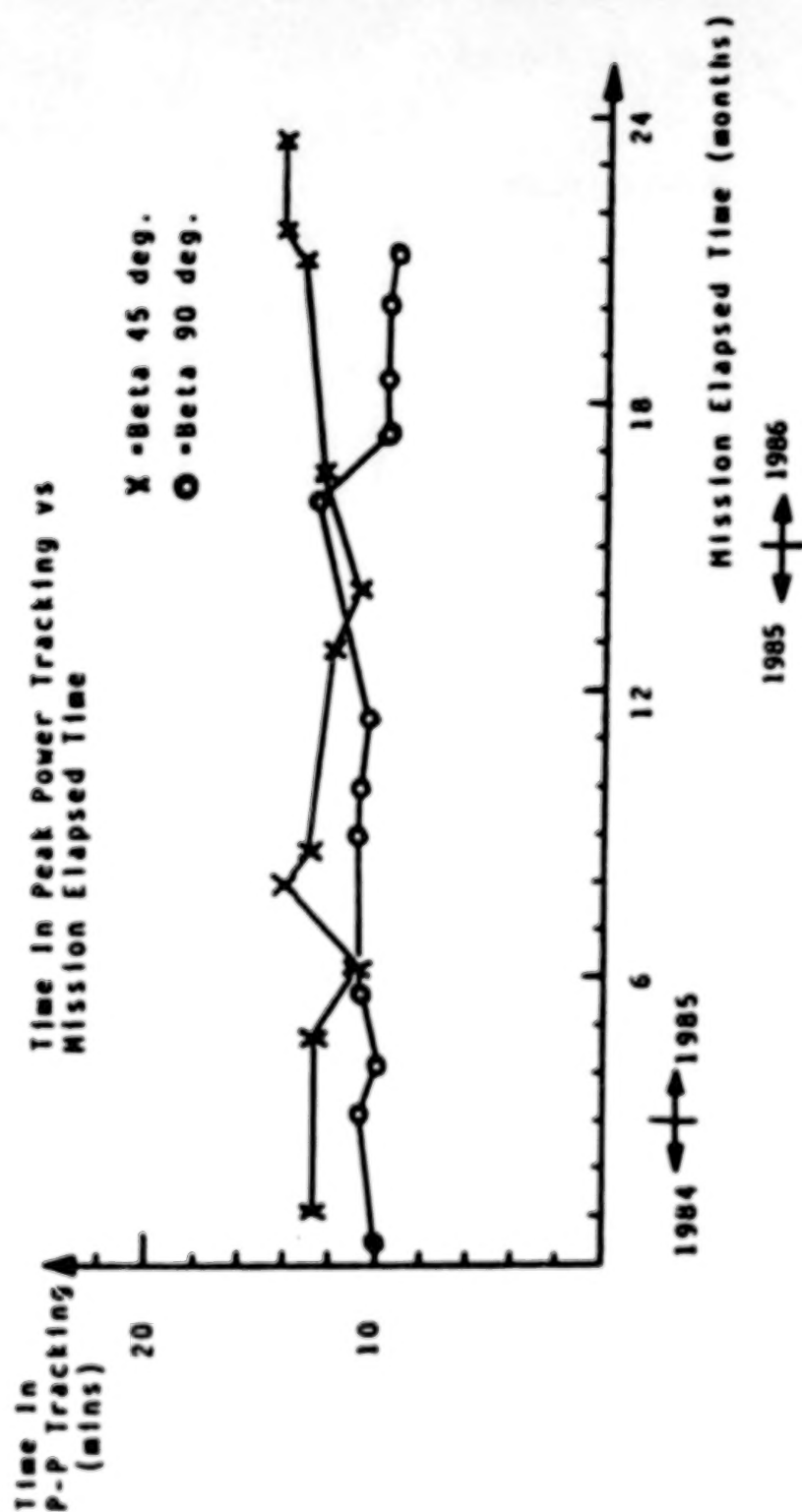


Figure 3. Time Spent Peak-Power Tracking.

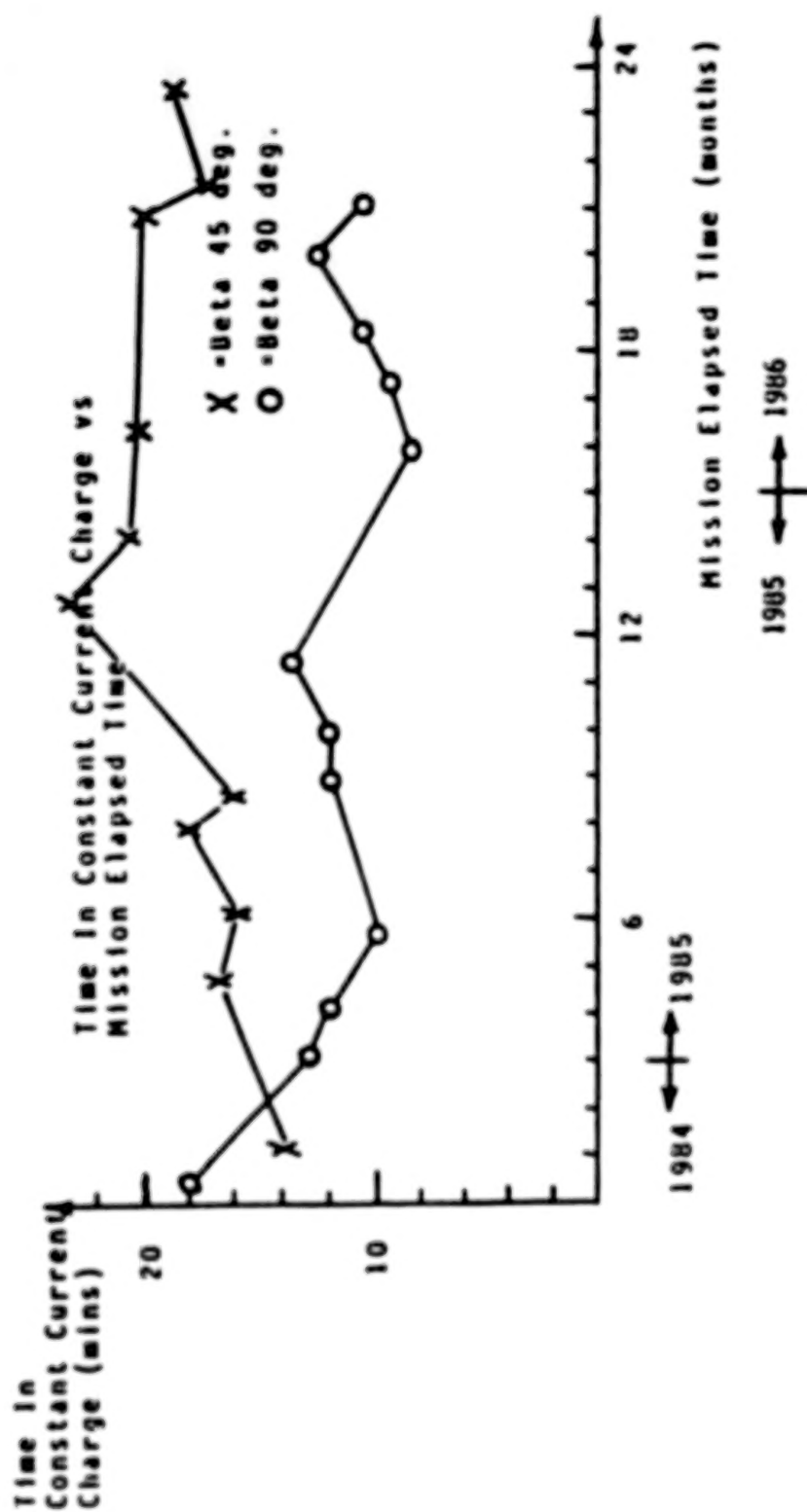


Figure 4. Time Spent in Constant Current Mode.

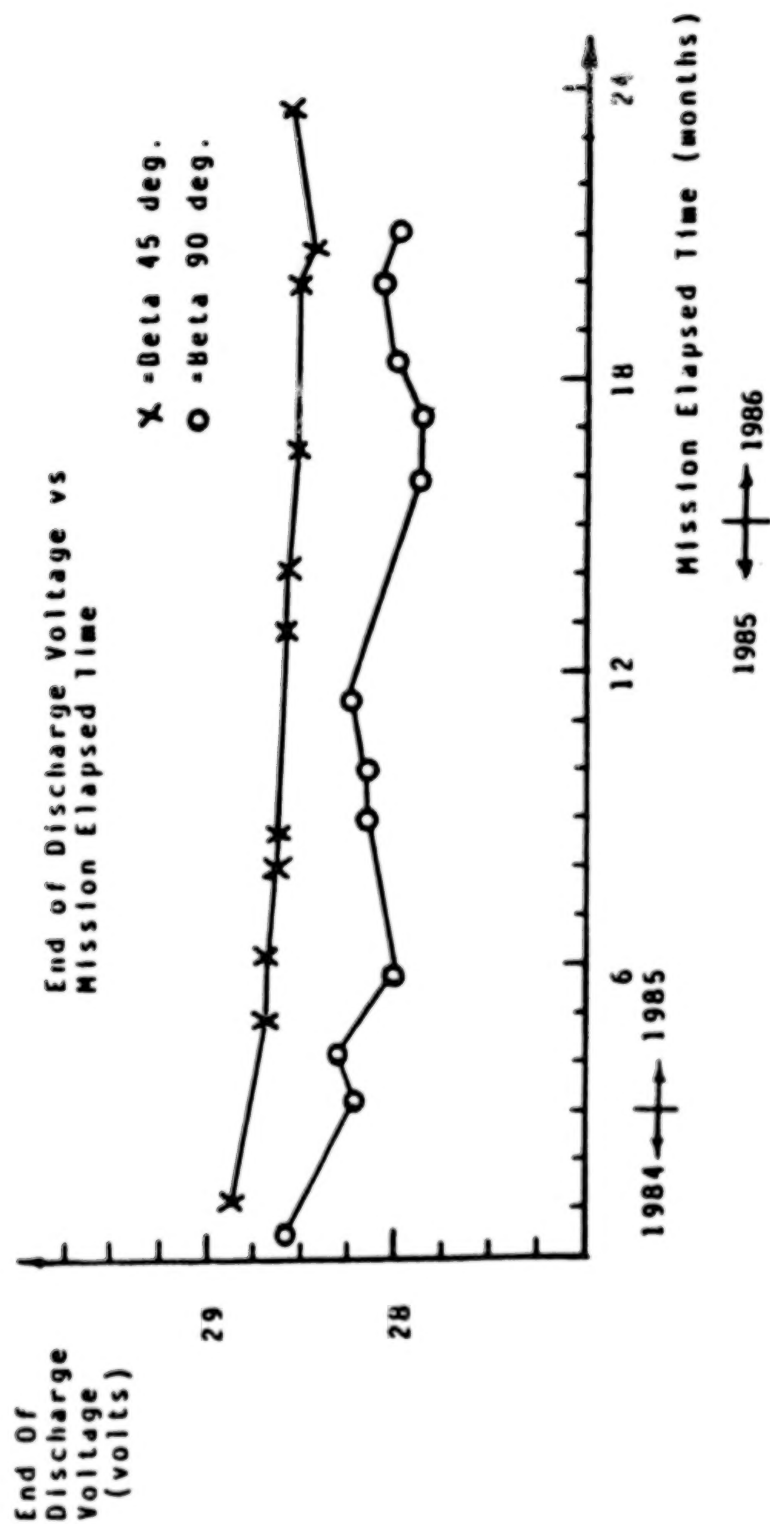


Figure 5. End of Discharge Voltage.

Loads : No power amplifier usage

Current at End-of-Discharge : 10 +/-1.5 amps.

Of the three parameters trended only the End of Discharge Voltage versus mission elapsed time (Figure 5) shows any discernable trend. The plot shows a slight decrease in the end of discharge voltage over the two-year period.

References

1. P. C. Lyman, ERBS Power Subsystem Trend Data, Ball Aerospace Systems Division, SER ERBS 05-57, Rev. B, 09-19-86

EFFECTS OF LONG TERM STORAGE ON AEROSPACE NICKEL CADMIUM CELL PERFORMANCE

Thomas Y. Yi
Space Power Applications Branch, Code 711
NASA/Goddard Space Flight Center
Greenbelt, MD 20771

SUMMARY

A study currently being performed at NASA/Goddard Space Flight Center (GSFC) to evaluate the long term effects on aerospace nickel cadmium cells is described. A number of 6Ah and 12Ah capacity cells which have been stored in shorted condition for 9 to 11 years at the GSFC have been selected for this study. Of the three tests which have been initiated (initial and final destructive analyses of the test cells, GSFC electrical characterization tests, and life cycling tests) only the GSFC electrical characterization tests have been completed; other tests are scheduled to be completed by February, 1987. The preliminary electrical performance data from the life cycling test and chemical composition data from the destructive testing indicate no anomalous behavior.

PRECEDING PAGE BLANK NOT FILMED

INTRODUCTION

Investigation of long term storage effects on aerospace nickel cadmium cell performance is an important topic that has generated little interest. Although many works have been published on the performance of a nickel cadmium cell, relatively few studies have been addressed on the effects of prolonged storage of these cells in the recent years.

This topic is especially important to NASA in that we are interested in the reliability of a cell which has been stored for an extended period of time after activation. Cells for a flight project are procured, tested, made into battery packs, and placed in cold storage well in advance of the launch date. Inevitably because of launch delays, the question of cell reliability as a function of storage time is often asked. Originally NASA/Goddard Space Flight Center (GSFC) placed an arbitrary 18 months age limit on nickel cadmium cells held in storage for a spacecraft launch; this judgment limit was later extended to 24 to 36 months. At present we at GSFC do not like to store cells for more than 3 to 4 years after activation prior to the launch date, although there are data supporting storage periods of up to 5 years. With more studies on the topic of storage effects we may be able to extend our storage time limit.

A number of studies have addressed the issue of the long term storage effects on nickel cadmium cells [1-13]. Bogner who tested the cells after a 6-month storage at 10°C reported that the capacity of the cell packs was as good or better after storage [2]. Scott has studied the effects of storing batteries, which were shorted and stored at 5 to 10°C, over a 4-year period. He found no appreciable adverse effect over this time frame, and he suggested that the batteries can be store up to 5 years when the cells are shorted, and at a fairly low temperature [3]. Similarly Stanley reported that shorted storage has proved to be effective for up to 5 years without significant degradation [4]. Thierfelder et al. reported that the swelling of the positive plates and the decrease in overcharge protection are found to be the life limiting characteristics during prolonged storage [5]. They recommended a maximum cell age of 3.5

years at time of spacecraft launch for a 7.5 year mission. Brahim et al. found that the cells retained a significant efficiency after 5 years of storage [6]. However Hobbs et al., based on their initial data, suggest that storage effects will constitute a major problem [7]. They later reported reductions in capacity between 1% and 75% after a 3 year storage period mode, depending on the cell model, storage temperature, and storage time [8]. I would like to point out that the nickel cadmium cells studied by Brahim et al. and Hobbs et al. were of commercial grade, not of aerospace quality.

Most of the aerospace cells used in the above studies were manufactured in the 1960's, whereas the cells used in this study, in the 1970's. The cells used in this study resemble the present day nickel cadmium cells in characteristics and construction more closely than most of the cells used in the above works. Because the cells used in this study were fabricated at a later date, these cells have been manufactured under refined process and under better quality control than most of those cells in the above works; these cells have been manufactured and tested, adhering closely to NASA/GSFC Specification 74-15000, Specification for Manufacturing of Aerospace Nickel-Cadmium Storage Cells [14].

This study was initiated to investigate the effects of long term storage on aerospace nickel cadmium cells via electrical acceptance testing, simulated flight conditions at both real time and accelerated time testing, and destructive analysis. The cells selected for this study have been stored at room temperature under shorted condition in the Battery Lab at GSFC for 9 to 11 years. The results from the study will be compared with previous data on these cells, namely from the initial acceptance data at GSFC, and from the life cycling data on cells from the same lot at NASA Battery Facility at Naval Weapons Support Center (NWSC) in Crane, IN. We have selected General Electric (G.E.) 6Ah and 12Ah nickel cadmium cells for this study. These cells have been chosen because of their relative abundance in the Battery Lab, and also because of availability of their GSFC acceptance data and NWSC life cycling data. Specific information on these cells is mentioned elsewhere [15-20]. The test plans along with the preliminary data were first presented at the 1985 NASA/GSFC Battery

Workshop [21-22].

TEST DESCRIPTION

For this study twelve cells have been selected from each of the IUE (International Ultraviolet Explorer satellite) 6Ah and 12Ah cell lots at the Battery Lab at GSFC. Of the 12 cells within a lot, 2 cells underwent destructive analysis at Bowie State College in Bowie, MD, following the procedures outlined in the NASA document X-711-74-279 [23]. The remaining 10 cells from each lot were fabricated into two 5-cell packs, one of which was tested at the Battery Lab at GSFC, and the other at NWSC. The steps in the GSFC electrical characterization test are outlined in Table 1. The operating parameters of the NWSC life testing packs are listed in Table 2. The 6AH test pack is currently undergoing accelerated geosynchronous orbit cycling (GEO), whereas the 12AH pack is operating at real time low earth orbit (LEO) cycling. These test parameters were deliberately chosen to operate under the same operating conditions as pack 231A for the 6AH pack, and pack 8G for the 12AH pack at NWSC [24-31]. The specifics of the GSFC and NWSC tests were reported at the 1985 NASA/GSFC Battery Workshop, and are available elsewhere [21-22].

RESULTS AND DISCUSSION

Only those tests at GSFC have been completed at this time. Therefore, the bulk of the discussion will be on the results from those tests.

GSFC Electrical Characterization Tests

Electrical characterization tests as outlined in Table 1 in the Test Description section has been

completed on the selected G.E. 6Ah and 12Ah cells. Figures 1 and 2 compare the cell capacities at different charge rates and temperatures for the 6Ah and 12Ah cells, respectively. The preliminary indication shows that both the 6Ah and 12Ah cells have improved their cell capacities after 9 to 11 years of storage. Moreover both the cell and third electrode voltages at end-of-charge (EOC) have either remained the same or have increased after the storage period.

Our observation that cell capacities increase with storage time is of great concern. Although such observation has been reported by Bogner [2], it is generally believed that cells degrade over long length of time, principally due to degradation of the separator material, nylon. Real time synchronous orbit tests and some LEO test have shown a gradual increase in the cell ampere-hour capacities during the early cycles of life testing. Such increases may result either from incomplete formation of the positive plates during cell manufacturing, or from inadequate active "excess charged" negative capacity at the beginning of cycling [32]. Scott found that a very large percentage of changes is introduced during acceptance testing, and that very little additional changes during shorted storage [11]. The tested nickel cadmium cells have been stored shorted after some 30 cycles of testing in the original acceptance test. These two ideas suggest that the tested IUE cells are more affected by the GSFC electrical characterization test than by storage. If so, the tested IUE cells may exhibit a slight increase in their cell capacities at beginning-of-life (BOL); we must wait until the life tests are completed to reach any conclusion.

All the 6AH cells have met the performance specification as outlined in the Cell Acceptance Test Plan [33-34]. From Fig. 1, we note that for either test dates, we see the generally observed cell behavior that cell capacities increase with cycling time, and that the lowest capacity is seen during the overcharge test where the temperature is at 0°C. For the 12AH cells, similar behaviors were noted (see Fig. 2). Nearly all the plots from the GSFC electrical characterization tests, of cell voltage versus time, and of third electrode voltage versus time, exhibited normal cell characteristics.

The third electrode voltage plots for one cell (S/N 014) among the 6Ah cells displayed abnormal behavior, however. This particular cell showed no change in the third electrode voltage for the discharge portions during the second capacity check and during the overcharge test (see Fig. 3 and 4, respectively). For the charge portions of the second capacity check and overcharge test, its third electrode voltage did not change until the cell was fully charged (see Fig. 5 and 6, respectively). Such behaviors for both the charge and discharge periods were not observed in the first capacity check and in the subsequent capacity check or burn-in cycles.

This anomalous behavior of the third electrode is not a cause for an alarm. The third electrode voltage is an "unpredictable" parameter. Baer reported that during his testing of the IUE cells, the third electrode voltage test data revealed a very high degree of nonuniformity [20]. His finding was in accord with Scott and Rusta [32] who stated that from the life cycling data and from flight experience the third electrode performance is not reliable over long periods of time. Besides, the third electrode was not utilized to control charge and discharge, but rather it was used to provide additional data.

NWSC Life Tests

Life tests for both the 6AH pack and 12AH pack are scheduled to be completed by February, 1987. To date, the 6AH pack, which is labelled as pack 231C at NWSC, has undergone 9 accelerated shadow periods; the 12AH pack, which is labelled as pack 8I, has undergone about 5000 LEO cycles. The latest data from NWSC on packs 231C and 8I are plotted in Figures 7 and 8, respectively. In Fig. 7, pack 231C has completed its eighth shadow period, i.e., equivalent of 4 years of synchronous cycling. The plot of cell capacity check for pack 231C is shown in Figure 9; the cells have not lost any capacities after eight shadow periods. In Fig. 8, pack 8I has completed 4552 LEO cycles. These plots exhibit normal cell characteristics.

Destructive Analyses

At the beginning of this study, four cells have been sent to Bowie State College, MD, for destructive analysis; the test analyses show no anomalies. Eight more cells will be undergo destructive analysis once the NWSC tests on the cells are completed.

CONCLUSION

This study was initiated to better understand the effects of long term storage on nickel cadmium cells. The selected cells have passed the GSFC electrical characterization tests; they have been life tested for over 5000 LEO cycles and 9 accelerated GEO shadow periods without failure. Because the tests are still ongoing, no conclusions will be made until all the tests have been completed.

REFERENCES

1. DiStefano, S. et al., "Studies of the Effect of Aging on the Components of Sealed Nickel Cadmium Cells." *Proc. Symp. on the Nickel Electrode*, Fall Meeting of the Electrochem. Soc., pp. 216-223.
2. Bogner, R. S. et al., "Cycle Life and Storage Test Results." *1976 GSFC Battery Workshop*, NASA X-711-77-28, pp. 215-222.
3. Scott, W., "Long-Term Storage Effects Update." *1977 GSFC Battery Workshop*, NASA Conference Publication 2041, pp. 219-222.
4. Stanley, C., *Spacecraft Testing, 5-Year Storage Life*, USAF/SAMSO Contract F04701-71C-0131, Report 16439-93-002-602, TRW Systems Group, 1976.
5. Thierfelder, H. E. et al., "Nickel Cadmium Cell Age Sensitivity Study." *Proc. Intersoc. Eng. Conf.*, Vol. 1, 1984, pp. 319-323.
6. Braham, R. W. et al., "On the Aging of the Nickel Cadmium Systems." *Power Sources*, Vol. 6, 1977, pp. 129-159.
7. Hobbs, B. S. et al., "Aspects of Nickel Cadmium Cells in Single Cycle Applications - The Effect of Long Term Storage." *J. Appl. Electrochem.*, Vol. 8, 1978, pp.305-311.

8. Hobbs, B. S., "Short Circuit Storage Testing of Nickel Cadmium Cells." The City University Report No. 80/26/023, Final Summary Report, London, England, 6/80.
9. Harkness, J., "Storage Effects on Cells." 1977 GSFC Battery Workshop, NASA Conference Publication 2041, pp. 223-242.
10. Dunlop, J., "Storage Experience." 1973 GSFC Battery Workshop, pp. 81-91.
11. Scott, W., "Cells Shorted for Years." 1975 GSFC Battery Workshop, NASA X-711-76-21, pp. 201-207.
12. Scott, W., "Effect of Long Term Activated Shorted Storage." 1974 GSFC Battery Workshop, NASA X-711-74-348, pp. 125-139.
13. Halpert, G., "Effect of Storage Modes on Nickel-Cadmium Cell Condition." 1983 Space Power Workshop, Los Angeles, CA, 3/16/83.
14. "Specification for the Manufacture of Aerospace Nickel Cadmium Storage Cells," NASA/GSFC Specification 74-15000, March 1975.
15. Tiller, S. "TUE Flight Experience." 1978 GSFC Battery Workshop, NASA Conference Publication 2088, pp. 229-237.
16. Baer, D. "Cell Design." 1976 GSFC Battery Workshop, NASA X-711-77-28, pp. 89-95.
17. Tiller, S. "Update of the IUE Battery In-Flight Performance." 1979 GSFC Battery Workshop, NASA Conference Publication 2117, pp. 215-218.
18. Tiller, S. "Performance of the IUE Spacecraft Batteries After 70 Months." 1983 GSFC Battery Workshop, NASA Conference Publication 2331, pp. 353-365.
19. Tiller, S. "Status Report on the IUE Project Cell Life Test at NWSC-Crane." Internal Memorandum, Dec. 14, 1981.
20. Baer, D. Summary of the Manufacturing and Testing of 12AH Nickel-Cadmium Cells for the IUE Spacecraft. X-711-76-18, 1/76.
21. Yi, T. "Investigation of Long-Term Storage Effects on Aerospace Nickel-Cadmium Cell Performance." 1985 GSFC Battery Workshop, NASA Conference Publication 2434, pp. 249-254.
22. Yi, T, J. Power Sources, 18(1986) 191.
23. Halpert, G. and Kunigahalli, V. Procedure for Analysis of Nickel-Cadmium Cell Materials, NASA X-711-74-279, Rev. A, 1980.
24. Naval Weapons Support Center. Evaluation Program for Secondary Spacecraft Cells: Synchronous Orbit Testing of Sealed Nickel-Cadmium Cells, Contract S-53742-AG, WQEC/C 81-120A, 1981, pp. 114-133.
25. Naval Weapons Support Center. Evaluation Program for Secondary Spacecraft Cells: Synchronous Orbit Testing of Sealed Nickel-Cadmium Cells, Contract S-53742-AG, WQEC/C 81-120B, 1981, pp. 76-90.

26. Naval Weapons Support Center. *Evaluation Program for Secondary Spacecraft Cells: 16th Annual Report of Cycle Life Test*, Contract C-13105-D, WQEC/C 80-34, 1980, pp. 28-32.
27. Naval Weapons Support Center. *Evaluation Program for Secondary Spacecraft Cells: 17th Annual Report of Cycle Life Test*, Contract C-13105-D, WQEC/C 81-1, 1981, pp. 28-32.
28. Naval Weapons Support Center. *Evaluation Program for Secondary Spacecraft Cells: 18th Annual Report of Cycle Life Test*, Contract C-13105-D, WQEC/C 82-23, 1982, pp. 29-32.
29. Naval Weapons Support Center. *Evaluation Program for Secondary Spacecraft Cells: 19th Annual Report of Cycle Life Test*, Contract C-13105-D, WQEC/C 83-1, 1983, pp. 29-33.
30. Naval Weapons Support Center. *Evaluation Program for Secondary Spacecraft Cells: 20th Annual Report of Cycle Life Test*, Contract C-13105-D, WQEC/C 84-5, 1984, pp. 15-19.
31. Naval Weapons Support Center. *Evaluation Program for Secondary Spacecraft Cells: 16th Annual Report of Cycle Life Test*, Contract C-13105-D, WQEC/C 85-52, 1985, p. 36.
32. Scott, W. and Rusta, D. *Sealed Cell Nickel-Cadmium Battery Applications Manual*, NASA RP-1052, 12/79, pp. 350.
33. Tiller, S. *Battery Fabrication And Acceptance Test Plan for International Ultraviolet Explorer (IUE) 6AH Batteries*, NASA X-711-78-5, 1978.
34. Tiller, S. *Cell Acceptance Test Plan for Nickel-Cadmium Cells*, NASA X-711-76-143, 1976, pp. 17-19.

Table 1. Steps used in the GSFC Electrical Characterization Tests

Sequence Number	Test Condition Number	Test Description	Temperature (°C)	Current	Voltage Limits		Test Duration (hours)	
					Upper Limit (V)	Lower Limit (V)	Specified	Estimated
1	1	Conditioning Charge	25	C/20	1.51	0.80	48	—
2	2	Conditioning Discharge	25	C/2	1.51	0.80	—	3
		Resistive Drain	25	—	—	—	—	2
3	3	Conditioning Charge	25	C/10	1.51	0.80	24	—
4	2	Conditioning Discharge	25	C-2	1.51	0.80	—	3
		Resistive Drain/Temperature Stabilization	20	—	—	—	—	2
5	4	Capacity Charge	20	C/10	1.51	0.80	24	—
6	5	Capacity Discharge	20	C/2	1.51	0.80	—	3
		Resistive Drain	20	—	—	—	16	—
7	6	Charge Retention — Open Circuit	20	—	—	—	24	—
		Resistive Drain/Temperature Stabilization	10	—	—	—	—	2
8	7	Capacity Charge	10	C/20	1.53	0.80	48	—
9	8	Capacity Discharge	10	C/2	1.53	0.80	—	3
		Resistive Drain/Temperature Stabilization	0	—	—	—	—	2
10	9	Overcharge Charge	0	C/20	1.53	0.80	72	—
11	10	Overcharge Discharge	0	C/2	1.53	0.80	—	3
		Resistive Drain/Temperature Stabilization	10	—	—	—	—	2
12	11	Burn-in Charge #1	10	C/20	1.53	0.80	23	—
13	12	Burn-in Discharge #1	10	C/2	1.53	0.80	1	—
14	11	Burn-in Charge #2	10	C/20	1.53	0.80	23	—
15	12	Burn-in Discharge #2	10	C/2	1.53	0.80	1	—
16	11	Burn-in Charge #3	10	C/20	1.53	0.80	23	—
17	12	Burn-in Discharge #3	10	C/2	1.53	0.80	1	—
18	11	Burn-in Charge #4	10	C/20	1.53	0.80	23	—
19	12	Burn-in Discharge #4	10	C/2	1.53	0.80	1	—
20	11	Burn-in Charge #5	10	C/20	1.53	0.80	23	—
21	12	Burn-in Discharge #5	10	C/2	1.53	0.80	1	—
22	11	Burn-in Charge #6	10	C/20	1.53	0.80	23	—
23	12	Burn-in Discharge #6	10	C/2	1.53	0.80	1	—
24	11	Burn-in Charge #7	10	C/20	1.53	0.80	23	—
25	12	Burn-in Discharge #7	10	C/20	1.53	0.80	1	—
26	11	Burn-in Charge #8	10	C/20	1.53	0.80	23	—
27	13	Burn-in Capacity Discharge	10	C/2	1.53	0.80	1	—
		Resistive Drain/Temperature Stabilization	20	—	—	—	—	2
28	4	Capacity Charge	20	C/10	1.51	0.80	24	—
29	5	Capacity Discharge	20	C/2	1.51	0.80	—	3
		Resistive Drain	20	—	—	—	—	2

Table 2. Operating Parameters for NWSC Life Test Packs

	6AH Pack	12AH Pack
Life cycling regime	GEO	LEO
Duration (year, real time)	1	1
Temperature (°C)	10	0
Depth-of-discharge (%)	80	40
Orbit	25 day Eclipse	90 min
Charge	C/10	C/1.25
Discharge	C/1.5 (Eclipse)	C/1.25

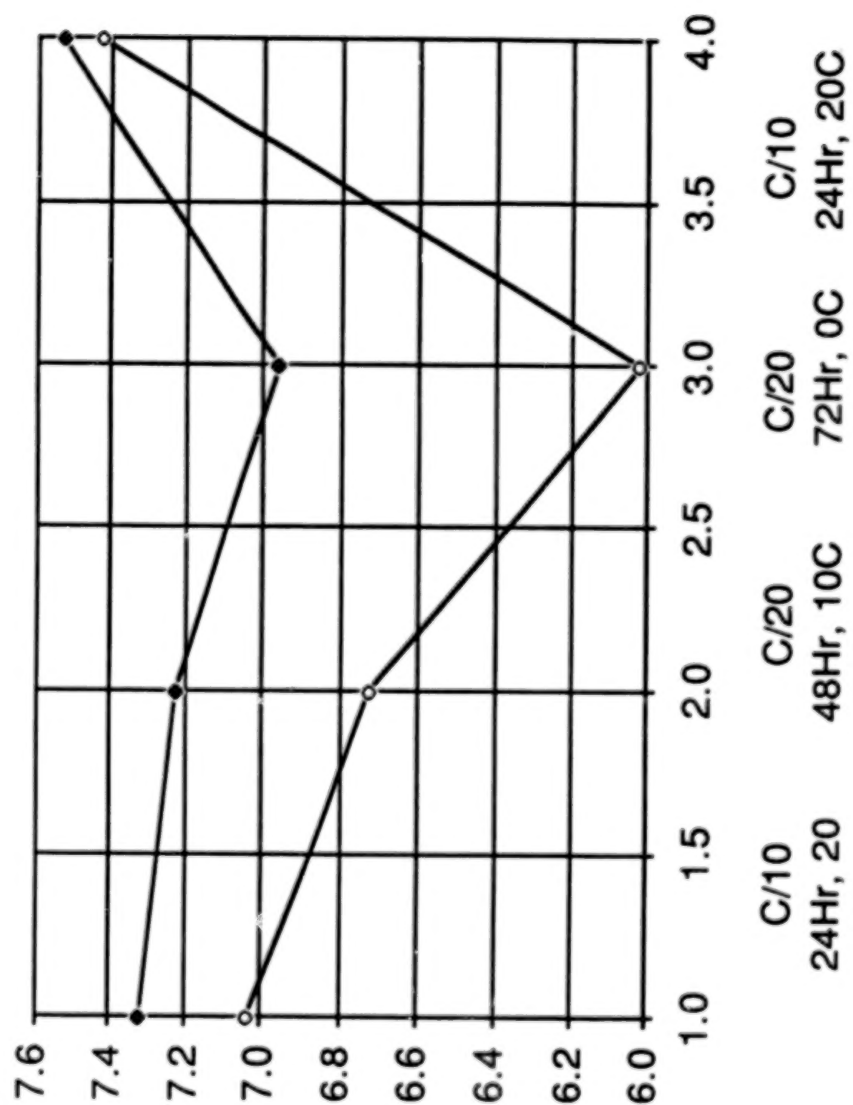


Figure 1. Comparison of 6AH Cell Capacities.

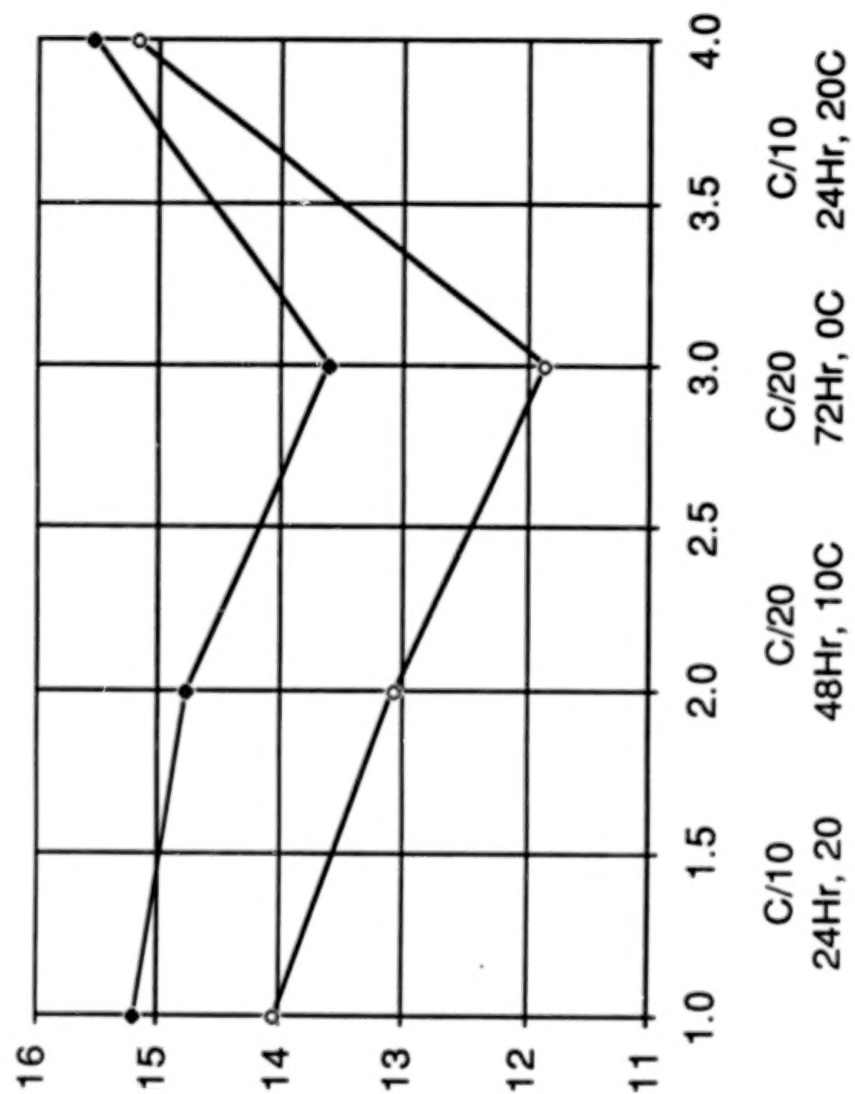


Figure 2. Comparison of 12AH Cell Capacities.

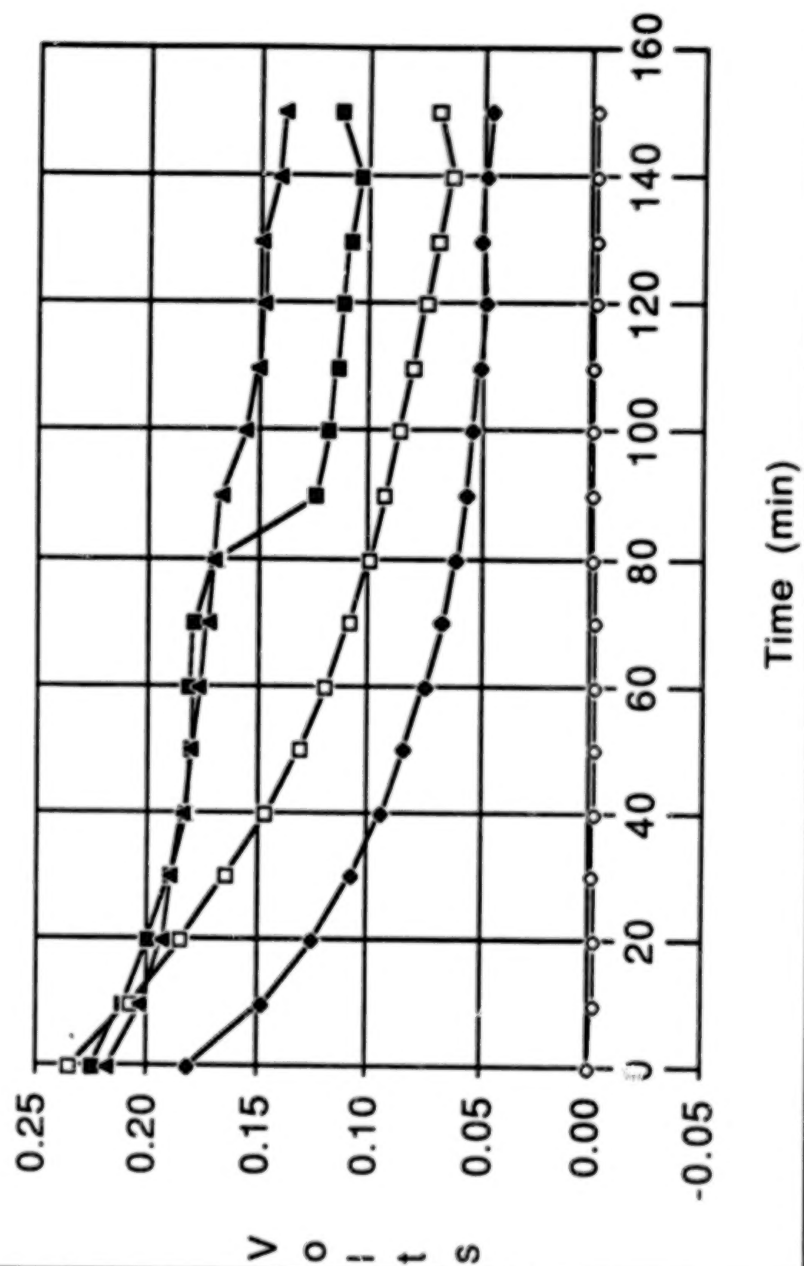


Figure 3. Capacity Discharge #2 6AH Cells [C/2, T=10C, Year=1986, 3rd Electrode].

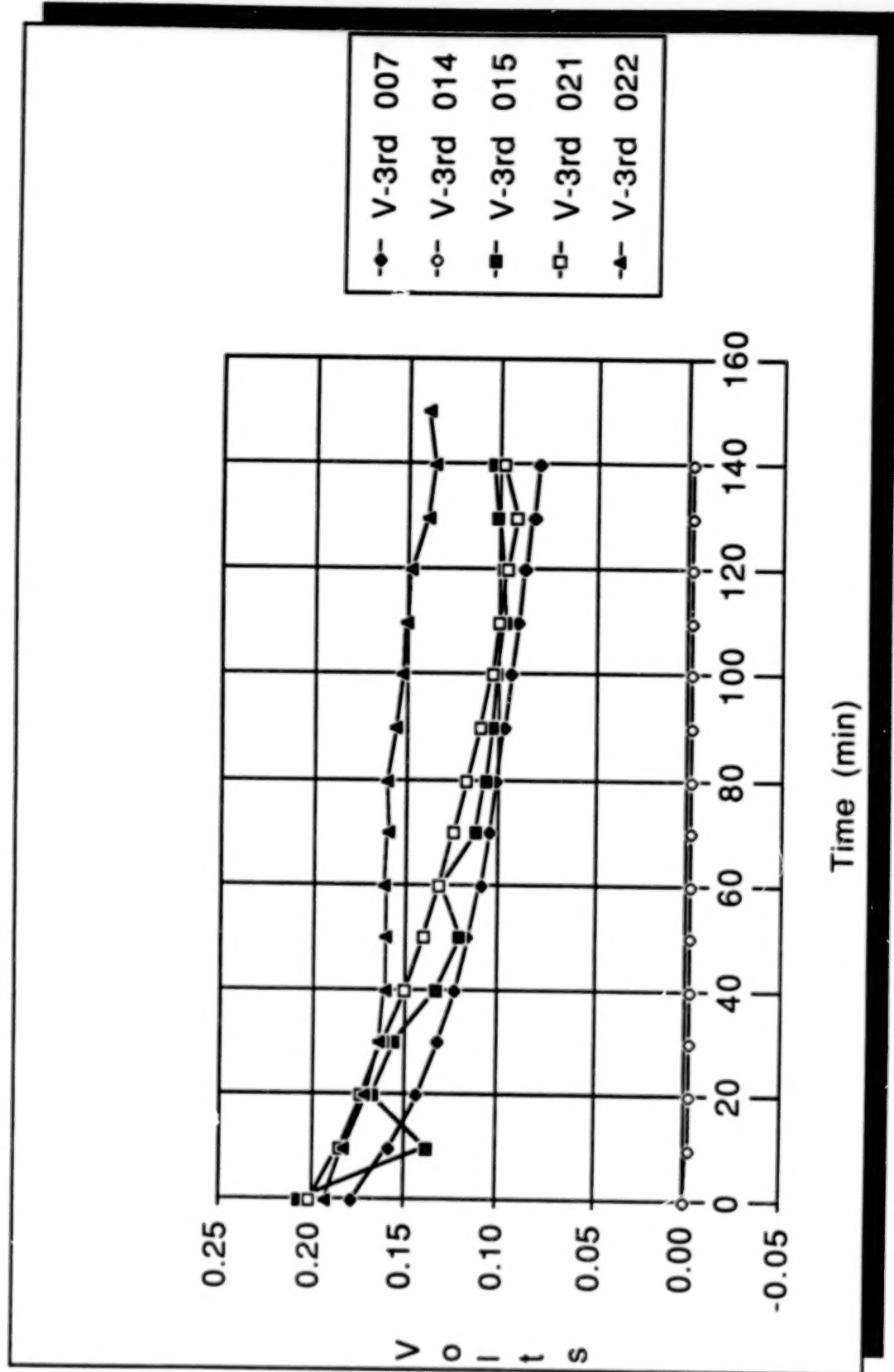


Figure 4. Overcharge Discharge 6AH Cells [C/2, T=0C, Year=1986, 3rd Electrode].

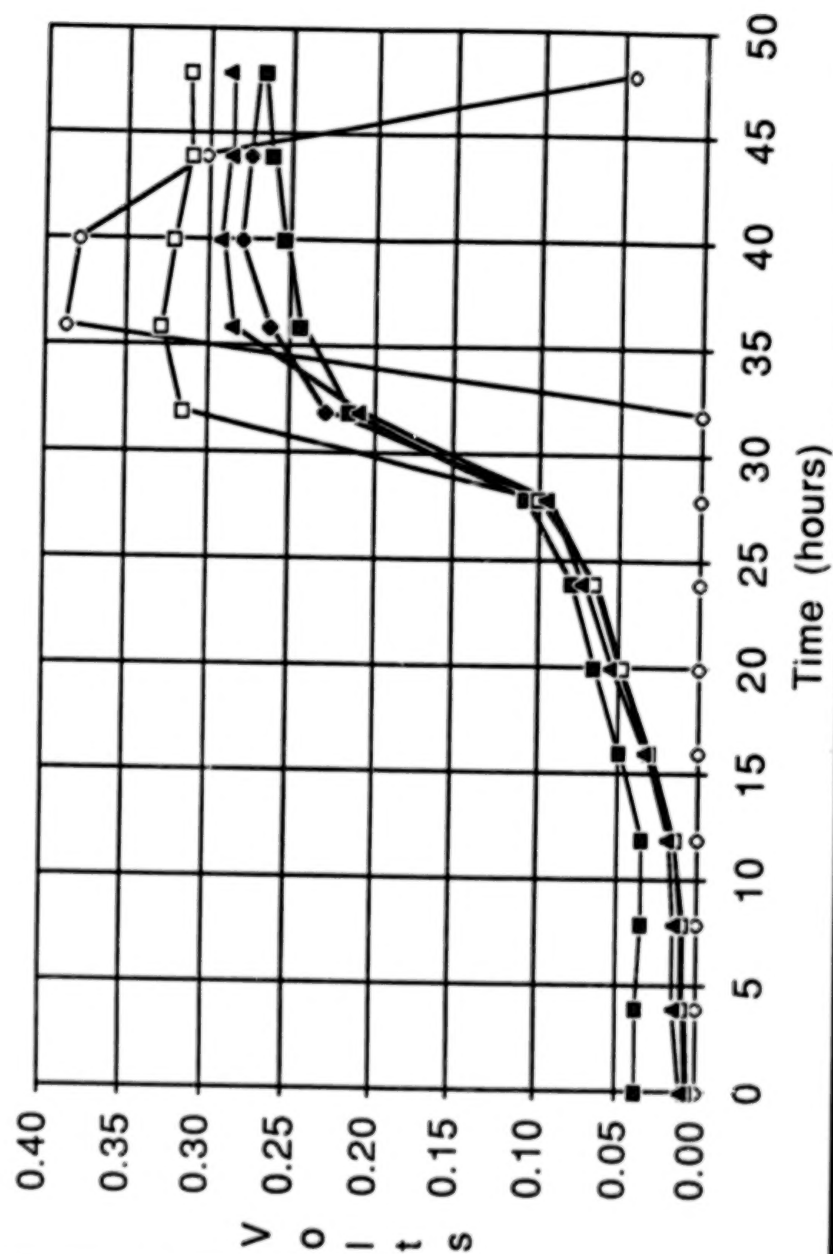


Figure 5. Capacity #2 Charge 6AH Cells [C/20, T=10C, Year=1986, 3rd Electrode].

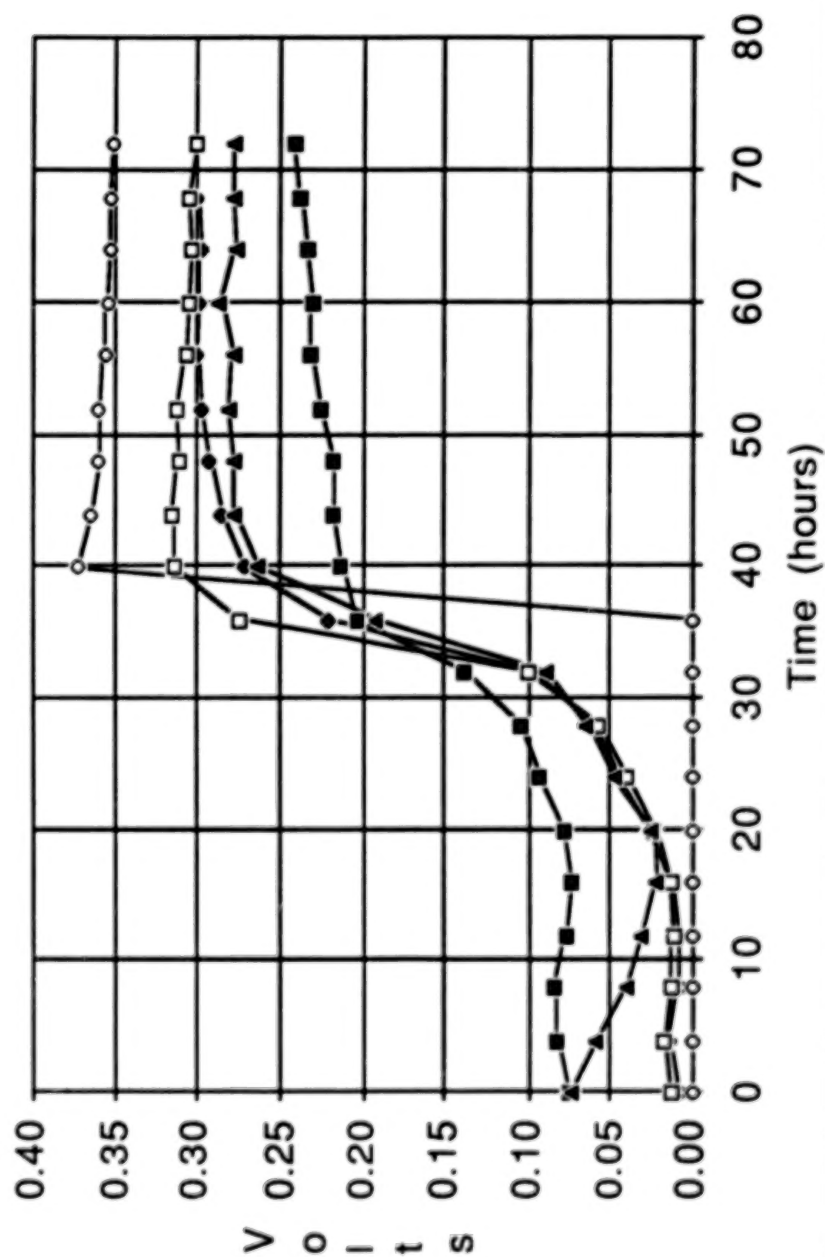


Figure 6. Overcharge Charge 6AH Cells [C/20, T=0C, Year=1986, 3rd Electrode].

Key: Cell No.
 Volt: Cell 1
 Volt: Cell 2
 Volt: Cell 3
 Volt: Cell 4
 Volt: Cell 5

Pack: 231C Manf: GE 6 AH
 Shadow # 8 - Cell Voltage vs Day
 Cycles: 259 to 283 Temp (C): 10 DOO (x): 80
 Chg .5A till 100% return, then .3A for 3 hrs, then .1A to EOC
 CX (PRIOR TO DAY 13 EVERY 4TH SHADOW-CELLS 1 THRU 5)

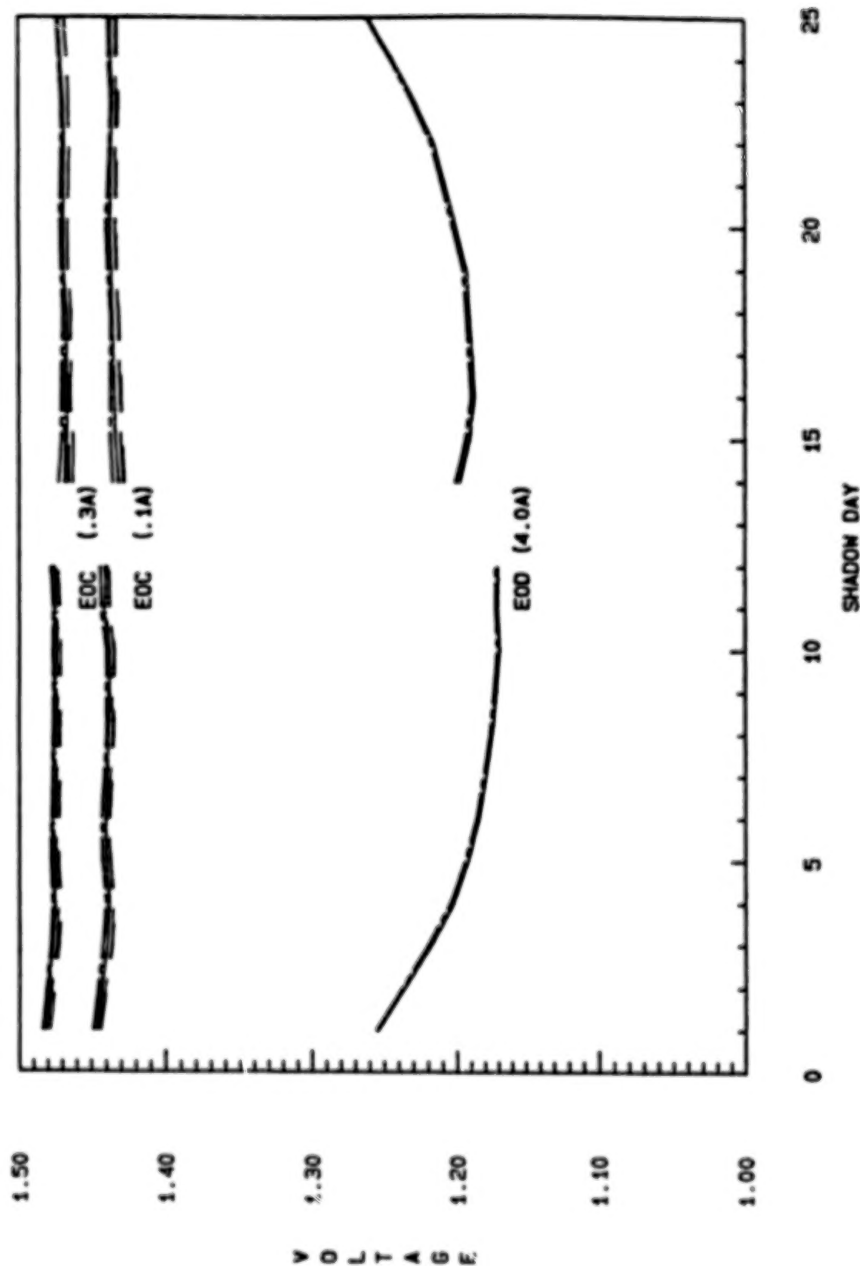


Figure 7. Pack #231C: Accelerated GEO Life Cycled at NWSC.

Pack: 81 IUE Manuf: GE 12 AH Cycle 4552
 Orbit: LEO Temp (C): 0 DOD (X): 40 GSFC Vt. Level: 7
 Voltage Limit (v/c): 1.490 Time to Vt. Limit (Hrs):
 Discharge (amp/Hrs): 9.6/.48 Charge (amp/Hrs): 9.6/1.00
 AH out: 4.615 AH in: 4.711 C/D RATIO: 1.021 EOC (I): .90

Key:

--- Current
 --- Cell 1
 --- Cell 2
 --- Cell 3
 --- Cell 4
 --- Cell 5

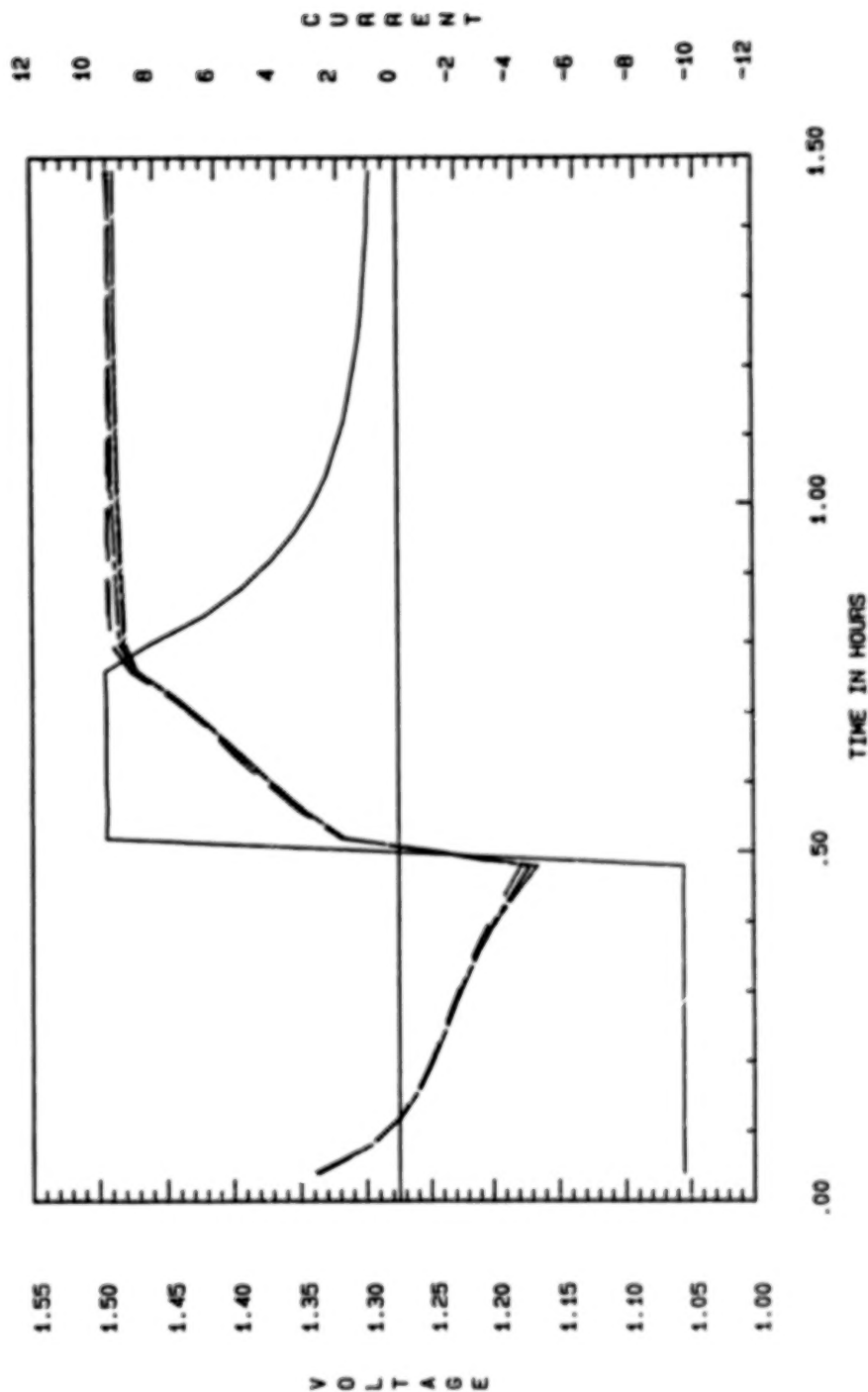


Figure 8. Pack #81: LEO Life Cycled at NWSC.

IUE
 Pack: 231C Manf: GE 6 AH
 Capacity Check - Shadow # 8
 Cycle: 271 Temp (C): 10 Rate (amps): 4.0
 Note: Follows 12th day of shadow period

Key: Cell No.
 --- Volt: Cell 1
 --- Volt: Cell 2
 --- Volt: Cell 3
 --- Volt: Cell 4
 --- Volt: Cell 5

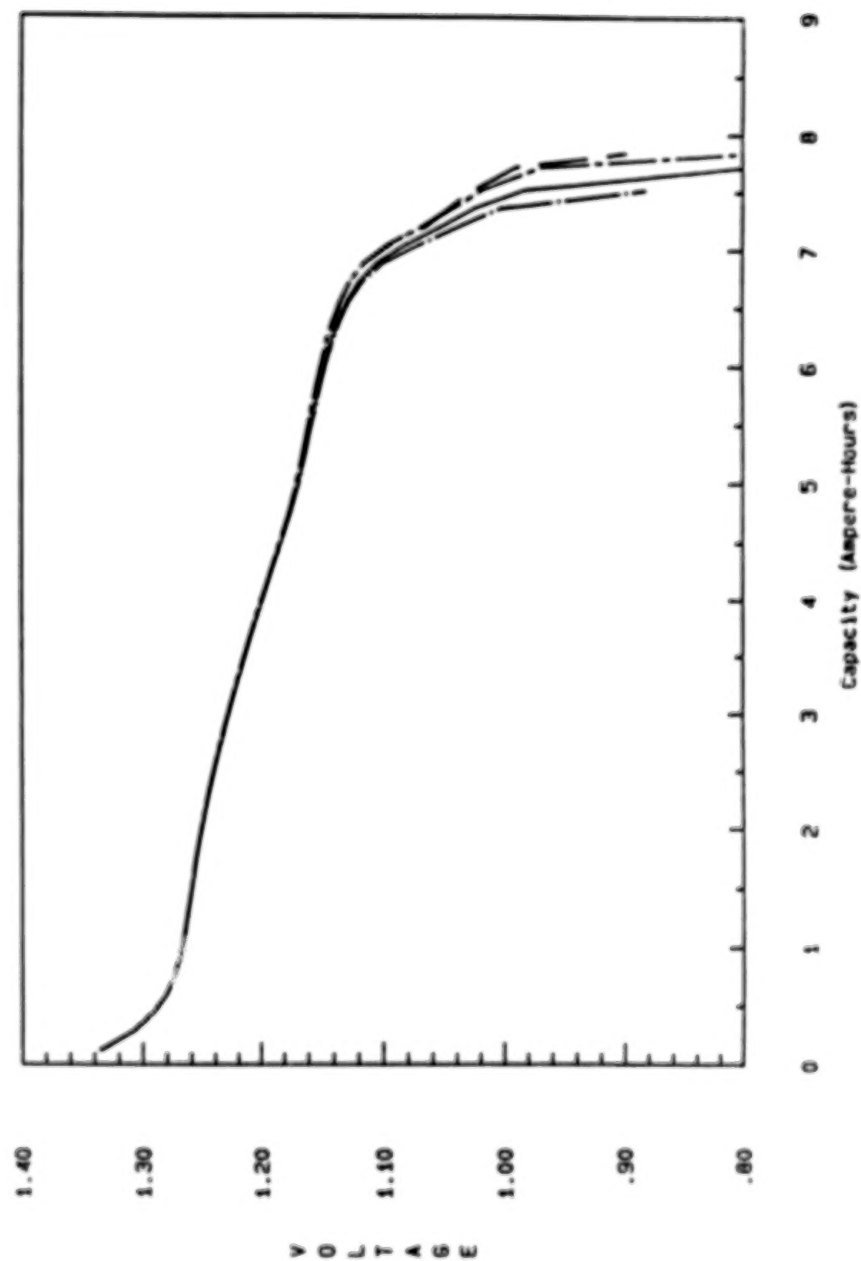


Figure 9. Pack #231C: Capacity Check During the Eighth Shadow Period.

QUALIFICATION TESTING OF GENERAL ELECTRIC 50 Ah NICKEL-CADMIUM CELLS WITH PELLON 2536 SEPARATOR AND PASSIVATED POSITIVE PLATES

George W. Morrow
Goddard Space Flight Center
Greenbelt, MD 20771

SUMMARY

Forty-two 50 Ah nickel-cadmium cells were delivered to the Goddard Space Flight Center (GSFC) by General Electric (GE) in February, 1985 for the purpose of evaluating and qualifying a new nonwoven nylon separator material, Pellon 2536, and the new GE positive plate nickel attack control gas passivation process. Testing began in May, 1985 at the Naval Weapons Support Center (NWSC) in Crane, Indiana with GSFC standard initial evaluation tests. Life cycling in both Low Earth Orbit (LEO) and Geosynchronous Orbit (GEO) began in July, 1985 with approximately 6500 LEO cycles and three GEO eclipse seasons complete at this writing. After early problems in maintaining test pack temperature control, all packs are performing well but are exhibiting higher than normal charge voltage characteristics.

INTRODUCTION

In the early 1980's, Pellon Corporation announced that it would discontinue the manufacture of aerospace nickel-cadmium nonwoven nylon separator material, Pellon 2505 ml. That announcement meant that a new separator material would have to be developed and qualified for aerospace use.

Pellon 2536, very similar to 2505 ml, was chosen in 1984 as the new separator material. In the meantime, GE had developed a new positive plate process to reduce the amount of attack on the nickel sinter structure during active material impregnation. This process, therefore, also needed to be tested to determine the effect, if any, it would have on the well defined performance characteristics and life of the space cells. Therefore, a test program was put together by the GSFC to evaluate and qualify both the separator and positive plate process. Cell fabrication for this program was initiated in early 1984 at GE and the cells were delivered in February, 1985.

CELL DESCRIPTION

The 50 Ah nickel-cadmium cells being tested in this program were activated with electrolyte during the 37th week of 1984. All cells have dual, nickel braze, ceramic-to-metal terminal seals and welded prismatic cases with a nominal case wall thickness of 0.0265 inch. Cells undergoing test are made up of 4 designs: 1) NASA standard with Pellon 2505 ml separator, old positive plate processing, and teflonated negative plates (42BO50AB20); 2) Pellon 2536 separator, old positive plate processing, and teflonated negative plates (42BO50AB25); 3) Pellon 2505 ml separator, gas passivated positive plate processing, and teflonated negative plates (42BO50AB26); and 4) Pellon 2536 separator, gas passivated positive plate processing, and teflonated negative plates (42BO50AB27). Cell design data is presented in Table 1. The cells were manufactured to GE Manufacturing Control Document (MCD) 232A2222AA-84 and acceptance tested at GE to Acceptance Test Procedure P24A-PB-222 prior to delivery.

TEST OBJECTIVES

The objectives of this test program are: 1) to evaluate the effects of Pellon 2536 separator material and the new GE positive plate nickel attack control gas passivation process on cell performance and life and 2) to qualify these changes for use in NASA/GSFC spacecraft applications.

INITIAL EVALUATION TEST RESULTS

The standard initial evaluation test used by the GSFC is outlined in Figure 1. Results of the initial evaluation tests were reported at the 1985 NASA/GSFC Battery Workshop and, therefore, will only be summarized here.

First, packs with the GE gas passivated positive plates exhibited higher peak and end-of-charge voltages during capacity and overcharge tests. Peak voltages were as much as 20 mV higher than other packs. Second, capacity test results for all packs compared well. Capacities ranged between 58.7 Ah and 63.2 Ah. Third, packs with the GE gas passivated positive plates recovered to a lower voltage during voltage recovery tests following 16 hour resistive short down. Voltage differential between packs was as much as 35 mV. Fourth, internal resistance, charge retention, and pressure versus capacity returned test results compared well between all packs.

LIFE CYCLE EVALUATION TEST DESCRIPTION

The identification of each test pack and the test matrix outlined is detailed in Table 2. There were initially 3 cycling regimes in this test: LEO 40% DOD and 20°C (L4020), LEO 40% DOD and 0°C (L4000), GEO 80% DOD and 20°C (G8020). All four cell designs are being tested in the the L4020 regime (packs 150A-150D) while only the old positive, 2536 separator and passivated positive, 2536 separator designs are tested in the G8020 regime (packs 150H and 150I) and only the passivated positive, 2536 separator design is tested under the L4000 regime (pack 150G). Because of problems encountered with maintaining 0°C and cell divergence in the pack, the L4000 pack temperature was raised to coincide with the L4020 packs at cycle 2920.

In the L4020 regime, the cells are discharged at a 0.8C rate (40 amperes) for 30 minutes and charged at a 0.8C rate to a voltage clamp at which point the current is allowed to taper for the remainder of the 60 minute charge period. The voltage clamp was initially selected to assure a percent recharge (C/D) of

112 \pm 2 percent. All LEO packs undergo a capacity check at the normal cycling discharge rate to 0.75 volts/cell every six months.

The G8020 regime is a real-time GEO regime with a 42-day eclipse period occurring twice per year. During shadow periods the cells are discharged at a 0.667C rate (33 amperes). Following each shadow, the packs are charged at a 0.1C rate (5 amperes) to 115 percent recharge (C/D) or 1.48 volts any cell, whichever occurs first. At that time, the rate is reduced to a 0.017C rate (0.83 ampere). During periods of continuous charge (all sun periods), the packs are trickle charged at the 0.017C rate. The packs are reconditioned to 0.75 volt/cell before each eclipse season. All test packs contain 5 cells.

LIFE CYCLE EVALUATION TEST RESULTS

At this time, the L4020 packs have experienced approximately 6500 cycles while the L4000 pack has seen 3600 cycles. The G8020 packs have gone through 3 eclipse seasons. Problems were encountered early in the cycle life test in controlling the internal cell temperatures in the L4020 packs. Temperatures at various locations in the packs rose to as high as 28°C and temperature imbalance between the cells caused severe cell voltage divergence. Because the capability of providing active cooling to the individual packs was not available, it was decided that the environmental chamber temperature be lowered to 10°C in order to maintain a 15°C internal pack temperature at the hottest point. This was done at cycle 2900. Since that time, cycling has continued without anomaly.

Current cycling endpoint data is presented in Table 3. This data shows that packs 150A through 150D compare very well in performance with all end-of-discharge (EOD) voltages between 1.03 and 1.10 volts/cell and charge/discharge ratios between 1.03 and 1.05. These EOD voltages are in the range expected from previous tests run on NASA standard 50 Ah cells at 40% DOD. All packs are operating at the same voltage clamp. Figures 2 through 5 are typical cycle plots for packs 150A through 150D. These plots correspond to the cycle prior to the scheduled 1 year capacity check. Figures 6 through 9 are the discharge curves for the 1 year capacity check. The second plateau characteristic is very noticeable at

the normal cycling DOD. The capacities of all packs compare fairly well and range between 43 and 50 Ah.

Problems related to temperature were also experienced with the L4000 pack (150G). At 0°C, cell divergence within the pack occurred at approximately cycle 2833. In the next 50 cycles, the voltage clamp was adjusted numerous times without avail. At cycle 2920, the environmental chamber temperature was raised to 10°C to maintain a pack temperature of 15°C at the hottest point. Cycling has continued since that time without anomaly. It appears, therefore, that differences in charge efficiency between the cells at cold temperatures caused pack imbalance. This is being investigated and will be reported on at a later date.

Through 3 eclipse seasons, the G8020 packs (150H and 150I) have performed without anomaly. Reconditioning discharges prior to eclipse season 2 for packs 150H and 150I are presented in Figures 10 and 11 respectively. These curves show that there has been no loss of capacity and that both packs are performing comparably. A measure of the number of ampere-hours in and out for each day during eclipse season 2 is presented in Figures 12 and 13. These figures show the discharge profile for each day in the eclipse season and show the capacity returned during each charge at both the high rate and low rate. End-of-charge and end-of-discharge voltages are shown in Figures 14 and 15 for both packs. Both packs are performing well with minimum EOD voltages of approximately 1.15 volts/cell at 80% DOD. A slight divergence in cell EOC voltages at the high rate charge is apparent from Figure 14. These voltages come back together during the subsequent low rate charge period.

CONCLUSIONS

Slightly higher charge voltages as well as increased voltage divergence has been observed in all gas passivated positive plate test packs. This is most clearly seen in overcharge tests and LEO cycling test voltage clamp settings. Performance at low temperatures has also been a problem with pack 150G.

This problem is being investigated and may prove to be associated with low temperature charge efficiency.

Overall, performance of all cell designs has been acceptable with no extreme differences observed with Pellon 2536 separator or the GE gas passivated positive plates. Life cycle testing will continue to failure.

REFERENCES

1. Morrow, G. W., "Qualification Testing of General Electric 50 Ah Nickel-Cadmium Cells with New Separator and New Positive Plate Processing," The 1985 Goddard Space Flight Center Battery Workshop, NASA CP 2382, pages 159-168.
2. Morrow, G. W., "Qualification Testing of General Electric 50 Ah Nickel-Cadmium Cells with New Separator and New Positive Plate Processing," Journal of Power Sources, vol. 18, nos. 2 and 3, September 1986, pages 135-144.

Table 1: CELL DESIGN DATA

	NASA		OLD		NEW		NEW	
	STANDARD		POSITIVE	SEPARATOR	POSITIVE	SEPARATOR	POSITIVE	SEPARATOR
	Pos.	Neg.	Pos.	Neg.	Pos.	Neg.	Pos.	Neg.
Post No.	31069	45008	31069	45008	45046	45008	45046	45008
Flooded Cap. Ah	59.23	130.06	59.23	130.06	60.62	130.06	60.62	130.06
Theoretical Cap Ah	78.50	149.71	78.50	149.71	74.86	149.71	74.86	149.71
Utilization %	76	87	76	87	81	87	81	87
No. of Plates	16	17	16	17	16	17	16	17
Plate Area (dm ²)	1.422	1.422	1.422	1.422	1.422	1.422	1.422	1.422
Plate Thickness (in.)	0.027	0.031	0.027	0.031	0.027	0.031	0.027	0.031
Loading Hydrate (g/dm ²)	12.21	15.86	12.21	15.86	12.12	15.86	12.12	15.86
Electrolyte (cc)	166	157	162	155				
Separator	Pellon 2505	Pellon 2536	Pellon 2505	Pellon 2536	Pellon 2505	Pellon 2536	Pellon 2536	Pellon 2536
Precharge Ah	20.83	21.25	21.40	20.97				

TABLE 2:
LIFE CYCLING TEST MATRIX

ORBIT	DOD	TEMP (°C)	NASA STD. CELLS	OLD POS. NEW SEP.	NEW POS. OLD SEP.	NEW POS. NEW SEP.
LEO	40	20	PACK 150A 42B050AB20 S/N 2-7	PACK 150B 42B050AB25 S/N 2-7	PACK 150C 42B060AB26 S/N 2-8	PACK 150D 42B060AB27 S/N 3-6,11,12
GEO	80	20		PACK 150H 42B050AB25 S/N 1,8-12		PACK 150I 42B050AB27 S/N 1,7-10
LEO	40	0				PACK 150G 42B050AB27 S/N 2,13-16

TABLE 3: CURRENT CYCLING AND ENDPOINT DATA

PACK	VT LIMIT (V/CELL)	EOD V (V/CELL)	EOC I (AMPS)	C/D	CAPACITY 1 YR. (AH)
150A	1.468	1.05	3.25	1.05	50.3
150B	1.468	1.06	3.50	1.05	45.3
150C	1.468	1.03	2.75	1.03	43.8
150D	1.468	1.10	3.05	1.04	43.1

- PHENOLPHTHALEIN LEAK TEST
- THREE CAPACITY TESTS
- INTERNAL RESISTANCE TEST
- CHARGE RETENTION TEST, 20°C
- INTERNAL SHORT TEST
- CHARGE EFFICIENCY TEST, 20°C
- OVERCHARGE TESTS, 0° AND 35°C
- PRESSURE VERSUS CAPACITY TEST
- PHENOLPHTHALEIN LEAK TEST

Figure 1. Initial Evaluation Test Regime.

REGUALIFICATION-LIFE CYCLING

Pack: 150A Manuf: GE 50 AH Cycle 5835
 Orbit: LEO Temp (C): 10 DOD (X): 40 GSFC Vt. Level: 7
 Voltage Limit (v/c): 1.470 Time to Vt. Limit (Hrs):
 Discharge (Amp/Hrs): 40.0/.48 Charge (Amp/Hrs): 40.0/1.00
 AH out: 19.196 AH in: 20.103 C/D RATIO: 1.047 EOC (I): 3.25
 Cell Design: NASA Standard

Key: Current
 --- Cell 1
 --- Cell 2
 --- Cell 3
 --- Cell 4
 --- Cell 5

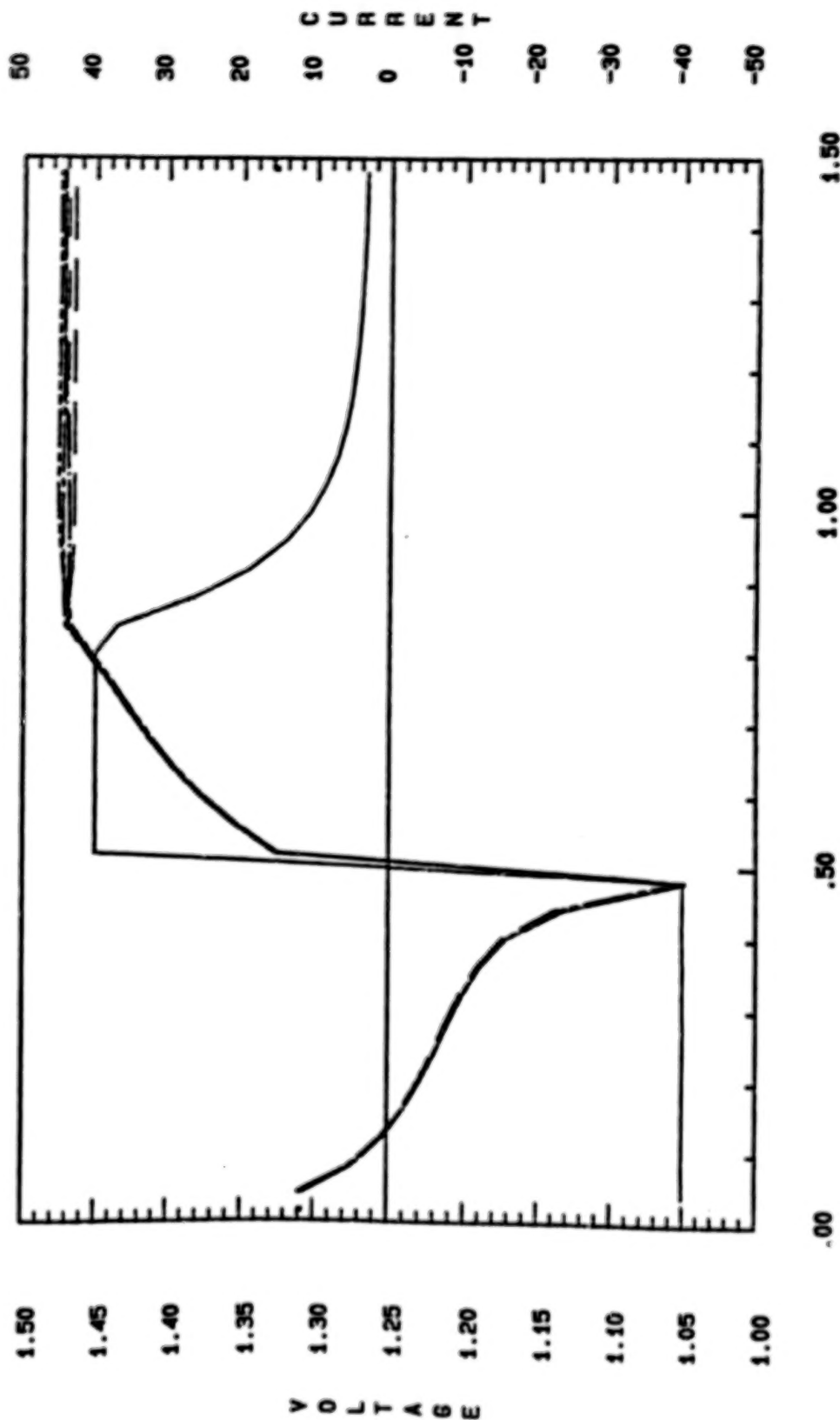


Figure 2.

REGUALIFICATION-LIFE CYCLING

Pack: 1508 Manuf: GE 50 AH Cycle 5836
 Orbit: LEO Temp (C): 10 DOD (X): 40 GSFC Vt. Level: 7
 Voltage Limit (v/c): 1.470 Time to Vt. Limit (hrs):
 Discharge (Amp/Hrs): 40.0/.48 Charge (Amp/Hrs): 40.0/1.00
 AH out: 19.212 AH in: 20.186 C/D RATIO: 1.051 EOC (I): 3.50
 Cell Design: Old Positive, New Separator

Key:
 --- Current
 --- Cell 1
 --- Cell 2
 --- Cell 3
 --- Cell 4
 --- Cell 5

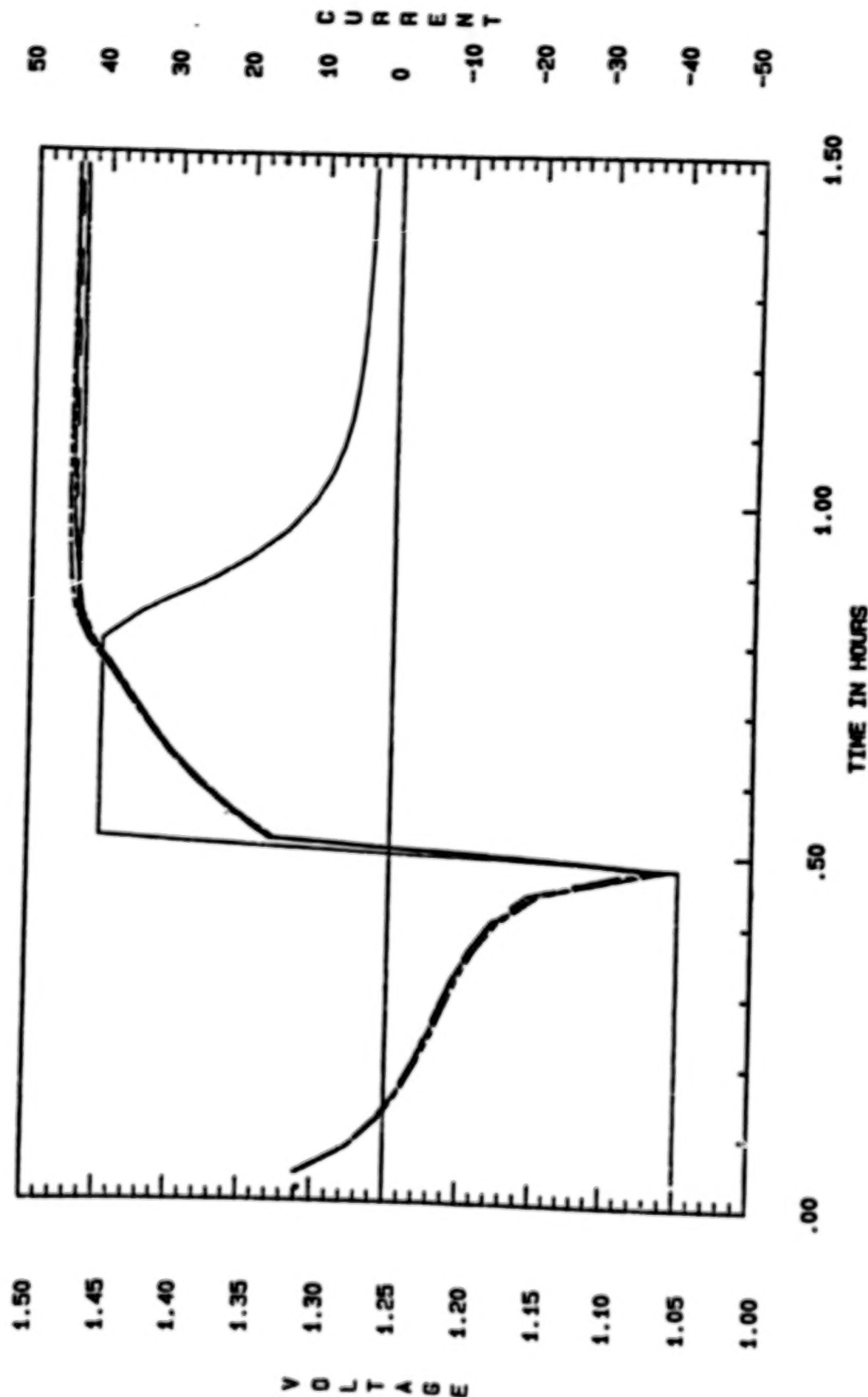


Figure 3.

REGUALIFICATION-LIFE CYCLING

Pack: 150C Temp (C): 10 50 AH Cycle 5834
 Orbit: LEO Manuf: GE 000 (3): 40 GSFC Vt. Level: 7
 Voltage Limit (v/c): 1.470 Time to Vt. Limit (hrs):
 Discharge (Amp/Hrs): 40.0/.48 Charge (Amp/Hrs): 40.0/1.00
 AH out: 19.186 AH in: 19.833 C/D RATIO: 1.034 EOC (I): 2.75
 Cell Design: New Plate, Old Separator

Key:
 --- Current
 --- Volt: Cell 1
 --- Volt: Cell 2
 --- Volt: Cell 3
 --- Volt: Cell 4
 --- Volt: Cell 5

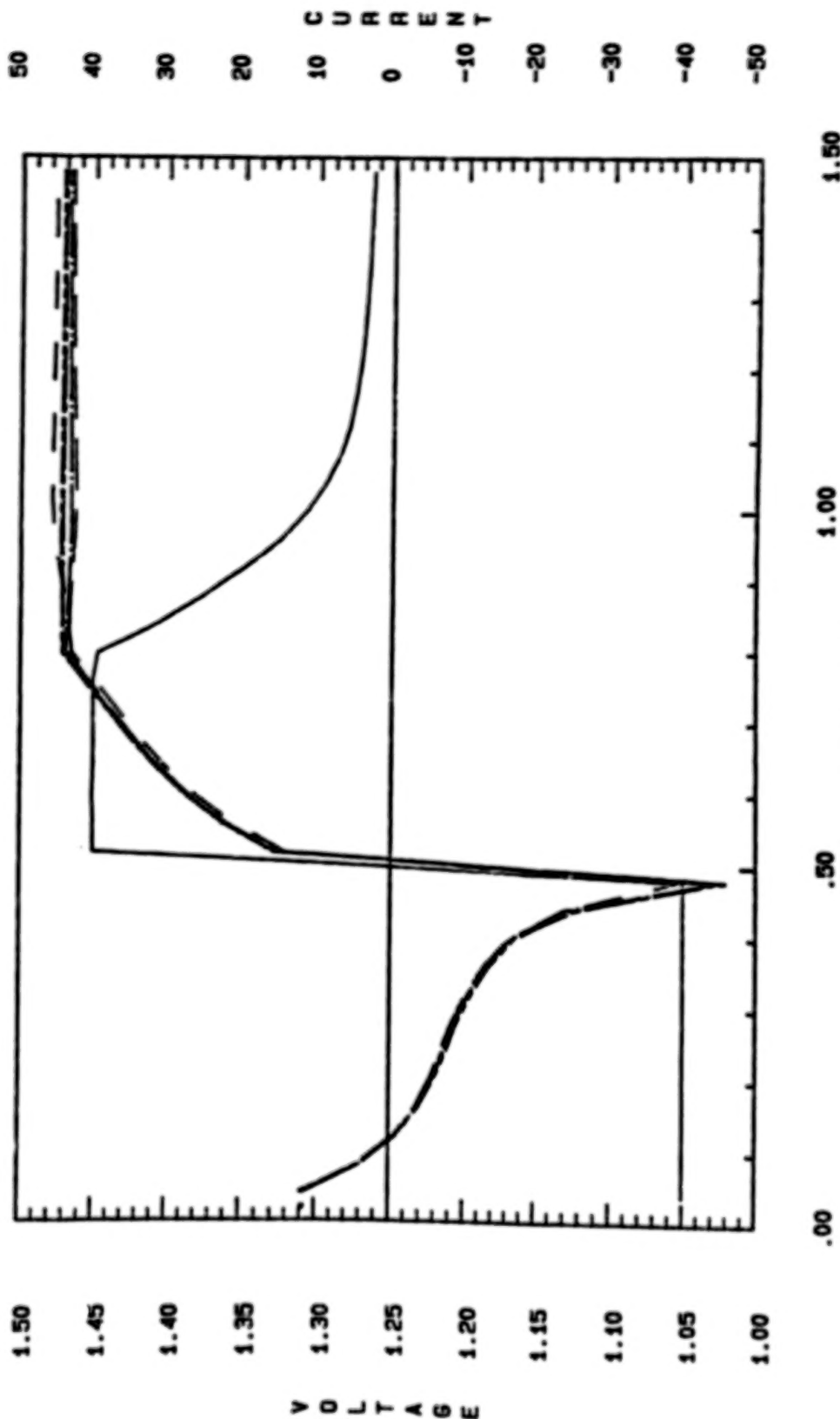


Figure 4.

REGUALIFICATION-LIFE CYCLING

Pack: 1500 Manuf: GE 50 AH Cycle 5832
 Orbit: LEO Temp (C): 10 DOD (X): 40 GSFC Vt. Level: 7
 Voltage Limit (v/c): 1.470 Time to Vt. Limit (hrs): 40.0/1.00
 Discharge (Amp/Hrs): 40.0/.48 Charge (Amp/Hrs): 40.0/1.00
 AH out: 19.212 AH in: 19.964 C/D RATIO: 1.039 EOC (I): 3.05
 Cell Design: New Plate, New Separator

Key: Current
 --- Volt: Cell 1
 --- Volt: Cell 2
 --- Volt: Cell 3
 --- Volt: Cell 4
 --- Volt: Cell 5

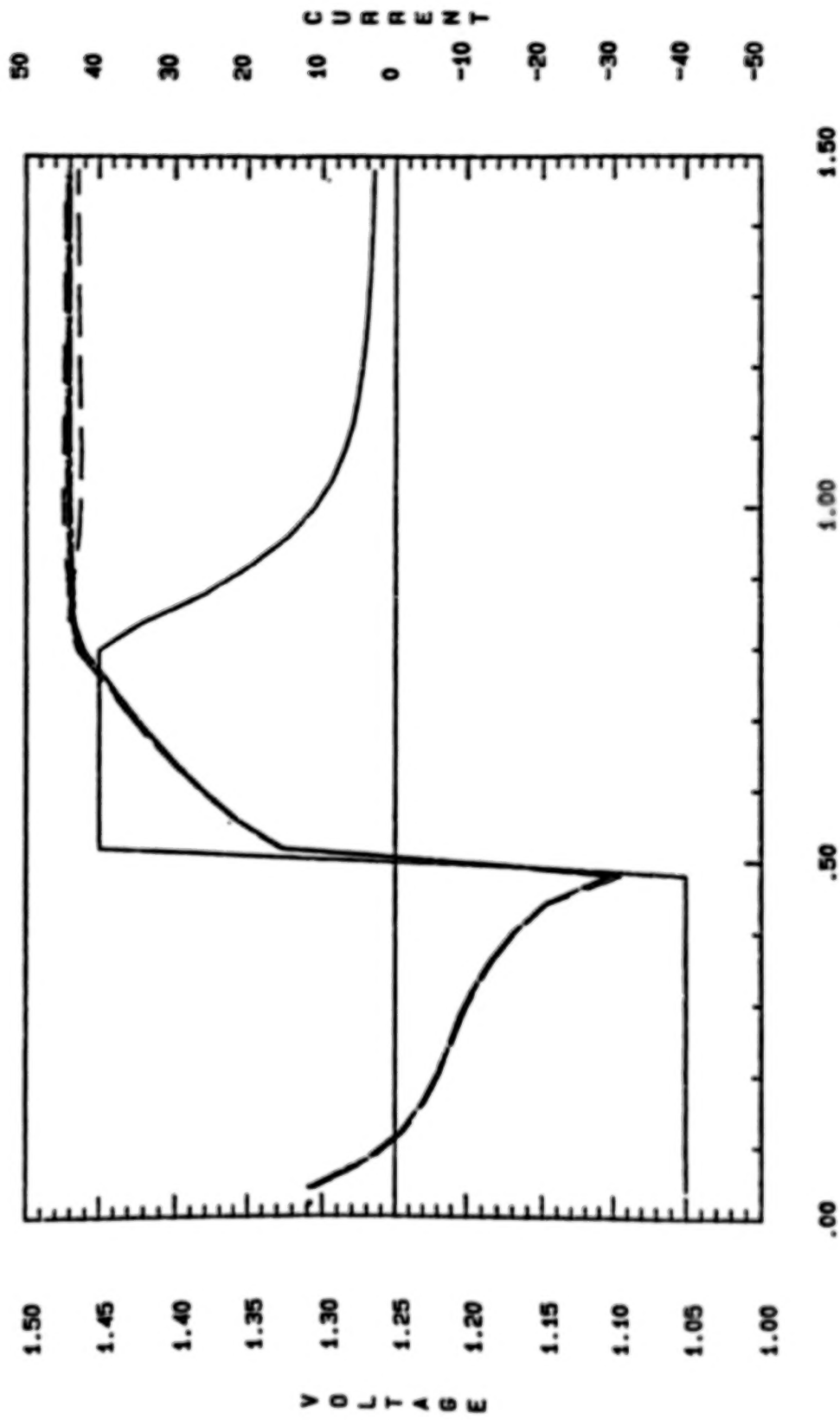


Figure 5.

REGUALIFICATION

Capacity Check

Pack: 150A Manf: GE 50 AH

Cycle: 5836 Temp (C): 10 Rate (Amps): 40.0

Note: CX to .75 volts any cell at 12 months of life.

Cell Design: NASA Standard

Key:	Cell No.
—	Volt: Cell 1
—	Volt: Cell 2
—	Volt: Cell 3
—	Volt: Cell 4
—	Volt: Cell 5

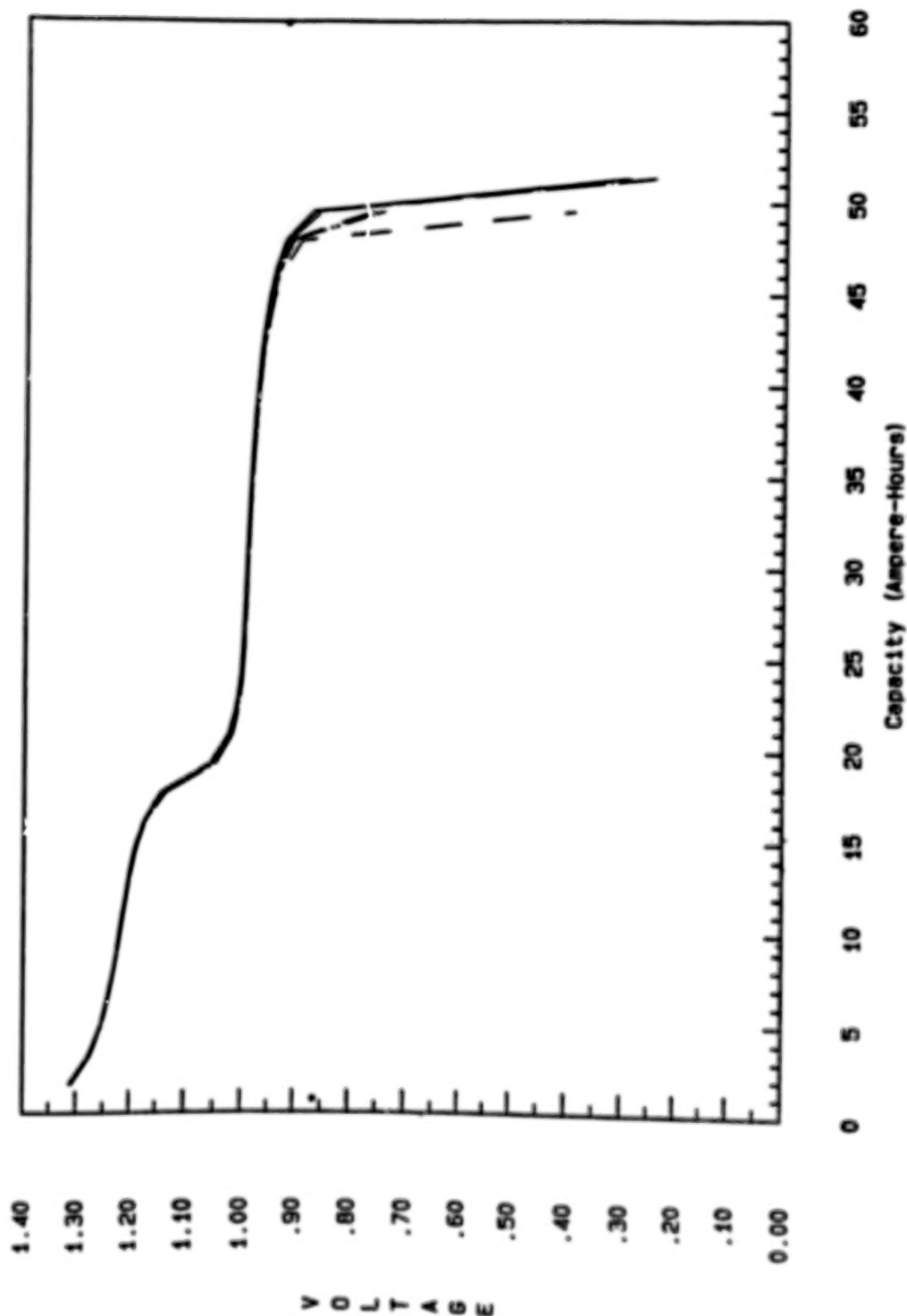


Figure 6.

REGUALIFICATION

Capacity Check

Peck: 1508 Manf: 6E 50 AH

Cycle: 5837 Temp (C): 10 Rate (Amps): 40.0

Note: CX to .75 volts any cell at 12 months of life.

Cell Design: Old Positive, New Separator

Key:	Cell No.
—	Cell 1
- -	Cell 2
- -	Cell 3
- -	Cell 4
- -	Cell 5

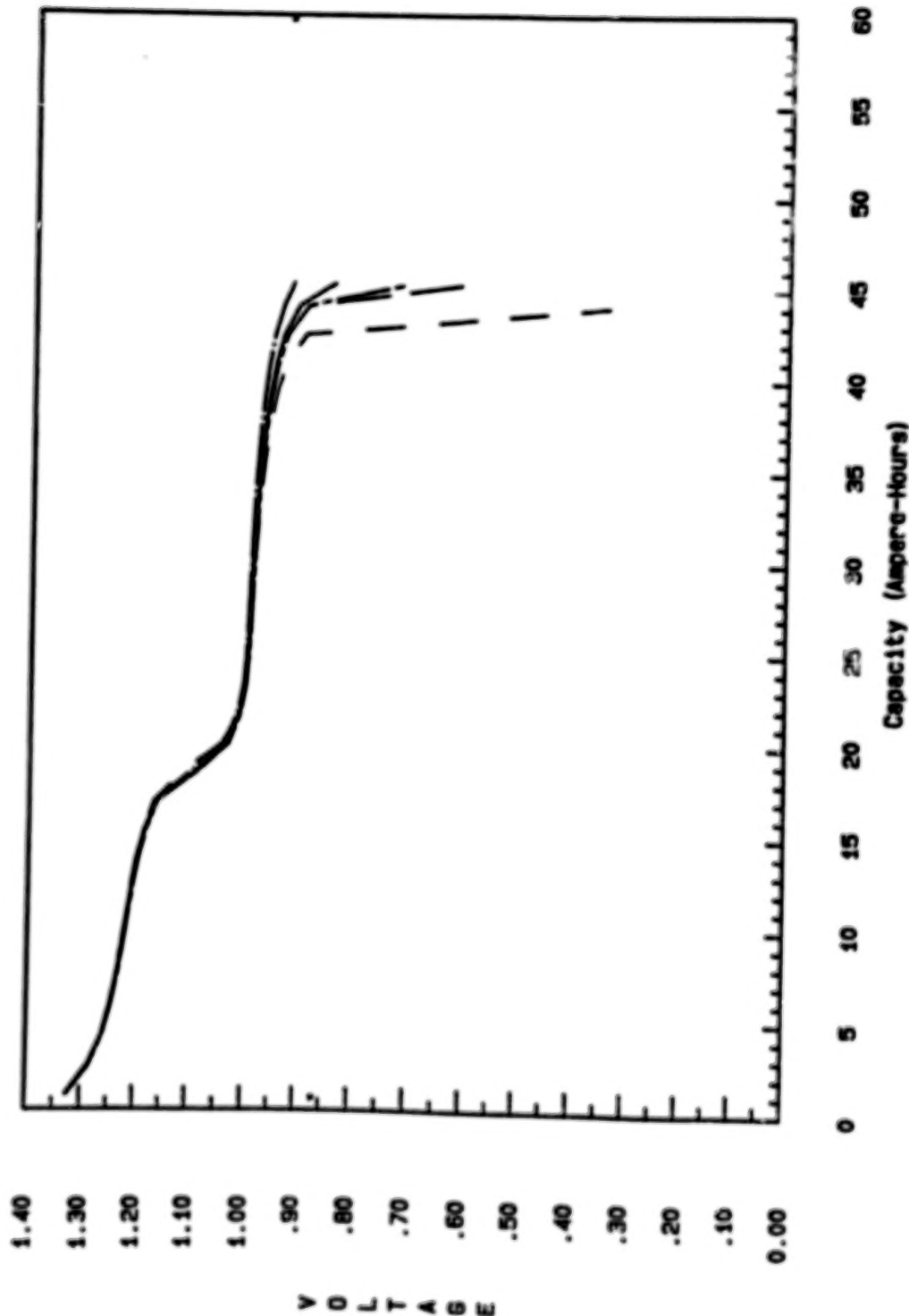


Figure 7.

REGUALIFICATION

Capacity Check

Pack: 150C Manf: GE 50 AH

Cycle: 5835 Temp (C): 10 Rate (Amps): 40.0

Note: CX to .75 volts each cell at 12 months of life.

Cell Design: New Plate, Old Separator

Key:	Cell No.
—	Cell 1
- -	Cell 2
- - -	Cell 3
- - - -	Cell 4
- - - - -	Cell 5

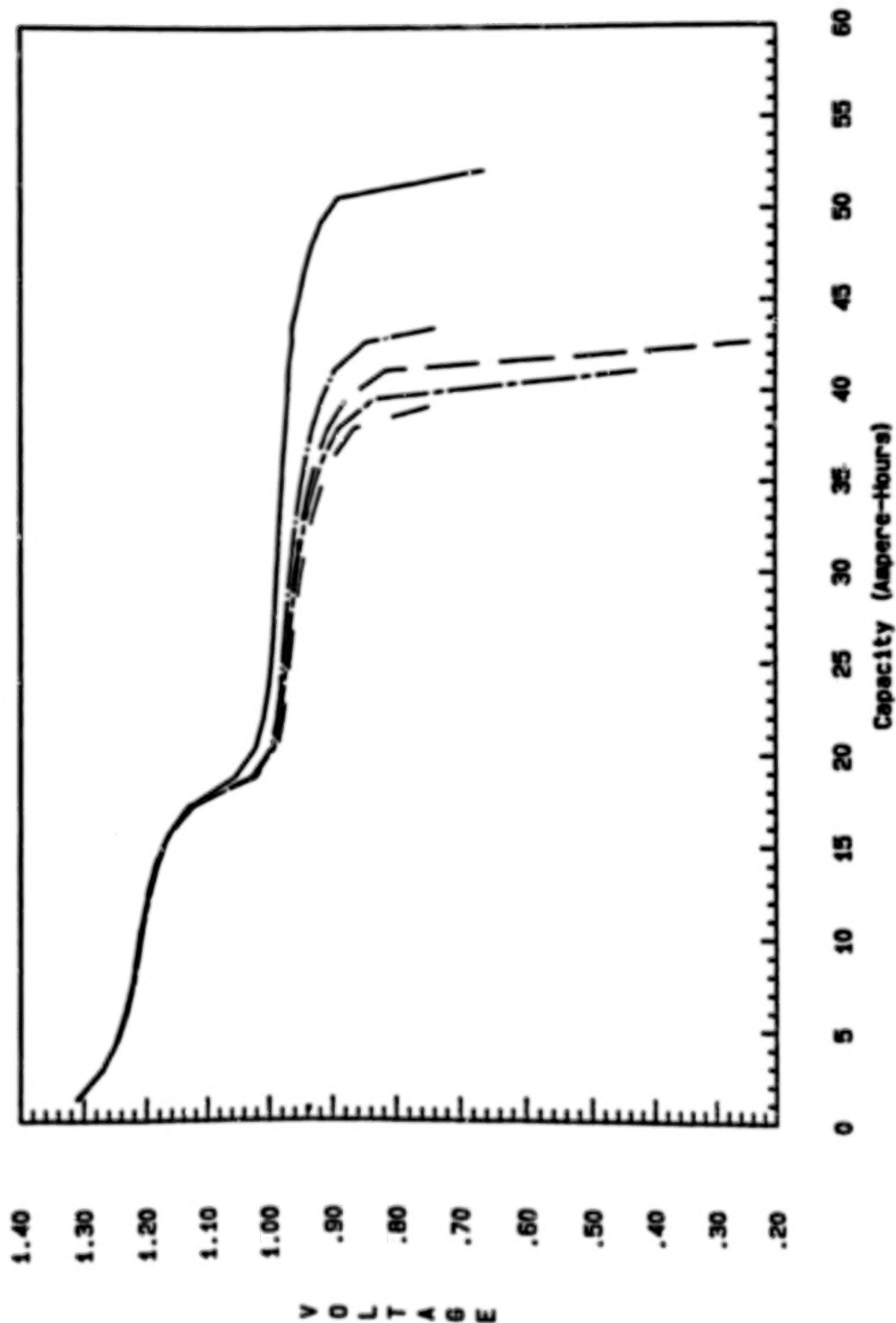


Figure 8.

REQUALIFICATION

Capacity Check

Pack: 1500 Manf: GE 50 AH

Cycle: 5833 Temp (C): 10 Rate (Amps): 40.0

Note: CX to .75 volts any 11 at 12 months of life.

Cell Design: New P e, New Separator

Key:	Cell No.
—	Cell 1
—	Cell 2
—	Cell 3
—	Cell 4
—	Cell 5

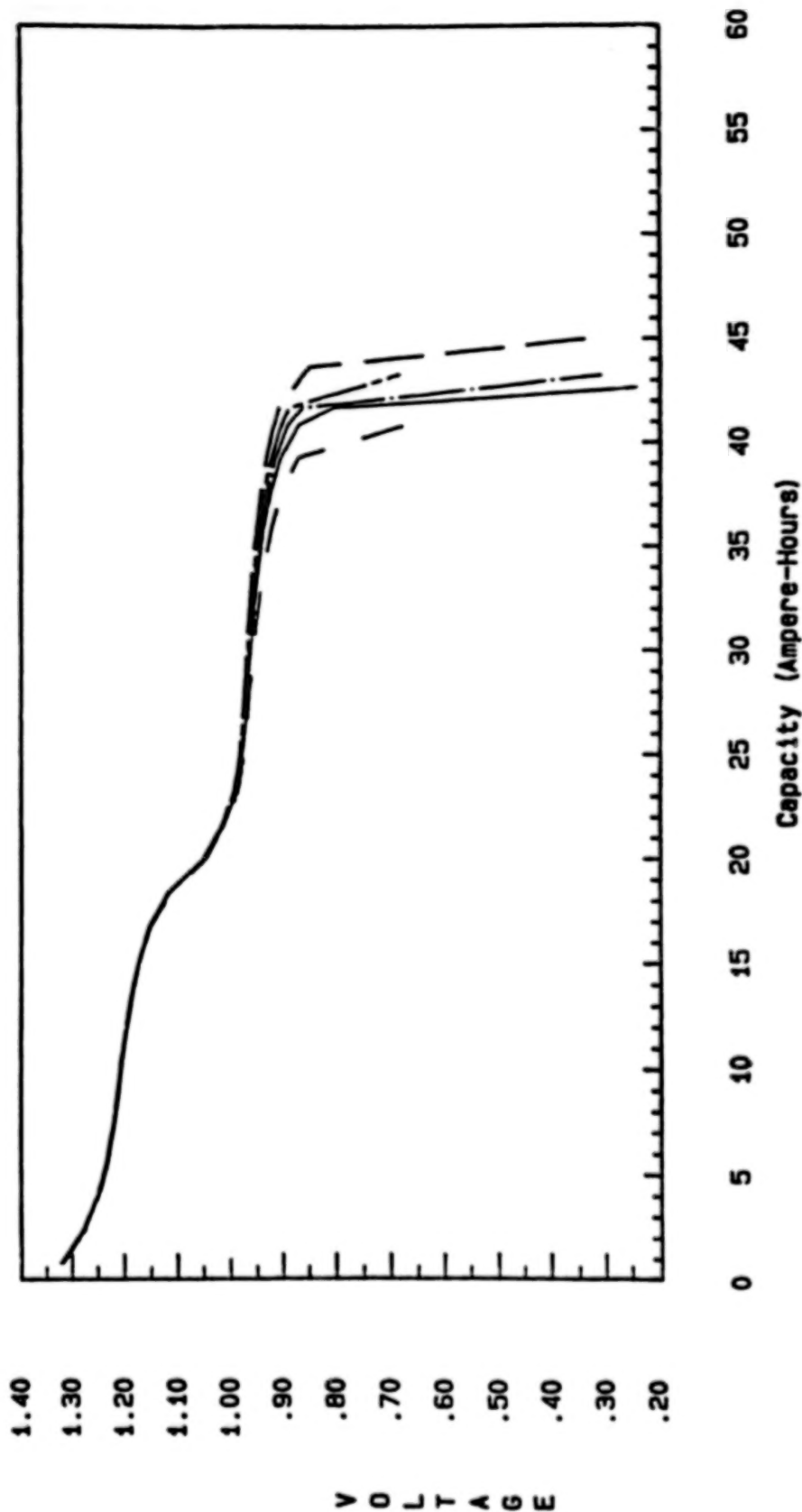


Figure 9.

REQUALIFICATION

Pack: 150H Manf: 6E 50 AH

Reconditioning - Prior to Shadow # 2

Cycle: 162 Temp (C): 20 Rate (Amps): 33.3

Note: Followed 4 mo. float at .83 amp

Key: Cell No.	
—	Volt: Cell 1
—	Volt: Cell 2
—	Volt: Cell 3
—	Volt: Cell 4
—	Volt: Cell 5

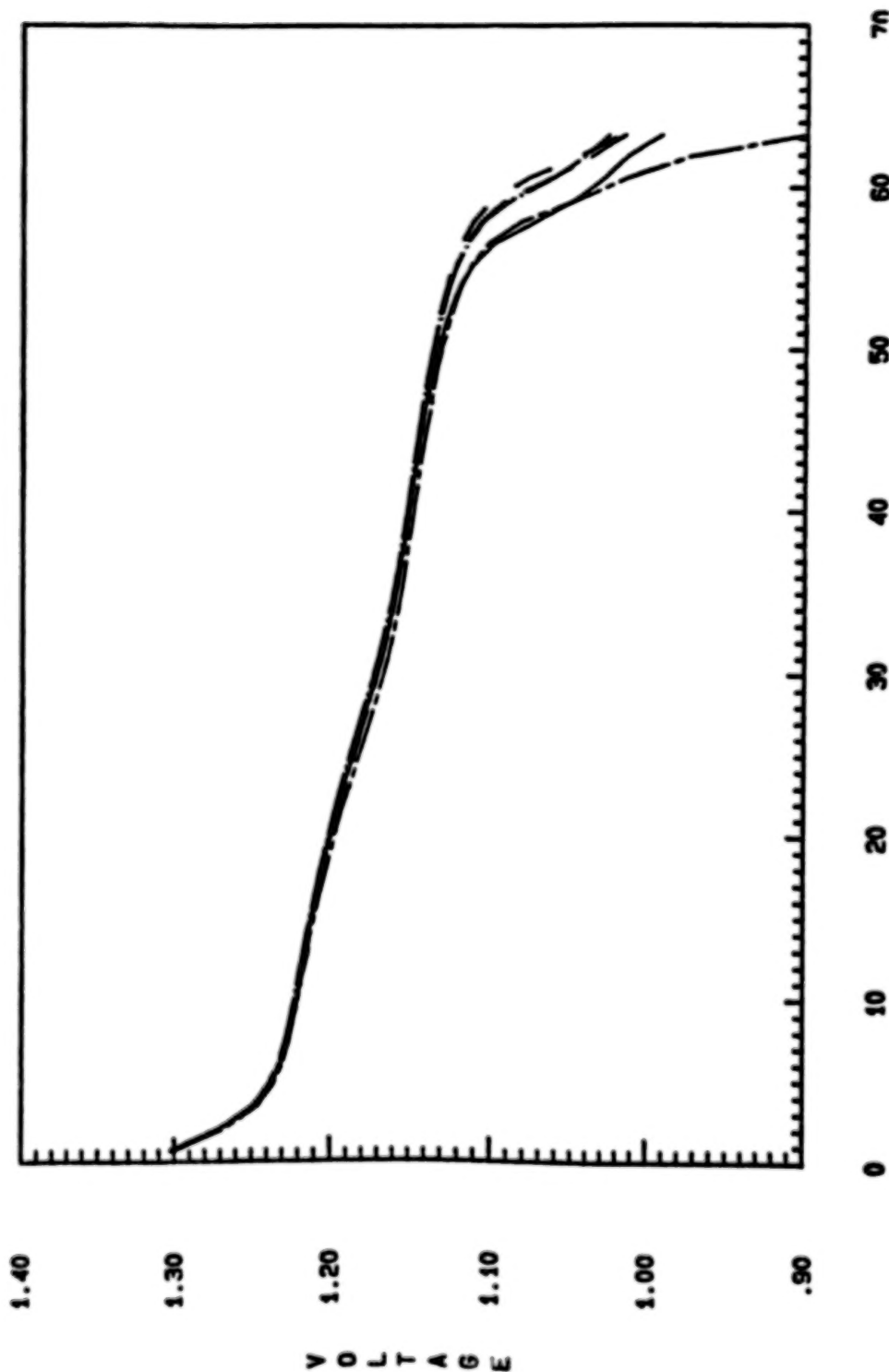


Figure 10.

REQUALIFICATION

Pack: 150I Manf: GE 50 AH
 Reconditioning - Prior to Shadow # 2
 Cycle: 162 Temp (C): 20 Rate (Amps): 33.3
 Note: Followed 4 mo. float at .63 amp

Key: Cell No.

—	Volt: Cell 1
—	Volt: Cell 2
—	Volt: Cell 3
—	Volt: Cell 4
—	Volt: Cell 5

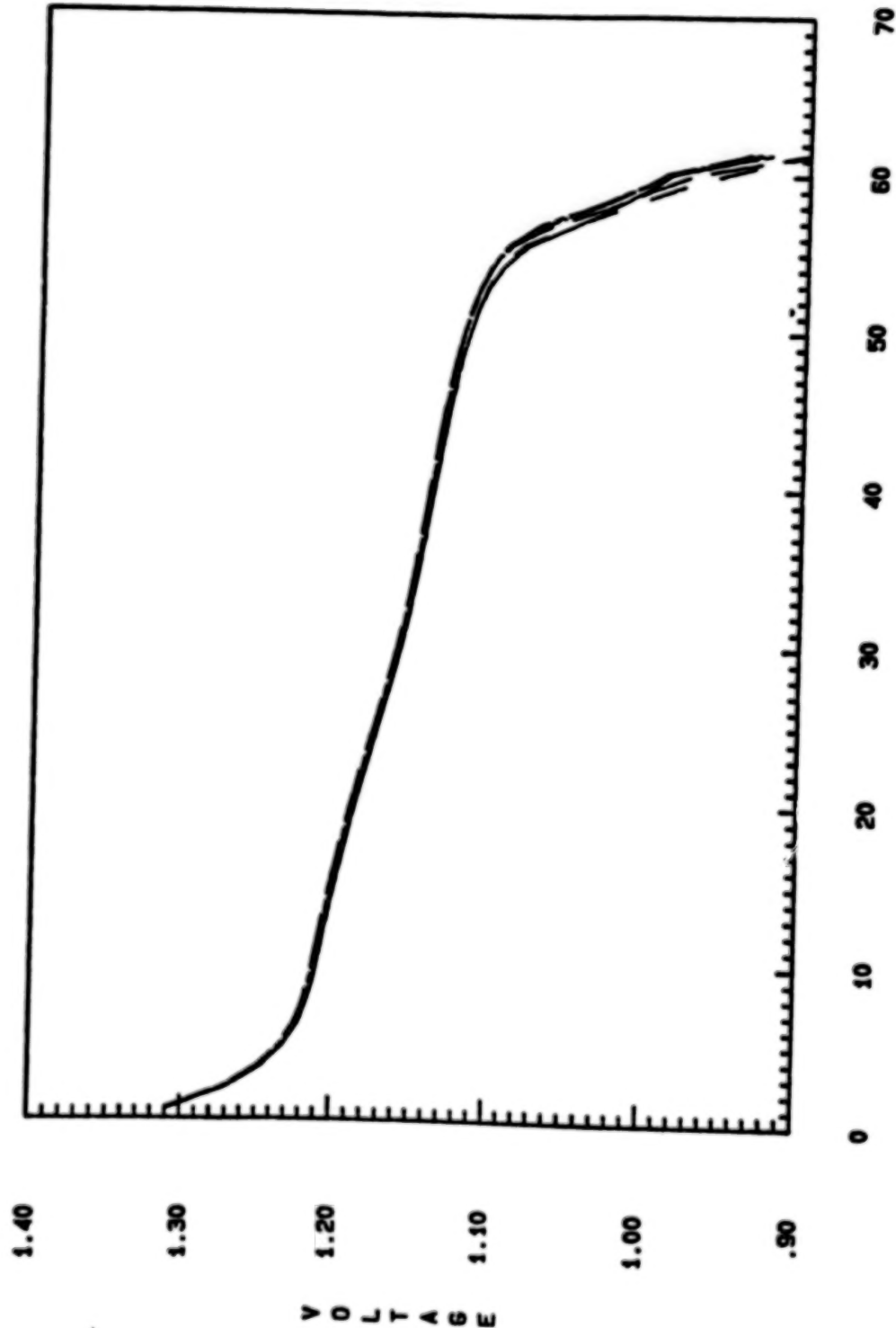


Figure 11.

REGUALIFICATION

Pack: 150H Manf: 6E 50 AH

Shadow # 2 - Ampere-Hours vs Day

Cycles: 177 to 217 Temp (C): 20 DOD (X): 80

Dchg (33.3A). Chg (5.0A till 115% or 1.49v any cell then .83A)

Key: _____
Ampere Hours

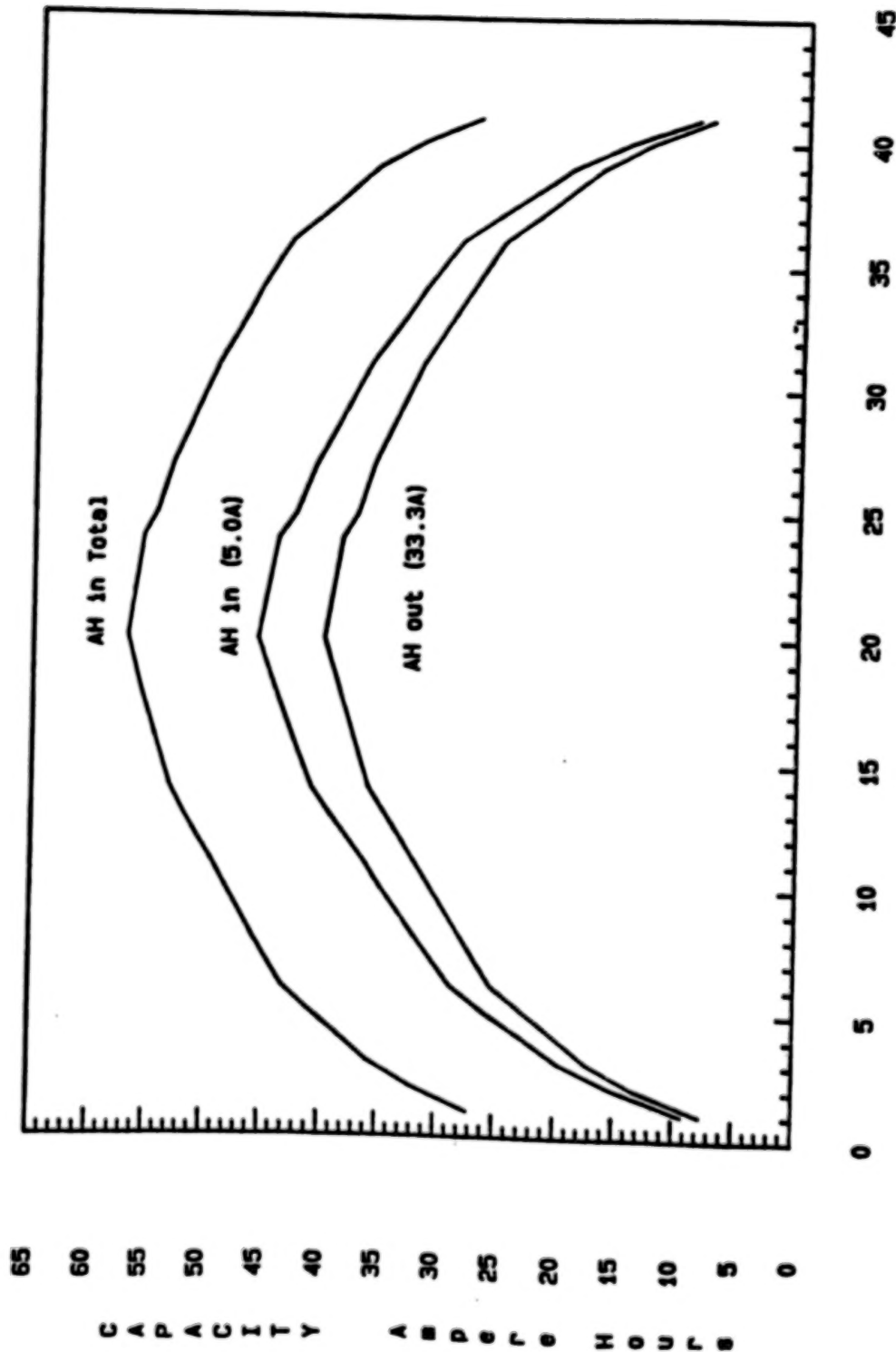


Figure 12.

REGUALIFICATION

Peck: 150I Manf: 6E 50 AH

Shadow 2 - Ampere-Hours vs Day

Cycles: 177 to 217 Temp (C): 20 DOD (X): 80

Dchg (33.3A). Chg (5.0A till 115% or 1.49v any cell then .83A)

Key: _____
Ampere Hours

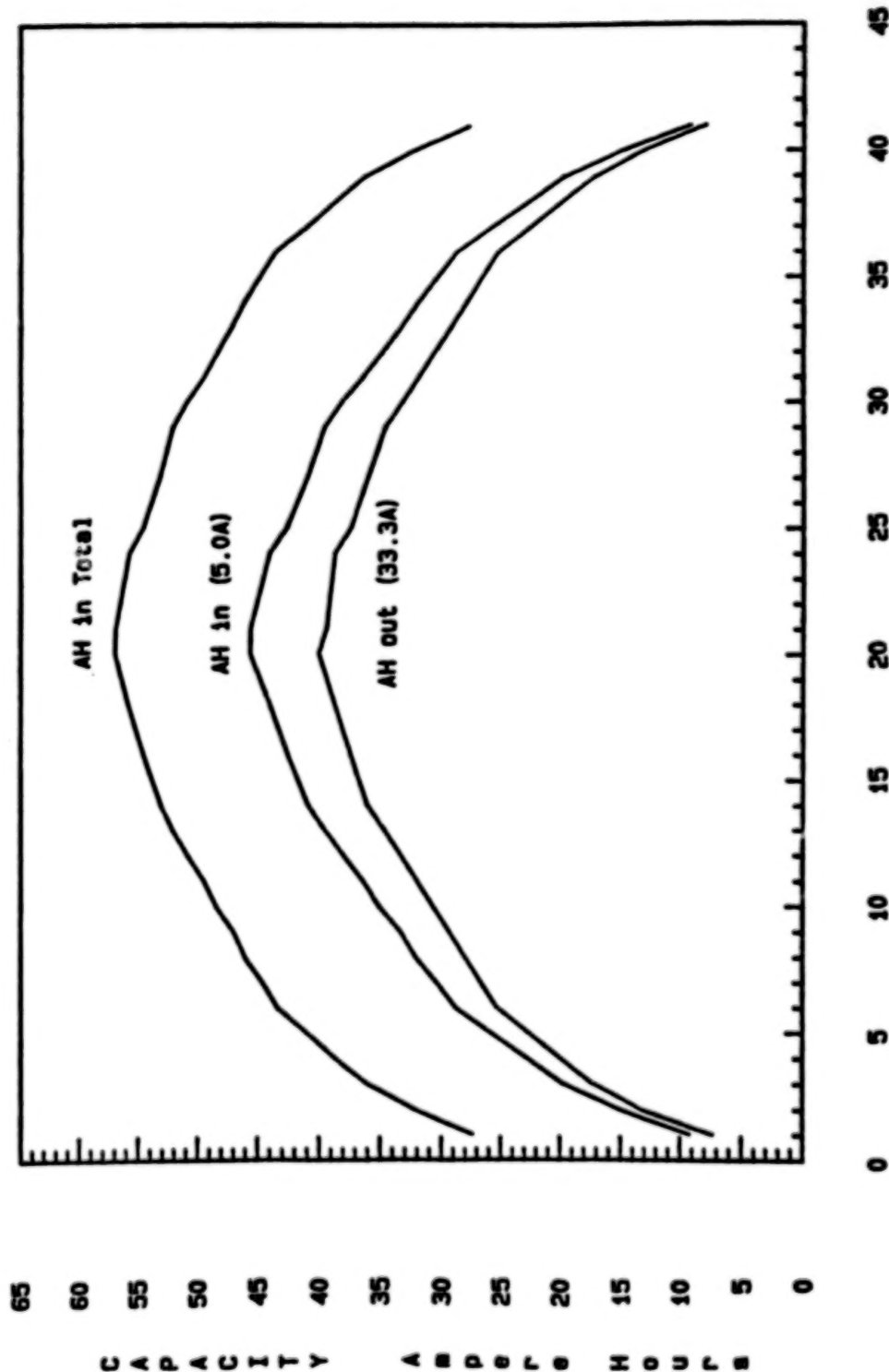


Figure 13.

REQUALIFICATION

Pack: 150H Manf: GE 50 AH

Shadow 2 - Cell Voltage vs Day

Cycles: 177 to 217 Temp (C): 20 DOD (X): 80

Charge was 5.0A till 115% return or 1.49 volts any cell then .83A

Key:	Cell No.
---	Cell 1
---	Cell 2
---	Cell 3
---	Cell 4
---	Cell 5

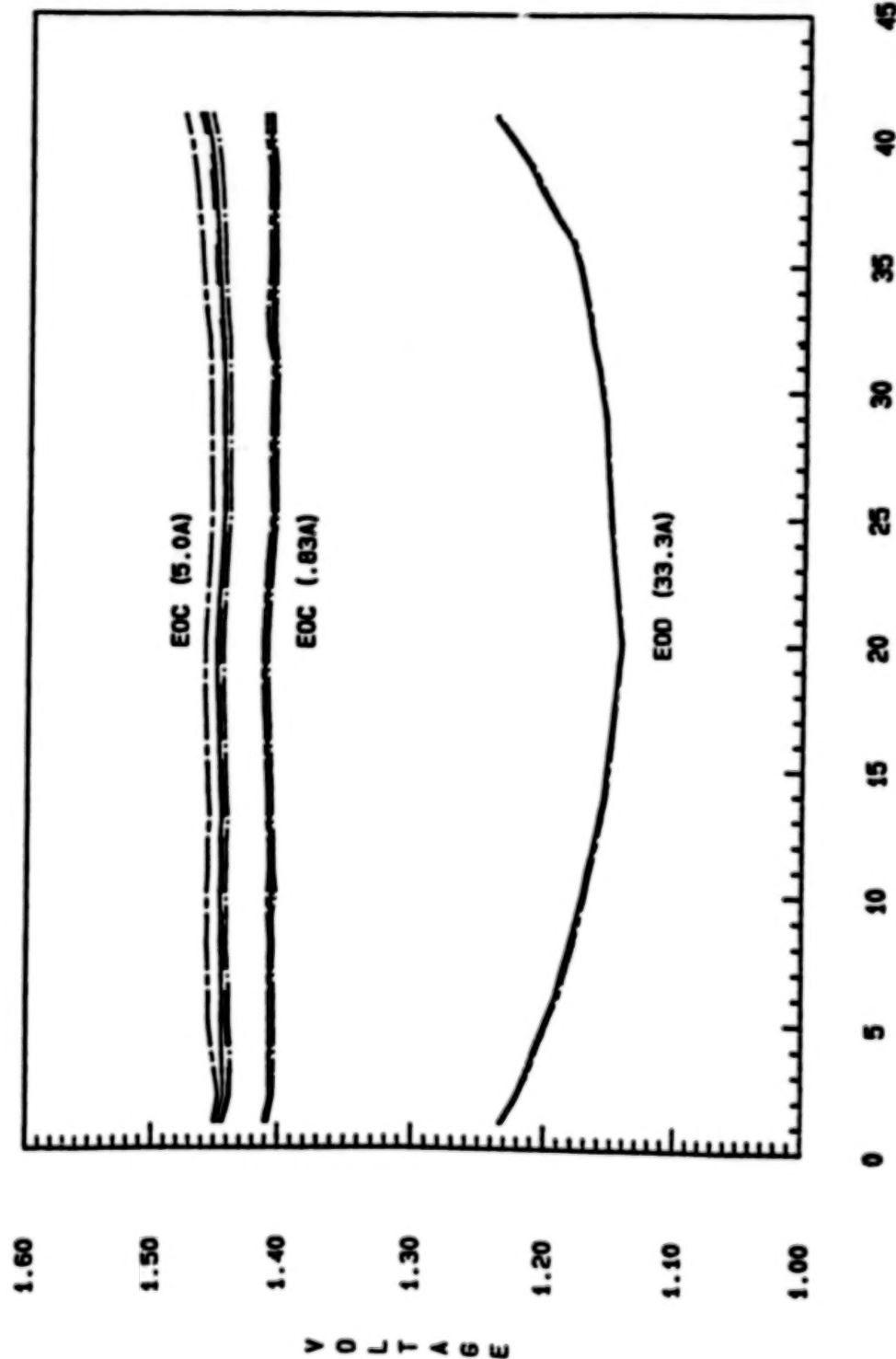


Figure 14.

REGUALIFICATION

Pack: 150I Manf: GE 50 AH

Shadow # 2 - Cell Voltage vs Day

Cycles: 177 to 217 Temp (C): 20 DOD(X): 80

Charge was 5.0A till 115% return or 1.49 volts any cell then .83A

Key:	Cell No.
---	Cell 1
---	Cell 2
---	Cell 3
---	Cell 4
---	Cell 5

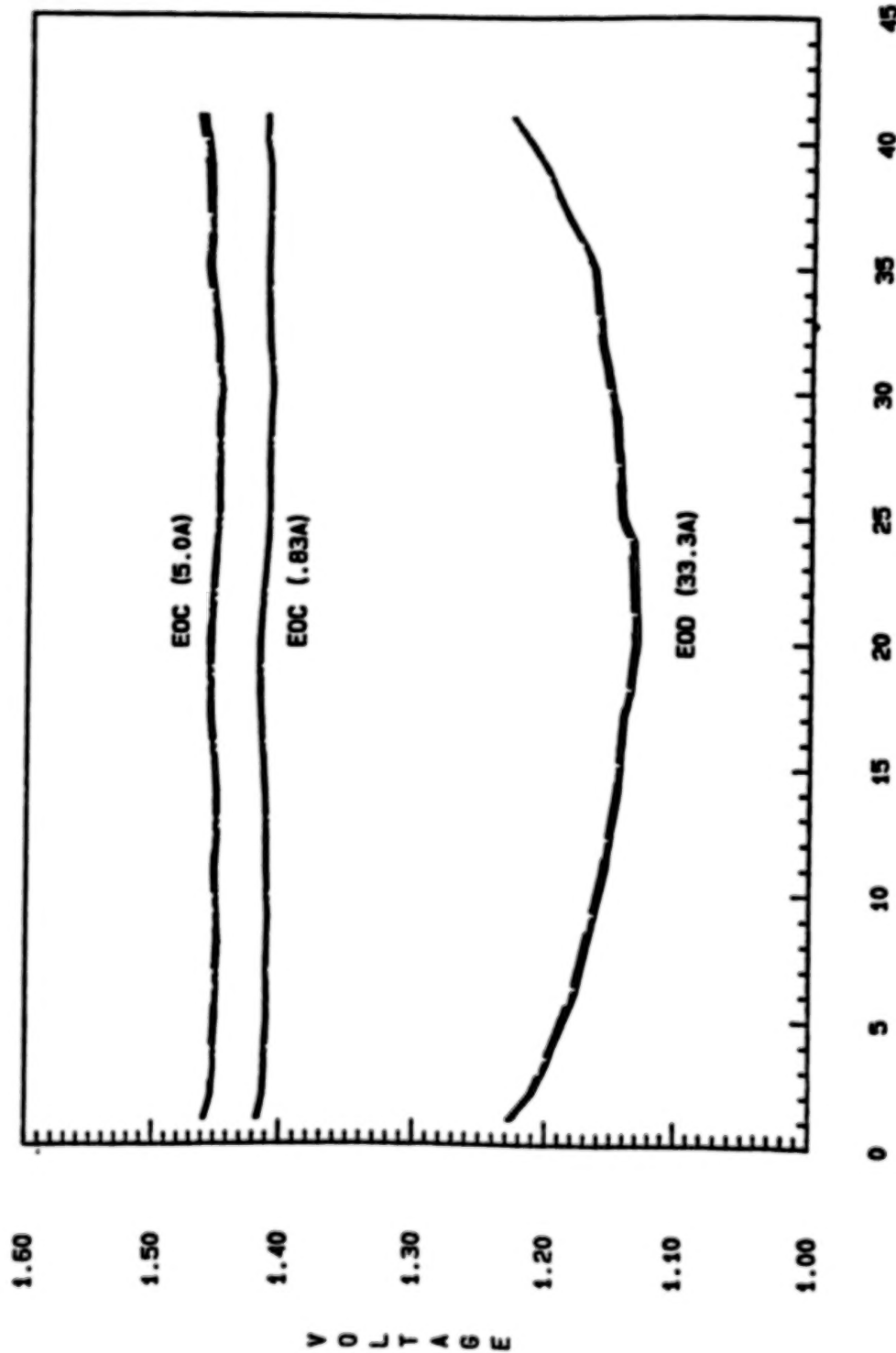


Figure 15.

FLIGHT EXPERIENCE OF SOLAR MESOSPHERE
EXPLORER'S POWER SYSTEM OVER
HIGH TEMPERATURES RANGES

Jack Faber*
Daniel Hurley**

This paper summarizes the performance of the power system on the Solar Mesosphere Explorer (SME) satellite for the life of the mission and the techniques used to ensure power system health. Early in the mission high cell imbalances in one of the batteries resulted in a loading scheme which attempted to minimize the cell imbalances without causing an undervoltage condition. A short term model of the power system allowed planners to predict depth of discharge using the latest available data. Due to expected orbital shifts the solar arrays experience extended periods of no eclipse. This has required special conditioning schemes to keep the batteries healthy when the eclipses return. Analysis of the SME data indicates long term health of the SME power system as long as the conditioning scheme is continued.

INTRODUCTION

SME was launched 6 Oct 1981 into a nearly circular polar orbit at an altitude of 534 km. The satellite was injected at an inclination of 97.5 degrees to maintain a near 3AM-3PM sun-synchronous orbit. However, since SME has no onboard mechanism for adjusting its orbit the natural orbital perturbations have caused the orbit plane to precess out of

- * SME Mission Analyst Manager, Laboratory for Atmospheric and Space Physics, University of Colorado, Boulder, Colorado.
- ** SME Flight Analyst, Laboratory for Atmospheric and Space Physics, University of Colorado, Boulder, Colorado.

the shadow of the earth. The duration of each orbits eclipse has varied from a high of 32 minutes to the current low of 0 minutes. This has caused fluctuations of electrical shelf temperatures, which have ranged from 20 to 60 degrees C.

DESCRIPTION OF SME'S POWER SYSTEM

SME has an unregulated, direct energy transfer power system. Power is generated by eleven parallel diode protected solar array panels, with three additional switchable panels. The energy is stored in two nickel-cadmium batteries containing 21 cells each. While charging to each battery can be disabled, both batteries can discharge through a diode even when commanded off line. Overcharge protection is provided by a shunt regulator that has been commanded to shunt at the lowest of four voltage-temperature (V/T) levels. Undervoltage protection is provided by logic that will turn off all nonessential loads if the voltage drops below 23.7 volts.

The batteries were build by SAFT in the spring of 1977 for use on the P-78 satellite. They were used during P-78 ground tests from Oct 1977 through Sep 1978 and then placed in cold storage. The batteries were tested on Sept 1979 and then returned to cold storage before being placed in SME on Sept 1980. Prior to launch the batteries were cycled approximately 100 times to less than 20% DOD and approximately 20 times to more than 50% DOD (ie. conditioning cycles). In all ground testing battery two was observed to have slightly higher capacity and better balance than battery one.

EARLY MISSION SUMMARY

During the first 4 years of the mission the battery temperatures varied between 15 and 30 degrees C (Fig. 1). Since the angle between the solar arrays and the sun has been kept at a constant 37 degrees the driver for this fluctuation was the yearly solar intensity (Fig. 2). The duration of eclipse has varied little during this period (Fig. 3). The cell imbalance monitors on board, which averages and compares the voltage on each half of each battery, began to rise in both batteries but especially in battery one. In late 1981 battery one was taken off line automatically by the cell monitor. Five days later, battery two was commanded off line to provide deeper conditioning than one eclipse could provide. During the remainder of the mission, on one eclipse per day, optional loads were commanded on to cause a 10% discharge of the batteries to 24.5 volts (Fig. 4). This was combined with some loading during charge to reduce the charge rate to C/10.

TEMPERATURE PROBLEMS WITH BATTERY ONE

During the fall of 1985 the duration of eclipse dropped to less than 20 minutes, for the first time in the mission, and the temperature of the electrical shelf began to rise. However, the temperature of battery one rose an additional 7 degrees C above the electrical shelf (Fig. 5). This additional temperature rise caused battery one to heat the shelf above that predicted for the observed duration of eclipse. Battery one had become a heat source for the electrical shelf. Also, cell imbalances in battery one began to rise during charge and the amount of heat generated by battery one continued to increase. By reducing the charge rate to c/10 the cell imbalances in battery one were brought under control and the temperatures stabilized. Consideration was given, at that time, to taking battery one off line. However, since it was not possible to accurately determine the sharing between the two batteries and since the temperatures were under control battery one was left on line.

NO ECLIPSE

As the first period of no eclipse approached, the temperature of battery one began to increase more rapidly than that of the other electrical shelf monitors. It was decided, at that time, to take battery one off line. The results of taking battery one off line were dramatic. Within 10 hours, the temperature of battery one dropped 18 degrees C and the temperature of battery two dropped 4 degrees C. At this time, the battery temperatures again matched the electrical shelf temperatures. The voltage of battery one dropped 5 volts during the next 30 hours. As the voltage of battery one continued to drop, a decision was made to leave it off-line for the remainder of the mission (Fig. 6).

After the satellite entered the period of no eclipse, battery two was also taken off line. At that time it became possible to recalibrate the current monitors of battery two. Recalibration confirmed the coefficients had been underestimating the share of discharge battery two provided at temperatures above 30 degrees C. It is estimated battery two will be able to supply adequate power to avoid undervoltage during the 1987 eclipses. During the current period of no eclipse, battery two is conditioned by being taken off line for 5-7 days at approximately c/1000 discharge, then recharged for 30 minutes at c/10. After the 30 minutes, the bus voltage reaches shunt and the shunt control trickle charges the battery for an additional four hours, after which the conditioning cycle is repeated. If

trickle charge is allowed to continue for more than 4 hours a slight temperature increase is noted in battery two, indicating overcharge.

VOLTAGE PREDICTION

Prior to no eclipse, battery voltage was modeled as a function of the capacity removed from the battery. On a daily basis commands were loaded into the onboard memory. These commands controlled the times loads were turned on and off. Knowing the draw of each load and its duration, the capacity removed from the battery during each eclipse could be calculated and applied to the model to predict the battery voltage. During no eclipse, however, the battery trickle discharges, while offline. This trickle discharge is due to the small draw placed on the battery by the monitors. The value of this draw is unknown, since it is below the resolution of the monitors.

While battery two is offline, changes in voltage occur slowly. The slow change allows for accurate modeling of the battery's discharge curve (Fig. 7). In order to predicted the battery's voltage, over time, a simplification of the Shepherd equation was used.

$$E = E_s - K \left(\frac{Q}{Q - R} \right)^n - Nt + A_0 e^{(-BQ^{-n}t)} \quad (\text{Shepherd equation})$$

If the amount of current drawn from the battery is assumed constant, then the Shepherd equation (Ref. 1) can be simplified to give:

$$E = V - \frac{W}{1 - Xt} + Y_0 e^{(-Zt)} \quad (\text{simplified Shepherd equation})$$

The coefficients (V-Z) are adjusted until the predicted voltage matches the observed voltage.

CONCLUSION

Battery one, which was the weaker of the two batteries, failed initially in 1985 when the increase in sunlight caused it to be overcharged. The battery went into a thermal runaway condition in 1986 and was taken off line. The rapid drop in the voltage of battery one, once off line, was an indication of its weak condition. The current conditioning of battery two will tend to create a soft battery, due to the low discharge rate to shallow depths. Alternate conditioning cycles, however, are being investigated to insure battery two will be able to provide sufficient energy during the eclipses of 1987.

REFERENCES

1. C. M. Shepherd, "Design of Primary and Secondary Cells; II. An Equation Describing Battery Discharge," J. of the Electrochemical Society, Vol.112, No.7, July 1965 pp.657-664

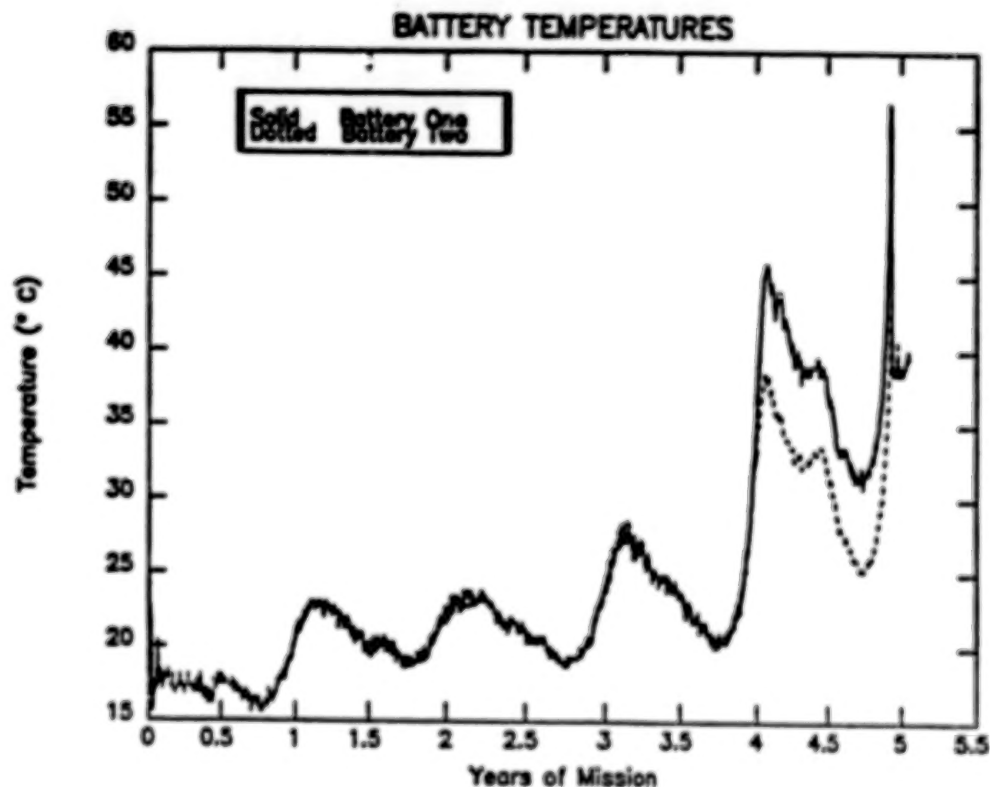


Figure 1.

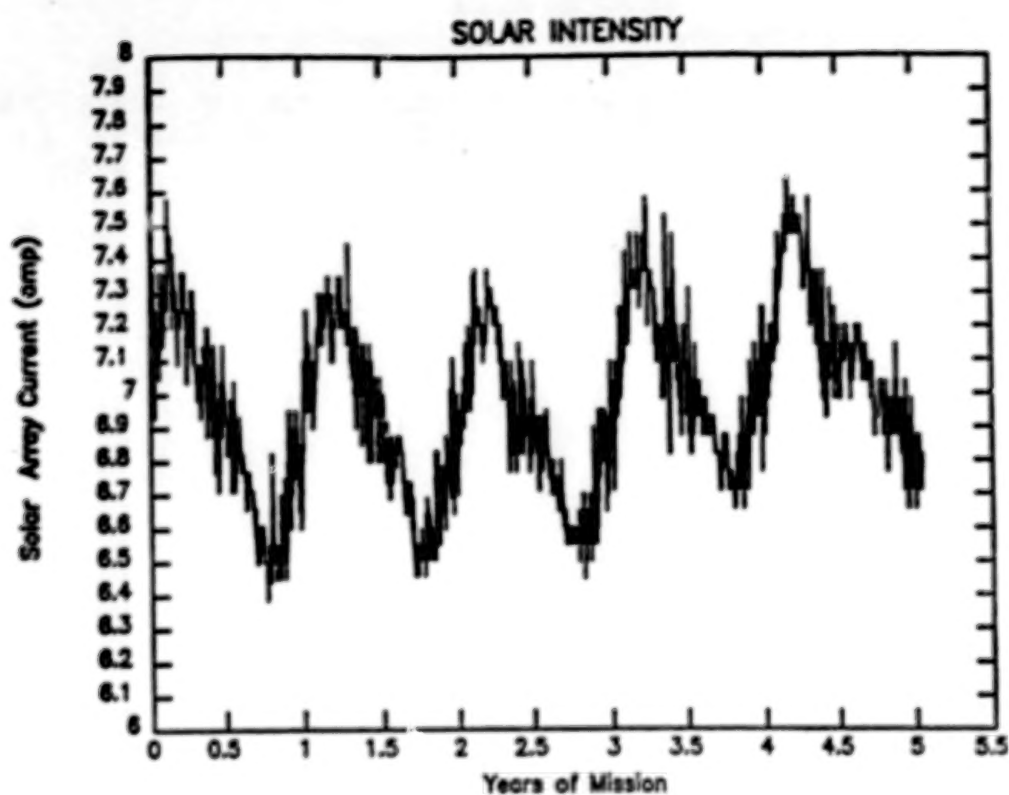


Figure 2.

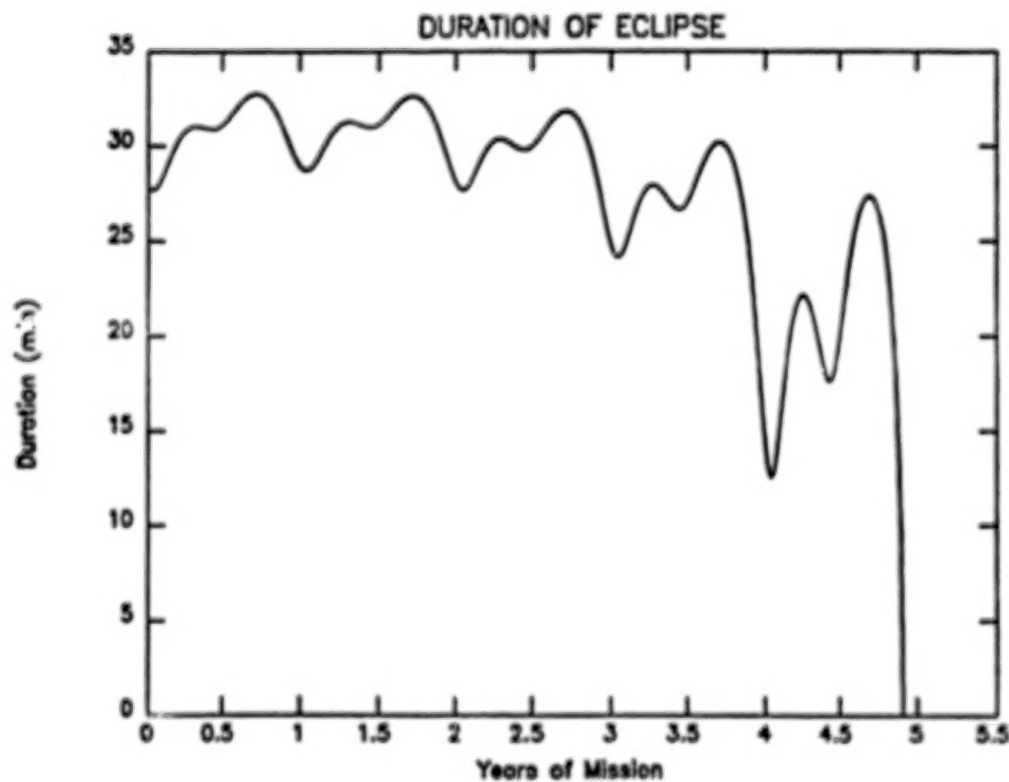


Figure 3.

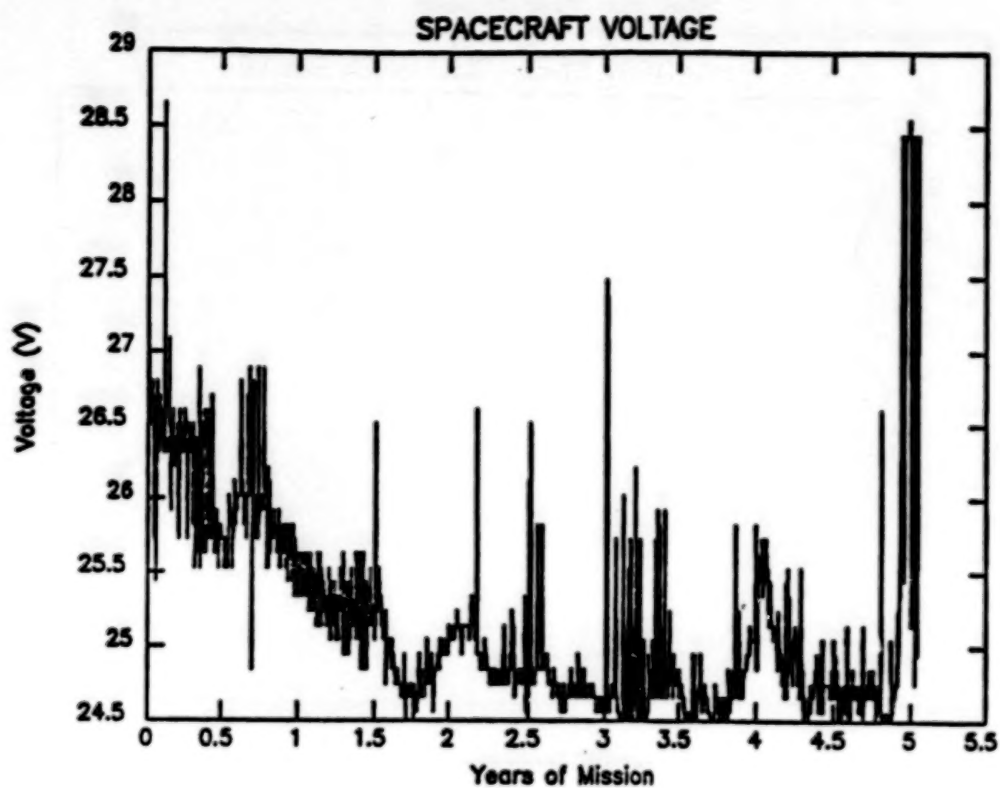


Figure 4.

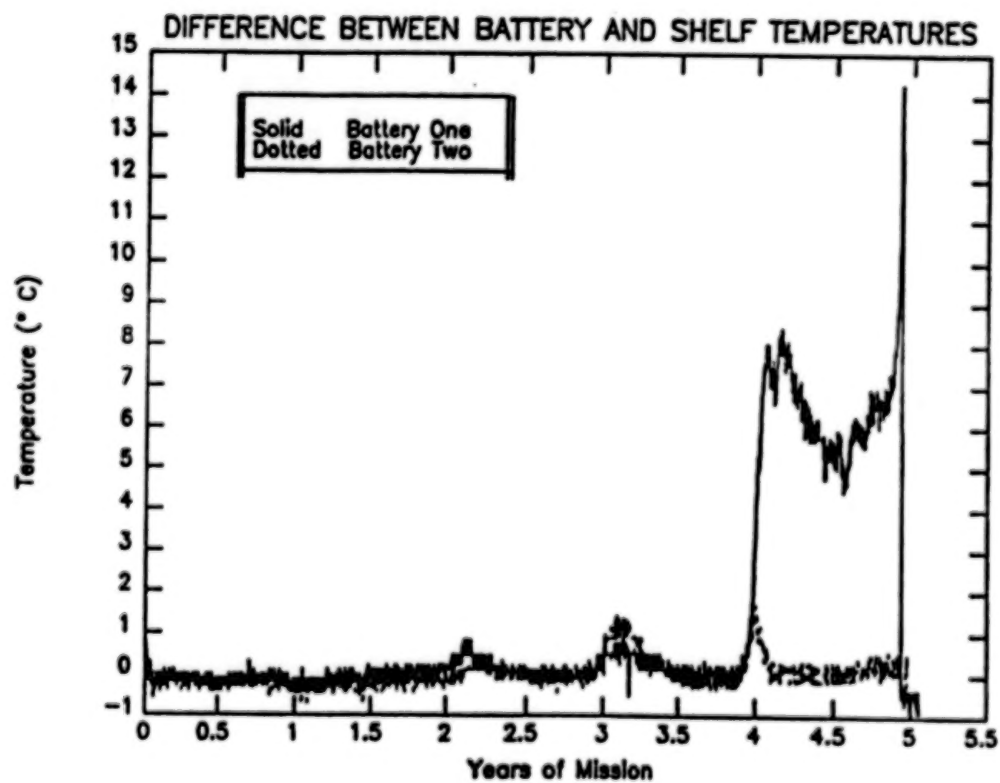


Figure 5.

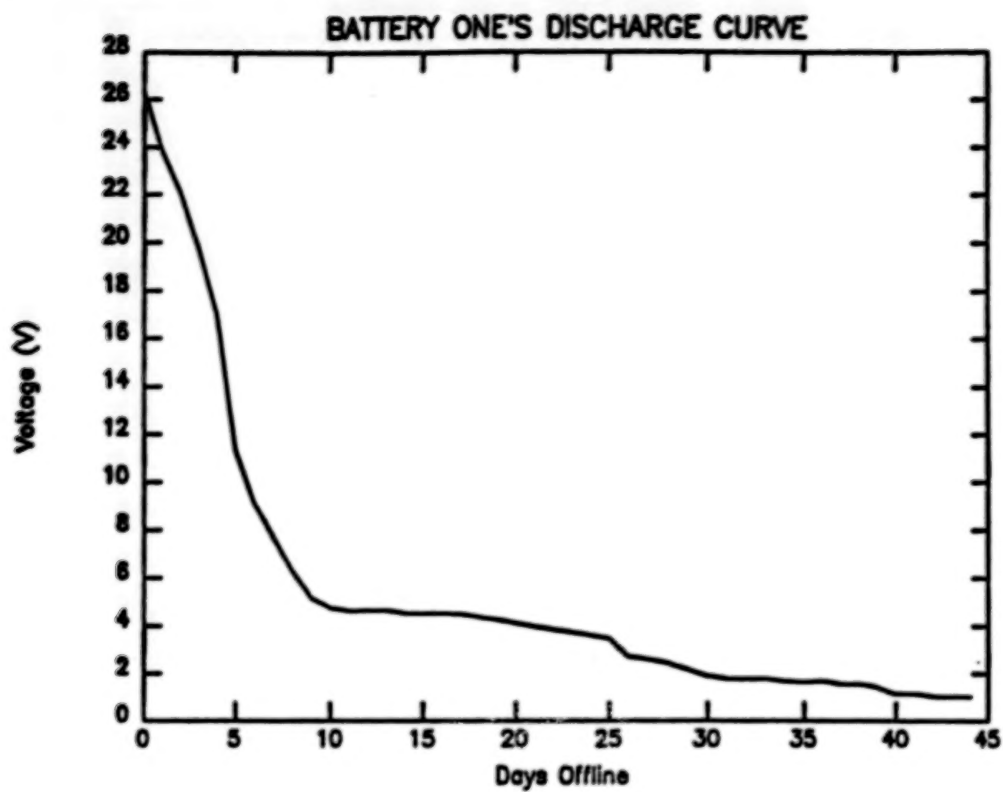


Figure 6.

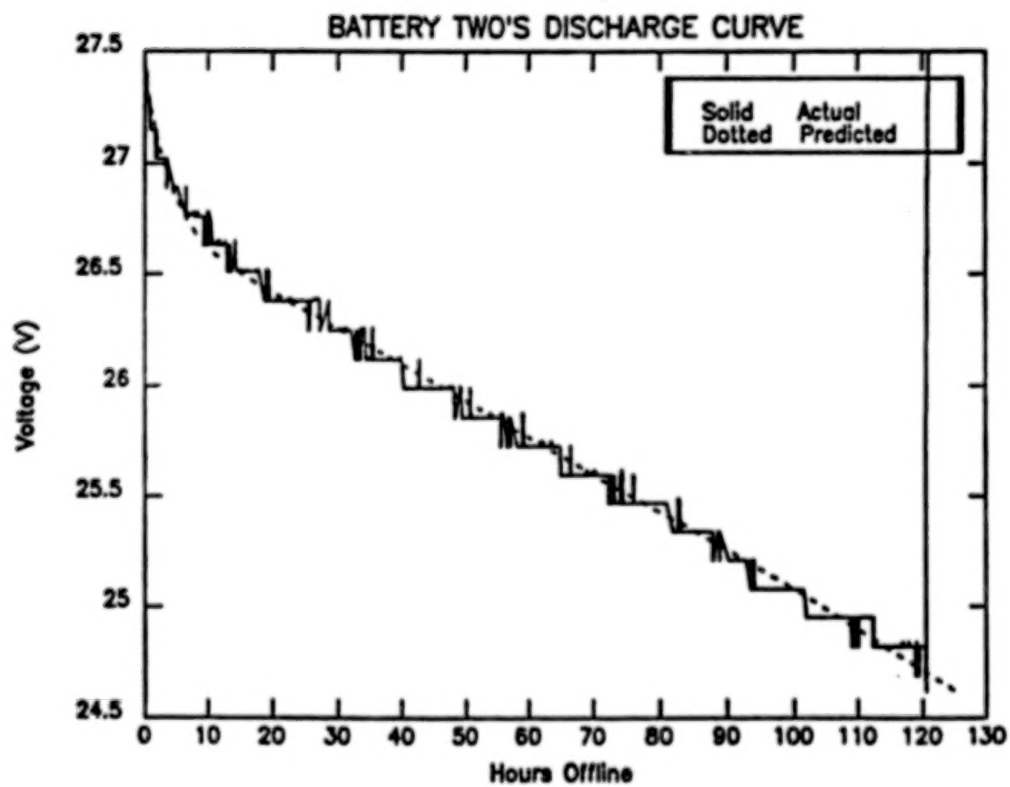


Figure 7.

SESSION IV

NICKEL CADMIUM DESIGN EVALUATION & COMPONENT TESTING

Chairman: G. Morrow, NASA/GSFC

REAL TIME CHARGE EFFICIENCY MONITORING FOR NICKEL ELECTRODES IN NICKEL AND NICKEL-HYDROGEN CELLS

A. H. Zimmerman
Chemistry and Physics Laboratory
The Aerospace Corporation
El Segundo, CA 90245

Introduction

The charge efficiency of nickel-cadmium and nickel-hydrogen battery cells is critical in spacecraft applications for determining the amount of time required for a battery to reach a full state of charge. The charge efficiency is the amount of charge stored relative to the amount being input to the battery by the battery charging system. As nickel-cadmium or nickel-hydrogen batteries approach about 90% state of charge or higher, the charge efficiency begins to drop towards zero, making estimation of the total amount of stored charge uncertain. Knowledge of the charge efficiency during real time operation could provide switch points for switching to trickle charge with minimum overcharge, battery charge control data for autonomous operation, or could allow automatic battery problem detection and responses in intelligent systems.

For nickel-cadmium batteries, which constitute most of the existing data base for space flight battery experience, it is difficult to accurately determine charge efficiency on a real time basis during uninterrupted operation. Charge efficiency estimates are typically based on prior history of available capacity following standardized conditions for charge and discharge. These methods work well as long as performance does not change significantly. Such performance changes may however make battery operation difficult as the batteries degrade towards the end of their life. The situation is potentially better for nickel-hydrogen batteries, for which internal cell pressures can provide an indication of the amount of charge stored. However such pressures can drift over long periods of operation, pressure monitoring hardware on each cell can be quite heavy, and the reliability of pressure monitoring strain gauges has been a problem. Thus a relatively simple method for determining charge efficiencies during real time operation for these battery cells would be a tremendous advantage. Furthermore such a method should ideally require monitoring of nothing more than the voltages of the battery cells. Such a method has been explored in this work, and appears to be quite well suited for application to nickel-cadmium and nickel-hydrogen battery cells.

Method for Determining Charge Efficiency

The charge efficiency of a nickel-cadmium or nickel-hydrogen cell that is nickel electrode limited as full charge is approached is given by

$$N = 1 - I_{ox}/I \quad (1)$$

where N is the fraction of the current I that is being stored in the cell. I_{ox} is the current going into evolution of oxygen, i. e. overcharge. The oxygen evolution current may be determined from the cell voltage using a

standard Tafel expression, assuming that the potential of the negative electrode does not change significantly as the cell goes into overcharge.

$$I_{ox} = I_0 \exp(KV) \quad (2)$$

where I_0 and K are empirically determined constants that define the rate of oxygen evolution as a function of cell voltage. These constants may be conveniently measured or updated without discharging the battery cell simply by measuring the cell voltage as a function of current when the cell is fully charged, a condition that causes all the current to go into oxygen evolution.

Cell Tests

The method outlined above was tested using both laboratory cells and sealed 6Ah NiCd cells. The laboratory cells had a nickel electrode, a Hg/HgO reference electrode, and a nickel metal counter electrode, and used 31% KOH as electrolyte. The temperature of all cells tested was controlled to within ± 0.1 deg C using a regulated temperature bath that pumped cooling fluid through a copper block into which the cells were mounted. All tests were both controlled and monitored by a microprocessor, which operated from an uninterruptible power system. Independent under- and over-voltage interlocks were included in the system for cell safety in the event of an equipment malfunction.

The first tests that were done involved simply charging the cell followed by discharge at a C/2 rate (the C rate discharges the nameplate cell capacity in a one hour period). Typical voltages during charge at a C/10 rate for both laboratory cells and a 6 Ah NiCd cell are indicated in Fig. 1. While the cell was at a full state of charge, the current/voltage curve for oxygen evolution was measured by reducing the current from the C/10 charge rate to C/20, C/50, and C/100. At each charge rate the cell voltage was allowed to stabilize before being recorded. The steady-state oxygen evolution voltages were corrected for the ohmic voltage drops within the cell, which was a negligible correction for charge rates of C/10 or lower. The capacity stored in the cell was plotted as a function of time on charge at a C/10 rate. Typical data are indicated in Figs. 2 and 3 for 0 deg C and 23 deg C operation of the laboratory cells. Using the measured voltages during recharge with the measured oxygen evolution current/voltage curves, the charge efficiency was calculated from Eq. (1) and the total stored capacity was compared to the data of Figs. 2 and 3. This procedure gave good agreement with the experimental results as long as the voltage rollover observed as the cell went into overcharge was not significant, such as at 0 deg C. Voltage rollover is defined in Fig. 1. The voltage rollover observed in both laboratory cells and sealed NiCd cells was taken into account by assuming that this effect was due to an offset in the overcharge voltage that occurred as the state of charge increased to where oxygen began to be given off. Such an offset could arise from changes in the nickel electrode as it goes into oxygen evolution, or from changes in the negative electrode potential resulting from the oxygen generation. When such a voltage offset correction was applied by subtracting the offset from the voltages measured prior to rollover, excellent agreement was obtained between the measured capacity and that calculated. (At rollover the offset was exponentially attenuated according to the width of the rollover peak). The calculated results are indicated in Figs. 2 and 3 for both capacity and charge efficiency as a function of charge time. Calculations were also done that optimized the agreement between the data and the calculated results

by adjusting the amplitude of the voltage offset. These calculations indicated that optimum agreement was obtained when the offset was the same as the amplitude of the voltage rollover.

The results of similar tests for a 6 Ah NiCd cell are indicated in Fig. 4 at 23 deg C. While the amplitude of the voltage rollover is greater in this cell than in the laboratory cells of Figs. 2 and 3, excellent agreement between the measured and the calculated capacity is obtained when the overcharge potentials are corrected for the amplitude of the voltage rollover. The data of Figures 1-4 indicate that while the voltage behavior during charge may be significantly affected by both temperature and prior cell history, the measured voltage behavior maintains a good correlation with the charge efficiency characteristics.

The capability to predict charge efficiencies from voltage for a single cycle is of some use, however of more practical use is the ability to determine charge efficiencies during continuous cycling, which is how battery cells are used in space applications. The most sensitive test of the charge efficiency calculation is to charge a cell to near full charge, then to cycle it a number of times at about 50% DOD using a charge return of 100.0%. Since no additional charge is being returned to compensate for overcharge (oxygen evolution), the cell should gradually decrease in state of charge. This test was done for both laboratory cells and a 6 Ah NiCd cell. After 12 cycles the cell was discharged to determine its state of charge. The voltage of the cell during the cycling was used to calculate the state of charge and charge efficiency continuously during the cycling, giving the results in Figs. 5 and 6 for the laboratory and 6 Ah cells respectively. The agreement between the measured capacity after the cycling and that calculated from the cell voltage alone is excellent. The current voltage relationship used to determine oxygen evolution as a function of voltage was determined both before and after the 12 cycles, and was found to only exhibit small changes with cycling. Such changes in oxygen evolution voltages are likely to occur quite slowly during long-term cycling, and may be easily considered in charge efficiency calculations by periodically measuring the overcharge voltage as a function of current.

Requirements for System Application

For the method evaluated here to be applied to determining charge efficiency and state of charge in a battery system, several requirements must be met. The first of these is that individual cell voltages be provided to a processing facility, whether on the ground or part of the power system. The system must also have the ability to periodically determine the overcharge voltage as a function of current. This can be done when the battery is at full charge during sunlit periods for geosynchronous applications. For low-earth orbit applications such measurements may be possible during trickle charge or by varying the VT level while the battery is fully charged. In systems where temperatures may vary significantly during recharge, methods to correct the magnitude of the voltage rollover as a function of temperature must be established. The evaluation of such methods in life tests can provide data to indicate how well they work over long term operation.

Conclusions

A method has been demonstrated to effectively allow the charge efficiency of

NiCd and NiH₂ cells to be monitored in real time, using only voltage measurements as inputs. With further evaluation such a method may provide a means to better manage charge control of batteries, particularly in systems where a high degree of autonomy or system intelligence is required.

Charge Voltages for Laboratory and 6 Ah NiCd Cells

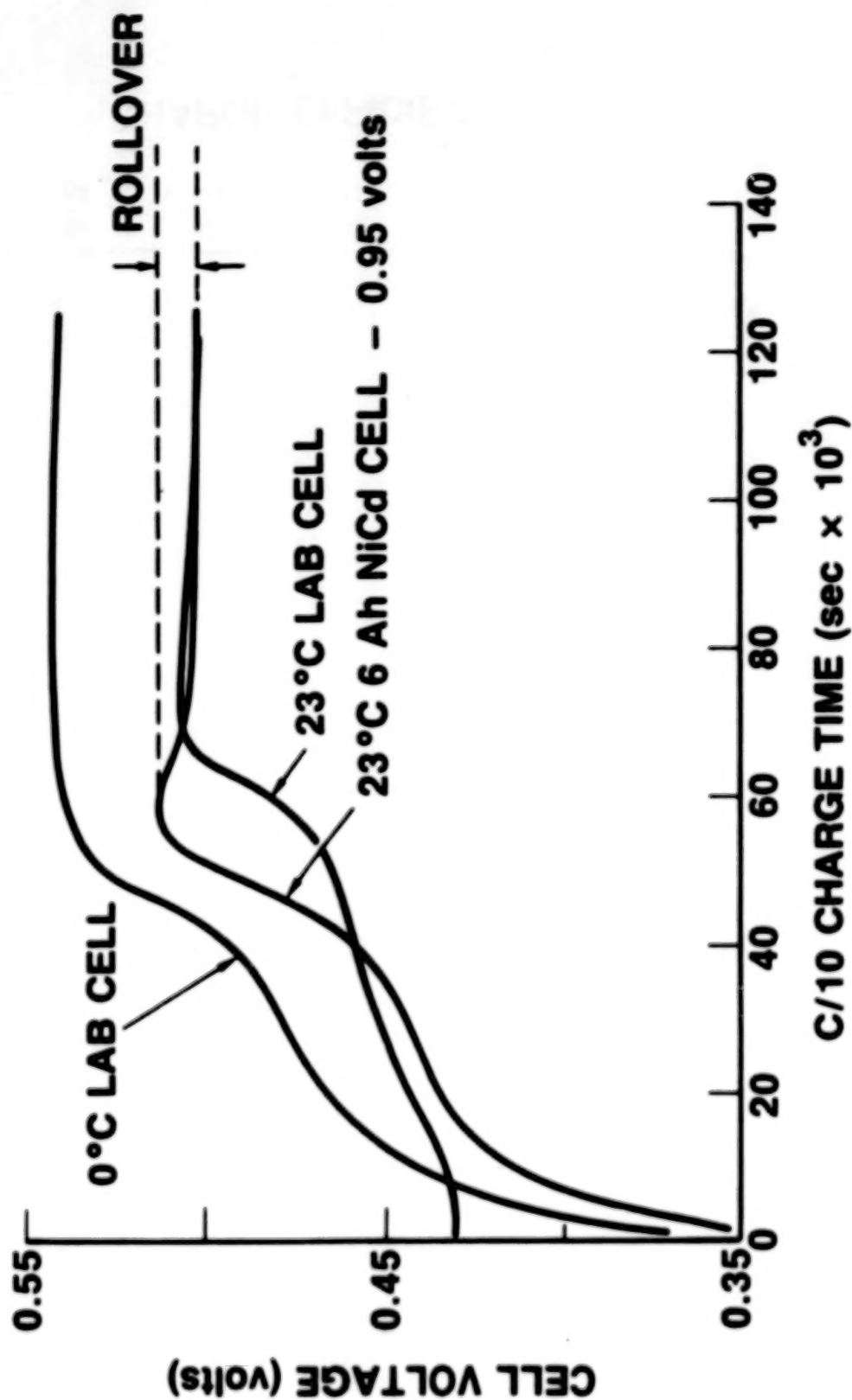


Figure 1.

Capacity and Charge Efficiency as a Function of Charge Time at C/10 (2mA/cm²) for Nickel Electrode

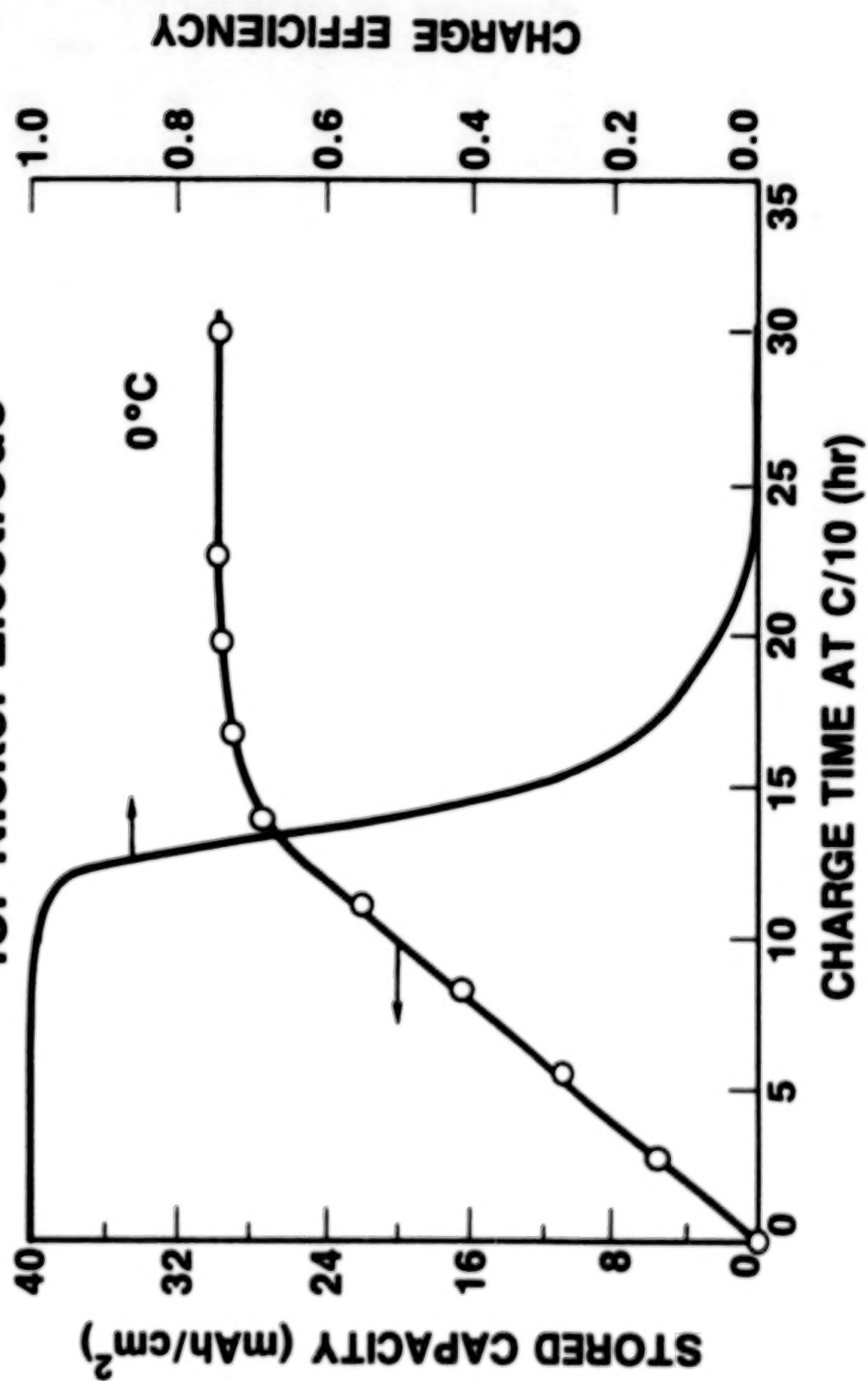


Figure 2.

Capacity and Charge Efficiency as a Function of Charge Time at C/10 (2mA/cm²) for Nickel Electrode

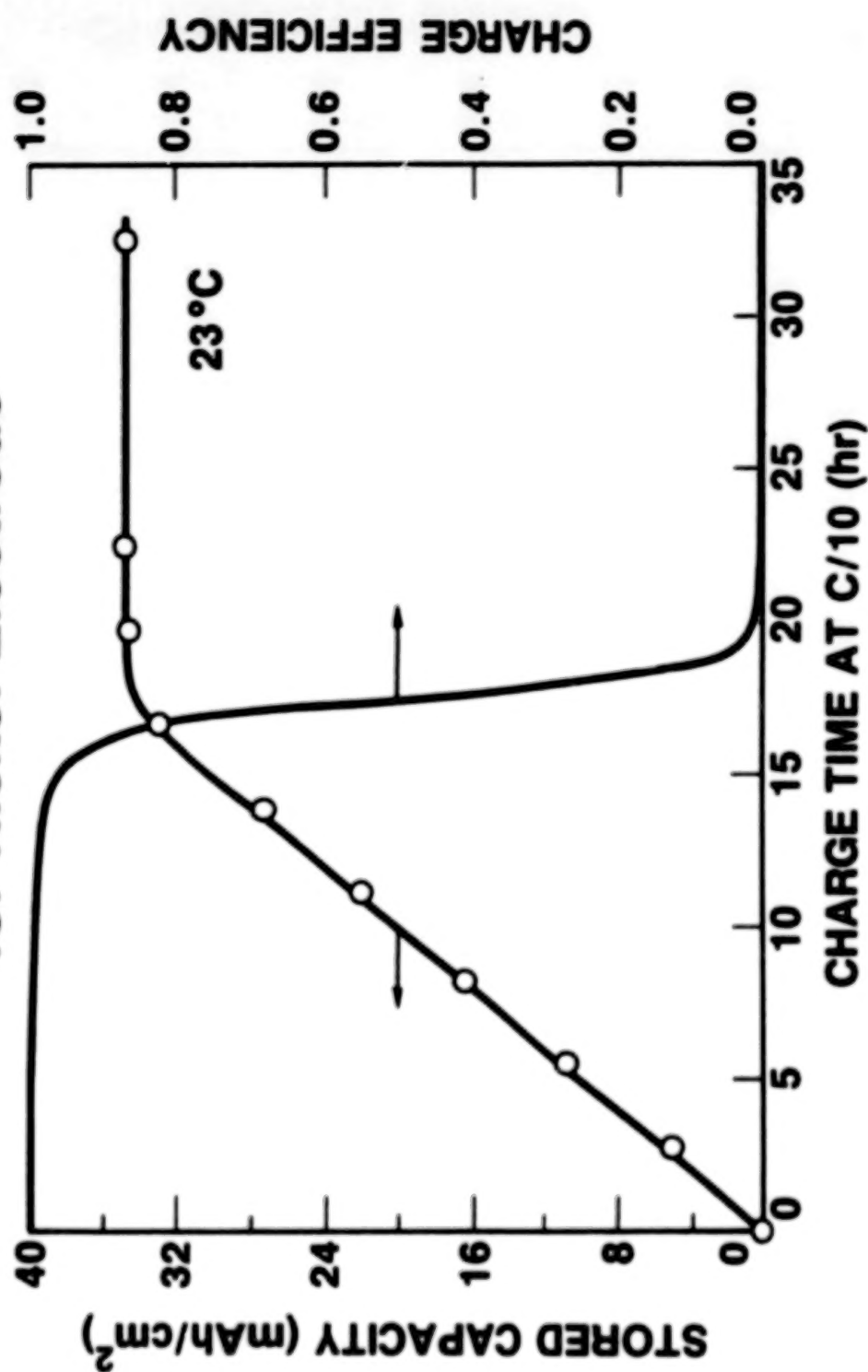


Figure 3.

Capacity and Charge Efficiency as a Function of Charge Time at 0.6A for a 6 Ah NiCd Cell

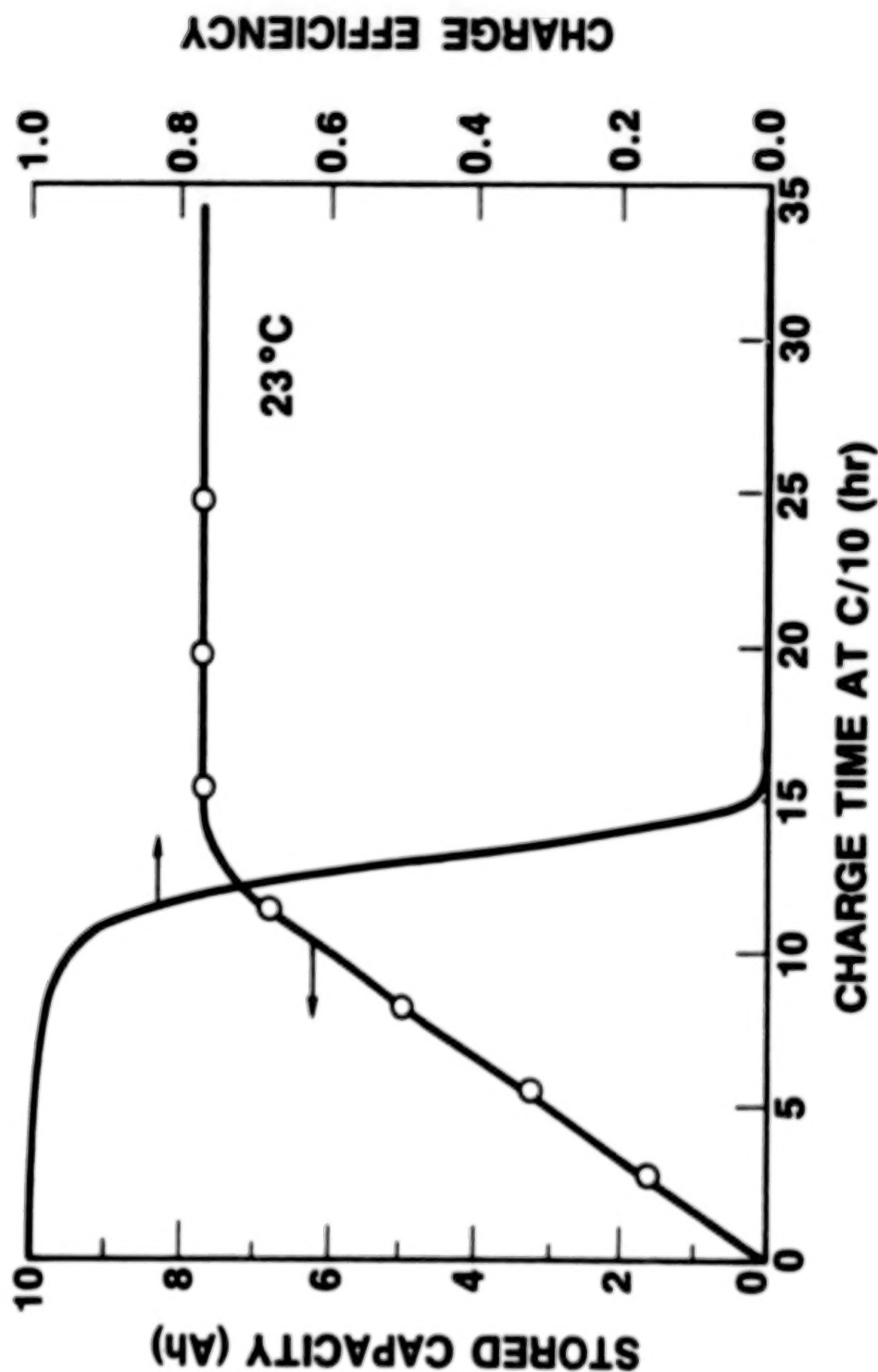


Figure 4.

Predicted Capacity and Charge Efficiency
12 CYCLES FOR NICKEL ELECTRODE AT 0°C CALCULATED
FROM VOLTAGE DATA

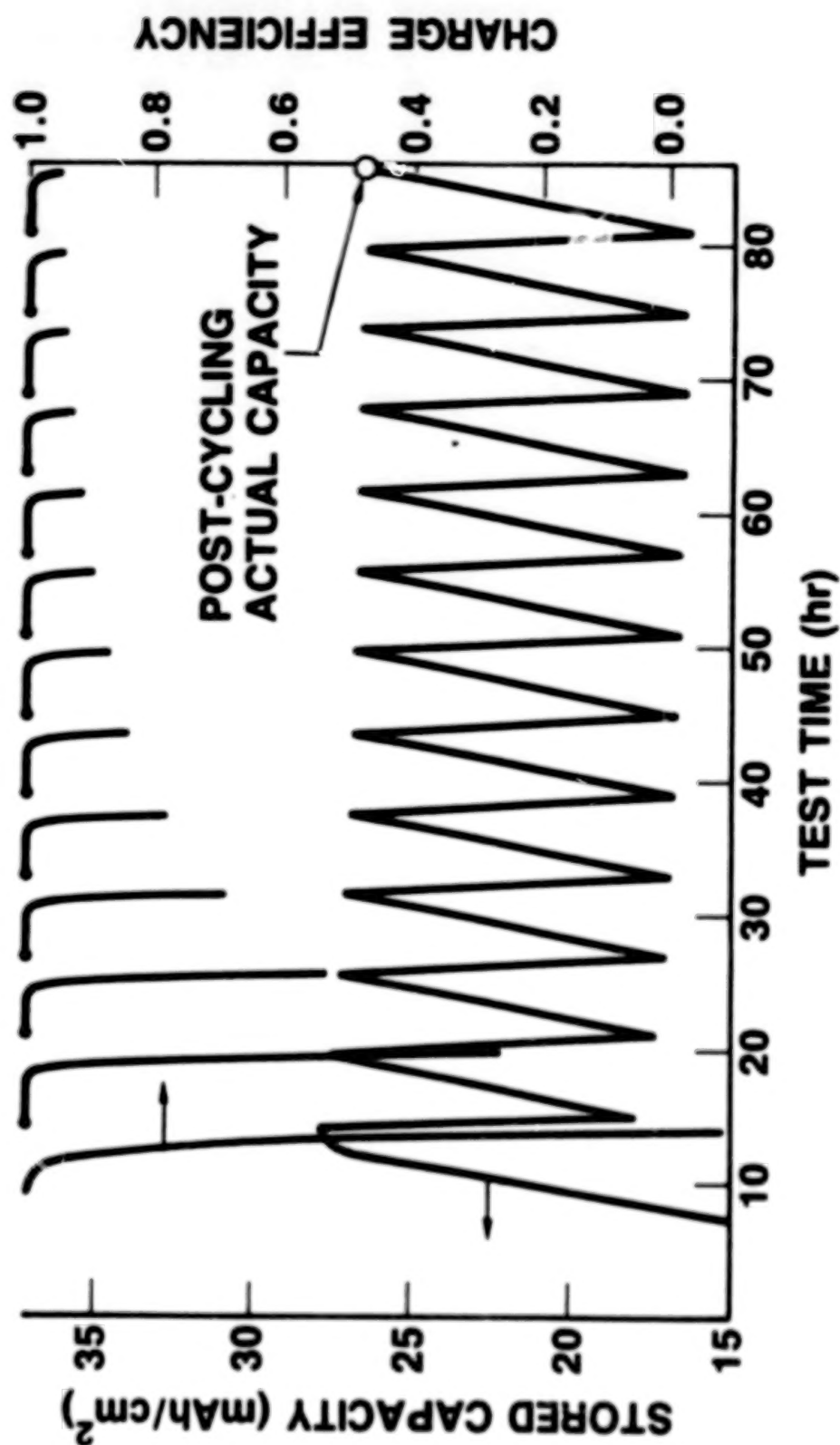


Figure 5.

Predicted Capacity and Charge Efficiency

12 CYCLES FOR 6 Ah NiCd CELL AT 23°C CALCULATED FROM VOLTAGE DATA

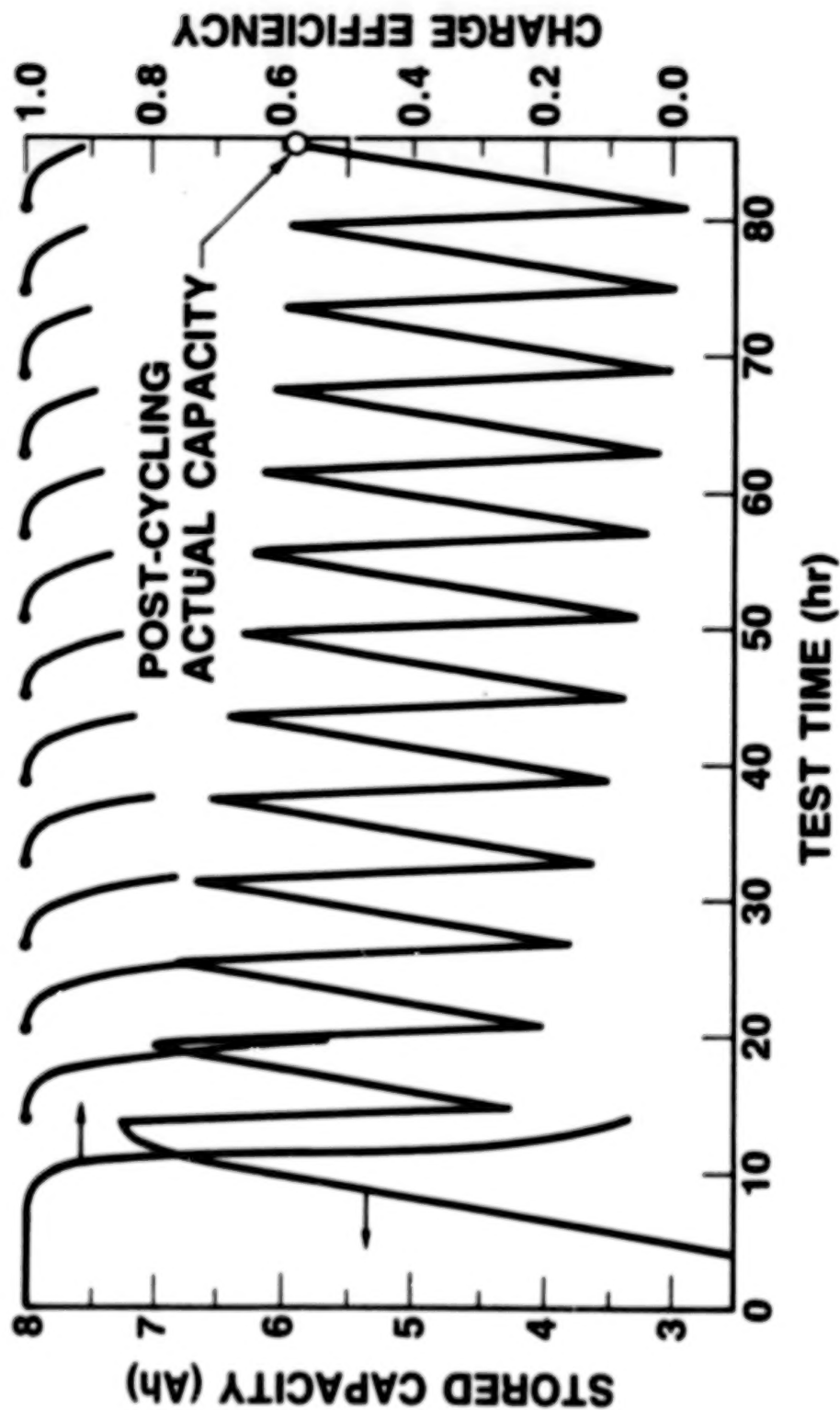


Figure 6.

Real Time Charge Efficiency Monitoring for Nickel Electrodes in NiCd and NiH₂ Cells

**A. H. ZIMMERMAN
THE AEROSPACE CORPORATION
EL SEGUNDO, CALIFORNIA**

**PRESENTED AT THE GODDARD SPACE FLIGHT CENTER
BATTERY WORKSHOP
18-19 NOVEMBER 1986, GREENBELT, MARYLAND**

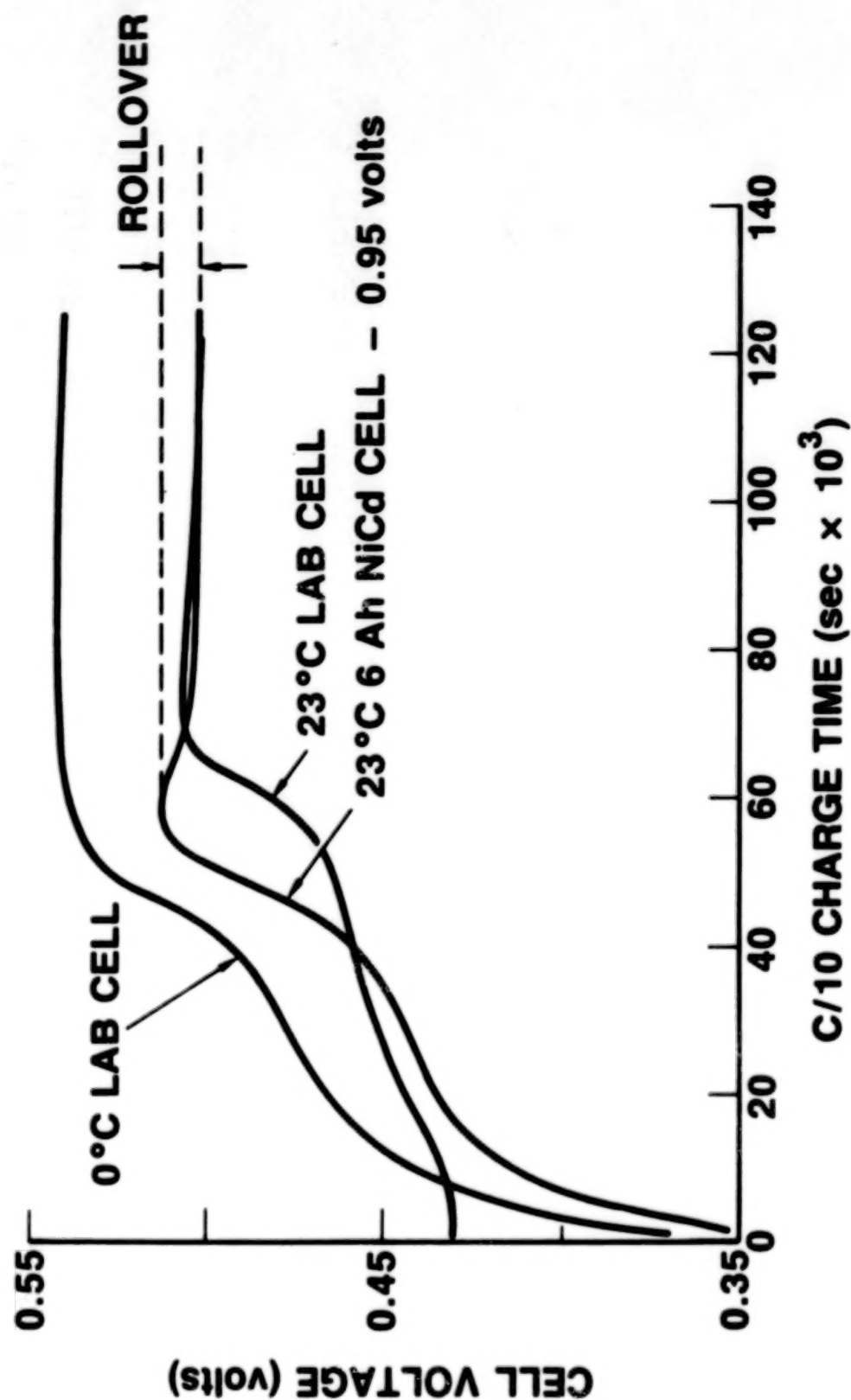
Objectives

- **DEVELOP METHOD FOR ACCURATELY DETERMINING
REAL-TIME CHARGE EFFICIENCY**
 - **NICKEL ELECTRODE LIMITED CELLS AT FULLY
CHARGED STATE**
- **DEMONSTRATE CAPABILITY TO FOLLOW STATE OF
CHARGE DURING CYCLING**
- **METHOD MUST BE EASILY AUTOMATED FOR AUTONOMOUS
OR INTELLIGENT POWER SYSTEMS**
 - **DEPENDS ON STANDARD MEASUREMENTS (voltage,
current, time) ONLY**

Approach

- CHARGE EFFICIENCY ASSUMED TO BE GOVERNED BY OXYGEN EVOLUTION RATE FROM NICKEL ELECTRODE
 - $\text{EFFICIENCY} = 1 - I_{\text{ox}}/I$
- OXYGEN EVOLUTION RATE CAN BE PREDICTED BASED ON NICKEL ELECTRODE VOLTAGE
 - $I_{\text{ox}} = I_0 e^{KV}$
- PRIMARY ASSUMPTIONS:
 - CONSTANTS INDEPENDENT OF STATE OF CHARGE
 - NEGATIVE ELECTRODE VOLTAGE NOT AFFECTED BY OXYGEN GENERATED AT POSITIVE

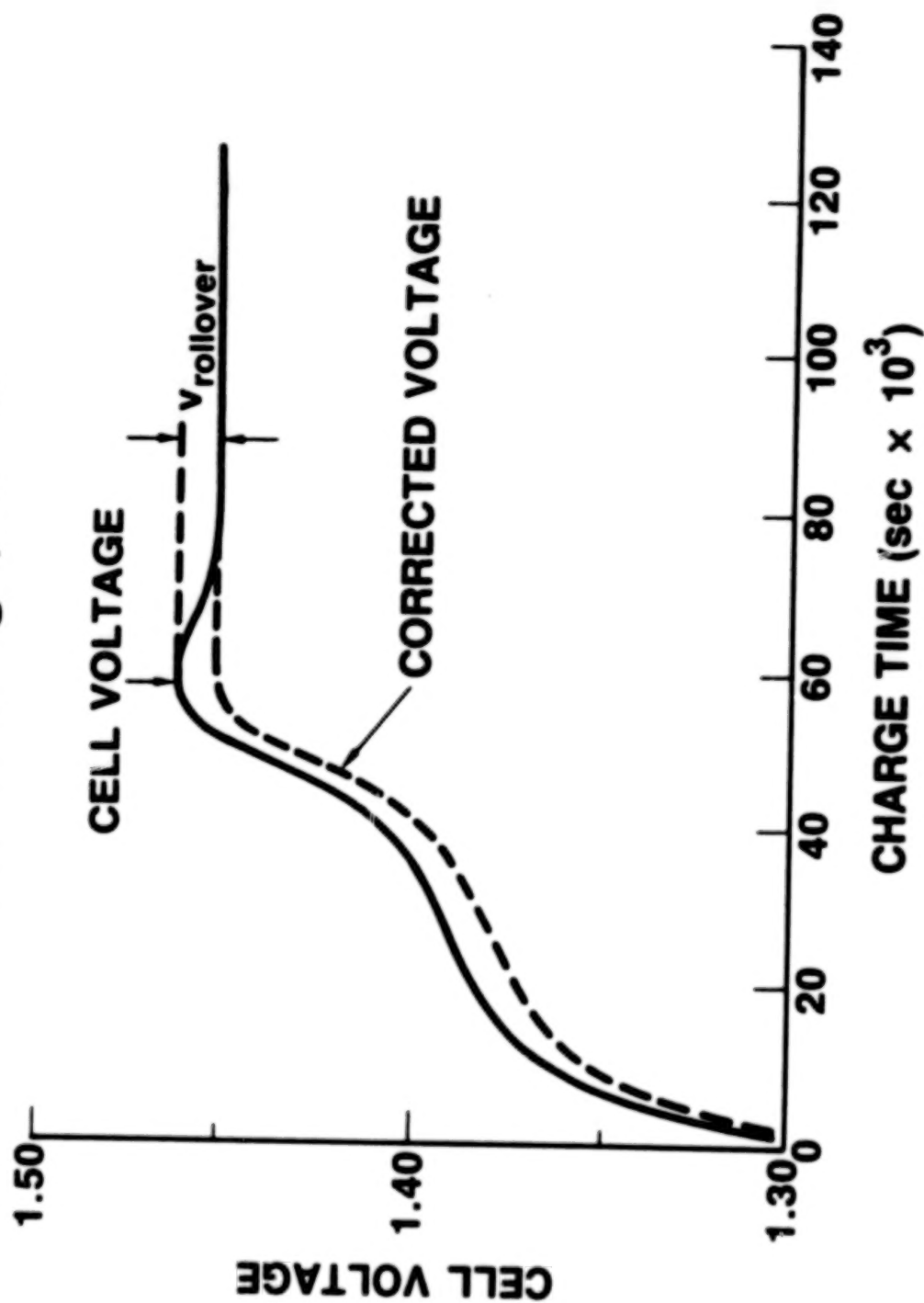
Charge Voltages for Laboratory and 6 Ah NiCd Cells



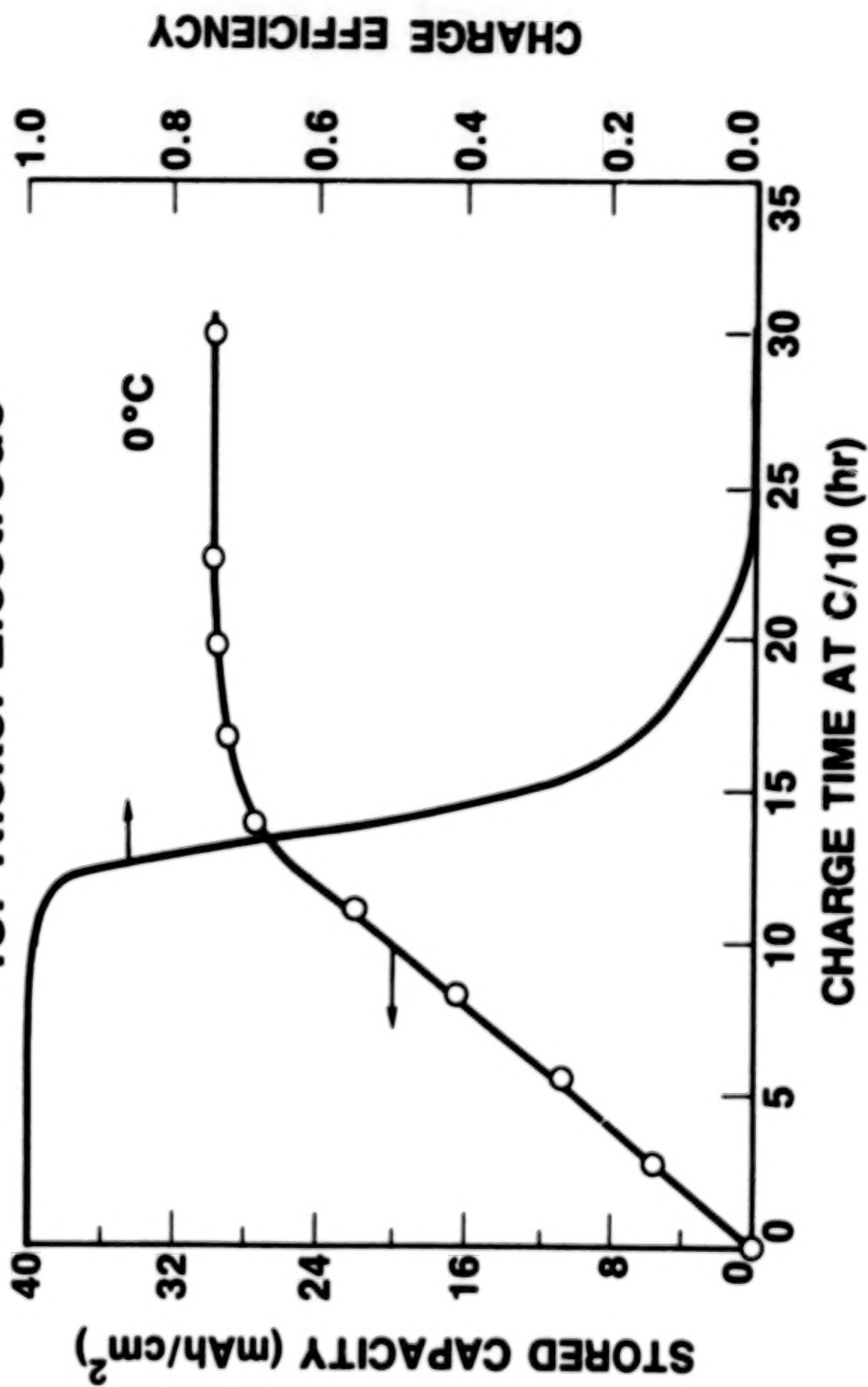
Modified Approach

- ASSUME THAT VOLTAGE ROLLOVER REPRESENTS A NEGATIVE OFFSET TO OXYGEN EVOLUTION VOLTAGE
- CORRECT MEASURED VOLTAGE FOR THIS OFFSET,
 $V' = V - V_{\text{rollover}}$
 - CORRECTION IS NOW A FUNCTION OF STATE OF CHARGE, TEMPERATURE, AND CURRENT

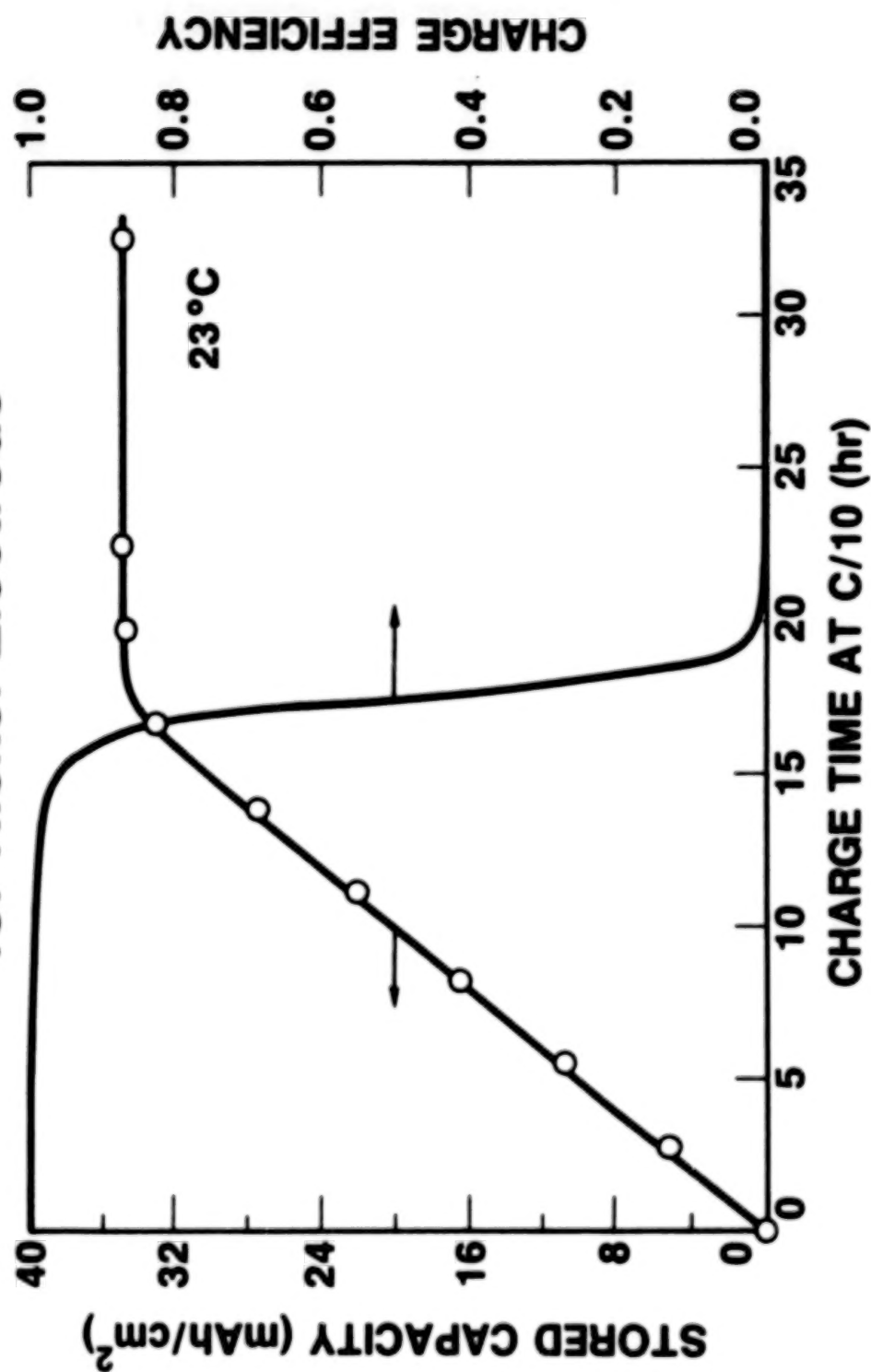
Correction to NiCd Cell Voltage for Rollover, C/10 Charge, 23°C



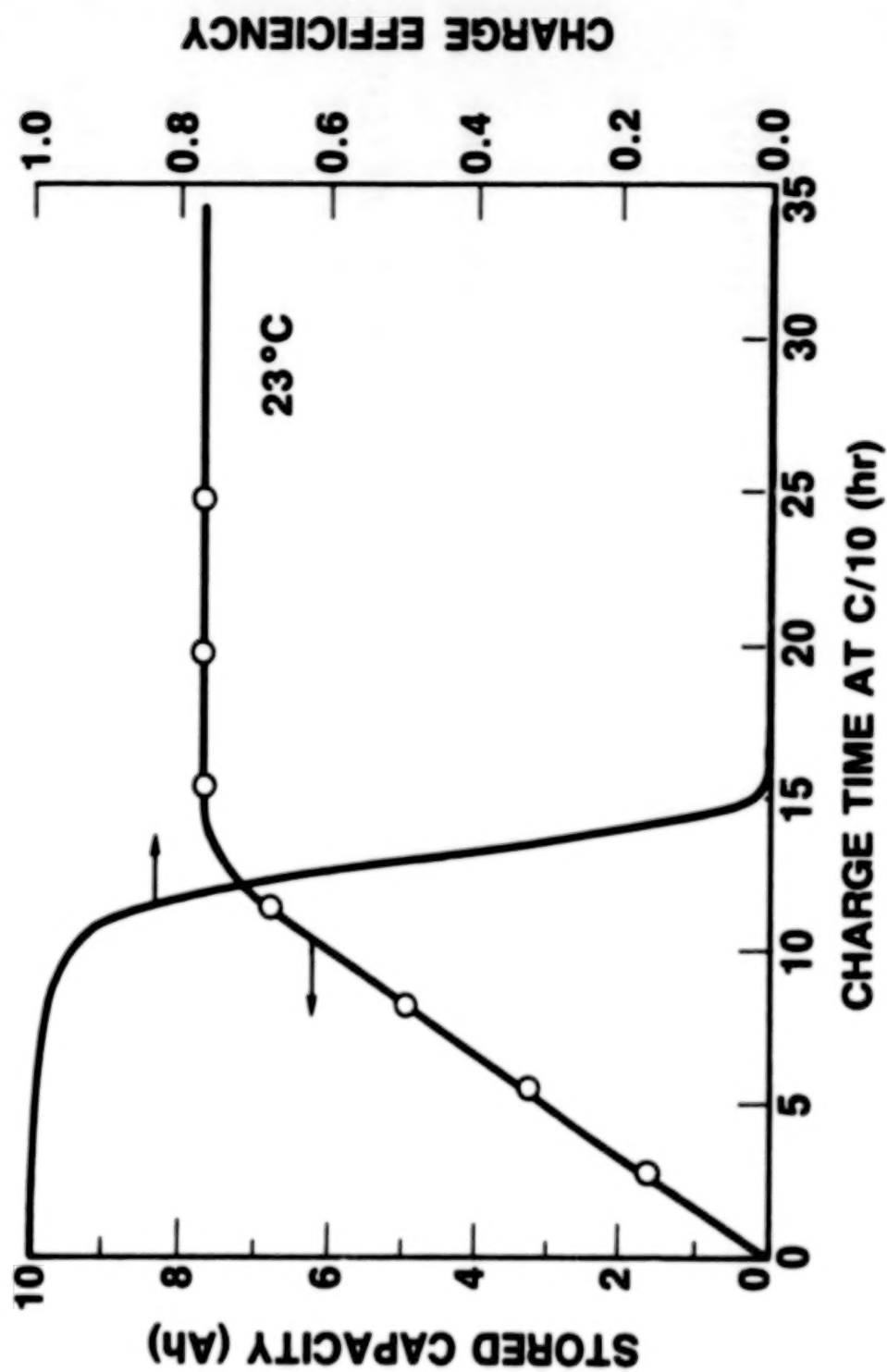
Capacity and Charge Efficiency as a Function of Charge Time at C/10 (2mA/cm²) for Nickel Electrode



Capacity and Charge Time as a Function of Charge Time at C/10 (2mA/cm²) for Nickel Electrode



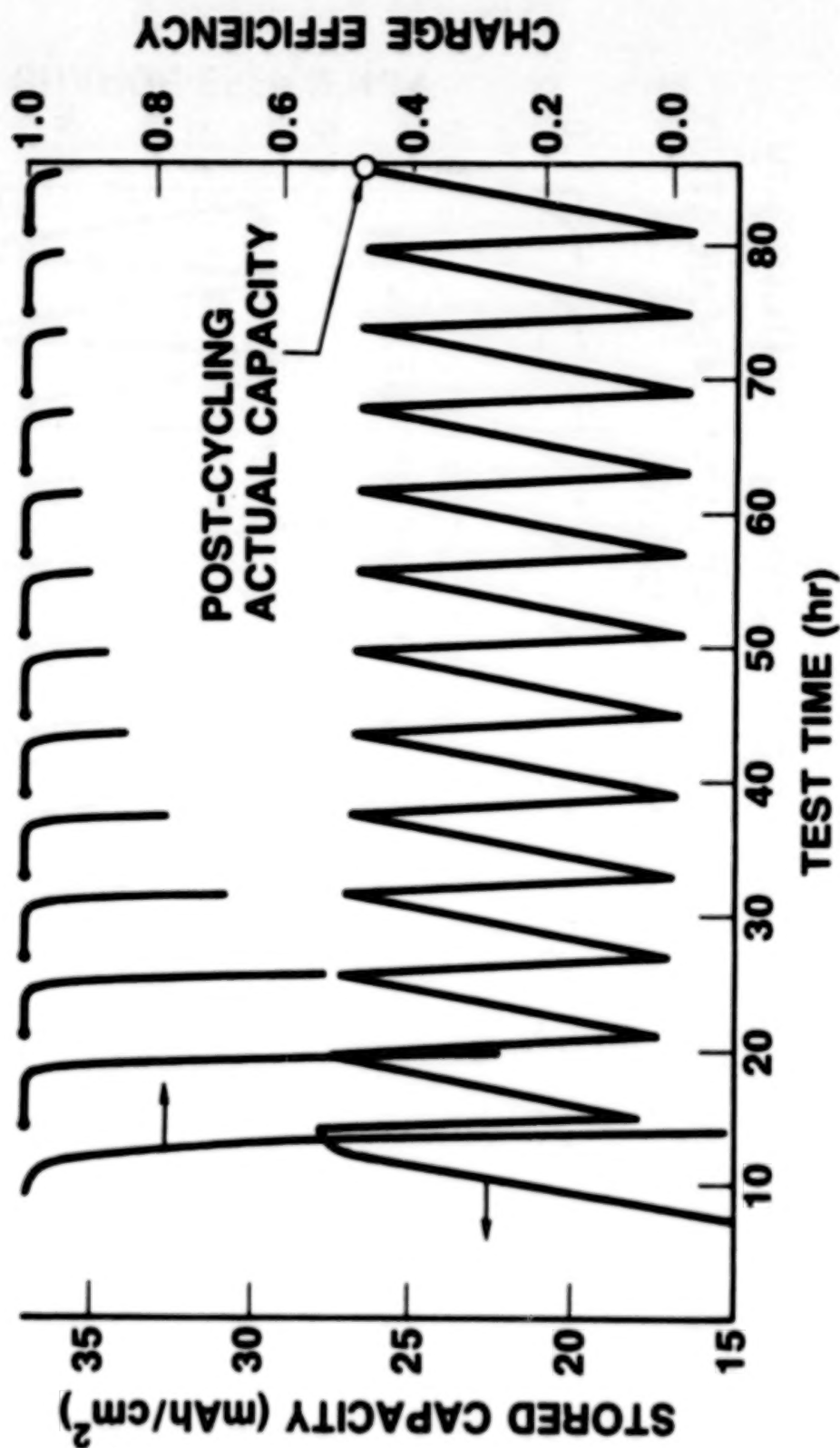
Capacity and Charge Efficiency as a Function of Charge Time at 0.6A for a 6 Ah NiCd Cell



Procedure for Monitoring Charge Efficiency During Cycling Operation

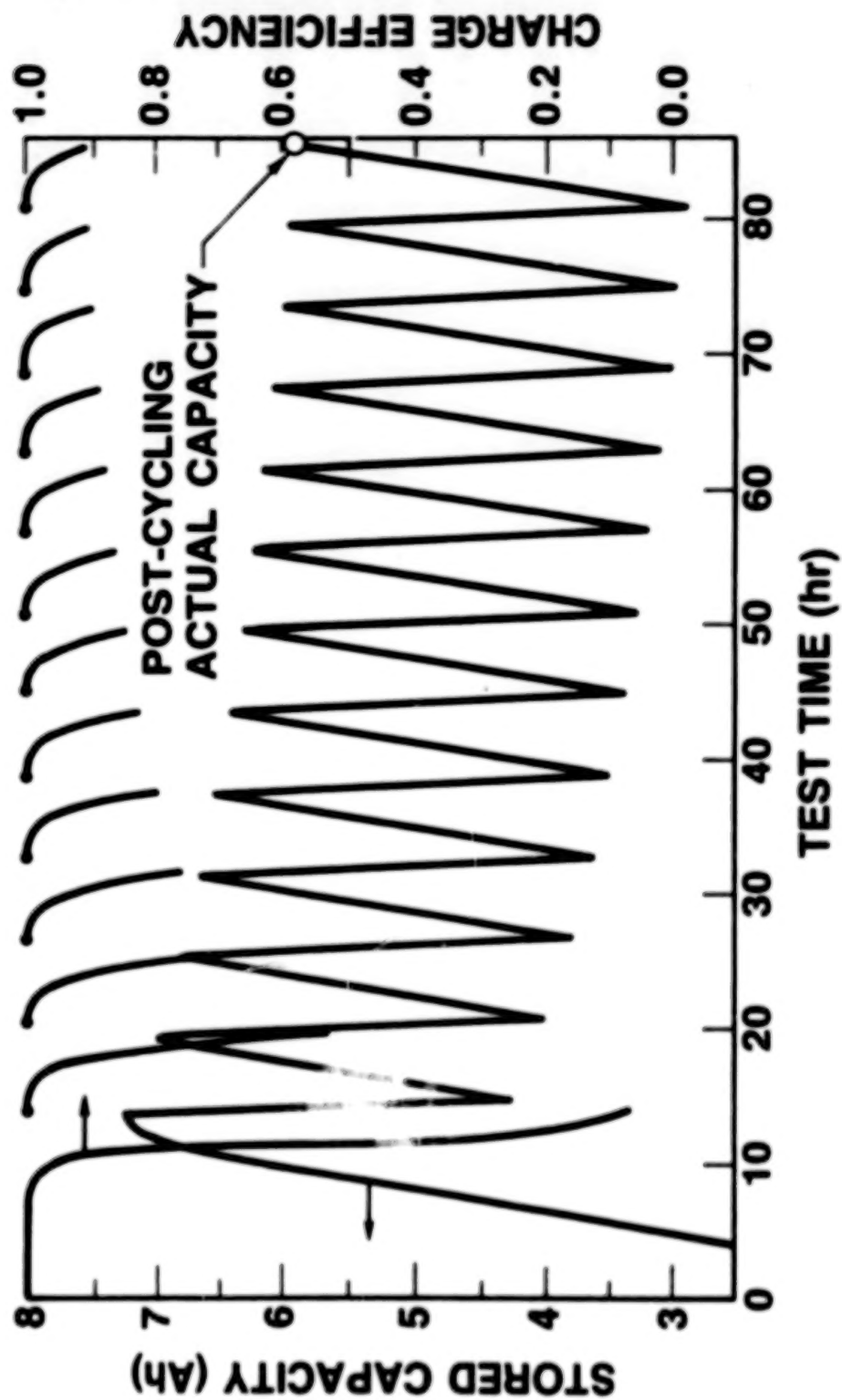
- **CHARGE FULLY AT C/10**
 - DETERMINE ROLLOVER CORRECTION AS FUNCTION OF STATE OF CHARGE
 - DETERMINE OXYGEN EVOLUTION CONSTANTS AFTER FULL CHARGE IS REACHED FROM OVERCHARGE VOLTAGE AT C/10, C/20, C/50, C/100
- **CYCLE 12 TIMES**
 - DISCHARGE 50% OF RATED CAPACITY AT C/2
 - RECHARGE 100% OF CAPACITY DISCHARGED, USING C/10 CHARGE
- **MEASURE STORED CAPACITY AFTER 12 CYCLES**

Predicted Capacity and Charge Efficiency **12 CYCLES FOR NICKEL ELECTRODE AT 0°C CALCULATED** **FROM VOLTAGE DATA**



Predicted Capacity and Charge Efficiency

12 CYCLES FOR 6 Ah NiCd CELL AT 23°C CALCULATED FROM VOLTAGE DATA



Conclusions

- CHARGE EFFICIENCY CAN BE ACCURATELY MONITORED USING NiCd OR NiH₂ CELL VOLTAGES
(Applicable to NiH₂ as well as NiCd)
- METHOD OUTLINED HERE IS SELF-CORRECTING:
 - OXYGEN EVOLUTION POTENTIALS MAY BE PERIODICALLY CHECKED
 - ACCURACY OF METHOD IMPROVES AS CELL STATE OF CHARGE DECREASES
- METHOD SHOULD BE SUITABLE FOR AUTONOMOUS DETECTION OF ANOMALOUS CONDITIONS DURING OPERATION (short circuits, recharge problems, etc.)

N888

11039

UNCLA

STATISTICALLY DETERMINED NICKEL CADMIUM
PERFORMANCE RELATIONSHIPS

Sidney Gross
Boeing Aerospace Company
Seattle, Washington 98124

A considerable amount of data are customarily taken on aerospace nickel cadmium cells to control manufacture, to verify that the cells will be acceptable, and to select well-matched cells for assembly into batteries. These data provide an opportunity for statistical analysis on data distribution and the interrelationships between parameters. This information can be helpful in understanding behavior, for use in quality control, and in identifying possible problems with individual cells or with lots of cells, and even for manufacturing process control (Figure 1). This is also a logical approach for analysis of a common data pool for Ni/Cd cells. Since the data required for analysis is already available during manufacture, there is little additional cost involved for data acquisition. In fact, computerized data handling will save money in data processing. Furthermore, data analysis should be able to help screen out unnecessary tests, for additional cost saving.

A statistical analysis was performed on sealed nickel cadmium cell manufacturing data and cell matching data. The cells subjected to the analysis were 30 AH sealed Ni/Cd cells, made by General Electric Co. A total of 213 data parameters was investigated, including such information as plate thickness, amount of electrolyte added, weight of active material, positive and negative capacity, and charge-discharge behavior (Figure 2). Statistical parameters determined include the maximum and minimum values, arithmetic mean, variance, standard deviation, skewness, kurtosis, and data histograms (Figures 3 and 4). Figure 5 shows a typical data histogram with very little skewness or kurtosis, whereas, Figure 6 shows another which is skewed and has a high kurtosis. Statistical analyses were made to determine possible correlations between test events; for example, if there is any connection between end of charge voltage and pressure, or between electrolyte amount and capacity.

The data show many departures from normal distribution. Some departures are inherent in the physical behavior of cells, and others are due to manufacturing bias. For example, in one lot of cells, the data fall in two distinct groups, which were identified as caused by manufacturing variations from batch processing. Skewing of pressure data sometimes occurred very strongly and appeared to be related to removal and rework of the high pressure cells.

Statistical relationships between data obtained during one test event and another were also obtained. The analysis used was the rank-difference method for coefficient of correlation, producing coefficients that can range from -1.0 to +1.0 for perfect positive correlation and perfect negative correlation, respectively. Completely random results would yield a correlation of 0. For example, the relationship between cell pressures for 30 AH cells at two unrelated test conditions was evaluated 20 hours into the charge at 3.0 amperes and 75°F versus 72 hours into the charge at 1.5 amperes and 32°F. Correlation coefficients for five lots averaged 0.62, showing that there is a definite relationship (Figure 7). Pressure at 72 hours of charge also correlates with pressure after two hours of discharge. Pressure does not correlate very well with voltage, however, and its correlation with pressure at the end of charge on the last cycle is good for only one of the four lots.

Sometimes two parameters would show a strong positive correlation for some lots but not for others. This behavior appeared to be the result of important differences between lots. In analyses of five lots, this was found to be the case for correlations of pressure vs. voltage (ranging 0.097 to 0.47), early life pressure vs. pressure after cycling (ranging -0.187 to 0.604), end of charge voltage vs. KOH volume (ranging 0.026 to 0.987), open circuit voltage 24 hours after removing shorting wires vs. 1.0 hours afterwards (ranging 0.306 to 0.972, Figure 8), and also vs. open circuit voltage 24 hours after 15 A/1 minute charge following 16 hours shorting (-0.054 to 0.998, Figure 8).

Occasionally, there are interesting surprises, though upon reflection these are understandable. For example, thickness of the cells, measured at the center, correlates very well with the final cell weight (Figure 9), and also correlates well with the open circuit voltage 24 hours after a 15 A/1.0 min charge following 16 hours shorting. Data are not available to determine whether these correlations would hold also for other lots.

The end of charge voltage after 31 cycles is found to correlate well with that same voltage at the first cycle (Figure 10). It also correlates well with capacity. For only one of the four lots did KOH final volume and end of charge voltage appear to be related.

Capacity to 1.0 V and capacity to 1.15 V were found to be closely related, though with some departure for one of the lots. Interestingly enough, capacity to 1.0 V on one test did not correlate, for three of the four lots, with capacity to 1.0 V for another test (Figure 11). The test conditions for test 7 were C/20 charge for 72 hours at 0°C, and discharge at C/2 at 0°C.

Product consistency from one lot to another is an important attribute for aerospace applications. It is clear from these examples that there are some significant differences between these lots. Statistical analyses are seen to be an excellent way to spot those differences. Also, it is now proven beyond doubt that battery testing is one of the leading causes of statistics.

ACKNOWLEDGEMENT

This paper is based upon work performed under JPL Contract 953984, W.O. 342-19. The support and suggestions by Sam Bogner are gratefully acknowledged.

TECHNOLOGY

- o Investigate interrelationships between parameters
- o Help understand behavior

MANUFACTURING PROCESSING CONTROL

- o Identify long-term changes in processes
- o Identify batch-to-batch differences
- o Common data pool for Ni/Cd cells

QUALITY CONTROL

- o Identify problems with individual cells
- o Identify problems with cell lots
- o Help select matched cells for batteries

COST

- o Data are already available
- o Computerized data-handling will save money
- o Analysis can help screen out unnecessary tests

Figure 1. Advantages of Statistical Data Analysis.

- o 30 AH sealed NiCd cells
- o Used manufacturing data and cell matching data
- o 213 data parameters were investigated; e.g.,
 - o Plate thickness
 - o Amount of electrolyte
 - o Weight of active material
 - o Positive and negative capacity
 - o Charge-discharge behavior
 - o Many others
- o Multiple manufacturing lots

Figure 2. Basis for Analysis.

- o Maximum and minimum values
- o Arithmetic mean
- o Variance
- o Standard deviation
- o Skewness
- o Kurtosis
- o Data histograms
- o Correlations between test events

Figure 3. Statistical Analysis.

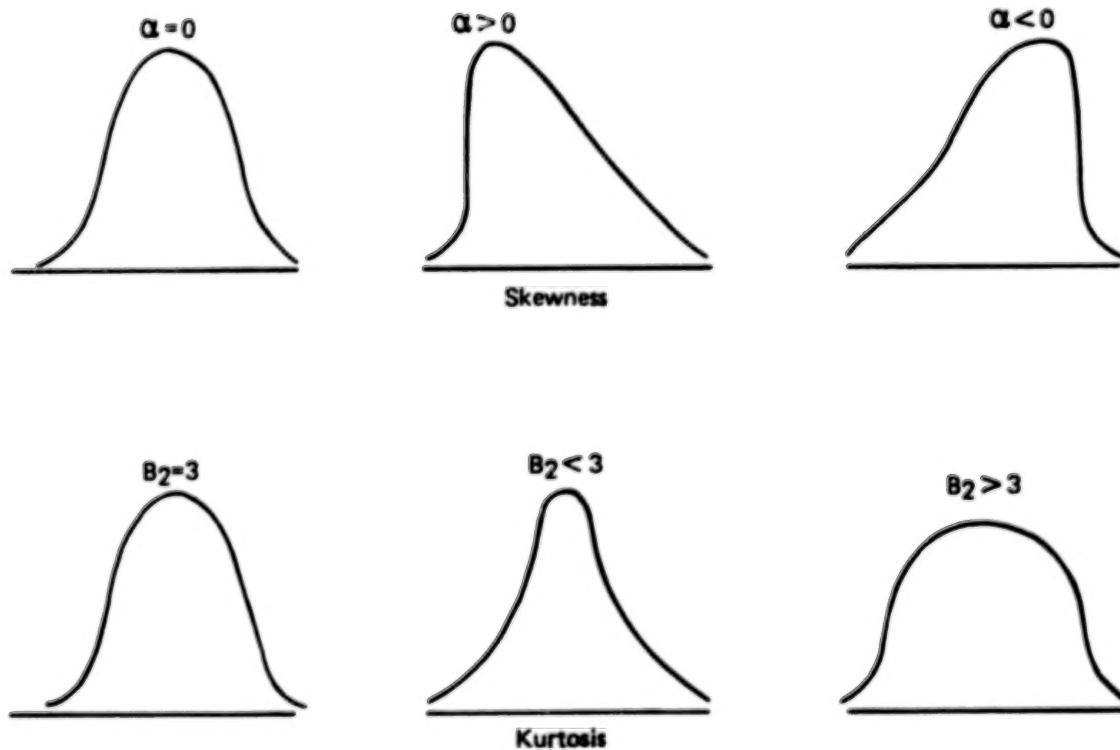


Figure 4. Statistical Terms.

HISTOGRAM FOR TAP DATA

MIN	MAX	TESTA	LOT#	VARIABLE	D.S.7A	AMIV
35.20	35.43	90	1			
35.43	35.66	27	94			
35.66	35.89	50	40	95		
35.89	36.12	37	57	61	62	65
36.12	36.35	1	2	3	5	10
36.35	36.58	7	8	14	34	45
36.58	36.81	4	11	13	14	15
36.81	37.04	18	19	54	55	74
37.04	37.27	17				
37.27	37.50	6	30	40		

MINIMUM VALUE= 35.200
 STANDARD DEVIATION= .417
 SKEWNESS= -.338
 KURTOSIS= 3.205
 MEAN= 36.462
 -2 ST. DEV. = 35.627
 -1 ST. DEV. = 36.044
 +1 ST. DEV. = 36.879
 +2 ST. DEV. = 37.296

Figure 5. Capacity to 1.0 Volt.

Pressure at 72 hours of charge versus:

	<u>Correlation Coefficient</u>			
	Lot 5	Lot 6	Lot 7	Lot 8
Voltage at 72 hours	0.097	0.390	0.264	0.255
Pressure at 20 hours	0.663	0.589	0.447	0.792
Pressure at 120 minutes of discharge	0.492	0.582	0.916	0.799
Pressure at end of charge, last cycle	0.484	0.343	0.604	-0.222

Figure 7. Pressure Effects.

Open circuit voltage 24 hours after removing shorting wires versus:

	<u>Correlation Coefficient</u>			
	Lot 5	Lot 6	Lot 7	Lot 8
OCV 1.0 hour after removing wires	0.306	0.319	0.942	0.972
OCV 24 hours after 15A/1.0 min charge following 16 hr shorting	-0.054	0.637	0.003	0.998

Figure 8. Open Circuit Voltage Effects.

Cell center thickness versus:

	<u>Correlation Coefficient</u>
	Lot 8
OCV 24 hrs after 15A/1.0 min charge following 16 hr shorting	0.996
Final cell weight	0.997

Figure 9. Cell Thickness Effects.

End of charge voltage at cycle 31 versus

	Correlation Coefficient			
	Lot 5	Lot 6	Lot 7	Lot 8
EOCV at cycle 1	1.000	1.000	1.000	0.999
Capacity to 1.0V	0.999	1.000	0.871	0.990
KOH final volume	0.131	-0.061	0.186	0.976

Figure 10. End of Charge Voltage Effects.

Capacity to 1.0V (C/10 chg 14 hr, C/2
disch, 75°F) versus:

	Correlation Coefficient			
	Lot 5	Lot 6	Lot 7	Lot 8
Capacity to 1.15V, same test (B)	0.996	0.999	0.912	0.560
Capacity to 1.0V, test 7	0.191	-0.116	0.187	0.811
End of charge voltage, cycle 31	0.999	1.000	0.871	0.980

Figure 11. Capacity Effects.

TEST SUMMARY FOR ADVANCED H₂ CYCLE NI-CD CELL

Lee Miller

Eagle-Picher Industries, Inc.

ABSTRACT

To improve operational tolerances and mass, the H₂ gas recombination design provisions of the Ni-H₂ system have been incorporated into the sealed Ni-Cd system. Produced is a cell design capable of operating on the "H₂ cycle" versus the normal "O₂ cycle". Three (3) test cells have now completed approximately 4,300 LEO (90 minute) cycles at 20% DOD. Performance remains stable although one (1) cell exhibited a temporary pressure anomaly.

INTRODUCTION

This paper is intended as a test summary update on a small group of cells which evolved from development efforts previously reported in the NASA/GSFC Battery Workshop.⁽¹⁾

Three (3) 50 AH rated, space type, Ni-Cd battery cells were equipped with standard, Ni-H₂ type, catalytic gas electrodes as shown in Exhibit No. 1. These cells incorporated no discharged negative electrode capacity or "overcharge protection". H₂ gas evolution at the negative electrode during charge is expected and intended in this design.

By connecting (electrically) the cell case directly to the cell positive terminal, the evolved H₂ gas would be expected to be recombined rapidly by the reactions summarized in Exhibit No. 2.

DESIGN ADVANTAGES

If the concept proves successful, it is believed the design will offer the advantages listed in Exhibit No. 3. These advantages should allow the production of a sealed Ni-Cd cell design which can tolerate higher charge rates over a wider temperature range while offering a longer cycle life at a higher DOD.

In addition, a lower mass or improved specific energy should be achieved by elimination of the present weight associated with the negative electrode discharged or overcharge protection capacity increment. This improvement relative to a current "O₂ cycle" cell design is summarized in Exhibit No. 4.

TEST SUMMARY

The three (3) 50 AH rated cells were equipped with pressure gages and mounted in a thermal control system. Shorting straps were connected from the positive terminal of each cell to its case. The charge/discharge cycle was controlled automatically to a fixed time at a constant current. A limited test budget necessitated manual data acquisition which imposed the need for some data extrapolation to the actual end point.

Test parameters and major events are summarized in Exhibit No. 5. In general, stable performance continues to be maintained.

The capacity measurements were performed via reconditioning cycles from a fully charged state.

Because of pressure recovery, no examination of the one (1) anomalous cell has been performed yet to determine the cause of its performance diversion. It is suspected in these "first build" test cells a high resistance may have temporarily developed in the catalytic electrode-to-positive electrode circuit.

Test data was only summarized to approximately cycle number 3,360 because a large group of cells from another program were introduced into the thermal control system. A higher test temperature required by the large group of cells precludes a direct comparison with the earlier cycle data.

CONCLUSION

Testing is continuing on a small group of "H₂ cycle", sealed Ni-Cd cell designs with successful results. To date, 4,300 LEO cycles have been achieved at a 20% DOD.

The goal is to demonstrate concept feasibility leading to the production of an advanced sealed, Ni-Cd cell design offering improved operational tolerance and lower mass.

REFERENCES

(1) Miller, L. (Eagle-Picher Industries): "An Advanced Ni-Cd Battery Cell Design". Proc. 1985 Goddard Space Flight Center Battery Workshop, NASA Conference Publication 2434, GSFC Greenbelt, Maryland, November 19-21, 1985.

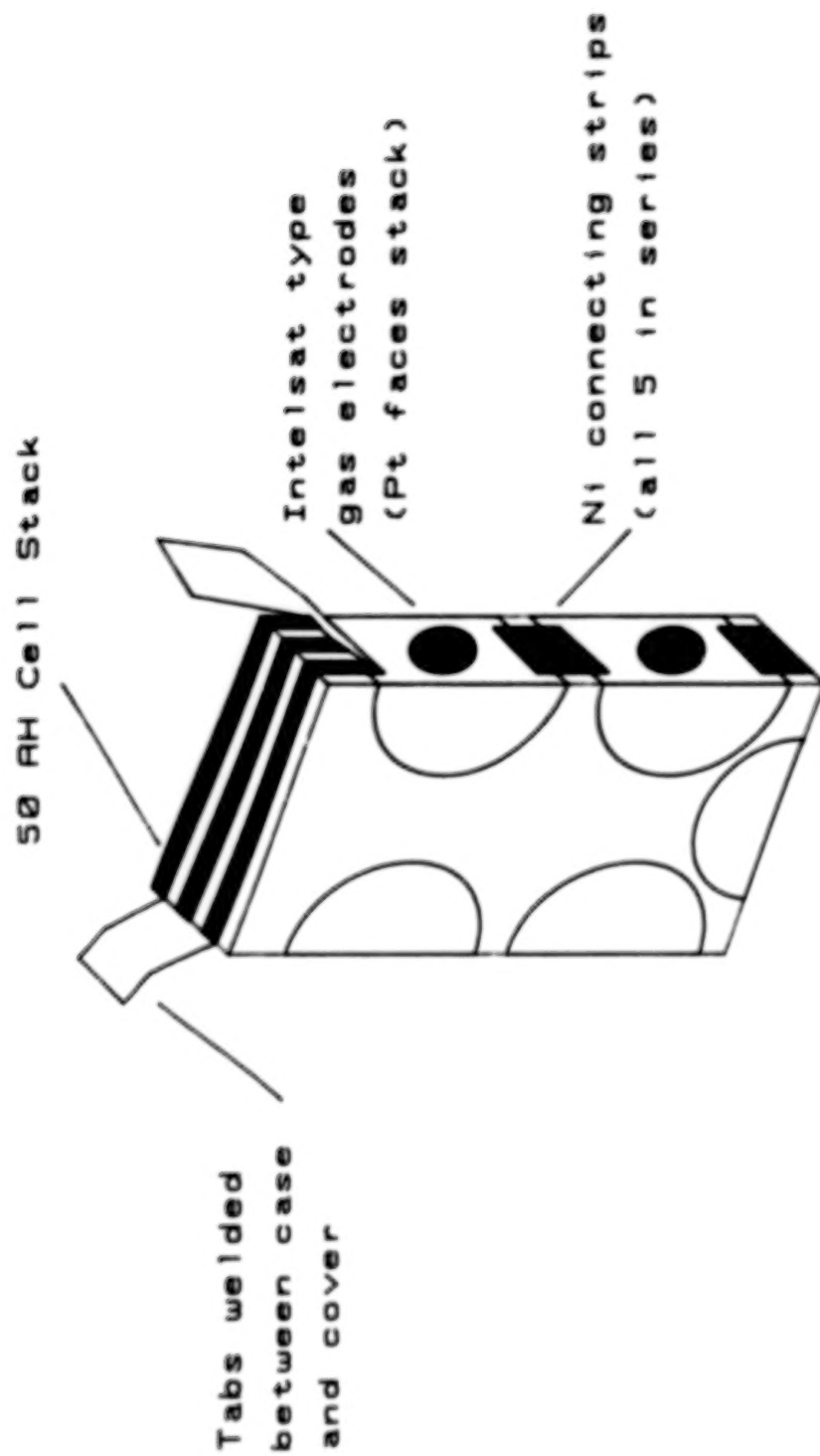
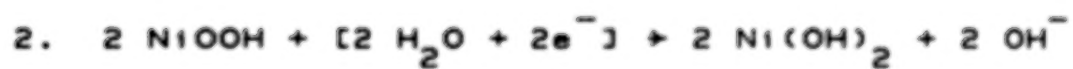


Figure 1. Ni-Cd Test Cell Assembly Sketch.



COMBINED REACTION

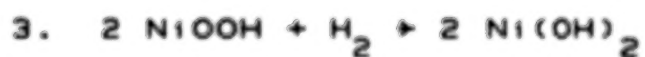


Figure 2. Sealed Nickel-Cadmium Gas Electrode Reaction.

1. INCREASED OPERATIONAL TOLERANCE.
2. ACCOMMODATE INORGANIC SEPARATOR CANDIDATES.
3. FUNCTION WITH INCREASED ELECTROLYTE QUANTITIES.
4. LOWER OPERATING PRESSURES.
5. HIGHER SPECIFIC ENERGIES.

Figure 3. H_2 Cycle Ni-Cd Cell Design Advantages.

	<u>O₂ CYCLE</u>	<u>H₂ CYCLE</u>
POSITIVE GROUP	456 GMS	456 GMS
NEGATIVE GROUP	633	508*
ELECTROLYTE	223	223
SEPARATOR	18	18
CELL COVER	25	25
CELL CAN	<u>98</u>	<u>98</u>
TOTAL	1,453 GMS	1,328 GMS
SPECIFIC ENERGY	45.4 WHR/KG	49.7 WHR/KG

* ASSUMPTIONS:

1. NEGATIVE/POSITIVE RATIO = 1.8:1.0
2. REMOVED DISCHARGED NEGATIVE CAPACITY (OVERCHARGE PROTECTION) = 125 GRAMS (70% OF EXCESS CAPACITY)

Figure 4. Light-Weight 50 AH Ni-Cd Cell Design.

CHARGE: 60 MINUTES/10.0 AMPS

DISCHARGE: 36 MINUTES/16.0 AMPS

RETURN: 1.04 FACTOR

TEMPERATURE: 10⁰C

CYCLES TO DATE: 4,300

DOD: APPROXIMATELY 20%

MAJOR EVENTS:

I. INITIAL PERFORMANCE - (APPROX. CYCLE 30)

END-OF-CHARGE \bar{X} = 1.68 VOLTS

END-OF-DISCHARGE \bar{X} = 1.24 VOLTS

END-OF-CHARGE
PRESSURE \bar{X} = -20 IN. OF HG

II. CAPACITY MEASUREMENT - (APPROX. CYCLE 500)

MEASURED CAPACITY \bar{X} = 59.0 AH

III. CAPACITY MEASUREMENT - (APPROX. CYCLE 1,500)

MEASURED CAPACITY \bar{X} = 58.0 AH

Figure 5. Life Test Summary.

IV. TEST ANOMALY - (APPROX. CYCLE 2,800)

ONE (1) CELL PRESSURE DIVERSION (END-OF-CHARGE)

<u>APPROX. CYCLE</u>	<u>PRESSURE</u>
2,800	-21 IN. OF HG
2,930	64 PSI
3,050	81 PSI
3,180	33 PSI
3,310	-18 IN. OF HG

V. CURRENT PERFORMANCE - (APPROX. CYCLE 3,360)

END OF CHARGE \bar{X} = 1.67 VOLTS

END OF DISCHARGE \bar{X} = 1.23 VOLTS

END OF CHARGE
PRESSURE \bar{X} = -22 IN. OF HG

Figure 5. Continued.

FNC

A NEW TECHNOLOGY IN NI-CD BATTERIES

BACKGROUND TO FNC DEVELOPMENT

- **1895 POCKET AND TUBULAR CELL DEVELOPMENT**
- **1930 SINTERED CELL DEVELOPMENT**
- **1983 FIBER-STRUCTURED NICKEL ELECTRODES-FNC**

ORIGINAL PAGE IS
OF POOR QUALITY

FNC

FIBER STRUCTURED NICKEL ELECTRODES



FNC Fibre Structure, as seen under an electron microscope

FNC CHARACTERISTICS

- **THICKNESS AND SIZE CAN BE EASILY CHANGED**
- **PURE ACTIVE MATERIALS ARE USED**
- **HIGH CONDUCTOR DENSITY**
- **HIGH ELASTICITY OF THE STRUCTURE**
- **HIGH POROSITY**

FNC PERFORMANCE ATTRIBUTES

- **IMPROVED CHARGE EFFICIENCY**
- **HIGH CAPACITY WITH LITTLE WATER LOSS**
- **CAPACITY MAINTAINED WITH USE**
- **WIDE OPERATING TEMPERATURE RANGE**

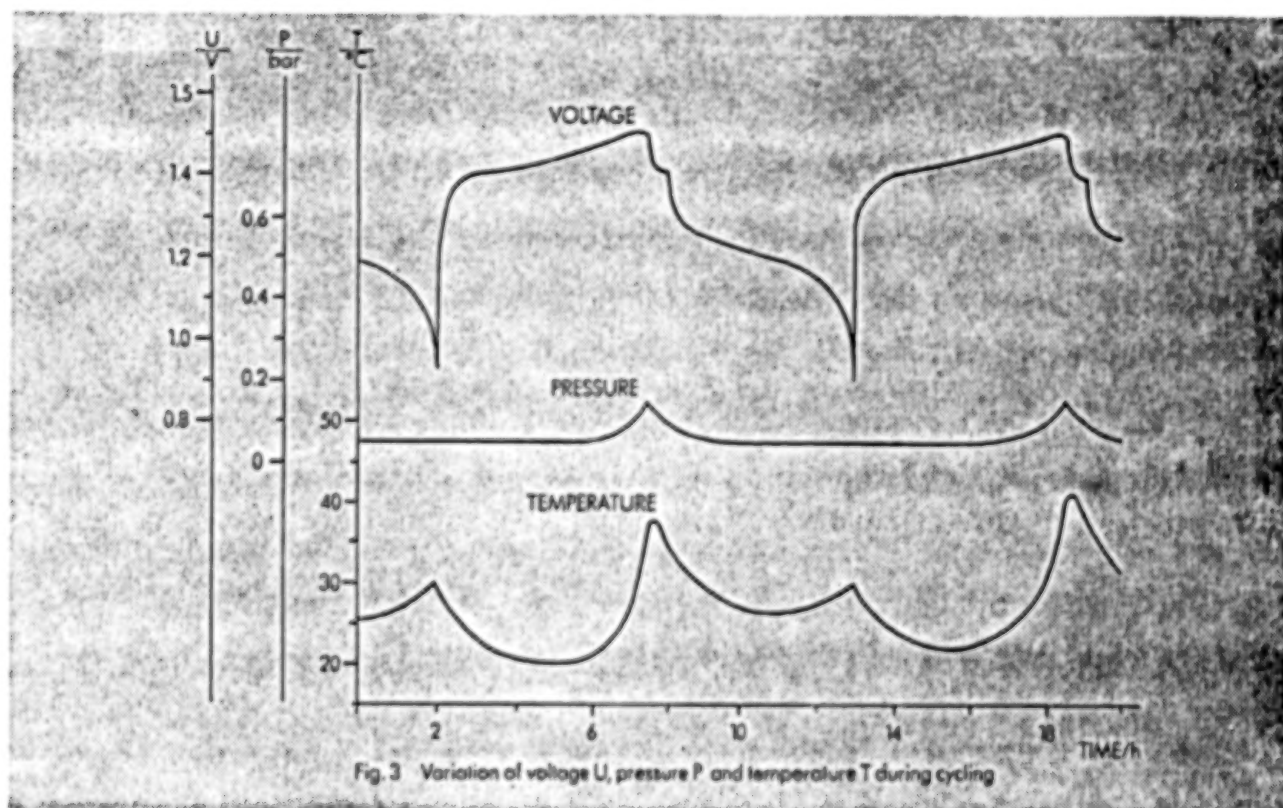
FNC

SEALED CELLS

FNC SEALED CELL CHARACTERISTICS

- **FLAT VOLTAGE CURVE**
- **SHARP TEMPERATURE RISE**
- **NEGATIVE PRESSURE**
- **LIGHT WEIGHT**
- **HIGH RECOMBINATION RATES**

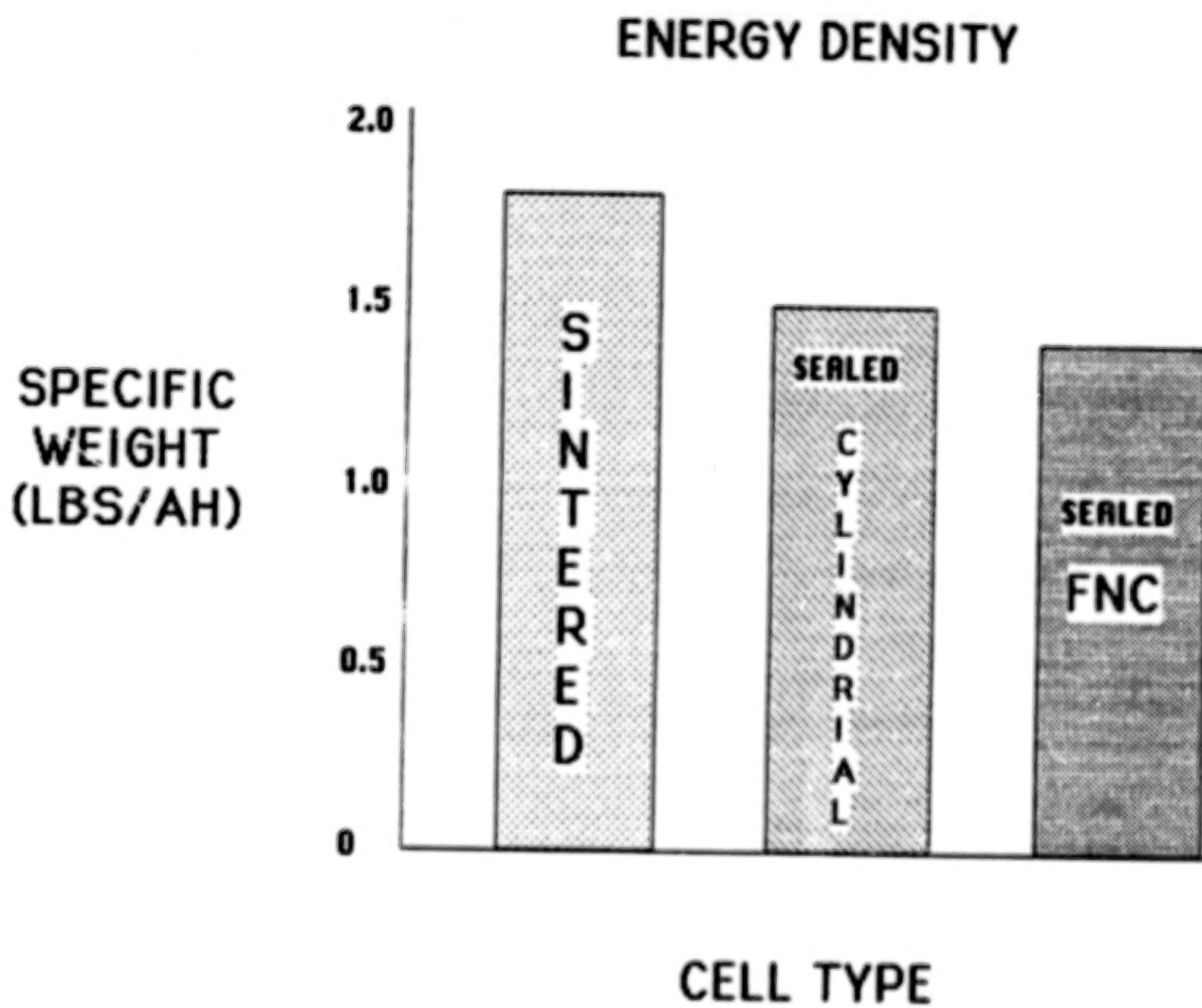
FNC SEALED CELL PERFORMANCE



ORIGINAL PAGE IS
OF POOR QUALITY

FNC SEALED CELL PERFORMANCE FACTS

- **HIGH CHARGE RATE (1 C)**
- **10 C DISCHARGE RATES**
- **10 TO 20 % OVERCHARGE FOR FULL CAPACITY**
- **3% CAPACITY LOSS AFTER 1000 DEEP CYCLES**
- **HIGHER ENERGY DENSITY**



FNC SEALED CELL MAINTENANCE

- **NO WATER REPLACEMENT**
- **NO LOSS OF CAPACITY/FADING WITH USE**
- **NO CELL SWELLING AND SELF DESTRUCTION**

VENTED FNC BATTERY APPLICATIONS

- TRACTION
- UTILITIES
- UPS

SEALED FNC BATTERY APPLICATIONS

- BACKUP POWER SUPPLIES
- ON BOARD AIRCRAFT
- HIGH PERFORMANCE MAINTENANCE FREE APPLICATIONS

1986 NASA/GSFC BATTERY WORKSHOP
LIST OF PARTICIPANTS

Julio Acevedo
NASA/Headquarters
Code RP
Washington, DC 20546
(202) 453-2844

Walter Alsbach
INTELSAT
3400 International Drive, NW
Washington, DC 20008
(202) 944-6988

Harry Alward
Eveready Battery
39 Old Ridgeberry
Danbury, CT 06817
(203) 974-7480

Jon Armantrout
Lockheed
1111 Lockheed Way
Sunnyvale, CA 94086
(408) 742-2453

Daniel Augenstene
DOJ
8199 Backlick Road
Lorton, VA 22079
(202) 234-2800 Ext. 3198

Charles Badcock
Aerospace
P.C. Box 92957
Mail Stop M2-275
Los Angeles, CA 90009
(213) 336-5180

James Barnes
NSWC
Code R33
Silver Spring, MD 20903-5000
(301) 394-1312

Wilbert Barnes
NRL
Code 7714
4555 Overlook Ave., SW
Washington, DC 20375
(202) 767-6517

Albert Bates
Naval Air Development Center
Code 3042
Jacksonville Road
Warminster, PA 18974
(215) 441-2584

Carl Baxam
Tracor Battery Tech. Center
3805 Mt. Vernon Avenue
Alexandria, VA 22305
(703) 769-6833

Dick Beauchamp
Johnson Controls
P.O. Box 591
Milwaukee, WI 53201
(414) 228-2361

Klaus von Benda
DAUG Ltd.
P.O. Box 85
W. German
D-7300 Esslingen
WEST GERMANY
0711-1746010

Chuch Bennett
General Electric
3198 Chestnut Street
Philadelphia, PA 19101
(215) 823-2183

J. Bentley
Yardney
82 Mechanic Street
Pawcatuck, CT 02891
(203) 599-1100

E. Berry
Aerospace
P.O. Box 92957
Mail Stop M4-988
Los Angeles, CA 90009
(213) 648-6273

Samuel Birken
Aerospace
P.O. Box 92957
Mail Stop M4-986
Los Angeles, CA 90009
(213) 336-6080

R.F. Bis
NSWC
Code R-33
Silver Spring, MD 20903-5000
(301) 394-1312

Carole Bleser
Eagle-Picher
P.O. Box 5234
Colorado Springs, CO 80931
(303) 392-4266

R.S. Bogner
Hughes Aircraft Co.
P.O. Box 92919
Airport Station
MS S41/A315
Los Angeles, CA 90009
(213) 648-3755

Donald Bondeson
Martin Marietta
P.O. Box 179
Mail Stop S8032
Denver, CO 80201
(303) 977-6132

Francis Boyce
RCA
13305 Finsbury Ct. #1
Laurel, MD 20708
(301) 763-7110

J. Brill
Eagle-Picher
P.O. Box 47
Joplin, MO 64802
(417) 623-8000

Ralph Brodd
Gould
35129 Curtis Blvd.
Eastlake, OH 44094
(216) 953-5065

Richard Broderick
GTE
1700 Old Meadow Road
McLean, VA 22102
(703) 848-0421

Kathleen Burch
Comsat
18725 Purple Martin Lane
Gaithersburg, MD 20879
(301) 428-4000 ext. 2251

Robert Byrnes
U.S. Army
27 Kelvin Drive
Stafford, VA 22554
(202) 695-3516

Uno Carlsson
Fairchild
20301 Century Blvd.
Germantown, MD 20879
(301) 428-6022

Howard Carpenter
Eveready Battery
39 Old Ridgeberry
Danbury, CT 06817
(203) 794-7549

Alan Casperd
British Aerospace
Argyle Way, Stevenage
Hertfordshire
ENGLAND
SG1-2AS
438-73-6482

Robert Cataldo
NASA/Lewis Space Center
21000 Brook Park Road
Cleveland, OH 4416
(216) 433-5254

Divna Cipris
Allied Signal
P.O. Box 1021-R
Morristown, NJ 07960
(201) 455-2880

Virginia Clay
Martin Marietta
P.O. Box 179
M/S D1744
Denver, CO 80201
(303) 977-9467

Steven Cohen
RCA Americom
4 Research Way #2-8
Princeton, NJ 08540
(609) 987-4118

P. Chetty
Fairchild
Germantown, MD 20874
(301) 428-6947

Young Cho
Drexel University
Dept. of Mechanical Engineering
Chestnut & 32nd Street
Philadelphia, PA 19104
(215) 895-2425

Leo Christensen
Pellon Co.
20 Industrial Ave.
Chelmsford, MA 01824
(617) 256-6588

James Ciesla
Electrochem
10000 Wehrle Drive
Clarence, NY 14031
(716) 759-2828

Joe Connolly
AT&T
50 Lawrence Road
Springfield, NJ 07081

Dennis Cooper
INTELSAT
3400 International Drive, NW
Washington, DC 20008
(202) 944-7349

A.H. Cox
British Aerospace
Argyle Way, Stevenage
Hertfordshire
ENGLAND
SG1-2AS
438-73-6482

Walter Cox
NSWC
Code R33
Silver Spring, MD 20903-5000
(301) 394-1312

Glenn Cruze
Duracell
Bldg. 9 Berkshire Industrial Park
Bethsc, CT 06801
(203) 791-3284

Harry Culver
NASA/Goddard Space Flight Center
Code 711.1
Greenbelt, MD 20771
(301) 286-6841

F.S. Cushing
3-E Laboratories
840 W. Main Street
Lansdale, PA 18936
(215) 362-7012

Ivan Danzig
6812 Wild Rose Court
Springfield, VA 22152
(202) 695-3516

Patrick Davis
NSWC
Code R33
Silver Spring, MD 20903-5000
(301) 394-1312

John Day
NASA/Goddard Space Flight Center
Code 711.2
Greenbelt, MD 20771
(301) 286-5752

Mark DeWitt
Rockwell
P.O. Box 3644
Seal Beach, CA 90740-7644
(818) 594-1829

Rodney Dixon
SAFT - Li Div
109 Beaver Court
Cockeysville, MD 21030

Mike Dommeniconi
Lockheed Missile & Space Company
1111 Lockheed Way
B/158 O/M210
Sunnyvale, CA 94086
(418) 756-6149

Sam Donley
Aerospace Corporation
Mail Stop M2-275
P.O. Box 92957
Los Angeles, CA 90009
(213) 336-4103

A. Donnet
INTELSAT
3400 International Drive, NW
Washington, DC 20008
(202) 944-7245

Orville Dunham
National Standard
P.O. Box 1620
Corbin, KY 40701-1620
(606) 528-2141

J.D. Dunlop
Comast Labs
22300 Comsat Drive
Clarksburg, MD 20871
(301) 428-4545

Alan Eales
British Aerospace
Argyll Way, Stevanage
Hertfordshire
ENGLAND
438-736880

Martin Earl
COMSAT Labs
22300 Comsat Drive
Clarksburg, MD 20871
(301) 428-4503

Wally Ebner
Honeywell
104 Rock Road
Horsham, PA 19044

Tim Edgar
Gates Co.
P.O. Box 5887
Denver, CO 80217
(303) 744-4614

Chris Edghill
McDonnell Douglas
P.O. Box 516
Dept 354, Bldg 32, Lv 3
MS 83
St. Louis, MO 63166

Marlon Enciso
NASA/Goddard Space Flight Center
Code 711.1
Greenbelt, MD 20771
(301) 286-5070

Michael Enoch
Orbital Systems, Ltd.
P.O. Box 700
Lanham, MD 20706
(301) 731-5650

Bill Eppley
Honeywell
104 Rock Road
Horsham, PA 19044

James Epstein
Battery Engineering
1636 Hyde Park Avenue
Hyde Park, MA 02136
(617) 361-7555

M.D. Farrington
Farrington Lockwood Company Ltd.
P.O. Box 6797, Station J
Ottawa, Ontario
CANADA K2A 3Z4
(613) 226-7314

David Feder
Electrochemical Energy
35 Ridgedale Ave.
Madison, NJ 07940
(201) 377-0163

Tony Felts
NWSC Crane
Code 30524
Crane, IN 47522
(812) 854-1593

Sergio Ferreira
EMBRATEL
Ave Pres Vargas, 1012
605 Centro Rio de Janeiro,
BRAZIL
CEB 20070
55-21-216-8641

Charles Fleischmann
Honeywell
104 Rock Road
Horsham, PA 19044

Jack Fober
University of Colorado
5525 Central
Boulder, CO 80309
(303) 492-1884

Robert W. Francis
The Aerospace Corporation
P.O. Box 92957
Los Angeles, CA 9009
(213) 336-6273

Kenneth Fuhr
Martin Marietta
P.O. Box 179
Denver, CO 80201
(303) 971-5529

James Garver
NRL
Code 7714
4555 Overlook Ave., SW
Washington, DC 20375-5000
(202) 767-9075

Steve Gaston
RCA
P.O. Box 800
Princeton, NJ 08540
(609) 426-3349

Pete George
NASA/Marshall Space Flight Center
Huntsville, AL 35812

Joe Gessler
SAFT - Li Div
109 Beaver Court
Cockeysville, MD 21030

H. Gibbard
Power Conversion

Al Gillis
NASA/Goddard Space Flight Center
Code 405
Greenbelt, MD 20771
(301) 286-6332

Richard Giovannoni
W.R. Grace
7379 Route 32
Columbia, MD 21044
(301) 531-4342

Olga Gonzalez-Sanabria
NASA/Lewis Research Center
21000 Brookpark Road
Mail Stop 309-1
Cleveland, OH 44135
(216) 433-5252

Lester Gordy
U.S. Army
8219 Running Creek Ct.
Springfield, VA 22153
(202) 695-3516

Tom Gostonski
Code 743.1
NASA/GSFC
Greenbelt, MD 20771
(30) 286-3326

Hal Grady
Foote Mineral Co.
Route 100
Exton, PA 19341
(215) 363-6500

John Gray
Boeing
P.O. Box 3999
Seattle, WA 98124
(206) 773-3710

Robert Green
GTE
1700 Old Meadow Road
McLean, VA 22102
(703) 848-0452

Gerald Griffin
Altus
1610 Crane Court
San Jose, CA 95112
(408) 436-1300

Michael Grimm
SAFT
109 Beaver Ct
Cockeysville, MD 21030

Frank Gross
Martin-Marietta
P.O. Box 179
Denver, CO 80201

Sidney Gross
Boeing Aerospace Co.
MS 8K-35
P.O. Box 3999
Seattle, WA 98124
(206) 773-5744

Randy Haag
NWSC
Code 30524
Crane, IN 47522
(812) 854-1593

Steve Hafner
SAFT - Li Div.
109 Beaver Ct.
Cockeysville, MD 21030
(301) 666-3200

Arnold Hall
Yardney
82 Mechanic Street
Pawcatuck, CT 02891
(203) 599-1100

Steve Hall
NWSC
Code 30524
Crane, IN 47522
(812) 854-1593

Gerald Halpert
JPL
4800 Oak Grove Drive
Pasadena, CA 91109
(213) 354-5474

V.M. Halsall
Johnson Controls Inc.
5757 N. Greenbay Avenue
Milwaukee, WI 53201
(414) 228-2437

Mark Halverson
RCA
4 Research Way
Princeton, NJ 08540
(609) 987-4297

Dieter Harden
AEG Aktiengesellschaft
Industriestr 29
D-2000 Wedel
WEST GERMANY

Alan Harkness
Ballard Research
1164 15th Street W.
North Vancouver, BC
CANADA V7P 1MP
(604) 986-4104

David Harma
Yardney Battery Division
82 Mechanic Street
Pawcatuck, CT 02891
(203) 599-1100 x 254

Lowell Harmon
Westinghouse
NASA/GSFC
Code 480.1
Greenbelt, MD 20771
(301) 286-6143

E. Hendee
Telesat Canada
333 River Road
Ottawa, Ontario
CANADA
(613) 746-5920

Thomas Hennigan
T.J. Hennigan Assoc.
900 Fairoak Avenue
N. Hyattsville, MD 20783
(301) 559-0613

Gregg Herbert
APL
Johns Hopkins Road
Laurel, MD 20707
(301) 792-5000 Ext. 8604

Terry Hershey
Aerospace
P.O. Box 92957
El Segundo, CA 90009-2957
(213) 336-6273

Bob Higgins
Eagle-Picher
P.O. Box 47
Joplin, MO 64802
(417) 623-8000

Albert Himy
Navy
P.O. Box 1652
Hyattsville, MD 20788-0652
(301) 699-7630

G.F. Hoff
NSWC Code R-33
Silver Spring, MD 20903-5000
(301) 394-1312

Gerhard Holleck
EIC Laboratories
111 Downey Street
Norwood, MA 02062
(617) 769-9450

Harry Holter
Naval-Sea Systems Command
Comdr NSSC Code 06G231
Washington, DC 20362-5101
(202) 692-2080

Robert Hooper
U.S. Army
HQDA Room 1E668
Attn: DAEN-ZC
Pentagon
Washington, DC 20310-2600
(202) 695-3520

Franklin Hornbuckle
Fairchild
20301 Century Blvd.
Germantown, MD 20874-1127
(301) 428-6221

Paul Howard
Howard Association
P.O. Box 280
Greensboro, MD 21639
(301) 482-6088

Daniel Hurley
University of Colorado
5525 Central
Boulder, CO 80309
(303) 492-1884

Warren Hwang
Aerospace
P.O. Box 92957
Mail Stop M2-275
Los Angeles, 90009
(213) 336-6962

David Icenhower
U.S. Navy
Naval Ship R&D Center
Code 2721
Annapolis, MD 21402
(301) 267-2748

Thierry Jamin
CNES
French National Space Study
CST/DRT/TVE/ME
18 Ave. E. Belin
31055 Toulouse Cedesc
FRANCE
61-27-49-38

Ain Jenkins
MBB Space System Group
P.O. Box 801169
8000 Munich 80
WEST GERMANY

Daniel Johnson
Eveready Battery
P.O. Box 45035
Westlake, OH 44145
(216) 835-7619

Joseph Jolson
Catalyst Research
3706 Crondall Lane
Owings Mills, MD 21117
(301) 356-2400

Quentin Kampf
Pellon
221 Jackson Street
Lowell, MA 01852
(818) 594-1829

Katalin Keener
Eagle-Picher
P.O. Box 5234
Colorado Springs, CO 80931
(303) 392-4266

John Kelly
Exide Co.
19 W. College Avenue
Yardley, PA 19067

Alain Kerouanton
SAFT - Li Div.
109 Beaver Court
Cockeysville, MD 21030
(301) 666-3200

Randy Kientz
General Electric
P.O. Box 114
Gainesville, FL 32602
(904) 462-3557

Edison Kipp
Kipp
914 Schooner Court
Annapolis, MD 21401

David Kirkpatrick
Lockheed Missiles & Space Co.
1111 Lockheed Way
B/158 O/M201
Sunnyvale, CA 94086
(408) 756-6149

Martin Klein
Energy Research
3 Great Pasture Road
Danbury, CT 06810
(201) 792-1460

Chip Koehler
Ford Aerospace Co.
3939 Fabian Way
Mail Station G-45
Palo Alto, CA 94303

Paul Krehl
Electrochem Ind.
10000 Wehrle Drive
Clarence, NY 14031
(716) 759-2828

M. Kronenberg
Duracell
37 A Street
Needham, MA 02194
(617) 449-7600

Ben Lamb
Naval Research Lab
4555 Overlook Ave.
Washington, DC 20375-5000
(202) 767-6534

Paul Leigh
APL
Johns Hopkins Road
Laurel, MD 20707
(301) 792-5000 Ext. 8604

Joel Levinthal
Allied Bendix Aerospace
P.O. Box 17880
Jacksonville, FL 32245-7880
(904) 739-4203

S. Levy
Sandia National Lab
Code 2523
Albuquerque, NM 87185-5800
(505) 844-8029

Herman Lewis
McDonnell Douglas
5301 Boisa Avenue
A3-354/10-3
Huntington Beach, CA 92647
(714) 896-3137

David Linden
Consultant
78 Lovett Avenue
Little Silver, NJ 07739
(201) 741-2271

Joseph Lundquist
W.R. Grace
7379 Route 32
Columbia, MD 21044
(301) 531-4342

Chuck Lurie
TRW
One Space Park
R4/1028
Redondo Beach, CA 90278
(213) 536-3503

Tyler Mahy
CIA
c/o OTS
Washington, DC 20505
(202) 351-3912

N. Margalit
Tracor
3805 Mt. Vernon Avenue
Alexandria, VA 22305
(703) 769-6800

Lynn Marcoux
BTC Engineering Ltd.
1164 15th Street, West
N. Vancouver, BC
V7P 1M9 CANADA
(604) 966-4104

Dean Maurer
AT&T
600 Mountain Avenue
Room 1E207
Murray Hill, NJ 07060
(201) 582-3237

Richard Maurer
APL
Johns Hopkins Road
Laurel, MD 20707
(301) 953-4009

Joseph McCann
RCA
9012 Stevens Lane
Lanham, MD 20706
(301) 763-7577

Joe McDermott
Martin-Marietta
P.O. Box 179
Denver, Co 80201

Bruce McDonald
Duracell
Berkshire Ind. Park
Building 9
Bethel, CT 06801
(203) 791-3258

Greg McDonald
MCI
P.O. Box 291
Clarksburg, MD 21671
(301) 540-5408

John Metcalfe
Canadian Astronautics
1050 Morrison Drive
Ottawa, ON
K2H 8K7, CANADA
(613) 820-8280

George Methlie
CIA
2120 Nathhoa Court
Falls Church, VA
(703) 533-1499

John Meyer
APL
John Hopkins Road
Laurel, MD 20707
(301) 792-5000 Ext. 8604

Vern Mielke
NASA/Goddard Space Flight Center
Code 711.1
Greenbelt, MD 20771
(301) 286-8477

Ron Mikkelson
General Dynamics
P.O. Box 85990
MZ 24-8720
San Diego, CA 92123
(619) 547-3706

Martin Milden
Aerospace
P.O. Box 92957
Mail Stop M5-720
Los Angeles, CA 90009
(213) 648-5225

Gene Miller
APL
Johns Hopkins Road
Laurel, MD 20707
(301) 792-5000 Ext. 8604

Lee Miller
Eagle-Picher
P.O. Box 47
Joplin, MO 64802
(417) 623-8000

Tim Miller
Air Force Space Comm.
1028 Mahattan Ave., #1
Hermosa Beach, CA 90254

Tom Miller
NASA/Lewis Research Center
21000 Brookpark Road
Mail Stop 501-17
Cleveland, OH 44135
(216) 433-6300

Don Mitchell
Honeywell
104 Rock Road
Horsham, PA 19044

George Morrow
NASA/GSFC
Code 711.2
Greenbelt, MD 20771
(301) 286-6691

Harry Moses
NRL
828 Glen Allan Drive
Baltimore, MD 21229
(202) 767-3683

Carl Mueller
NSWC
Code R33
White Oak
Silver Spring, MD 20903-5000
(301) 394-2472

Buddy Murray
Martin Marietta Corporation
P.O. Box 179
Mail Stop S-4017
Denver, CO 80201
(303) 971-8731

Kim Nagal
U.S. Army
203 S. Yoakum Parkway
Alexandria, VA 22304
(703) 370-8014

Rich Niederberger
SAFT - Li Div.
109 Beaver Court
Cockeysville, MD 21030
(301) 666-3200

L. Norton
NASA/Marshall Space Flight Center
Code EB12
Huntsville, AL 35812

Robert Nowak
Office of Naval Research
Code 113 ES
800 N. Quincy Street
Arlington, VA 22217-5000
(703) 696-4409

D. Oldham
British Aerospace
Argyle Way, Stevenage
Hertfordshire, England
SG1-2AS
438-73-6482

Joseph Omasta
Martin Marietta
P.O. Box 179
Denver, CO 80201
(303) 971-8731

Tim Ostwald
Ball Aerospace
P.O. Box 1062
Boulder, CO 80306
(303) 939-4443

Burton Otzinger
Rockwell
P.O. Box 3644
Seal Beach, CA 90740-7644
(818) 594-3724

Boone Owens
Boone Owens, Inc.
4707 Lyndale Ave., N.
Minneapolis, MN 55430
(612) 645-2514

Charles Palandati
4915 56th Avenue
Hyattsville, MD 20781

Bob Patterson
TRW
One Space Park
Redondo Beach, CA 90278

Eugene Pearlman
RCA
P.O. Box 800
Princeton, NJ 08540
(609) 426-3349

Edward Pfeffer
AT&T
50 Lawrence Road
Springfield, NJ 07081
(201) 467-7332

David Pickett
Hughes Aircraft
Box 92919
Mail Stop S41/A315
Los Angeles, CA 90009
(213) 648-2128

F. Porter
APL
Johns Hopkins Road
Laurel, MD 20707
(301) 792-5000 Ext. 8604

Geoff Prentice
Johns Hopkins University
Department of Chemical Engineering
Baltimore, MD 21218
(301) 338-7006

Khrushow Press
SAFT - Li Div
109 Beaver Court
Cockeysville, MD 21030
(301) 666-3200

Vincent Puglisi
General Electric
P.O. Box 114
Gainesville, FL 32602
(904) 462-4457

N. Raman
SAFT - Li Div.
109 Beaver Court
Cockeysville, MD 21030
(301) 666-3200

Guy Rampel
General Electric
P.O. Box 114
Gainesville, FL 32602
(904) 462-3521

Robert Richards
Martin Marietta
P.O. Box 179
Denver, CO 80201
(303) 971-5525

Paul Ritterman
COMSAT
2250 E. Imperial Hwy
El Segundo, CA 90245
(213) 416-9106

Ernest Rodriguez
NASA/GSFC
Code 711.2
Greenbelt, MD 20771
(301) 286-6202

Howard Rogers
Hughes
P.O. Box 92919
S-41/A315
Los Angeles, CA 92919
(213) 648-0480

Teresa Romanofsky
NASA/Lewis Research Center
21000 Brookpark Road
Mail Stop 501-17
Cleveland, OH 44135
(215) 433-5363

Gilbert Roth
NASA/Headquarters
Code LB
Washington, DC 20546
(202) 453-8341

Pierre Rousseau
SAFT
156 Ave de Metz
Romainville, FRANCE
93230
48-43-93-61

Frank Scalici
Intelsat
(202) 944-7353

Steve Schiffer
RCA
P.O. Box 800
Princeton, NJ 08540
(609) 426-3349

David Schmidt
General Electric
P.O. Box 861
Gainesville, FL 32602
(904) 462-4752

Schmidt
RCA Americom
P.O. Box 95
Edsall Road
Sussex, NJ 07461
(201) 827-7900

Dean Schneebeck
Martin Marietta Corp.
Mail Stop S-4017
P.O. Box 179
Denver, CO 80201
(303) 971-8731

Wolfgang Schuler
Dornier Systems
N.R. Schulge
NASA/Headquarters
Code QP
Washington, DC 20546
(301) 453-1869

Jean-Pierre Schultze
SAFT
156 Ave de Metz
Romainville, France
93230
48-43-93-61

Kenneth Schwer
McDonnell Douglas
P.O. Box 516
E454/Bldg. 74B
Mail Stop 409
St. Louis, MO 63166
(314) 839-7023

Nicky Serr
NASA/Marshall Space Flight Center
Code EB12
Huntsville, AL 35812

Richard Shaw
Martin Marietta
P.O. Box 179
Mail Stop S0550
Denver, CO 80201
(303) 971-8731

Willard Scott
TRW
One Space Park
R4/1028
Redondo Beach, CA 90278
(213) 536-3503

Charles Scuilla
CIA
5501 Starboard Ct.
Fairfax, VA 22032
(703) 351-3912

J. Searcy
Sandia National Lab
Code 2523
Albuquerque, NM 87185-5800
(505) 844-3649

Eddie Seo
Gates Co.
P.O. Box 5887
Denver, CO 80217
(303) 744-4614

Jack Sindorf
Johnson Controls
900 E. Keefe Ave
Milwaukee, WI 53212
(414) 228-2719

Luther Slifer
7023 Dolphin Road
Lanham, MD 20706
(301) 552-1761

Marc Smith
GTE
1700 Old Meadow Road
McLean, VA 22102
(703) 848-0414

John Smithrick
NASA/Lewis Research Center
21000 Brookpark Road
Cleveland, OH 44135

Frank Snow
U.S. Navy - SPAWAR
Attn: PMW 142-4
Washington, DC 20363-5100
(202) 692-2290

Ray Sperber
GTE
1700 Old Meadow Road
McLean, VA 22102

Robert Staniewicz
SAFT - Li Div
109 Beaver Ct.
Cockeysville, MD 21030

Robert Stearns
General Electric
P.O. Box 8555
Philadelphia, PA 19101
(215) 354-1505

Sal Stefano
JPL
4800 Oak Grove Drive
Mail Stop 122-123
Pasadena, CA 91109
(818) 354-6320

Richard Stirling
ITE
6901B Distribution Dr.
Beltsville, MD 20705
(301) 937-8200

Joe Stockel
U.S. Govt.
Washington, DC 20505
(703) 351-2065

Ralph Sullivan
APL
Johns Hopkins Road
Laurel, MD 20707
(301) 792-5000 Ext. 8604

Subbarao Surampudi
JPL
Mail Stop 277-212
4800 Oak Grove Drive
Pasadena, CA 91109
(818) 354-0352

David Surd
Catalyst Research
3706 Crondall Lane
Owings, Mills, MD 21117
(301) 356-2400

William Swartz
APL
Johns Hopkins Road
Laurel, MD 20707
(301) 792-5000 Ext. 8604

Larry Swette
Giner, Inc.
14 Spring Street
Waltham, MA 02254-9147
(617) 899-7270

Benjamin Tausch
Martin Marietta
P.O. Box 3430
Sunnyvale, CA 94088-3430
(408) 752-4175

J. Taylor
MOLI Energy
3958 Myrtle Street
Burnaby, BC Canada
V5C 4G2
(604) 437-6927 Ext. 404

Bob Tenkman
Xetron
40 West Crescentville Rd
Cincinnati, OH 45246

Larry Thaller
NASA/Lewis Research Center
21000 Brookpark Road
Cleveland, OH 44135
(216) 433-6146

Helmut Thierfelder
General Electric
P.O. Box 8555
Philadelphia, PA 19101
(215) 354-2027

Dorena Thompson
Eagle-Picher
P.O. Box 47
Joplin, MD 64802
(417) 623-8000

Smith Tiller
NASA/Goddard Space Flight Center
Code 711.2
Greenbelt, MD 20771
(301) 286-6489

Hari Valdyanthan
COMSAT
22300 Comsat Drive
Clarksburg, MD 20871
(301) 428-4507

Jean-Francois Valobra
SA Matra
31 Rue Des Cosmonautes
Zl du Palays
31077 Toulouse Cedex
FRANCE
61-39-61-39

Henry Vandewall
SPAR Aerospace

K. Vasanth
NSWC
Code R-32
10901 New Hampshire Ave.
Silver Spring, MD 20903-5000
(301) 394-3549

Jean Verniolle
ESA/ESTEC
Keplerlaan 1
2200 AZ Noordwijk
Netherlands
31-1719-83868

Don Verrier
TRW
One Space Park
R4/1028
Redondo Beach, CA 90278
(213) 536-3503

James Waggoner
Catalyst Research
3706 Crondall Lane
Owings Mills, MD 21117
(301) 356-2400

Harry Wajsglas
NASA/Goddard Space Flight Center
Code 711.1
Greenbelt, MD 20771
(301) 286-6158

Harry Wannemacher
NASA/Goddard Space Flight Center
Code 711.1
Greenbelt, MD 20771
(301) 286-5914

Don Warnock
U.S. Air Force
AFWAL/POO5-2
Wright-Patterson AFB, OH 45433-6563
(513) 255-6241

Glenn Waterman
ULDC
7915 South 1530 West
West Jordan, UT 84084
(801) 561-9385

Thomas Watson
Catalyst Research
3706 Crondall Lane
Owings Mills, MD 21117
(301) 356-2400

Donald Webb
McDonnell Douglas
P.O. Box 516
E454/Bldg. 74B
Mail Stop 409
St. Louis, MO 63166
(314) 233-2404

Irwin Weinstock
Catalyst Research
3706 Crondall Lane
Owings Mills, MD 21117
(301) 356-2400

Eileen Whitlock
U.S. Army - SLAG
5925 Quantrell Avenue
Alexandria, VA 22312
(703) 941-3347

Thomas Willis
AT&T
600 Mountain Avenue
Murray Hill, NJ 07060
(201) 582-3545

Richard Wissoker
GTE
520 Winter Street
Waltham, MA 02154-1275
(617) 466-3216

Richard Wojcik
Department of Communications
P.O. Box 11490
Station H
Ottawa, ON
K2H 6S2 CANADA
(613) 998-2429

R. Wolstencroft
British Aerospace
Argyle Way
Stevenage Herts, ENGLAND

Arley Wright
ITE
6901B Distribution Dr.
Beltsville, MD 20705
(301) 937-8200

David Yalom
AT&R, Inc.
10813 East Nolcrest Dr.
Silver Spring, MD 20903
(301) 593-1973

Thomas Yi
NASA/GSFC
Code 711.2
Greenbelt, MD 20771
(301) 286-3051

A. Zimmerman
Aerospace
P.O. Box 92957
Mail Stop M2-275
Los Angeles, CA 90009
(213) 648-7415

Adrian Zolla
Altus
1610 Crane Ct
San Jose, CA 95112
(408) 436-1300

Report Documentation Page

1. Report No. NASA CP- 2486		2. Government Accession No.		3. Recipient's Catalog No.	
4. Title and Subtitle The 1986 Goddard Space Flight Center Battery Workshop				5. Report Date September 1987	
				6. Performing Organization Code 711.0	
7. Author(s) G. Morrow and T. Yi, Editors				8. Performing Organization Report No. 87B0408	
				10. Work Unit No.	
9. Performing Organization Name and Address Goddard Space Flight Center Greenbelt, Maryland 20771				11. Contract or Grant No.	
				13. Type of Report and Period Covered Conference Publication	
12. Sponsoring Agency Name and Address National Aeronautics and Space Administration Washington, D.C. 20546-0001				14. Sponsoring Agency Code	
15. Supplementary Notes					
16. Abstract This document contains the proceedings of the 19th annual Battery Workshop held at Goddard Space Flight Center, Greenbelt, Maryland on November 18-19, 1986. The Workshop attendees included manufacturers, users and Government representatives interested in the latest developments in battery technology as they relate to high reliability operations and aerospace use. The subjects covered include lithium cell technology and safety improvements, nickel-cadmium separator and electrode technology along with associated modifications, flight experience and life testing of nickel-cadmium cells, and nickel-hydrogen applications and technology.					
17. Key Words (Suggested by Author(s)) Batteries, Electro-Chemical, Nickel-Cadmium, Lithium, Nickel-Hydrogen			18. Distribution Statement Unclassified-Unlimited Subject Category 33		
19. Security Classif. (of this report) Unclassified	20. Security Classif. (of this page) Unclassified	21. No. of pages 394	22. Price A17		

**END
DATE
FILMED**

JAN 13 1988